Substructural Condition Assessment of Bridge Structures Under Moving Vehicles

By

Solmaz Pourzeynali Miankouh

A thesis submitted in fulfilment of the requirements for the degree of

Doctor of Philosophy

Centre for Infrastructure Engineering (CIE)

WESTERN SYDNEY
UNIVERSITY

March 2020

`

Certificate of Authorship/originality

I certify that the work in this thesis has not previously been submitted for a degree nor has been submitted as part of requirements for a degree except as fully acknowledged within the text.
I also certify that the thesis has been written by me. Any help that I have received in my research work and the preparation for the thesis itself has been acknowledged. In addition, I certify that all information sources and literature used are indicated in the thesis.

Solmaz Pourzeynali Miankouh

30/03/2020

`

Abstract

Bridge infrastructures are continuously subject to degradation, due to aging, their operational environment, and excess loading, which places users at risk. It has now become a major concern worldwide, where the majority of bridge infrastructures are approaching their design life, and the number of bridges in poor condition is increasing. This compels the engineering community to develop robust and reliable methods for continuous monitoring of bridge infrastructures. Most of the existing methods are time-consuming, labour-intensive, and expensive or they are not robust enough to be used in real-world applications. To address this problem, new methods need to be developed, and rather than numerical verifications laboratory and field tests should be carried out for experimental validation.

In this research project, condition assessment of bridge structures under moving vehicles is investigated. The bridge subjected to a moving vehicle is subjected to one type of forced vibration test, with no need for traffic interruption and extensive experimental arrangements. Using moving vehicles as an exciter has the ability to induce structural vibration with a large enough amplitude and reasonable signal-to-noise ratio.

There have been many attempts made in the condition assessment of bridges. However, in most cases the bridge is subjected to non-moving loads or known moving loads. Moreover, road surface roughness can hugely affect the dynamic behaviour of a vehicle as well as the interaction force between a vehicle and a damaged bridge structure. Therefore, bridge structural damage and moving loads should be identified together, which has not been studied extensively. In this study, firstly the identification of moving loads based on the explicit form of the Newmark-β method is proposed and verified, and then simultaneous identification of moving loads and structural parameters is presented. Moving load identification in existing studies is commonly formulated in state space, which is sensitive to discretization and sampling rate. Numerical and experimental studies indicate the efficiency and robustness of the method considering different levels and locations of damage, vehicle speed, and road surface roughness.

For small structures, simultaneous identification of moving loads and structural parameters employing the finite element model of the whole structure is reasonable, however, the situation is completely different when it comes to large and complex structures. The identification of structural damage is an inverse problem that is also ill-posed in the presence of noise. When dealing with large and complex structures, accuracy and convergence will become significant issues and the efficiency of the method will be degraded. More response

`

measurements are needed which means the requirement of more labour, installation difficulties, and expenses. As the number of unknowns increases, this problem will become more challenging.

To address this dilemma, the substructure condition assessment has been proposed. Utilizing this method, a bridge model can be split into many substructures. Substructures which are more vulnerable to damage or are of more importance can be chosen as target substructures. A substructure has a considerably smaller number of DOFs in comparison with the whole structure and the number of unknown parameters is also reduced. However, substructures are not isolated from the remaining structure and interface forces between substructures have to be applied as dynamic forces to substructures.

The substructure condition assessment method in civil engineering is commonly employed for buildings and beams under non-moving loads or known loads. This project is believed to be among the few studies on condition assessment of bridge structures under moving vehicles considering uncertainties such as noise, vehicle speed, and road surface roughness. In this method, measurements are used directly. There is no need for complete measurements at the interface nodes as well as no need for interface force measurements. The moving vehicle is unknown and only the location and speed of the vehicle is needed to be known in advance.

For substructure condition assessment, two cases have been investigated, in one of which the finite element model (FEM) of the whole structure is available and in another one, only the FEM of the target substructure is available. Model updating is carried out based on a dynamic response sensitivity method and local damage is simulated as a reduction in element stiffness.

Experimental and numerical studies on a bridge structure subject to moving loads indicate the robustness and efficiency of the proposed techniques to deal with road roughness, and vehicle speed in moving load identification as well as detecting and quantifying structural damage. The proposed techniques have the potential to reduce the number of sensors needed for bridge structural health monitoring as well as to reduce the computational effort and costs while enhancing the accuracy.

`

To my husband and parents

`

Acknowledgments

This PhD project could not have been completed without the support and guidance of a number of people whose contribution I wold like to acknowledge.

Firstly, I would like to acknowledge the financial support received from the Australian Research Council under the discovery program grant number of "DP160103197".

Furthermore, I would like to express my sincere thanks to my supervisor, Prof. Bijan Samali, who provided me with the opportunity to work on this great project, and for his continuous support, immense knowledge and motivation, as well as my co-supervisor, Dr. Maria Rashidi, for her constant encouragement, invaluable suggestions and emotional support during this research. Additionally, I would like to thank my external supervisor from the University of Technology Sydney, A/Prof. Xinqun Zhu, for his support of my Ph.D. studies.

My sincere gratitude goes to Prof. Siu-Seong Law at Beijing Jiaotong University for his invaluable technical guidance. I was surprised by his knowledge and passion in this field, and he has become my role model for positive characteristics, time management, and communication skills.

In addition, I would like to thank structural laboratory manager, Mr. Robert Marshal, and all structural laboratory technical staff, in particular Mr. Ali Ghari Zadeh, for his patience, time, efforts, and invaluable technical advice in performing experimental tests.

I thank Dr. Mehri Makki Alamdari and Dr. Hamed Kalhor for their kind support, Ms. Linda Brown for her great support in library affairs, Ms. Ann Buckie for proof reading, and the reviewers for donating their valuable time to read my thesis. In particular, I am grateful to Dr. Arash Bahar for enlightening me with my first glance of Ph.D. research.

I would like to express my special thanks to my husband for his great patience, motivation and support during this journey to achieve my goal, as well as to extend my gratitude to my lovely parents who have been tolerating the far distance, and have always supported me, support without which I could not imagine this and other achievements in my life. I also appreciate my brothers for supporting me spiritually throughout writing this thesis and my life in general.

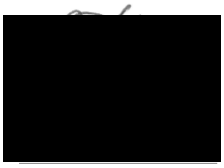

Solmaz Pourzeynali Miankouh

30/03/2020

`

Table of Contents

`

`

`

`

List of figures

`

`

`

`

`

`

`

List of tables

`

`

`

Chapter 1. Introduction

1.1. Research significance

The quality and condition of bridge infrastructures are key indicators of productivity growth, economic development, social and environmental wellbeing. However, they are always subjected to degradation because of aging, their environment, and excess loading. Now it has become a worldwide concern that a large proportion of bridge infrastructures require significant and immediate maintenance because of long-term under-investment during past decades which will impose constraints on all parts of the economy and society (Engineers Australia 2010).

The Australia Infrastructure Report Cards provide information on the quality of Australia's infrastructures, the first of which was released in 1999 with others published in 2005 and 2010. According to these reports, in 1999 the national engineering construction spending on infrastructure was $23.96 billion and the overall grade was "D", indicating a poor condition for which critical changes were required to improve the infrastructure condition to be fit for its future purpose. By 2005, the budget was increased by 28% to $30.68 billion, and the assessment result was lifted to "C+", indicating an adequate result but major changes were still required to improve the infrastructure condition to be fit for its purpose. By 2010, this amount increased by a further 53% to $46.99 billion, and the national assessment remained unchanged at "C+" (Engineers Australia 2010).

Almost the same conditions exist in the United States. Bridge infrastructure in U.S. Infrastructure Report Card in 2017 was graded "C+" which is the same as that in 2013 (American Society of Civil Engineers 2017). There are 614,387 bridges in the U.S., 39% of which (4 in 10) have been in operation for 50 years or more, with an additional 15% having been in operation for 40-49 years. The intended design life of those bridges is 50 years. As mentioned in this report, 9.1% of the nation's bridges were considered structurally deficient in 2016, while receiving traffic averaging in 188 million trips across them each day. There was always a concern about insufficient investment in infrastructures to meet current and future demands. The catastrophic Minnesota River Bridge collapse in 2007 and the Washington State Bridge collapse in 2013 in the USA both highlight the significant need for a cost-effective and systematic maintenance strategy for transporting infrastructure.

Structural health monitoring of bridges using sensor technology has attracted the attention of many researchers for monitoring the structural performance and assessing the condition of aging bridge structures. An early warning will be obtained if there are changes in

`

the load pattern or response mechanism. The condition-based maintenance strategy is an effective way to reduce maintenance costs to satisfy current and future requirements. This has been included in the new bridge design code AS5100, introduced in 2017. In this research project, a substructure condition assessment for bridge structures under moving loads is proposed which is highly reliable for damage detection and can hugely reduce costs while also saving time. Utilising this method, the bridge model can be split into many substructures. Substructures which are more vulnerable to damage or which are of more importance can be chosen as target substructures for condition assessment studies.

1.2. Background

Condition assessment of bridge structures based on vibration measurements has attracted increasing interest among researchers (Brownjohn 2007; Carden & Fanning 2004; Doebling, S. W., Farrar & Prime 1998; Fan & Qiao 2011). There are mainly two types of dynamic vibration tests: the ambient vibration test and the forced vibration test (Chen, GW, Beskhyroun & Omenzetter 2014; Farrar, C.R. et al. 1999; Green 1995; Peeters, B., Maeck & Roeck 2001; Womack & Halling 1999). In this research project, condition assessment of bridge structures under moving vehicles is investigated. A bridge subjected to a moving vehicle is exposed to one type of forced vibration test, with no need for traffic interruption and extensive experimental arrangements. Using moving vehicles as an exciter has the potential of inducing structural vibration with a large enough amplitude and reasonable signal-to-noise ratio (Chen, S, Xia & Zhang 2007; González & Hester 2013; Hester & González 2012; Law, S. S. & Zhu 2009; Malekjafarian, Abdollah, McGetrick & OBrien 2015; Siringoringo & Fujino 2012; Sun, Z, Zhang & Tong 2013; Zhu, Xiang et al. 2019; Zhu, XQ & Law 2015).

The dynamic interaction force between vehicles and road surface is one type of external excitation that can be intensified by structural damage, road surface roughness and vehicle speed and can degrade bridge structures. Therefore, it is of high importance to simultaneously identify moving loads and structural damage while considering road surface roughness. Although there have been extensive attempts to identify moving loads with known structural parameters (Chan, THT, Yu & Law 2000; Chan, THT et al. 2001; Daniel & Kortiš 2017; Law, S. S. & Zhu 2011; Yu & Chan 2007; Zhu, XQ & Law 2016), or to identify structural parameters while knowing moving loads, it seems their simultaneous identification has not been studied enough. Some of the existing studies are for structures subject to known moving loads, non-moving loads, or moving masses (Jayalakshmi & Rao 2017; Lu & Law 2007; Sun, H & Betti 2014; Zhang, Qingxia, Jankowski & Duan 2010a, 2010b; Zhang, Q., Jankowski & Duan 2012).

`

Zhu and Law (2007) presented a method based on displacement measurements to simultaneously identify moving loads and crack damage. They verified the method numerically considering different levels of noise and road roughness. The method is not sensitive to noise but is sensitive to road roughness, and it requires a full-sensor placement. This method was later extended by Law and Li (2010) and numerically verified. The results of this comprehensive study indicated that a sufficient number of sensors is needed as well as the accuracy of identified moving loads can hugely affect the precision of damage detection. Feng et al. (2015) proposed a method using a limited number of sensors. A Bayesian inference-based regularization approach was applied to solve the ill-posed least squares problem for unknown vehicle axle loads. They verified their method numerically at different vehicle speeds and noise levels. However, they did not take into account the effect of roughness and the method has load identification errors over mid supports.

Abbasnia et.al. (2015) developed a sensitivity-based damage detection method referred to as Adjoint Variable Method (AVM), and the effectiveness of the proposed technique has been numerically investigated. The method is sensitive to noise greater than 1.4% and the effect of road roughness is not explored. Obrien et al. (2015) suggested a method based on strains and deflections measurements, yet results indicate that strain measurements are effective only when the sensor is close to the damage zone. Furthermore, the method is sensitive to damage location and it can be identified well only if it is close to the centre of the beam.

In summary, it can be seen that most of the successful studies of simultaneous identification of damage and moving loads, which consider a moving vehicle as an excitation source, have not studied the effect of road roughness or they are not verified experimentally. Therefore, in this research work, simultaneous identification of moving load and structural damage considering a four-degree model for a moving vehicle is carried out. The effects of uncertainties such as measurement of noise, road surface roughness, and the vehicle speed is investigated, and the proposed technique is verified by both numerical example and experimental tests.

To do simultaneous identification of moving load and structural damage, firstly the identification of moving loads based on the explicit form of the Newmark-β method is proposed and verified. Moving load identification in existing studies is commonly formulated in state space, which is sensitive to discretization and sampling rate (Chan, THT, Yu & Law 2000; Chan, THT et al. 2001; Daniel & Kortiš 2017; Law, S. S. & Zhu 2011; Yu & Chan 2007; Zhu, XQ & Law 2016).

`

For small structures simultaneous identification of moving loads and structural parameters with the finite element model of the whole structure is reasonable, however, the situation is completely different when it comes to large and complex structures. The identification of structural damage is an inverse and ill-posed problem. When dealing with large and complex structures, accuracy and convergence will become issues and the efficiency of the method will be degraded. Hence, more response measurements are needed which means more labour, installation difficulties, and expenses. As the number of unknowns increases, this problem will become more challenging.

Koh et al. (1991) proposed the application of substructure identification in civil engineering for the first time, and three numerical examples were studied including a shear building, a plain frame building, and a truss bridge. Utilising this method, the bridge model can be split into many substructures. Substructures which are more vulnerable to damage or which are of more importance can be chosen as target substructures. A substructure has a considerably smaller number of degrees of freedom (DOF) in comparison with the whole structure and the number of unknown parameters is also reduced. However, substructures are not isolated from the remaining structure and interface forces between substructures have to be applied as dynamic forces to substructures.

There are some substructure damage detection approaches which require interface response measurements (Koh, C. G., Hong & Liaw 2003; Trinh & Koh 2012; Yun & Bahng 2000; Yun & Lee 1997); however, it is sometimes impossible to measure the interface responses especially when it comes to rotational responses. Furthermore, most of the time domain methods are developed and verified for structures under non-moving loads (Kun, Law & Zhu 2015; Law, S, Pinghe & Li 2014; Law, S. S. & Yong 2011; Law, S. S., Zhang & Duan 2010; Tee, Koh & Quek 2009; Trinh & Koh 2012).

Law and Yong (2011) studied two substructural damage detection methods in time domain based on the state-space method and iterative updating model. In one of the methods, the finite element model (FEM) of a whole structure may be utilised to identify any external forces, while in another only a target substructure's FEM is available and interface forces, as well as external forces, are all taken as excitations identified in state space. Once loads are identified a damage identification method may then be applied to detect damage in the target substructure. The method is numerically verified by a truss structure under a non-moving load. This method is sensitive to noise in load identification which will increase by the number of unknown external forces, leading to errors in damage detection. However, damage location and extent can still be properly identified.

`

Li and Law (2012a) developed a method and verified it by a 30 m simply supported box-section bridge deck structure subject to moving loads. This numerical example includes 60 flat shell elements and 396 DOFs in total. Under moving load excitation, the method can identify simulated damage even at 5% noise, however several small false positives exist, originating from model condensation in the forward response reconstruction or smearing effect which will increase by noise. The method is also sensitive to sensor placement. Zhu et al., (2013) developed a method which was verified numerically by a 3-span frame and a simply supported beam under a moving load. They have studied limited substructure cases without considering uncertainties such as road roughness and speed as well as the dynamic behaviour of a more realistic vehicle. The method is worthy for identification of damage however it is sensitive to noise when it comes to moving load identification, which may originate from the sensitivity of the state-space method to discretization or sampling rate.

As reviewed, most of the time domain methods are developed and verified for structures under non-moving loads and they are commonly formulated by state-space methods suffering from the errors of discretization and sampling ratio. Furthermore, substructure condition assessment of bridges under moving vehicles considering uncertainties such as road surface roughness and vehicle speed needs more investigation. Liu et al. (2014) developed and verified the explicit form of the Newmark-β method for a force identification of a full structure under a non-moving load. It is shown to be superior to the state space method. Also, Liu et al. (2015) proved the superiority of this method for interface force identification of substructures while the structure is under non-moving load. Here, the explicit form of the Newmark-β method is developed for moving load identification and damage identification, either for a full structure or for a substructure.

In this study, strain and acceleration measurements are used as inputs. There is no need for complete measurements at interface nodes as well as no need for interface force measurements. The moving vehicle is unknown and only the location and speed of it is needed to be known in advance. This project is believed to be among the few studies on condition assessment of bridge structures under moving vehicles considering uncertainties such as noise, vehicle speed, and road surface roughness with numerical and experimental verifications.

1.3. Research objectives and innovation

The main objectives of this thesis are summarized as follows:

1) Moving load identification based on the explicit form of the Newmark-β method
2) Simultaneous identification of structural damage and moving loads

`

3) Substructure condition assessment of bridge structures under moving load with or without having the finite element model of the whole structure
4) Verifying the proposed techniques by numerical and experimental studies in the laboratory
5) Further verifying using a cable-stayed bridge in the field

The effects of sensor placement, measurement noise, road roughness, vehicle speed, and damage location on the accuracy of the proposed techniques have been investigated. The main advantage of identifying moving loads based on the explicit form of the Newmark-β method is its superiority to the state space method in discretization and data sampling rate. Through simultaneous identification of structural damage and moving loads, the effect of road roughness and other uncertainties which affect the dynamic interaction force between vehicle and road surface can be considered. Although there is an extensive attempt to identify moving loads with known structural parameters, or identifying structural parameters with knowing moving loads, it seems their simultaneous identification has not been studied enough.

Furthermore, choosing a moving vehicle as a source of excitation has several advantages over other excitation sources as follows:

1) There are no traffic interruptions
2) Analysis is performed under operational environment conditions
3) Analysis is performed continuously
4) There is no need for exceptional experimental arrangements or techniques
5) The number of sensors and amount of expense is reduced
6) There is the ability for excitation of structural vibrations with a large amplitude and high signal-to-noise ratio

The main advantages of substructure condition assessment of structures are as follows:

1) There will be a reduction in DOFs and unknown parameters using substructure identification, resulting in a lesser number of sensors which have to be installed.
2) The computation effort will be reduced significantly, and computation convergence will be more easily achieved.
3) The uncertainty surrounding boundary conditions, material, and physical parameters decreases using this approach, and since it is often difficult to achieve complete accuracy in a finite element model of a large-scale structure for system identification, this method helps in increasing accuracy.

With the above considerations, it is beneficial to extend the substructure approach into bridge structures. This approach has mainly been studied for other structures such as buildings

`

or beams under non-moving loads or known moving loads. This project is believed to be the first essential study on substructure condition assessment of bridge structures under moving vehicles considering road surface roughness and vehicle speed. The proposed method is verified experimentally.

1.4. The layout of the thesis

This thesis includes eight chapters. Chapter 1 is an introduction to the background, innovation, and layout of this thesis. Chapter 2 presents the literature review on vibration-based condition assessment of structures with a focus on time-domain methods for sub/full structure condition assessment of bridges subject to moving vehicles excitations.

Chapter 3 proposes a technique for moving load identification based on the Newmark-β method. In this chapter, the technique is numerically verified by a single-span simply supported beam and a three-span continuous bridge subject to a four-degree moving vehicle. The effects of the sensor location, measurement noise, vehicle speed, and road surface roughness, as well as side/mid supports on the accuracy of this method are investigated.

Chapter 4 includes a time-domain technique based on the Newmark-β method for simultaneous identification of moving loads and structural damage. The response sensitivity method is applied in an iterative procedure to update the finite element model of the structure using the simulated acceleration responses of a damaged structure. Damage is simulated by elemental stiffness reduction and mass is assumed unchanged. The effects of damage location/extension, sensor location, measurement noise, vehicle speed and road surface roughness, as well as mid/side supports, are numerically verified by studying a single-span simply supported bridge and a two-span continuous bridge.

Chapter 5 conducts a substructure condition assessment of bridge structures based on the above techniques. The intact finite element model of the substructure is available, and the study is performed both with and without having the finite element model of the whole structure. In both of the studies, no measurement is needed at interface nodes; however, the interface forces should be identified based on the above techniques. The effects of the chosen substructure, sensor location, vehicle speed, road surface roughness, and measurement noise are numerically investigated by a single-span simply-supported bridge. Acceleration measurements are numerically simulated.

Chapter 6 delivers an experimental study in the laboratory to verify the proposed techniques experimentally. The set up mainly includes a 3m single-span simply-supported beam excited by a four-wheel car being pulled through the beam by an electronic motor. In the

`

first part of this chapter, strain measurements are used to identify moving loads running on the intact beam. The effects of the sampling frequency and vehicle speed are investigated. Strains are reconstructed by inputting the identified load into the equation of motion of the beam and are then compared with the measured values to evaluate the effectiveness and accuracy of the proposed method for damage identification. In the next part, strain and accelerometer measurements are used for simultaneous identification of structural parameters and moving loads as well as substructure condition assessment of the beam before and after inducing damage. The results before inducing damage are considered as a reference to evaluate the effectiveness of the proposed techniques. The effects of the sampling frequency, vehicle speed, and damage location/extension have been investigated.

Chapter 7 delivers a field study on a 45m cable-stayed bridge located in Western Sydney to verify the effectiveness of the proposed method. This bridge was fitted with accelerometers, strain gauges, and a data acquisition system in 2016 to capture and record any vibrations. A car is passed through this bridge, data recorded and analysed for moving load identification. The method has been successful in identifying the moving loads; however, it is suggested to add more sensors to increase the accuracy of load identification which is needed for damage detection. Chapter 8 provides a summary of the derived conclusions and a discussion on future studies.

`

`

Chapter 2. Literature Review

2.1. Introduction

Condition assessment of bridge structures based on vibration measurements has attracted increasing interest among researchers. There are mainly two types of dynamic vibration tests: the ambient vibration test and forced vibration test. In section 2.2, a review is conducted on studies which have investigated the characteristics of these two test methods and have compared them. Then in section 2.3, the reasons why moving vehicles are used as an excitation source in this research work are explained, and a brief review is presented on indirect bridge health monitoring techniques. Structural Health Monitoring methods of bridges under moving vehicles can generally be divided into three categories: those based on bridge responses (direct bridge health monitoring), those based on vehicle responses (indirect bridge health monitoring), and those based on both vehicle and bridge responses. Direct health monitoring methods, which will be the focus of the current research, are reviewed in section 2.4.

The direct bridge health monitoring approach can be divided into three categories: Those with unknown traffic excitations, those with known moving loads, and those based on identifying moving loads and bridge damage iteratively. A review on the first two groups is presented in section 2.4, and since the focus of this thesis is on the third category, a comprehensive review on simultaneous identification of moving loads and structural parameters is presented in section 2.5.

For small structures simultaneous identification of moving loads and structural parameters with the finite element model of the whole structure is reasonable, however, the situation is completely different when it comes to large and complex structures. The identification of structural damage is an inverse problem that is also ill-posed in the presence of noise. When dealing with large and complex structures, accuracy and convergence will become important issues and the efficiency of the method will be degraded. More response measurements are needed which means more labour, installation difficulties, and expenses. As the number of unknowns increases, this problem will become more challenging. To address this problem, the substructure condition assessment of bridge structures is proposed in this project, a review of which is presented in section 2.6. A summary of this chapter is presented in section 2.7. The technique of substructure condition assessment has mainly been studied for other structures such as beams and buildings. This project is believed to be the first essential study on condition assessment of bridge structures under moving vehicles using substructure identification methods.

`

2.2. Excitations for condition assessment of bridge structures

Bridge condition assessment and damage detection processes have attracted increasing interest from the research community. Aging, environmental and excess loads submit bridges to continuous degradation, and now that many of them are or will soon be approaching the end of their design lives there is an increasing danger of incidents developing. Instances of sudden bridge collapses are on the rise worldwide. Early detection and warning of a bridge becoming unsafe can help in saving human lives and reducing any economic impact (Zhu, et al. 2014) .

Structural condition assessment of bridge structures based on vibration measurements has attracted the interest of many researchers for over three decades (Brownjohn 2007; Carden & Fanning 2004; Doebling, S. W., Farrar & Prime 1998; Fan & Qiao 2011).

There are mainly two kinds of dynamic vibration tests: the ambient vibration test (AVT) and the forced vibration test (FVT), both of which are reliable methods to obtain the modal parameters of bridge structures. The sources of excitation in AVT are mainly the vehicles traveling through or underneath the bridge, wind, and ground support excitations, which are widely distributed and uncontrollable. The excitation source in FVT is a controlled input force applied on one point of the bridge structure by an exciter, which is larger than the ambient forces. AVT permits the measurements of structural vibration under its operational condition, however FVT requires shutting down traffic during the tests, making use of heavy and expensive equipment, as well as requiring high supplies of power (Chen, et al. 2014) . As an example, shakers anchored to the bridge deck for forced vibration tests can be seen in Figure 2-1.

Figure 2-1: Shakers anchored to the bridge deck for forced vibration test (Chen *et al*. 2014)

`

There has been some research conducted on the feasibility aspects of AVT and FVT. Green (1995) concluded that shakers are appropriate for short to medium span bridges (spans < 100 m), and AVT works better for medium to long-span bridges (spans > 70 m). Farrar et al. (1999) believes that there is not a consensus on the feasibility of one particular method, however, it seems that AVT is the most proper exciter for large bridge structures as well as for small bridges where traffic cannot be shut down during the test. Womack and Halling (1999) employed an eccentric mass shaker as an excitation source of two bridges in their study. They concluded that there should be a sufficient number of sensors to completely capture bridge motion. At the end spans of the nine-span bridge, it was difficult to pick up the bridge response over the noise.

Farrar et al. (2000) observed that excitation from impact hammer tests provided more reliable results than that from ambient sources in obtaining natural frequencies. On the other hand, Peeters et al. (2001) reported that ambient excitation and excitation from a shaker or drop weight impact all provided satisfactory results. Later, field studies were carried out on the 11-span Nelson St off-Ramp Bridge to experimentally investigate the feasibility and effectiveness of AVT and FVT. Based on the collected data from AVT and FVT, the identified frequencies, damping ratios and mode shapes of the bridge were compared. Satisfactory results were obtained by AVT through weak excitation levels (Chen, et al. 2014) .

Choosing the appropriate testing method for a particular bridge structure depends on many factors, such as bridge length, its structural type, and operational condition, and as such it is very important to choose the most proper one to obtain reliable results.

Choosing a moving vehicle as a source of excitation has been an active field of research over the past decade (Chen, S, Xia & Zhang 2007; González & Hester 2013; Hester & González 2012; Law, S. S. & Zhu 2009; Malekjafarian, Abdollah, McGetrick & OBrien 2015; Siringoringo & Fujino 2012; Sun, Z, Zhang & Tong 2013; Zhu, Xiang et al. 2019; Zhu, XQ & Law 2015). This is due to advantages such as no traffic interruption, capturing the dynamic response of the bridge under its operational condition, continuous monitoring and having no need for any especial experimental arrangements. A literature review on condition assessment of bridge structure under moving vehicles is presented in the next section.

`

2.3. Condition assessment of bridge structures under moving vehicles

Moving load based damage detection methods have attracted significant attention recently, as they have several advantages over other damage detection methods (He, Ren & Zhu 2017; Li, Jie & Zhao 2006; Link & Weiland 2009; Ouyang 2011; Zhu, Xiang et al. 2019; Zhu, XQ & Law 2015).

1) There are no traffic interruptions
2) Analysis is performed under operational environment conditions
3) Analysis is performed continuously
4) There is no need for exceptional experimental arrangements or techniques
5) The number of sensors and amount of expense is reduced

There is the ability for excitation of structural vibrations with a large amplitude and high signal-to-noise ratio

Structural Health Monitoring (SHM) methods of bridges under moving vehicles can generally be divided into three categories: those based on bridge responses (direct bridge health monitoring), those based on vehicle responses (indirect bridge health monitoring), and those which are based on both vehicle and bridge responses (Zhu, XQ & Law 2015). In direct bridge health monitoring, sensors are mainly instrumented on the bridge and the response measurements on the bridge are used to assess its structural condition. In indirect bridge health monitoring, sensors are installed only on the vehicle and the instrumented vehicle serves as both the exciter and moving sensor. These moving sensors collect data at different locations of the bridge structure, a result which is considered equivalent to a dense array of sensors.

Each of these approaches has its own advantages and disadvantages. To overcome the potential problems, a combination of both approaches can be used. The instrumented vehicles can be used to perform a quick scan of the bridge, and then more accurate damage detection of the suspected regions can be performed by collecting responses directly from the bridge deck, which is more sensitive to damage (Zhu & Law 2015) . Improving the accuracy as well as cost and computation efficiency of direct bridge health monitoring is the focus of this study. Indirect bridge health monitoring methods are reviewed in this section and direct health monitoring methods are reviewed in section 2.4, since this approach is the focus of this research.

2.3.1. Indirect bridge health monitoring

For indirect bridge health monitoring, sensors are installed only on the vehicle and the instrumented vehicle serves as both the exciter and moving sensor. The vehicle then collects data at different locations of the bridge structure, with the vehicle acting as a dense array of

`

sensors. It is obvious that this way, many bridges can be monitored in parallel. The process is economical, needing fewer sensors, and less experimental arrangements.

A literature review has been done on indirect bridge health monitoring by Malekjafarian et al. (2015). The advantages and disadvantages of different methods have been discussed and the challenges of indirect bridge health monitoring have been clarified for future work.

This method was first introduced by Yang et al. (2004), to attain the bridge frequencies from sensors installed on a vehicle. They performed a theoretical study on a simply supported bridge and the vehicle was modelled by a sprung mass. The feasibility of this method was verified by performing a test upon a field bridge with use of a two-wheel cart towed by a light truck (Lin & Yang 2005) . Later, more research was carried out to explore this method further and to provide experimental and fieldwork verification (Chan et al. 2013; Yang et al. 2013; Yang & Chen 2016). There was also some research conducted to consider the effects of bridge excitation levels (Kobayashi et al. 2008), as well as vehicle speed and acceleration (Yang & Chang 2009). The challenges arising with indirect bridge health monitoring based on natural frequency are as follows (Malekjafarian et al. 2015):

a) The effects of the road profile on vehicle responses, resulting in a reduction of the visibility of the bridge frequency;

b) Since bridge frequency can also change under a moving vehicle, it will become difficult to determine whether the change has resulted from the damage or vehicle movement.

There are also a few methods for indirect identification of bridge damping (Curadelli et al. 2008; Gonzalez 2012; Kim et al. 2014; McGetrick 2010; Modena 1999). Although these methods have been validated theoretically and experimentally, the potential application for bridge health monitoring and quantifying damping in practice is still difficult due to its complexity. Therefore, it is believed that focusing on other bridge parameters for bridge health monitoring is more reasonable (Malekjafarian et al. 2015) .

Identifying bridge mode shapes is of high importance since it can provide beneficial information about bridge condition. Discrepancies in mode shapes can be identified at points on a bridge which are related to locations of damage (Malekjafarian et al. 2015). The first identified attempt to study this can be attributed to Zhang et al. (2012). This study considered the moving vehicle crossing over the bridge while equipped with an accelerometer and shaker to artificially control the applied force. The study's method was confirmed for vehicle speeds of less than 18 km/h.

Yang et al. (2014) proposed a method based on obtaining instantaneous amplitudes-from the Hilbert transform of the band-pass filtered response of the vehicle. Similar to Zhang et al.

`

(2012), the accuracy of the method was confirmed with low vehicle speeds, 7.2, 14.4, and 28.8 km/h, and it should be noted that the accuracy reduced with an increase of vehicle speed. This method is very sensitive to road surface roughness. The influence of the measurement noise has not been considered in this method and an experimental study has been suggested for further investigation of findings. There are studies for mode shape identification (Malekjafarian et al. 2014; Oshima et al. 2014), some common challenges of which have been mentioned below for future studies (Malekjafarian et al. 2015).

a) It is sensitive to measurement noise;

b) There is low accuracy at high vehicle speeds;

c) More experimental studies are required.

Most of the above-mentioned studies are for extracting modal parameters of a bridge and they are not aimed towards structural damage detection. Damage detection of bridges does not explicitly need to identify bridge dynamic properties. Many indirect damage identification methods have been proposed, which are mainly based on moving force, operating deflection shape, displacement response, modal strain energy, and transmissibility.

In one of the earliest attempts, Bu et al. (2006) presented a damage identification method based on dynamic response sensitivity analysis. In this research, the damage index was defined in terms of bridge stiffness reduction. The effects of measurement noise, road surface roughness, and model errors were studied. It was concluded that identified results are acceptable and they are not sensitive to the uncertainties studied.

Kim et al. (2008) proposed a damage identification method for bridges under moving vehicles where the element stiffness index was adopted as the indicator of damage. Least-squares approximation, as a special case of the pseudo-inverse, was employed to solve the problem. The most important result of this study was that the vehicle speed did not greatly affect the damage identification results. However, other uncertainties, such as measurement noise, temperature variations, vehicle properties, and modelling uncertainties were not considered in this study.

Miyamoto and Yabe (2011, 2012) suggested a damage identification method for short to medium span reinforced/prestressed concrete bridges using a public bus. Sensitivity analysis and the substructure method were used in this study. In the field experiment it was found out that the method is feasible as long as the same bus is used for all measurements. This method is successful simply at judging the existence of damage in a bridge. They extended their study to consider more parameters such as weather, number of bus occupants, and vehicle speed (Yabe et al. 2013).

`

Li and Au (2014a) presented a damage detection method using a moving vehicle based on modal strain energy and the genetic algorithm. This method can determine the location of the damage by calculating a damage indicator from vehicle responses. This method is sensitive to the road profile and measurement noise (Li et al. 2014b) . Zhu et al. (2014) have proposed an innovative approach for indirect health monitoring of bridges under moving vehicles using equipped moving vehicles. By measuring the dynamic responses of the vehicle, extracted from sensors installed on the vehicle axles and body, they obtained the interaction force between the vehicle and bridge. Results of simulations conducted indicated that interaction forces were more sensitive to any local damage than the acceleration responses from the vehicle's axle or body. It should also be noted that further studies are needed to consider uncertainties related to the bridge-vehicle interaction system.

Kong et al. (2015) suggested a damage identification method using the vehicle transmissibility of the vehicle-bridge coupled system. Different damage indicators were used and the influences of several factors were studied, such as sensor location, road roughness, and vehicle speeds. In real world terms, this method is suitable for vehicle speeds between 36 km/h and 72 km/h, and it is sensitive to road roughness and low-frequency bridge responses.

There are also indirect health monitoring methods of damage detection based on wavelet transform. Nguyen and Tran (2010) identified the existence of damage and determined its location on a bridge by applying a Symlet wavelet transform to the displacement response of a moving vehicle. McGetrick and Kim (2013, 2014) applied Continuous Wavelet Transform (CWT) to the dynamic response of a passing vehicle over a bridge to identify damage and its location. The advantage of this method is that the vehicle needs only to spend a short length of time on the bridge. However, results indicate that the accuracy of this method is reduced at high speeds, the method relies on local anomalies in the signal, and the results can be compromised by edge effects (Malekjafarian et al. 2015) .

2.4. Direct bridge health monitoring

In direct bridge health monitoring, sensors are mainly instrumented on the bridge and the response measurements on the bridge are used to assess the structural condition. This type of approach can be divided into three categories: Those with unknown traffic excitations, those with known moving loads, and those based on identifying moving loads and bridge damage iteratively. A review on the first two groups is presented in this section, and since the focus of this thesis is on the third category, a review on simultaneous identification of moving loads and structural parameters is presented in section 2.5.

`

Mazurek and Dewolf (1990) conducted an experimental study on a two-span aluminium plate-girder bridge subject to light vehicular excitation. Structural damage was simulated by a release of supports and insertion of cracks. The aim was to investigate the feasibility of vibrational signature analysis in damage detection in highway bridges. Results indicated that the method is comparable with traditional methods for resonant frequencies and mode shapes, which are not sensitive to road roughness and vehicle velocity. Piombo et al. (2000) obtained the modal parameters of a bridge subjected to traffic excitation using acceleration data as ambient vibration. In this method, the wavelet estimation technique was used directly on transient data for the first time. The capability of this method was firstly inspected by analysing an analytical problem before implementing it on a real bridge, which was a simply supported bridge located in northern Italy. The analytical bridge was modelled as a three-span supported plate and the moving vehicle was modelled as a seven degrees-of-freedom system.

A damage detection method of a bridge structure was also proposed by Lee et al. (2002) using the excitation caused by existing traffic loading. In this method, the acceleration of the bridge was collected to estimate modal parameters which were then used as inputs for a neural network to detect the damage. This method was successful in finding the location and severity of the damage. Obrien et al. (2015) proposed a technique based on moving load identification and found out that moving load time history is more sensitive than direct displacement measurement to bridge damage.

In all these methods, bridge structural identification is based on measured responses of the bridge deck only, and traffic loading excitation data is unknown. There are also researches that have made use of traffic excitation data other than bridge responses to identify structural parameters. Chen et al. (2006a; 2006b; 2009) proposed a video-assisted project to get help from videos to glean basic data on vehicles passing the bridge. The basic data recorded the vehicle type, its speed and arrival time. Then, the data was synchronized with acceleration data from accelerometers, and structural parameters were identified offline. The method was verified by a short-span field bridge experiment.

Later, integrated structural health monitoring strategies, by which the image and sensor data from the bridge were integrated into a single computer, were introduced (Fraser, et al. 2010; Zaurin & Catbas 2011). Zaurin and Catbas (2011) used the unit influence line and Catbas et al. (2012) used the load rating of bridges as an index for monitoring bridge behaviour. Chen et al. (2015) proposed a method based on the stress line influence to detect the damage location in long-span suspension bridges. This method was verified by a case study on the Tsing Ma suspension bridge.

`

There are a lot of damage detection methods based on change in the natural frequencies, mode shapes or measured modal flexibility (Cawley & Adams 1979; Doebling, S.W. et al. 1996; Lim 1991; Narkis 1994; Pandey & Biswas 1994; Pandey, Biswas & Samman 1991; Ratcliffe 1997; Rizos, Aspragathos & Dimarogonas 1990; Wu, D & Law 2004). There are, however, many difficulties with the methods based on modal properties. Modal frequency methods can only detect large areas of damage and are easily affected by the surrounding environment or outside factors. Additionally, though vibrational modal shapes can provide more information on damage perceived, measurements taken are often incomplete and errors can occur (Li, J. , Hao & Lo 2015; Maia, Silva & Ribeiro 2001; Shimoi et al. 2015; Yan & Ren 2012; Zhu, Xiang et al. 2019).

Majumder and Manohar (2003) presented a time-domain method to detect damage in bridge structures. To verify the method, a beam structure subjected to the moving oscillator vibration was studied. The finite element model of the undamaged beam and structural and dynamic properties of the vehicle were considered to be known and vehicle-bridge interaction was also considered. Uncertainties, such as measurement noise, bridge deck unevenness, and incompleteness of measured data were considered in this method.

Nasrellah et al. (2010) studied the same problem based on the dynamic state estimation method, that employed particle filtering algorithms. Lu et al. (2009) suggested a local damage identification method based on the dynamic responses of the vehicle-bridge system. The finite element model updating based on response sensitivity was used to identify the damage of the bridge subjected to moving forces. This method was extended by Zhan et al. (2011) for bridges subjected to trains. In 2013, a crack identification method for beam-type structures under a moving vehicle was presented. In this method, an objective function based on the difference of the dynamic responses of the damaged beam and the mathematical model of the beam was defined and the optimisation problem solved by particle swarm optimisation (PSO) (Gokdag 2013) .

In all of the above methods, the moving load does not need to be measured or it is assumed to be known. However, the simultaneous identification of moving load and structural damage is of high importance since there is a strong bond between the input excitation of the structure and its condition. Road roughness affects the dynamic of moving vehicles, higher roughness intensifies the excitation which increases damage potential. Therefore, it is important to identify moving load and structural parameters iteratively considering uncertainties such as road roughness. This field has not been explored enough by researchers. A review of existing achievements is presented in the next section.

`

2.5. Simultaneous identification of moving loads and structural parameters

As mentioned in previous sections, the third category of direct bridge health monitoring is to identify structural parameters simultaneously with the moving load. A Moving vehicle is one type of excitation source, the dynamic interaction force between vehicle and road surface can be greatly affected by road surface roughness and vice versa. Considering this fact, repeated loading or overloading can degrade bridge structures. Therefore, it is of high importance to identify both moving loads and structural parameters simultaneously, considering road roughness and other uncertainties. Although there is an extensive attempt to identify moving loads with known structural parameters, or to identify structural parameters while knowing the moving loads, it seems their simultaneous identification has not been studied enough. Here, a brief review is performed on moving load identification based on known structural parameters and then a review on simultaneous identification of moving loads and structural parameters is presented.

Since direct measurement of the dynamic moving load is expensive, difficult and subject to errors, indirect identification methods from measured responses are desired, as they are easier and cheaper to carry out. Weigh-in-Motion (WIM) techniques have been developed to estimate the equivalent static axle loads, however, their results are reliable only if the road surface is smooth and the vehicle moves at low speeds (Gonz et al. 2012; Ojio et al. 2015; Wang, H et al. 2017). Unfavourable road roughness together with the dynamic effect of moving vehicles create interaction forces that can increase bridge damage two or four times compared to that from static axle forces. As a result, different methods have been proposed to identify moving loads consisting of both static and dynamic loads.

Moving load identification has been studied extensively in the past two decades and comprehensive literature reviews can be found in this field (Chan, THT, Yu & Law 2000; Chan, THT et al. 2001; Daniel & Kortiš 2017; Law, S. S. & Zhu 2011; Yu & Chan 2007; Zhu, XQ & Law 2016). Indirect identification techniques can be grouped into four groups, namely: the Time-Domain Method (TDM), the Frequency-Time Domain Method (FTDM), Interpretive Method I (IMI) and Interpretive Method II (IMII) (Law et al. 1997, Law et al. 1999, Chan and O'Connor 1990, Chan et al. 1999). In 2001, comparative studies carried out to numerically and experimentally explore the applicability of these four methods.

Chan et al. (2000) achieved a moving force identification by conducting field measurements on a pre-stressed concrete bridge. The gross vehicle weight and dynamic axle forces were determined with an acceptable margin of error. Zhu and Law (2001b) developed a generalized orthogonal function approximation based on the finite element formulation to

`

obtain the derivatives of the bridge modal responses. The moving loads were identified using the regularized least-squares method in the time-domain. The method was verified by numerical and experimental studies.

Moving load identification is an inverse problem and the ill-conditioning of the inverse problem can significantly affect the identification results. To improve the accuracy of moving load identification and provide bounds on the solution, Zhu and Law (2002) presented a time-domain method using a regularization technique. They concluded by numerical studies that a higher sampling frequency is needed when acceleration responses are used instead of strains. A relatively accurate model is required in this method. To address this problem, other regularization methods (González, Rowley & OBrien 2008; Law, S. S. et al. 2001; Law, S. S. & Fang 2001; Zhu, XQ & Law 2006) and techniques based on the Singular Value Decomposition (SVD) (Yu & Chan 2003) have been also used. Asnachinda et al. proposed an updated static component technique by which it is easier to select optimal regularization and verified the method experimentally in the laboratory (Asnachinda, Pinkaew & Laman 2008).

Deng and Cai in 2010 presented a method for dynamic load identification and verified it with computational simulations and field tests (Deng & Cai 2010; Deng & Cai 2011). Random vibration analysis of dynamic vehicle-bridge interaction considering road roughness was also studied (Lombaert & Conte Joel 2012). Wu and Law (2012) proposed a new stochastic moving load identification technique in which statistics of the time history of the moving force are identified from samples of the structural responses. This method is contrary to many approaches that treat the structure–load interaction problem as deterministic and is not sensitive to different levels of uncertainties.

A fully coupled method has been presented for reproducing road vehicle-bridge dynamic interaction (Oliva et al. 2013). It is based on finite element models. It is capable of considering geometric and material nonlinearities from both the vehicle and the structure, as well as simulating wheel-road separation. Furthermore, a force identification method in state space based on the Galerkin weak formulation has been proposed (Wang, T et al. 2015).

All these methods can identify forces or moving loads based on the known system parameters, such as the flexural stiffness of the bridge structure. In reality, unknown damages and unknown moving loads can exist together, influencing the response of the system. To address this problem, different algorithms have been developed using output only. The convergence of this problem is approved by Li and Chen (2003).

`

Hoshiya and Maruyama (1987) applied a weighted global iteration procedure to simultaneously identify moving and modal parameters of a simply supported beam. Extended Kalman filter was used in their method.

Zhu and Law (2007) presented a method based on displacement measurements to simultaneously identify moving loads and crack damage. They verified the method numerically via a 30 m simply supported beam for different levels of noise and road roughness. This study also attempted to verify the accuracy of identification in their method by examining the effect of the number of beam elements in the finite element model. Results showed that the use of orthogonal function expansion generated an insensitivity to measurement noise. As long as the sampling frequency is more than double the maximum frequency of interest of the responses excited by the moving load, this factor will not influence results of the method; the method is not sensitive to noise but it is sensitive to road roughness. Moving loads in all cases can be identified very well. This method has not been verified for a multiple span bridge or experimentally, and it requires a full-sensor placement. Furthermore, computation time has not been discussed. This method also has been extended by Law and Li (2010) and numerically verified by a three-span prestressed concrete box-section bridge under the action of a two-axle three-dimensional vehicle. The results of this comprehensive study have indicated that a sufficient number of sensors is needed as well as the accuracy of identified moving loads can greatly affect the accuracy of damage detection.

Lu and Law (2007) proposed a method based on the sensitivity of dynamic response to simultaneously identify moving loads and damage. Sinusoidal and impulsive forces with known locations were studied. One or two accelerometers with short record duration proved sufficient for acceptable results. The method was verified numerically by a 20 m single-span and a 30 m two-span continuous concrete beams as well as experimentally by a 2 m simply supported steel beam. This method is insensitive to noise, and force is identified very well. Reconstructed acceleration matches very well with the measured acceleration smoothed by an orthogonal function. Numerical results show no false alarm in any other adjacent undamaged elements which usually happens in other exiting methods, however, in experimental results there was considerable false identification of damage in adjacent elements. Computation time was not discussed in this study. Zhang et al. (2010a, 2010b) presented a method based on the Virtual Distortion Method for simultaneous identification of moving mass and structural damage. In this method a couple of masses are moving on a flat bridge at constant speeds. The moving masses and bridge are collectively considered a unit system exposed to constant moving external loads of the gravities of the masses. Numerical results show that this method

`

is robust to noise and can be used both offline and online. In these studies, the vehicle model is not considered as an excitation source and the effect of road surface roughness is not considered.

Zhang et al. (2012) developed a virtual distortion based method to simultaneously identify the excitation and damage. Results were verified numerically by a frame and experimentally by a cantilever beam. The excitation source for this study was not a moving load and only damage parameters were treated as the optimization variables. Later, Zhang et al. (2013) presented a method for simultaneous identification of moving vehicles and bridge damage considering road surface roughness. It is mentioned that vehicle parameters such as mass, stiffness, and damping are easier to identify than moving vehicles. Therefore, the vehicle parameters and structural damage were treated as optimization variables in the study. The above-mentioned method was numerically verified by a 200 m long three-span bridge, and the robustness of the method for model error and measurement noise was tested. Effects of different uncertainties such as different levels of road roughness, vehicle speed, damage location and extension, as well as computation time were not discussed.

Sun and Betti (2014) presented a hybrid artificial bee colony strategy to simultaneously identify structural parameters and, when possible, dynamic input time histories from incomplete sets of acceleration measurements. The method has been numerically verified by three types of frames. In this method, the non-moving load is considered as an excitation source. Furthermore, it is highly sensitive to measurement noise.

Feng et al. (2015) proposed a method of utilising a limited number of sensors to simultaneously identify bridge structural parameters and vehicle axle loads via an iterative parametric optimization process. The study applied a Bayesian inference-based regularization approach in an attempt to solve the ill-posed least squares problem for the unknown vehicle axle loads. Yet while this method was numerically verified over different vehicle speeds and levels of noise, both for a simply supported bridge and a three-span continuous bridge, the effect of roughness was not directly considered and the method has since shown load identification errors over mid supports.

Abbasnia et.al. (2015) developed a sensitivity-based damage detection method referred to as Adjoint Variable Method (AVM) to simultaneously identify moving loads and structural damage. The effectiveness of the proposed method is numerically illustrated by a two-span continuous girder and a plate. Numerical studies show this method is able to effectively reduce the computational cost in comparison with other traditional sensitivity methods. The method is sensitive to noise greater than 1.4% and the effect of road roughness is not explored.

`

Obrien et al. (2015) proposed a method for damage detection based on moving force identification. A two-dimensional vehicle-bridge interaction model is used for numerical verification. Both strains and deflections have been studied as measured responses. Results indicate that strain measurements are effective only when the sensor is close to the damage zone. Furthermore, the method is sensitive to damage location and it can be identified well only if it is close to the centre of the beam.

Jayalakshmi et al. (2017) presented an approach to simultaneously identify structural parameters and non-moving dynamic forces and verified them numerically by use of three examples of a simply supported beam, a building, and a truss bridge. This approach is based on a newly developed dynamic hybrid adaptive firefly algorithm (DHAFA) and a modified version of Tikhonov regularization plus the explicit form of the Newmark-β method. There are many limitations to reaching acceptable results by this method such as:

1) Sensors should be available at the location of dynamic forces,

2) One input force-time history should be known,

3) The known load should be in the range of 0.6 times to 1.5 times of the unknown forces. In practice however, these assumptions are not so simple to apply. Wang et al. (Wang, C, Du & Jiang 2018) developed a method for simultaneous identification of the load and unknown parameters where the excitation source is non-moving.

In summary, it can be seen that most of the studies of simultaneous identification of damage and load are for non-moving loads, and those which are for structures under moving loads are not investigated comprehensively for different uncertainties or are not verified experimentally. Therefore, in this research work, simultaneous identification of moving load and structural damage considering uncertainties such as noise, road surface roughness, and the vehicle speed is carried out and verified by both numerical example and experimental tests.

2.6. Substructure techniques for condition assessment of structures

The main challenge in structural identification is to save money and time as well as attain reasonable accuracy for identified parameters. Furthermore, because structural identification is a kind of inverse problem, which is naturally ill-conditioned, convergence will become a big challenge as the number of unknown parameters increases. Hence, different methods have been suggested to reduce the number of unknowns, one of which is a substructure identification method.

Koh et al. (1991) proposed the application of substructure identification in civil engineering for the first time. A substructure approach was developed to obtain stiffness and

`

damping coefficients of structures in the time domain from some measured responses due to dynamic loading. The method of extended Kalman filter with a weighted global iteration algorithm was used. The method was shown to be able to improve the accuracy and convergence of the structural parameters significantly in comparison with the conventional one. Three numerical examples were studied including a shear building, a plain frame building, and a truss bridge.

Yun and Lee (1997) compared two substructural identification methods for local damage detection: a direct method using the time histories of the measured responses, and an indirect method using substructural stiffness assessment. The latter was shown to be more stable in cases with more complex geometries. An auto-regressive and moving average with stochastic input (ARMAX) model and the sequential prediction method were used in this study and two numerical studies were carried out on a shear building model and a truss bridge model. Yun and Bahng (2000) proposed a method to estimate the stiffness parameters of a large structural system using neural network-based substructural identification. Two numerical examples carried out on a two-span truss and multi-story frames proved the effectiveness of this method.

Furthermore, Koh et al. (2003) presented progressive structural identification (PSI) in a time domain and substructural identification with and without overlap (SSI), in which interface forces have to be calculated by having all interface measurements. In this method, the concept of the quasi-static displacement vector is used to calculate the interface forces more easily and therefore fewer response measurements are required in comparison with the SSI method originally proposed by Koh et al. (1991). Although the proposed method can identify all structural parameters simultaneously, it involves some inaccuracies, since substructures are identified dependently to the remainder of the structure. To improve it, Trinh et al. (2012) presented an improved substructural identification method combined with multi-feature genetic algorithm (GA) to identify all structural parameters of large-scale structures. In this method, interface acceleration measurements are used directly, without estimating, to study the interaction effects for substructures. The method has been verified by both numerical and experimental studies on a 100-story shear building and a 10-story small-scale steel frame, respectively.

All the mentioned substructure damage detection approaches require interface response measurements; however, it is sometimes impossible to measure the interface responses, especially when it comes to rotational responses. Therefore, some researchers reconstructed these interface forces based on the frequency function or the transmissibility formulation. Koh et al. (2003) presented a method based on receptance theory in the frequency domain, by which

`

interface forces are eliminated by using enough response measurements in the substructure concerned and the genetic algorithm is used as an optimization tool. Two different beams and a structure with 50 DOFs are studied as numerical examples, showing the efficiency of this method.

Tee et al. (2009) developed a substructural identification strategy with incomplete measurements using the concept of model condensation. Force identification is formulated in state space and the damage is simulated by a reduction in structural stiffness. It has been verified numerically by a fairly large structural system with 50 DOFs and experimentally using an eight-story frame subject to non-moving loads of shaker and impulse hammer excitation. Law et al (2010) presented a method of damage detection using coupling forces between substructures under support excitation. Identification equations are formulated in state space. The method is verified by a numerical nine-bay three-dimensional truss structure.

Law and Yong (2011) studied two substructural damage detection methods in time domain based on the state space method and iterative updating model. In one of the methods, the FEM of a whole structure is available to identify external forces, while in another one only the FEM of a target substructure is available and interface forces, as well as external forces, are all taken as excitations and they are identified in state space. After identifying the loads, a damage identification method is then applied to detect damage in the target substructure. The method is numerically verified by a truss structure under a non-moving load. This method is sensitive to noise in load identification which will increase by the number of unknown external forces, leading to errors in damage detection. However, damage location and extent can still be fairly identified.

Trinh and Koh (2012) presented a substructure condition assessment based on a genetic algorithm. It has two significant advantages in comparison with previously existing methods, namely the direct use of acceleration measurements to consider interaction forces between substructures, and the use of an improved identification method based on multi-feature GA. Stiffness, damping, and mass have been simultaneously identified. The method has been verified numerically by a 100-story shear building and experimentally by a 10-story small-scale frame. Force is created by a shaker at a fixed location. The results of the proposed method are compared with the traditional method where the whole structure is assessed. Results indicate that the proposed method has improved accuracy significantly, however, there are still considerable errors in some cases.

Li et al. (2012) proposed a substructure condition assessment in the frequency domain based on the response reconstruction method. They verified their method numerically and

`

experimentally by use of a frame. The study considers excitation from a general force at the specific location. The finite element model of the intact substructure is needed in this method, while information on the remaining structure or interface nodes is not needed. There are some damage identification errors even when there is not any noise which may root in forward response reconstruction in the frequency domain. Studies show that the response reconstruction technique in the wavelet domain is more accurate than frequency domain and sampling duration will cause fewer errors.

Li and Law (2012b) proposed a substructure condition assessment method based on the response reconstruction method using the unit impulse response function in the wavelet domain. The information of responses and forces at interface nodes are not required, and only the FEM of the intact substructure and the acceleration responses of the damaged substructure are needed. They verified their method numerically by a 30 m simply supported box-section bridge deck structure subject to an earthquake. This numerical example included 60 flat shell elements and 396 DOFs in total. Their method is able to effectively identify damage at 10% noise, however it is not experimentally verified. Li and Law (2012a) also developed a substructure damage identification method based on the dynamic response reconstruction technique for a structure under moving vehicles. They verified their method using the same bridge under a moving load. Under moving load excitation, the method can identify simulated damages at 5% noise, however, several false positives exist originating from model condensation in the forward response reconstruction or smearing effect which will increase by noise. The method is also sensitive to sensor placement, and is not experimentally verified.

Zhu et al. (2013) developed a method to simultaneously identify damage and moving loads by a substructure study. Their method is based on the response sensitivity with respect to structural parameters and external forces. The equivalent external forces are represented by a Chebyshev Polynomial. They verified their method numerically by a 3-span frame and a simply supported beam under a moving load. They have studied limited substructure cases without considering uncertainties such as road roughness and speed as well as the dynamic behaviour of a more realistic vehicle. The method is fairly good to identify damage however it is sensitive to noise when it comes to moving load identification which may originate from the sensitivity of the state-space method to discretization or sampling rate.

Law et al. (2014) carried out an investigation on parallel decentralized damage detection of a structure based on a wavelet domain. The structure is divided into several substructures and non-moving forces, as well as the structural damage, are identified iteratively. It is shown that noise can significantly affect the accuracy of identified loads though this method is quite

`

promising for damage detection. This method was numerically verified by a simply supported plane truss structure.

Li and Hao (2014) proposed a substructural condition assessment based on wavelet-domain response reconstruction for structures under a non-moving load and verified it experimentally with a 7-story plane frame structure. Liu et al. (2014) developed and verified the explicit form of the Newmark-β method for a force identification of a full structure under a non-moving load, which is shown to be superior to the state space method. Liu et al. (2015) showed this superiority for interface force identification of substructures while the structure is under non-moving load. The method's robustness was checked at 5% noise and was numerically verified via a plane truss structure.

Generally, most of the time domain methods are developed and verified for structures under non-moving loads and they are commonly formulated by state space methods suffering from the errors of discretization and sampling ratio. Furthermore, substructure condition assessment of bridges under moving vehicles considering uncertainties such as road surface roughness and vehicle speed needs more investigation. Here, the explicit form of the Newmark-β method is developed for moving load identification and damage identification, either for a full structure or for a substructure. The effect of uncertainties such as road roughness, vehicle speed, and noise are also investigated.

2.7. Summary

Direct bridge health monitoring approaches are useful in damage detection of bridge structures; however, the method suffers from a disadvantage with the need for a large number of sensors, their installation, expenses and other factors.

Indirect bridge health monitoring has been successful in removing these challenges by using a moving vehicle as both the exciter and the sensor, but it is shown that vehicle acceleration responses are less sensitive to damage in the bridge in comparison with direct acceleration responses measured from the bridge deck. Some of the problems with indirect bridge health monitoring methods are as follows:

1- The accuracy of methods based on natural frequency, like a damage indicator, is reduced at high speeds and can be affected by environmental and operational conditions. This factor is not sensitive enough to damage and they are usually suitable for level one of structural health monitoring.

`

2- The accuracy of methods based on damping, like a damage indicator, can strongly be affected by environmental factors, such as temperature. Furthermore, this factor is very complex and difficult to measure in practice.
3- Although mode shapes have been shown to have good potential for condition assessment of bridges due to their sensitivity to damage, this is still a challenge. Using tapping vehicles is very expensive and it is accurate only for the first mode and at low speeds. Other methods, which do not use tapping vehicles, are of poor accuracy unless road roughness and measurement noise are ignored.
4- Wavelet-based methods of condition assessment are useful for all levels of condition assessment, but their accuracy is reduced at high speeds. Results are also not accurate in assessment of the beginning and the end of a bridge because of edge effects.
5- In most of studies, road roughness, measurement noise, and inherent uncertainties in the vehicle-bridge system are not considered properly.

To overcome the problems with direct and indirect health monitoring approaches, it is necessary to develop a technique to use measurements from the bridge deck, while using a lesser number of sensors, and reducing unknown parameters. To achieve this, the substructure condition assessment of bridge structures is proposed in this project. In this method, a large and complex bridge structure can be divided into smaller substructures for independent studies. It has been proved to be effective in damage detection of civil structures and is more sensitive to damage than equivalent global methods (DeVore 2013). The advantages of substructure condition assessment of structures are as follows:

1) There will be a lower number of degrees of freedom (DOFs) and unknown parameters using substructure identification, resulting in reducing the number of sensors which have to be installed.

2) The computation effort will be reduced significantly, and computation convergence will be achieved more easily.
3) Since it is difficult to precisely simulate the boundary conditions, material, and physical parameters, especially for large-scale bridge structures, this method will aid in increasing accuracy by reducing uncertainties.

With consideration of the above three advantages, it seems beneficial to extend the substructure approach into bridge structures. This approach has mainly been studied previously for other structures such as beams and buildings. This project is believed to be the first essential

`

study on condition assessment of bridge structures under moving vehicles using substructure identification methods.

`

`

Chapter 3. Moving load identification using the explicit form of the Newmark-β method

3.1. Introduction

In this chapter, the explicit form of the Newmark-β method is applied to identify moving loads passing through the bridge, considering road roughness. Response measurements are simulated through a dynamic analysis of the vehicle-bridge interaction (VBI) system. The general form of the explicit form of the Newmark-β method is generated to perform dynamic analysis of the vehicle-bridge interaction (VBI) system. The half-car model vehicle, with four degrees of freedom, is adopted in this study and the generalized Tikhonov Regularization method is used to provide bounds on the solution.

The dynamic of the vehicle-bridge interaction system is presented in section 3.2. In this section, equations regarding motion of the vehicle, bridge and vehicle-bridge coupled models are described. In section 3.3, the explicit form of the Newmark-β method is developed for the VBI system as well as for moving load identification. Furthermore, the generalized Tikhonov Regularization method is presented in this section. In sections 3.4 and 3.5, the method is verified by single-span simply supported and multi-span continuous bridges. The effects of sensor placement, measurement noise, vehicle speed, and road surface roughness are investigated in this section. Conclusions derived in this chapter can be found in section 3.6.

3.2. Dynamics of the vehicle-bridge interaction system

3.2.1. Road surface roughness

Road surface roughness distinctly affects the dynamic responses of both the bridge and vehicles. The ISO 8608 classifies road profiles from A to E according to their degree of roughness. In agreement with the ISO road roughness surface classification, a road profile can be calculated by the inverse Fourier transform of the road profile spectrum as follows (Agostinacchio, Ciampa & Olita 2014):

$$r(x) = \sum_{i=1}^{N} \sqrt{\Delta n}\,.\,2^{k}.\,10^{-3}.\,(\frac{n_0}{i.\Delta n})\cos\,(2\pi.\,i.\,\Delta n.\,x + \phi_i) \qquad 3\text{-}1$$

where x is a variable from 0 to L, L is the length of the bridge; $\Delta n = 1/L$; N is the number of data points which is equal to $L/B = T \times Sampling\ Frequency$, B is the sampling interval and T is the total time that the vehicle needs to pass the bridge; k is a constant integer increasing from 3 to 9, corresponding to the profiles from class A (very good surface) to class H (very poor surface) (See Table 3-1); $n_0 = 0.1\ \ cycles/m$; ϕ_i random phase angle distributed

`

uniformly between 0 and 2π. Randomly generated profiles can be seen in Figure 3-1 (Agostinacchio, Ciampa & Olita 2014).

A MATLAB code has been created to generate the surface roughness profile. It is noteworthy that since the code uses a random function to generate ϕ_i, running it multiple times will not result in the same road profiles. The Power Spectral Density (PSD) of road vertical displacement, $G_d(n_0)$, describes the road profile (see Table 3-2) the rougher the road, the higher the PSD value. Road profiles generated for a specific class have the same properties and similar PSDs. Reproducing the PSD from the generated road profile ensures the road profiles generated will match ISO 8606 classification. Figure 3-1 shows the simulated road profiles and their PSD. According to ISO 8606, the report shall include the displacement PSD versus spatial frequency, both on algorithmic axes.

In reality, it is dangerous to drive at high speeds on a road classified as level "C". Considering ride comfort and safety, the recommended maximum vehicle velocity for each level of road roughness is listed in Table 3-3 (Múčka 2018). In this paper, the results have been determined and tabulated considering this point.

Table 3-1: k values for ISO road roughness classification (Agostinacchio, Ciampa & Olita 2014)

Road Class		k
the upper limit	lower limit	
A	B	3
B	C	4
C	D	5
D	E	6
E	F	7
F	G	8
G	H	9

`

Table 3-2: ISO 8608 values of $G_d(n_0)$

Road class	$G_d(n_0)$ (*10^{-6} m^3) (n_0=0.1 cycles/m)	
	Lower limit	Upper limit
A	-	2^5
B	2^5	2^7
C	2^7	2^9

Table 3-3: Recommended maximum vehicle velocity as a function of ISO 8608 road classes

ISO 8608 road class the upper limit (*10^{-6} m^3)	A 32	B 128	C 512
V_{max} (m/s) for ride comfort threshold value, a_{2w}=1.2 m/s^2 (very uncomfortable)	>27	>27	~8.6
V_{max} (m/s) for ride safety threshold value, DLC=0.3 (very high)	>27	>27	~16

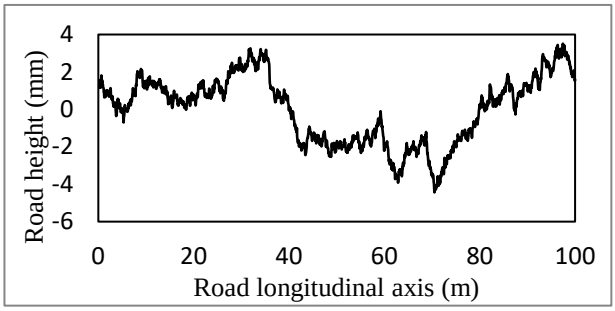

(a)Road profile-Class A

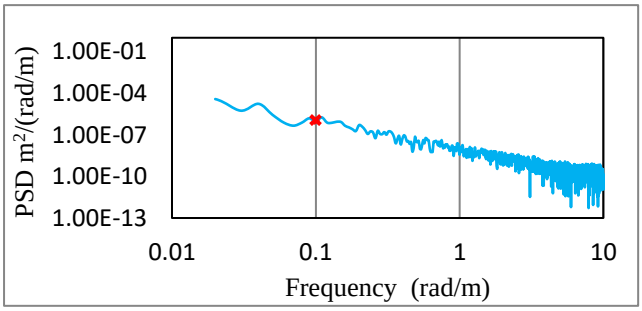

(b) PSD of road profile- Class A

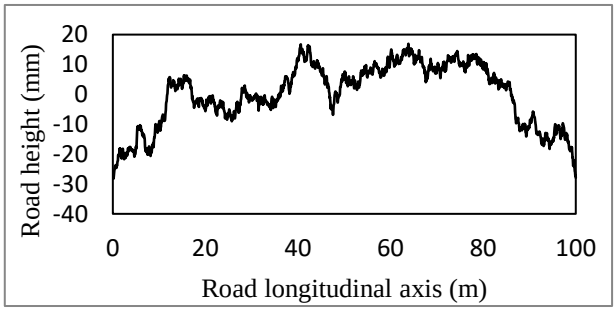

(c) Road profile-Class B

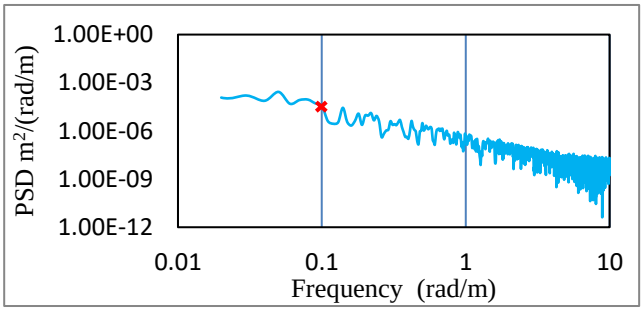

(d) PSD of road profile- Class B

Figure 3-1: Randomly generated road profiles and their spectra for classes A, B, and C

`

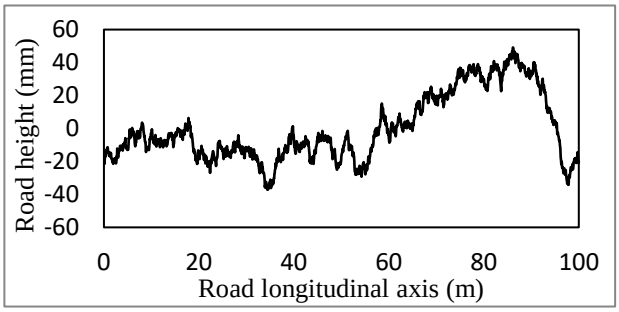

(e) Road profile-Class C

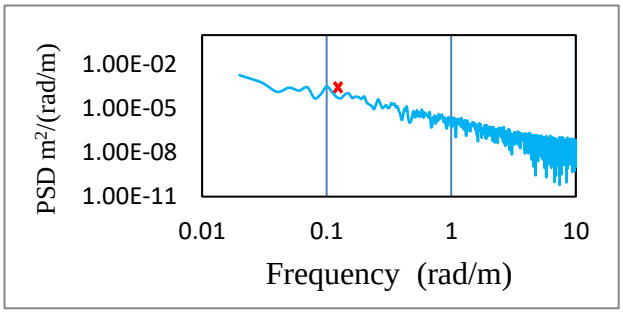

(f) PSD of road profile- Class C

Figure 3-1(continue): Randomly generated road profiles and their spectra for classes A, B, and C

3.2.2. Vehicle model

As shown in Figure 3-2, the vehicle–bridge interaction (VBI) system is modelled by a simply-supported or continuous bridge subject to a moving vehicle (Ferdek & Łuczko 2016), which is represented by a four-degree-of-freedom system. Here, m_v and I_v are the mass and the pitch moment of inertia of the vehicle body, respectively; m_{wf} and m_{wr} are masses of the front and rear axles, respectively; k_{sf}, k_{sr}, c_{sf} and c_{sr} are the linear suspension stiffness and the viscous damping parameters of the front and rear axles, respectively; k_{wf}, k_{wr}, c_{wf} and c_{wr} are the linear tire stiffness and the viscous damping parameters, respectively; l_f and l_r are the axle distances with respect to the gravity centre of the vehicle body; ρ is the mass per unit length of the bridge; EI is the flexural stiffness of the bridge, a product of Young's modulus E and the moment of inertia I; and y_{Bf} , y_{Br} , r_{Bf} and r_{Br} are the bridge displacements, and road profile displacements under the front and rear wheel moving on the bridge, respectively.

`

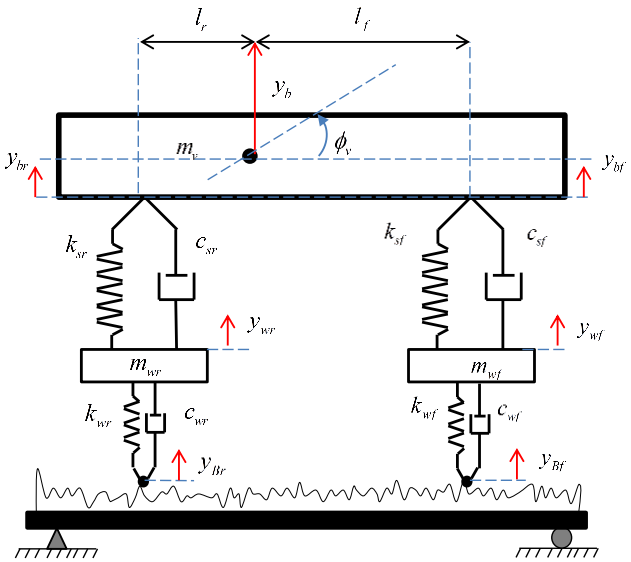

Figure 3-2: Vehicle-bridge interaction system

The equation of motion of the vehicle can be rewritten as (Ferdek & Łuczko 2016)

$$\begin{bmatrix} \frac{m_v l_r^2 + I_v}{l^2} & \frac{m_v l_f l_r - I_v}{l^2} & 0 & 0 \\ \frac{m_v l_f l_r - I_v}{l^2} & \frac{m_v l_f^2 + I_v}{l^2} & 0 & 0 \\ 0 & 0 & m_{wf} & 0 \\ 0 & 0 & 0 & m_{wr} \end{bmatrix} \begin{Bmatrix} \ddot{y}_{bf} \\ \ddot{y}_{br} \\ \ddot{y}_{wf} \\ \ddot{y}_{wr} \end{Bmatrix} + \begin{bmatrix} c_{vf} & 0 & -c_{vf} & 0 \\ 0 & c_{vr} & 0 & -c_{vr} \\ -c_{vf} & 0 & c_{wf} + c_{vf} & 0 \\ 0 & -c_{vr} & 0 & c_{wr} + c_{vr} \end{bmatrix} \begin{Bmatrix} \dot{y}_{bf} \\ \dot{y}_{br} \\ \dot{y}_{wf} \\ \dot{y}_{wr} \end{Bmatrix} + \tag{3-2}$$

$$\begin{bmatrix} k_{vf} & 0 & -k_{vf} & 0 \\ 0 & k_{vr} & 0 & -k_{vr} \\ -k_{vf} & 0 & k_{wf} + k_{vf} & 0 \\ 0 & -k_{vr} & 0 & k_{wr} + k_{vr} \end{bmatrix} \begin{Bmatrix} y_{bf} \\ y_{br} \\ y_{wf} \\ y_{wr} \end{Bmatrix} = \begin{Bmatrix} 0 \\ 0 \\ c_{wf}(\dot{y}_{Bf} + \dot{r}_{Bf}) + k_{wf}(y_{Bf} + r_{Bf}) \\ c_{wr}(\dot{y}_{Br} + \dot{r}_{Br}) + k_{wr}(y_{Br} + r_{Br}) \end{Bmatrix}$$

More details about how this formula is achieved can be found in the reference. Equation 3-2 can be simplified into Equation 3-3 and the vehicle frequency can be obtained by Equation 3-4.

$$\boldsymbol{M}_v \ddot{\boldsymbol{Y}}_v + \boldsymbol{C}_v \dot{\boldsymbol{Y}}_v + \boldsymbol{K}_v \boldsymbol{Y}_v = \boldsymbol{P}_v \tag{3-3}$$

Where

$$\boldsymbol{M}_v = \begin{bmatrix} \frac{m_v l_r^2 + I_v}{l^2} & \frac{m_v l_f l_r - I_v}{l^2} & 0 & 0 \\ \frac{m_v l_f l_r - I_v}{l^2} & \frac{m_v l_f^2 + I_v}{l^2} & 0 & 0 \\ 0 & 0 & m_{wf} & 0 \\ 0 & 0 & 0 & m_{wr} \end{bmatrix},$$

$$\boldsymbol{C}_v = \begin{bmatrix} c_{vf} & 0 & -c_{vf} & 0 \\ 0 & c_{vr} & 0 & -c_{vr} \\ -c_{vf} & 0 & c_{wf} + c_{vf} & 0 \\ 0 & -c_{vr} & 0 & c_{wr} + c_{vr} \end{bmatrix},$$

`

$$\boldsymbol{K}_v = \begin{bmatrix} k_{vf} & 0 & -k_{vf} & 0 \\ 0 & k_{vr} & 0 & -k_{vr} \\ -k_{vf} & 0 & k_{wf} + k_{vf} & 0 \\ 0 & -k_{vr} & 0 & k_{wr} + k_{vr} \end{bmatrix},$$

$$\boldsymbol{P}_v = \begin{Bmatrix} 0 \\ 0 \\ c_{wf}(\dot{y}_{Bf} + \dot{r}_{Bf}) + k_{wf}(y_{Bf} + r_{Bf}) \\ c_{wr}(\dot{y}_{Br} + \dot{r}_{Br}) + k_{wr}(y_{Br} + r_{Br}) \end{Bmatrix}, \text{ and } \boldsymbol{Y}_v = \begin{Bmatrix} y_{bf} \\ y_{br} \\ y_{wf} \\ y_{wr} \end{Bmatrix}$$

$$det(\boldsymbol{K}_v - \lambda \boldsymbol{M}_v) = 0 \qquad 3\text{-}4$$

where λ is an eigenvalue of $\boldsymbol{K}_v$ and $\boldsymbol{M}_v$.

3.2.3. Bridge model

The equation of motion of the bridge subjected to a moving vehicle can be written as:

$$\boldsymbol{M}_B \ddot{\boldsymbol{y}}_B + \boldsymbol{C}_B \dot{\boldsymbol{y}}_B + \boldsymbol{K}_B \boldsymbol{y}_B = \boldsymbol{N}_b \boldsymbol{F}_{int} \qquad 3\text{-}5$$

Where $\boldsymbol{M}_B$, $\boldsymbol{C}_B$, and $\boldsymbol{K}_B$ are the bridge mass, damping and stiffness matrices, respectively; $\boldsymbol{y}_B$, $\dot{\boldsymbol{y}}_B$, and $\ddot{\boldsymbol{y}}_B$ are the nodal displacement, velocity, and acceleration vectors, respectively. The beam bridge is discretised into n_{el} equally spaced elements with $n_{el} + 1$ nodes. Each node includes two degrees of freedom (DOFs), rotational and vertical translations. The total number of DOFs for the bridge is $ndof = 2 \times (n_{el} + 1)$.

The half vehicle model with two axles is used in this study and $(\boldsymbol{N}_b \boldsymbol{F}_{int})_{ndof \times 1}$ is an equivalent global load vector at each time instant. The matrix $\boldsymbol{N}_b$ is a $ndof \times 2$ transformation matrix that distributes interaction forces ($\boldsymbol{F}_{int}$) to equivalent nodal forces, which consists of the Hermitian shape function vectors at the DOFs of the beam elements where interaction forces are acting and zeros for the other entries, given by (Feng, Sun & Feng 2015; Law, S. S. et al. 2004)

$$\boldsymbol{N}_b = \begin{Bmatrix} 0 & \ldots. & 0 & \ldots. & N_{b1}((x_1(t), t) & \ldots.. & 0 & \ldots.. & 0 \\ 0 & N_{b2}((x_2(t), t) & \ldots.. & 0 & \ldots.. & 0 & \ldots.. & 0 & \ldots.. & 0 \end{Bmatrix}^T \qquad 3\text{-}6$$

Hermitian shape function vector for a load moving on an element (see Figure 3-3) is defined as follows:

`

$$\boldsymbol{N}_{bi} = \begin{Bmatrix} 1 - 3 \times \left(\frac{x_i(t)}{l}\right)^2 + 2 \times \left(\frac{x_i(t)}{l}\right)^3 \\ x_i(t) \times \left(\frac{x_i(t)}{l} - 1\right)^2 \\ 3 \times \frac{x_i(t)^2}{l} - 2 \times \left(\frac{x_i(t)}{l}\right)^3 \\ x_i(t) \times \left(\frac{x_i(t)}{l} - 1\right)^2 - \frac{x_i(t)}{l} \end{Bmatrix} \quad \text{3-7}$$

where i is the number of the load, x is the location of the load, and l is the element length, as shown in Figure 3-3.

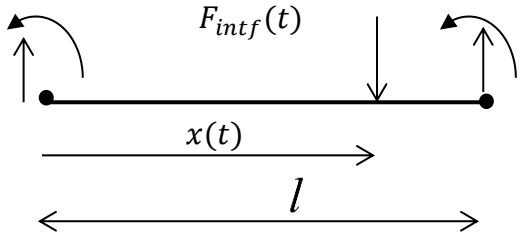

Figure 3-3: An element under moving load

$\boldsymbol{F}_{int} = \begin{Bmatrix} F_{intf}(t) \\ F_{intr}(t) \end{Bmatrix}$, $F_{intf}(t)$ and $F_{intr}(t)$ are the interaction forces acting on the bridge, which includes the static plus dynamic interaction forces between the two axles and the bridge, specifically,

$$\begin{aligned} F_{\text{int}f} &= -[c_{wf}(\dot{y}_{wf} - (\dot{y}_{Bf} + \dot{r}_{Bf})) + k_{wf}(y_{wf} - (y_{Bf} + r_{Bf}))] + W_f \\ F_{\text{int}r} &= -[c_{wr}(\dot{y}_{wr} - (\dot{y}_{Br} + \dot{r}_{Br})) + k_{wr}(y_{wr} - (y_{Br} + r_{Br}))] + W_r \end{aligned} \quad \text{3-8}$$

where $W_f = (m_v \times l_r/l + m_{wf})g$ and $W_r = (m_v \times l_f/l + m_{wr})g$ are the static loads at the front and the rear wheel locations, respectively; y_{Bf} , y_{Br} , r_{Bf} and r_{Br} are the bridge displacements, and road profile displacements under the front and rear wheel moving on the bridge, respectively. The bridge displacement under either of the wheels at each time step can be calculated by

$$y_{Bf} = \boldsymbol{N}'_{b1} y_B \qquad y_{Br} = \boldsymbol{N}'_{b2} y_B \quad \text{3-9}$$

In this study, Rayleigh damping is adopted for the bridge, i.e., $\boldsymbol{C}_B = \alpha \boldsymbol{M}_B + \beta \boldsymbol{K}_B$. The constants α and β can be obtained from $\alpha = 2\varsigma\omega_1\omega_2/(\omega_1 + \omega_2)$ and $\beta = 2\varsigma/(\omega_1 + \omega_2)$, where ς is the damping ratio, ω_1 and ω_2 are the first two natural frequencies respectively.

3.2.4. Vehicle-bridge coupled model

The vehicle and bridge models can be combined as follows:

`

$$\begin{bmatrix} \boldsymbol{M}_B & \mathbf{0} \\ \mathbf{0} & \boldsymbol{M}_v \end{bmatrix} \begin{Bmatrix} \ddot{\boldsymbol{y}}_B \\ \ddot{\boldsymbol{Y}}_v \end{Bmatrix} + \begin{bmatrix} \boldsymbol{C}_B & \mathbf{0} \\ \mathbf{0} & \boldsymbol{C}_v \end{bmatrix} \begin{Bmatrix} \dot{\boldsymbol{y}}_B \\ \dot{\boldsymbol{Y}}_v \end{Bmatrix} + \begin{bmatrix} \boldsymbol{K}_B & \mathbf{0} \\ \mathbf{0} & \boldsymbol{K}_v \end{bmatrix} \begin{Bmatrix} \boldsymbol{y}_B \\ \boldsymbol{Y}_v \end{Bmatrix} = \begin{Bmatrix} \boldsymbol{N}_b \boldsymbol{F}_{int} \\ \boldsymbol{P}_v \end{Bmatrix} \qquad 3\text{-}10$$

This equation can be rewritten as Equation 3-11. On the right-hand side of Equation 3-11, there are elements depending on bridge and vehicle responses which should be moved and coupled with the left-hand side. The final version of the vehicle-bridge coupled model is shown in Equation 3-12. Using the explicit form of the Newmark-β method, Equation 3-10 can be solved step-by-step to obtain the dynamic responses of the bridge and the vehicle. Due to the interaction of the system with moving loads; the mass, damping, and stiffness matrices as well as the force vectors of the system are time-dependent, and should be updated at each time instant. Having the dynamic responses of the bridge, the reference loads $\boldsymbol{F}_{\text{int}}$ can be calculated from Equation 3-5 or 3-8. This procedure algorithm can be seen in Figure 3-4.

$$\begin{bmatrix} \mathbf{M_B} & \mathbf{0} & \mathbf{0} & \mathbf{0} & \mathbf{0} \\ 0 & \dfrac{m_v l_r^2 + I_v}{l^2} & \dfrac{m_v l_f l_r - I_v}{l^2} & 0 & 0 \\ 0 & \dfrac{m_v l_f l_r - I_v}{l^2} & \dfrac{m_v l_f^2 + I_v}{l^2} & 0 & 0 \\ 0 & 0 & 0 & m_{wf} & 0 \\ 0 & 0 & 0 & 0 & m_{wr} \end{bmatrix} \begin{Bmatrix} \ddot{\mathbf{y}}_\mathbf{B} \\ \ddot{y}_{bf} \\ \ddot{y}_{br} \\ \ddot{y}_{wf} \\ \ddot{y}_{wr} \end{Bmatrix} +$$

$$\begin{bmatrix} \mathbf{C_B} & \mathbf{0} & \mathbf{0} & \mathbf{0} & \mathbf{0} \\ 0 & c_{sf} & 0 & -c_{sf} & 0 \\ 0 & 0 & c_{sr} & 0 & -c_{sr} \\ 0 & -c_{sf} & 0 & c_{wf} + c_{sf} & 0 \\ 0 & 0 & -c_{sr} & 0 & c_{wr} + c_{sr} \end{bmatrix} \begin{Bmatrix} \dot{\mathbf{y}}_\mathbf{B} \\ \dot{y}_{bf} \\ \dot{y}_{br} \\ \dot{y}_{wf} \\ \dot{y}_{wr} \end{Bmatrix} +$$

$$\begin{bmatrix} \mathbf{K_B} & \mathbf{0} & \mathbf{0} & \mathbf{0} & \mathbf{0} \\ 0 & k_{sf} & 0 & -k_{sf} & 0 \\ 0 & 0 & k_{sr} & 0 & -k_{sr} \\ 0 & -k_{sf} & 0 & k_{wf} + k_{sf} & 0 \\ 0 & 0 & -k_{sr} & 0 & k_{wr} + k_{sr} \end{bmatrix} \begin{Bmatrix} \mathbf{y}_\mathbf{B} \\ y_{bf} \\ y_{br} \\ y_{wf} \\ y_{wr} \end{Bmatrix} =$$

$$\begin{Bmatrix} (-\mathbf{N_{b1}} c_{wf} \underline{\dot{y}_{wf}} + \mathbf{N_{b1}} c_{wf} \underline{\dot{y}_{Bf}} - \mathbf{N_{b1}} k_{wf} \underline{y_{wf}} + \mathbf{N_{b1}} k_{wf} \underline{y_{Bf}}) + \\ (-\mathbf{N_{b2}} c_{wr} \underline{\dot{y}_{wr}} + \mathbf{N_{b2}} c_{wr} \underline{\dot{y}_{Br}} - \mathbf{N_{b2}} k_{wr} \underline{y_{wr}} + \mathbf{N_{b2}} k_{wr} \underline{y_{Br}}) \\ 0 \\ 0 \\ (c_{wf} \underline{\dot{y}_{Bf}}) + (k_{wf} \underline{y_{Bf}}) \\ (c_{wr} \underline{\dot{y}_{Br}}) + (k_{wr} \underline{y_{Br}}) \end{Bmatrix} + \begin{Bmatrix} (\mathbf{N_{b1}} k_{wf} r_{Bf} + \mathbf{N_{b1}} c_{wf} \dot{r}_{Bf} + \mathbf{N_{b1}} W_f) + \\ (\mathbf{N_{b2}} k_{wr} r_{Br} + \mathbf{N_{b2}} c_{wr} \dot{r}_{Br} + \mathbf{N_{b2}} W_r) \\ 0 \\ 0 \\ (c_{wf} \dot{r}_{Bf}) + (k_{wf} r_{Bf}) \\ (c_{wr} \dot{r}_{Br}) + (k_{wr} r_{Br}) \end{Bmatrix}$$

3-11

`

$$\begin{bmatrix} \mathbf{M_B} & \mathbf{0} & \mathbf{0} & \mathbf{0} & \mathbf{0} \\ \mathbf{0} & \frac{m_v l_r^2 + I_v}{l^2} & \frac{m_v l_f l_r - I_v}{l^2} & 0 & 0 \\ 0 & \frac{m_v l_f l_r - I_v}{l^2} & \frac{m_v l_f^2 + I_v}{l^2} & 0 & 0 \\ 0 & 0 & 0 & m_{wf} & 0 \\ 0 & 0 & 0 & 0 & m_{wr} \end{bmatrix} \begin{Bmatrix} \ddot{\mathbf{y}}_{\mathbf{B}} \\ \ddot{y}_{bf} \\ \ddot{y}_{br} \\ \ddot{y}_{wf} \\ \ddot{y}_{wr} \end{Bmatrix} +$$

$$\begin{bmatrix} \mathbf{C_B} & \underline{-\mathbf{N_{b1}} c_{wf} \mathbf{N}'_{\mathbf{b1}} - \mathbf{N_{b2}} c_{wr} \mathbf{N}'_{\mathbf{b2}}} & \mathbf{0} & \mathbf{0} & \underline{\mathbf{0} + \mathbf{N_{b1}} c_{wf}} & \underline{\mathbf{0} + \mathbf{N_{b2}} c_{wr}} \\ & \mathbf{0} & c_{sf} & 0 & -c_{sf} & 0 \\ & \mathbf{0} & 0 & c_{sr} & 0 & -c_{sr} \\ & \underline{\mathbf{0} - c_{wf} \mathbf{N}'_{\mathbf{b1}}} & -c_{sf} & 0 & c_{wf} + c_{sf} & 0 \\ & \underline{\mathbf{0} - c_{wr} \mathbf{N}'_{\mathbf{b2}}} & 0 & -c_{sr} & 0 & c_{wr} + c_{sr} \end{bmatrix} \begin{Bmatrix} \dot{\mathbf{y}}_{\mathbf{B}} \\ \dot{y}_{bf} \\ \dot{y}_{br} \\ \dot{y}_{wf} \\ \dot{y}_{wr} \end{Bmatrix} +$$

$$\begin{bmatrix} \mathbf{K_B} & \underline{-\mathbf{N_{b1}} k_{wf} \mathbf{N}'_{\mathbf{b1}} - \mathbf{N_{b2}} k_{wr} \mathbf{N}'_{\mathbf{b2}}} & \mathbf{0} & \mathbf{0} & \underline{\mathbf{0} + \mathbf{N_{b1}} k_{wf}} & \underline{\mathbf{0} + \mathbf{N_{b2}} k_{wr}} \\ & \mathbf{0} & k_{sf} & 0 & -k_{sf} & 0 \\ & \mathbf{0} & 0 & k_{sr} & 0 & -k_{sr} \\ & \underline{\mathbf{0} - k_{wf} \mathbf{N}'_{\mathbf{b1}}} & -k_{sf} & 0 & k_{wf} + k_{sf} & 0 \\ & \underline{\mathbf{0} - k_{wr} \mathbf{N}'_{\mathbf{b2}}} & 0 & -k_{sr} & 0 & k_{wr} + k_{sr} \end{bmatrix} \begin{Bmatrix} \mathbf{y}_{\mathbf{B}} \\ y_{bf} \\ y_{br} \\ y_{wf} \\ y_{wr} \end{Bmatrix} =$$

$$\begin{Bmatrix} (\mathbf{N_{b1}} k_{wf} r_{Bf} + \mathbf{N_{b1}} c_{wf} \dot{r}_{Bf} + \mathbf{N_{b1}} W_f) + (\mathbf{N_{b2}} k_{wr} r_{Br} + \mathbf{N_{b2}} c_{wr} \dot{r}_{Br} + \mathbf{N_{b2}} W_r) \\ 0 \\ 0 \\ (c_{wf} \dot{r}_{Bf}) + (k_{wf} r_{Bf}) \\ (c_{wr} \dot{r}_{Br}) + (k_{wr} r_{Br}) \end{Bmatrix}$$

3-12

The mass, stiffness, and damping matrices of the system in Equation 3-12 are square, and surface roughness influence has been considered on the right-hand side.

`

3.3. Moving load identification formulations

The Newmark-β method can be applied when establishing a relationship between output measurements and input loadings. Whenever the external load is known, bridge responses can be predicted by the forward analysis. However, in the real world, moving vehicles act as external loads and they are unknown. Identifying moving loads is an inverse problem, meaning to calculate moving loads using response measurements with the limited number of sensors installed on the bridge. It is an ill-posed least-squares problem. Here in this study, a known vehicle has been considered to verify the accuracy of the generated method, however, in the practical use of the generated method, it is not necessary to know the vehicle. By knowing the vehicle dynamic properties, the real interaction forces between the tires and road surface can be calculated and compared with the identified ones to check the method's accuracy.

3.3.1. Representation of the explicit form of the Newmark-β method

The equation of motion of any system has a format as follows:

$$\boldsymbol{M\ddot{y} + C\dot{y} + Ky = NF} \tag{3-13}$$

where mass, stiffness, damping, external force, and its influence matrix can be either time-dependent or constant. The representation of Equation 3-13 by the explicit form of the Newmark-β method for the case system is subject to a non-moving load as well as mass, stiffness, and damping of the system are constant during the time, is proposed by Liu et al. (2014). To simulate the response measurements in this study, the method is extended for a general system where the bridge is subject to a moving load, and the mass, stiffness, and damping matrices of the general system are time-dependent, and later the method is developed to identify moving loads.

In general, the representation of Equation 3-13 by the explicit form of the Newmark-β method is as follows:

$$\begin{bmatrix} \boldsymbol{y}_{i+1} \\ \boldsymbol{\dot{y}}_{i+1} \\ \boldsymbol{\ddot{y}}_{i+1} \end{bmatrix} = \begin{bmatrix} \boldsymbol{A}_0 \\ \boldsymbol{B}_0 \\ \boldsymbol{C}_0 \end{bmatrix}_{i+1} \boldsymbol{N}_{(i+1)}\boldsymbol{F} + \begin{bmatrix} \boldsymbol{A}_d & \boldsymbol{A}_v & \boldsymbol{A}_a \\ \boldsymbol{B}_d & \boldsymbol{B}_v & \boldsymbol{B}_a \\ \boldsymbol{C}_d & \boldsymbol{C}_v & \boldsymbol{C}_a \end{bmatrix}_{i+1} \begin{bmatrix} \boldsymbol{y}_i \\ \boldsymbol{\dot{y}}_i \\ \boldsymbol{\ddot{y}}_i \end{bmatrix} \tag{3-14}$$

where

$$\begin{aligned} \boldsymbol{A}_{0_{i+1}} &= \left(\widehat{\boldsymbol{K}}_{i+1}\right)^{-1}, \\ \boldsymbol{A}_{d_{i+1}} &= \left(\widehat{\boldsymbol{K}}_{i+1}\right)^{-1}\left[\frac{1}{\beta\Delta t^2}\boldsymbol{M}_{i+1} + \frac{\gamma}{\beta\Delta t}\boldsymbol{C}_{i+1}\right], \\ \boldsymbol{A}_{v_{i+1}} &= \left(\widehat{\boldsymbol{K}}_{i+1}\right)^{-1}\left[\frac{1}{\beta\Delta t}\boldsymbol{M}_{i+1} + (\frac{\gamma}{\beta} - 1)\boldsymbol{C}_{i+1}\right], \\ \boldsymbol{A}_{a_{i+1}} &= \left(\widehat{\boldsymbol{K}}_{i+1}\right)^{-1}\left[(\frac{1}{2\beta} - 1)\boldsymbol{M}_{i+1} + \frac{\Delta t}{2}(\frac{\gamma}{\beta} - 2)\boldsymbol{C}_{i+1}\right], \end{aligned} \tag{3-15}$$

`

$$\boldsymbol{B}_{0_{i+1}} = \frac{\gamma}{\beta\Delta t}\left(\widehat{\boldsymbol{K}}_{i+1}\right)^{-1},$$

$$\boldsymbol{B}_{d_{i+1}} = \frac{-\gamma}{\beta\Delta t}\widehat{\boldsymbol{K}}_{i+1}{}^{-1}\boldsymbol{K}_{i+1},$$

$$\boldsymbol{B}_{v_{i+1}} = \frac{\gamma}{\beta\Delta t}\widehat{\boldsymbol{K}}_{i+1}{}^{-1}\left[\left(\frac{\beta\Delta t}{\gamma} - \Delta t\right)\boldsymbol{K}_{i+1} + \frac{1}{\gamma\Delta t}\boldsymbol{M}_{i+1}\right],$$

$$\boldsymbol{B}_{a_{i+1}} = \frac{\gamma}{\beta\Delta t}\widehat{\boldsymbol{K}}_{i+1}{}^{-1}\left[\left(\frac{\beta\Delta t^2}{\gamma} - \frac{\Delta t^2}{2}\right)\boldsymbol{K}_{i+1} + (\frac{1}{\gamma} - 1)\boldsymbol{M}_{i+1}\right],$$

$$\boldsymbol{C}_{0_{i+1}} = \frac{\gamma}{\beta\Delta t^2}\widehat{\boldsymbol{K}}_{i+1}{}^{-1},$$

$$\boldsymbol{C}_{d_{i+1}} = \frac{-1}{\beta\Delta t^2}\widehat{\boldsymbol{K}}_{i+1}{}^{-1}\boldsymbol{K}_{i+1},$$

$$\boldsymbol{C}_{v_{i+1}} = \frac{-1}{\beta\Delta t^2}\widehat{\boldsymbol{K}}_{i+1}{}^{-1}(\boldsymbol{C}_{i+1} + \Delta t\boldsymbol{K}_{i+1}),$$

$$\boldsymbol{C}_{a_{i+1}} = \frac{\gamma}{\beta\Delta t^2}\widehat{\boldsymbol{K}}_{i+1}{}^{-1}\left[(\gamma - 1)\Delta t\boldsymbol{C}_{i+1} - \beta\Delta t^2(\frac{1}{2\beta} - 1)\boldsymbol{K}_{i+1}\right],$$

Where

$$\widehat{\boldsymbol{K}}_{i+1} = \boldsymbol{K}_{i+1} + \frac{1}{\beta\Delta t^2}\boldsymbol{M}_{i+1} + \frac{\gamma}{\beta\Delta t}\boldsymbol{C}_{i+1} \qquad 3\text{-}16$$

The general recursive relation can be written as:

$$\begin{bmatrix}\boldsymbol{y}_i\\ \dot{\boldsymbol{y}}_i\\ \ddot{\boldsymbol{y}}_i\end{bmatrix} = \begin{bmatrix}\boldsymbol{A}_0\\ \boldsymbol{B}_0\\ \boldsymbol{C}_0\end{bmatrix}_i \boldsymbol{N}_{(i)}\boldsymbol{F}_i + \begin{bmatrix}\boldsymbol{A}_d & \boldsymbol{A}_v & \boldsymbol{A}_a\\ \boldsymbol{B}_d & \boldsymbol{B}_v & \boldsymbol{B}_a\\ \boldsymbol{C}_d & \boldsymbol{C}_v & \boldsymbol{C}_a\end{bmatrix}_i \begin{bmatrix}\boldsymbol{y}_{i-1}\\ \dot{\boldsymbol{y}}_{i-1}\\ \ddot{\boldsymbol{y}}_{i-1}\end{bmatrix}$$

$$\begin{bmatrix}\boldsymbol{y}_{i-1}\\ \dot{\boldsymbol{y}}_{i-1}\\ \ddot{\boldsymbol{y}}_{i-1}\end{bmatrix} = \begin{bmatrix}\boldsymbol{A}_0\\ \boldsymbol{B}_0\\ \boldsymbol{C}_0\end{bmatrix}_{i-1} \boldsymbol{N}_{(i-1)}\boldsymbol{F}_{i-1} + \begin{bmatrix}\boldsymbol{A}_d & \boldsymbol{A}_v & \boldsymbol{A}_a\\ \boldsymbol{B}_d & \boldsymbol{B}_v & \boldsymbol{B}_a\\ \boldsymbol{C}_d & \boldsymbol{C}_v & \boldsymbol{C}_a\end{bmatrix}_{i-1} \begin{bmatrix}\boldsymbol{y}_{i-2}\\ \dot{\boldsymbol{y}}_{i-2}\\ \ddot{\boldsymbol{y}}_{i-2}\end{bmatrix} \qquad 3\text{-}17$$

$$\begin{bmatrix}\boldsymbol{y}_1\\ \dot{\boldsymbol{y}}_1\\ \ddot{\boldsymbol{y}}_1\end{bmatrix} = \begin{bmatrix}\boldsymbol{A}_0\\ \boldsymbol{B}_0\\ \boldsymbol{C}_0\end{bmatrix}_1 \boldsymbol{N}_{(1)}\boldsymbol{F}_1 + \begin{bmatrix}\boldsymbol{A}_d & \boldsymbol{A}_v & \boldsymbol{A}_a\\ \boldsymbol{B}_d & \boldsymbol{B}_v & \boldsymbol{B}_a\\ \boldsymbol{C}_d & \boldsymbol{C}_v & \boldsymbol{C}_a\end{bmatrix}_1 \begin{bmatrix}\boldsymbol{y}_0\\ \dot{\boldsymbol{y}}_0\\ \ddot{\boldsymbol{y}}_0\end{bmatrix}$$

The generated method can be applied to solve Equation 3-12 to simultaneously obtain bridge and vehicle responses.

To identify moving loads from Equation 3-5 where the mass, stiffness, and damping matrices are constant, Equation 3-17 can be represented by:

$$\begin{bmatrix}\boldsymbol{y}_i\\ \dot{\boldsymbol{y}}_i\\ \ddot{\boldsymbol{y}}_i\end{bmatrix} = \sum_{j=0}^{i-1} \begin{bmatrix}\boldsymbol{A}_d & \boldsymbol{A}_v & \boldsymbol{A}_a\\ \boldsymbol{B}_d & \boldsymbol{B}_v & \boldsymbol{B}_a\\ \boldsymbol{C}_d & \boldsymbol{C}_v & \boldsymbol{C}_a\end{bmatrix}^j \begin{bmatrix}\boldsymbol{A}_0\\ \boldsymbol{B}_0\\ \boldsymbol{C}_0\end{bmatrix} \boldsymbol{N}_{i-j}\boldsymbol{F}_{i-j} + \begin{bmatrix}\boldsymbol{A}_d & \boldsymbol{A}_v & \boldsymbol{A}_a\\ \boldsymbol{B}_d & \boldsymbol{B}_v & \boldsymbol{B}_a\\ \boldsymbol{C}_d & \boldsymbol{C}_v & \boldsymbol{C}_a\end{bmatrix}^i \begin{bmatrix}\boldsymbol{y}_0\\ \dot{\boldsymbol{y}}_0\\ \ddot{\boldsymbol{y}}_0\end{bmatrix} \qquad 3\text{-}18$$

Vector $\boldsymbol{x} \in R^{n_s \times 1}$ denoting the output of the structural system can be presented as follows:

$$\boldsymbol{x} = \boldsymbol{R}_a\ddot{\boldsymbol{y}} + \boldsymbol{R}_v\dot{\boldsymbol{y}} + \boldsymbol{R}_d\boldsymbol{y} \qquad 3\text{-}19$$

`

where $\boldsymbol{R}_a$, $\boldsymbol{R}_v$ and $\boldsymbol{R}_d \in R^{n_s \times N}$ are the influence matrices which are multiplied by the related measured responses, n_s is the dimension of the measured responses and N is the number of degrees of freedom of the structure.

Letting $\boldsymbol{R} = [\boldsymbol{R}_d \ \boldsymbol{R}_v \ \boldsymbol{R}_a]$, Equation 3-18 can be represented as follows:

$$\boldsymbol{x}(t_i) = \sum_{j=0}^{i-1} \boldsymbol{R} \begin{bmatrix} \boldsymbol{A}_d & \boldsymbol{A}_v & \boldsymbol{A}_a \\ \boldsymbol{B}_d & \boldsymbol{B}_v & \boldsymbol{B}_a \\ \boldsymbol{C}_d & \boldsymbol{C}_v & \boldsymbol{C}_a \end{bmatrix}^j \begin{bmatrix} \boldsymbol{A}_0 \\ \boldsymbol{B}_0 \\ \boldsymbol{C}_0 \end{bmatrix} \boldsymbol{N}_{i-j} \boldsymbol{F}_{i-j} + \begin{bmatrix} \boldsymbol{A}_d & \boldsymbol{A}_v & \boldsymbol{A}_a \\ \boldsymbol{B}_d & \boldsymbol{B}_v & \boldsymbol{B}_a \\ \boldsymbol{C}_d & \boldsymbol{C}_v & \boldsymbol{C}_a \end{bmatrix}^i \begin{bmatrix} \boldsymbol{y}_0 \\ \dot{\boldsymbol{y}}_0 \\ \ddot{\boldsymbol{y}}_0 \end{bmatrix} \quad \text{3-20}$$

Assuming zero initial conditions of the structure, the following equation can be written:

$$\boldsymbol{H}_k = \boldsymbol{R} \times \begin{bmatrix} \boldsymbol{A}_d & \boldsymbol{A}_v & \boldsymbol{A}_a \\ \boldsymbol{B}_d & \boldsymbol{B}_v & \boldsymbol{B}_a \\ \boldsymbol{C}_d & \boldsymbol{C}_v & \boldsymbol{C}_a \end{bmatrix}^k \begin{bmatrix} \boldsymbol{A}_0 \\ \boldsymbol{B}_0 \\ \boldsymbol{C}_0 \end{bmatrix} \quad \text{3-21}$$

Equation 3-20 can then be rewritten in the matrix convolution form in the time duration from t_1 to t_{tt} as

$$\boldsymbol{X} = \boldsymbol{H}_L \boldsymbol{F} \quad \text{3-22}$$

where tt is the number of time instants and

$$\boldsymbol{X} = \begin{bmatrix} \boldsymbol{x}(t_1) \\ \boldsymbol{x}(t_2) \\ \vdots \\ \boldsymbol{x}(t_{tt}) \end{bmatrix}, \boldsymbol{H}_L = \begin{bmatrix} \boldsymbol{H}_0 \boldsymbol{N}_{b_1} & 0 & \dots & 0 \\ \boldsymbol{H}_1 \boldsymbol{N}_{b_1} & \boldsymbol{H}_0 \boldsymbol{N}_{b_2} & \dots & 0 \\ \vdots & \vdots & \ddots & \vdots \\ \boldsymbol{H}_{tt-1} \boldsymbol{N}_{b_1} & \boldsymbol{H}_{tt-2} \boldsymbol{N}_{b_2} & \dots & \boldsymbol{H}_0 \boldsymbol{N}_{b_{tt}} \end{bmatrix}, \text{ and } \boldsymbol{F} = \begin{bmatrix} \boldsymbol{F}_{\text{int}}(t_1) \\ \boldsymbol{F}_{\text{int}}(t_2) \\ \vdots \\ \boldsymbol{F}_{\text{int}}(t_{tt}) \end{bmatrix} \quad \text{3-23}$$

where $\boldsymbol{X}$ is the assembled measured acceleration vector, $\boldsymbol{F}_{\text{int}}$ is the assembled unknown force vector, and $\boldsymbol{H}$ is known as the Hankel matrix of the bridge consisting of the system Markov parameters. It should be highlighted that $\boldsymbol{N}_{b_i}$ is time-dependent and should be updated at each time step. Provided that $\boldsymbol{H}_L$ can be identified in Equation 3-22, $\boldsymbol{F}$ can be determined from measured $\boldsymbol{X}$.

3.3.2. Regularized solution for moving load identification

The ordinary least squares solution (LSQ) for Equation 3-22 would lead to unbounded solutions because of the presence of noise in measurements, especially at the entrance and exit of the bridge. In order to provide a bounded solution, a regularisation technique can be used. Here, in this study, the damped least-squares method known as Tikhonov regularization (Aster, Borchers & Thurber 2005) has been adopted to minimize the function

$$\min\{\|\boldsymbol{H}_L \boldsymbol{F} - \boldsymbol{X}\|_2^2 + \lambda^2 \|\boldsymbol{L}(\boldsymbol{F} - \boldsymbol{F}_0)\|_2^2\} \quad \text{3-24}$$

where λ is the Tikhonov regularization parameter, $\boldsymbol{F}_0$ is an initial estimation of response and $\boldsymbol{L}$ is defined below (Golub, Heath & Wahba 1979; Hancen 2008):

`

$$\boldsymbol{L} = \begin{bmatrix} 1 & -2 & 1 & & \\ & 1 & -2 & 1 & \\ & & \ddots & \ddots & \ddots \\ & & 1 & -2 & 1 \end{bmatrix}_{(n-2)\times n} \quad \text{3-25}$$

where n is the number of samples (number of columns in $\boldsymbol{H}_L$). The generalized cross-validation (GCV) method is used to find the optimal regularization parameter (Golub, Heath & Wahba 1979; Hancen 2008).

3.3.3. The procedure of identification algorithm

In the numerical study, the procedure of moving load identification consists of two sections, namely: simulating measured responses and identifying moving loads. The main unknown parameter to be identified is the dynamic moving load, however, since this is a numerical study, measured responses should be simulated as well. Simulation of the measured responses is achieved through applying the Newmark-β method and solving Equation 3-12 (see Figure 3-4). Having the simulated measured responses of the bridge at selected points, moving loads are identified by solving Equation 3-22 (see Figure 3-5) .

Known parameters used are:

1) The bridge geometry and its material density,

2) Dynamic characteristics of the vehicle ($\boldsymbol{M}_{v,}\ \boldsymbol{C}_{v,}\ \boldsymbol{K}_{v}$),

3) The vehicle speed v and axle spacing l.

`

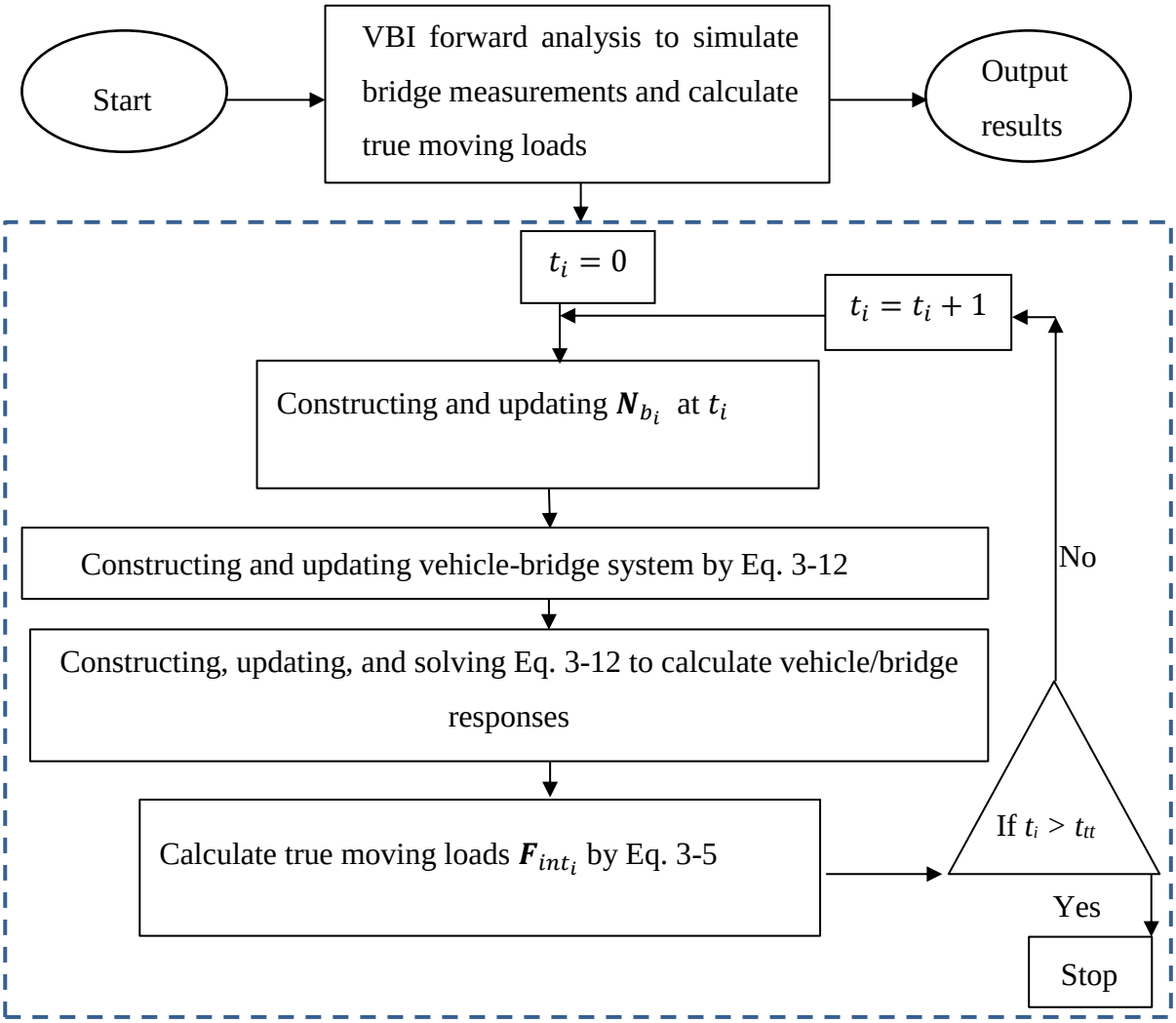

Figure 3-4: Algorithm for calculating the vehicle/bridge responses and the true moving loads by the Explicit form of Newmark-β method

`

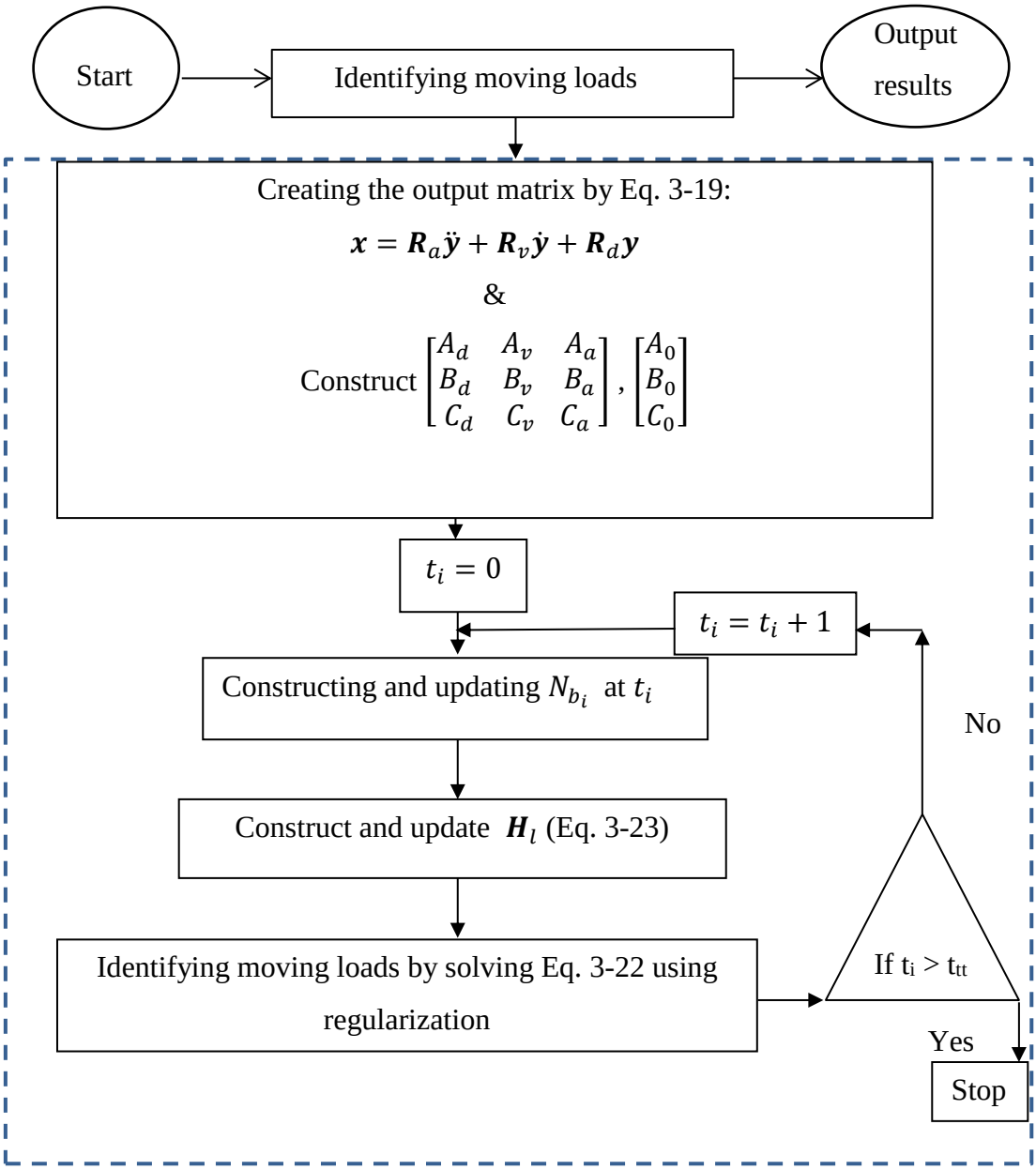

Figure 3-5: Algorithm for moving load identification by the explicit form of Newmark-β method

3.4. Numerical example 1: simply-supported single-span bridge

In this example, a simply supported single-span bridge with 30 m length subjected to the moving vehicle described in Table 3-4 is considered. The first five natural frequencies for the simply supported bridge are 3.9 Hz, 15.6 Hz, 35.1 Hz, 62.5 Hz, and 97.6 Hz, and the first four natural frequencies of the vehicle are 1.63 Hz, 2.29 Hz, 10.35 Hz, and 15.1 Hz, respectively. Table 3-4 and Table 3-5 list the parameter values of the vehicle (Mulcahy 1983) and bridge

`

subsystems, respectively. The effects of the number of sensors, surface roughness, vehicle speed, and measurement noise have been investigated.

Table 3-4: Vehicle parameters (Mulcahy 1983)

$m_v = 17735kg$	$m_{t1} = 1500\ kg$	$m_{t2} = 1000\ kg$
$I_v = 1.47 \times 10^5\ Nm^2$	$k_{s1} = 2.47 \times 10^6\ N/m$	$k_{s2} = 4.23 \times 10^6\ N/m$
$a_1 = 0.519\,m$	$k_{t1} = 1.75 \times 10^6\ N/m$	$k_{t2} = 3.5 \times 10^6\ N/m$
$a_2 = 0.481\,m$	$C_{s1} = 3 \times 10^4\ N/m/s$	$C_{s2} = 4 \times 10^4\ N/m/s$
$S = 4.27m$	$C_{t1} = 3.90 \times 10^3\ N/m/s$	$C_{t2} = 4.30 \times 10^3\ N/m/s$

Table 3-5: Bridge parameters

L= 30 m	EI=2.5*10^{10} N m^2	ρA=5*10^3 kg/m	Damping ratio for all modes= 0.02

3.4.1. Effect of the number of sensors and noise level

The vehicle moves on top of the beam at a constant speed of 15m/s, the road surface roughness level is "A" and the sampling frequency is considered 200 Hz. To investigate the effect of noise, the calculated responses are polluted with white noise as follows:

$$\boldsymbol{y} = \boldsymbol{y}_{real} + E_p std(\boldsymbol{y}_{real})\boldsymbol{N}_{oise} \quad 3\text{-}26$$

where $\boldsymbol{y}$ is a vector of polluted response, $\boldsymbol{y}_{real}$ is the vector of real responses, E_p is a noise level, and $\boldsymbol{N}_{oise}$ is a standard normal distribution vector with zero mean and unit standard deviation. To quantify the force identification accuracy, a percentage error is defined as $Error = \|\boldsymbol{F}_{true} - \boldsymbol{F}_{id}\|/\|\boldsymbol{F}_{true}\| \times 100\ \%$,

where $\boldsymbol{F}_{true}$ denotes the simulated true time-varying moving axle loads, and $\boldsymbol{F}_{id}$ is the identified loads by the proposed method.

The effects of different sensor placements are investigated as listed in Table 3-6. In case S7, seven accelerometers are equally spaced, and then in S6, S5, and S4, one accelerometer has been removed step by step to see the effect. In the case with three sensors, the third sensor is randomly placed to consider the case when a part of the bridge is inaccessible to install a sensor.

The relative percentage errors of identified loads from different sensor placements and at different noise levels are listed in Table 3-7. As can be seen in Table 3-7, without measurement noise, the identification errors are zero or close to zero, which shows the accuracy of the method. With noise, results from all sensor placements are slightly affected by the measurement noise level and the identification accuracy is decreased with the increase of the

`

noise level. It should be noted that since the road roughness and measurement noise are being generated randomly at each run of the program, the values of errors can be slightly more or less than these values. In general, it can be concluded that the method is reliable at different noise levels and sensor placements.

Table 3-6: Sensor Placement

Sensor case	Sensor No.	Sensor location (node no.)
S3	3	1/3L, 2/3L,4/5L
S4	4	1/8L, 1/4L, 1/2L, 3/4L
S5	5	1/8L, 1/4L, 1/2L, 3/4L, 7/8L
S6	6	1/8L, 1/4L, 1/2L, 5/8L, 3/4L, 7/8L
S7	7	1/8L, 1/4L, 3/8L, 1/2L, 5/8L, 3/4L, 7/8L

Table 3-7: The relative error (%) of the identified forces for different sensor placements

Sensor case	S3			S4		
Noise Level (%)	0	2	5	0	2	5
Front axle load	0.00	2.68	4.19	0.00	2.3	3.11
Rear axle load	0.25	2.80	3.71	0.23	2.73	3.18

Sensor case	S5			S6			S7		
Noise Level (%)	0	2	5	0	2	5	0	2	5
Front axle load	0.22	3.03	3.20	0.31	2.78	2.60	0.00	2.15	3.30
Rear axle load	2.90	4.12	4.03	2.42	2.92	3.29	0.24	2.01	3.85

Figure 3-6 and Figure 3-7 show the effect of the measurement noise level on moving load identification results by sensor placements S3 and S7, respectively. As can be seen, identified loads are fluctuating around the static load (100 kN). When loads are out of the bridge, the interaction forces are not identified as zero, this part of time history is excluded in calculating the errors.

`

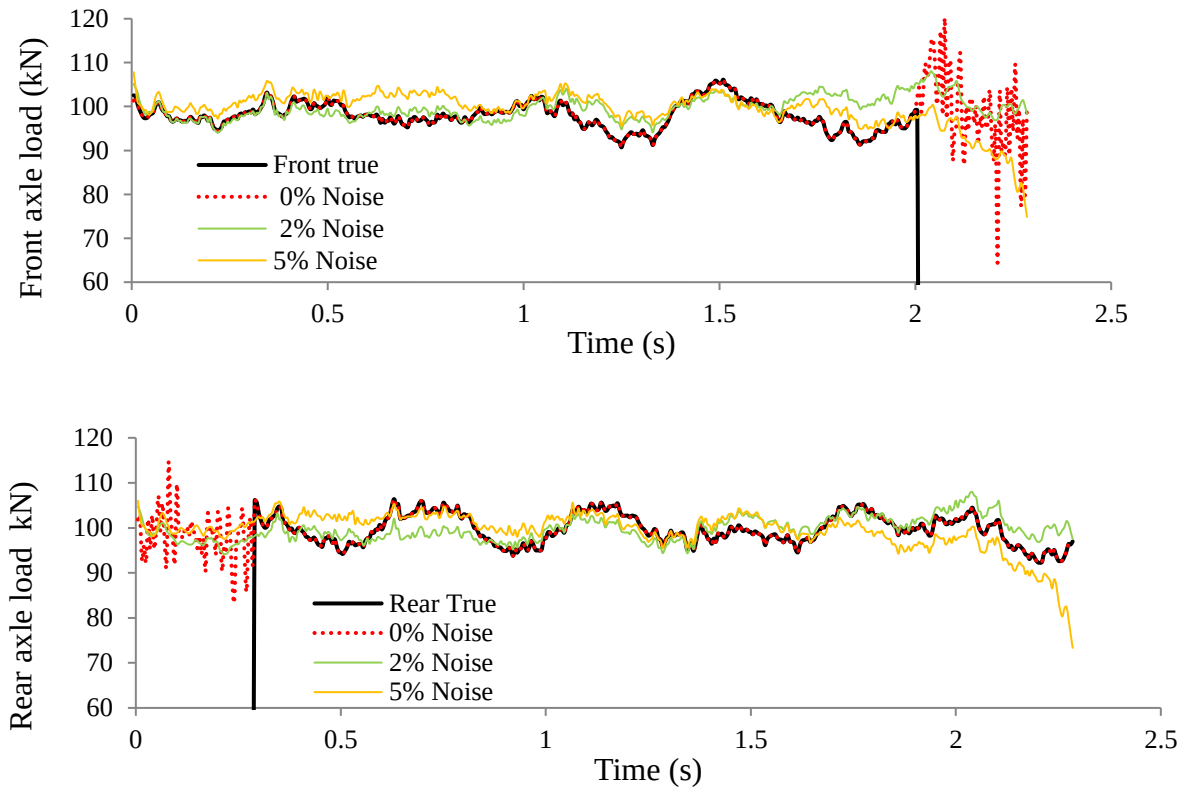

Figure 3-6: Identified loads at road roughness level A- speed 15 m/s- sensor placement S3;

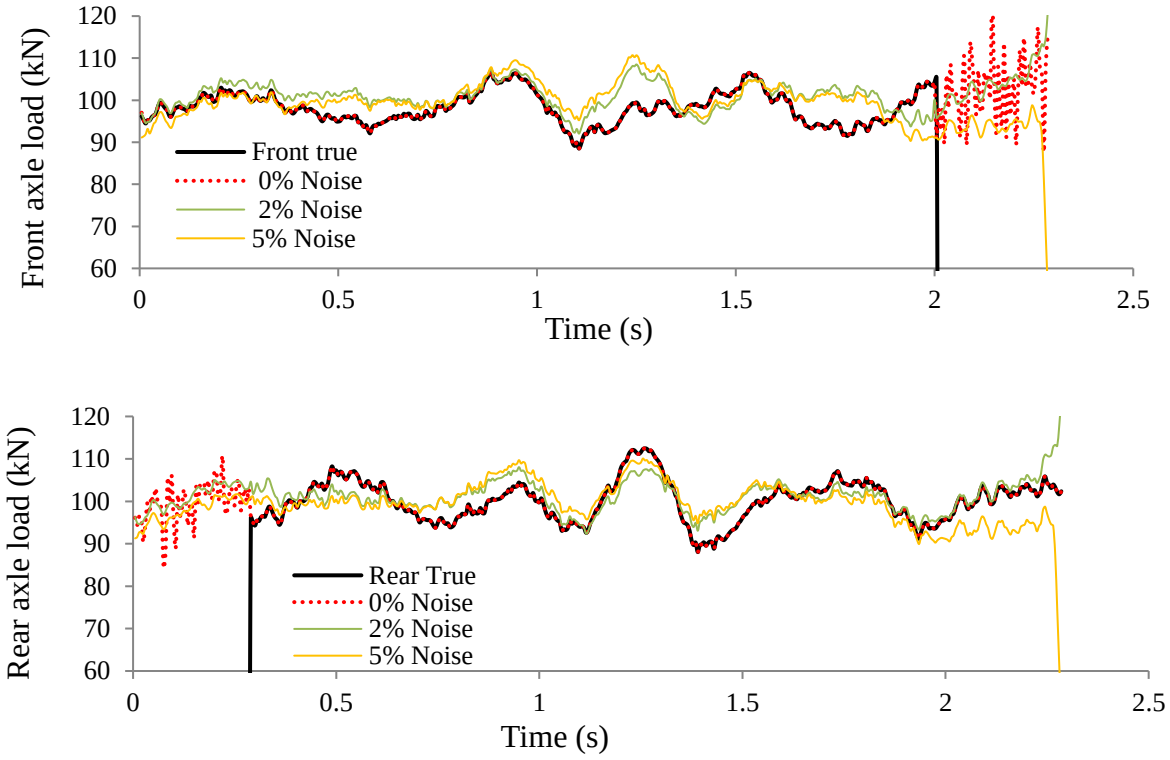

Figure 3-7: Identified loads at road roughness level A- speed 15 m/s- sensor placement S7;

`

3.4.2. Effect of vehicle velocity and road roughness level

In this section, the accuracy of the method at different vehicle speeds (10 m/s, 20 m/s, 30 m/s and 40 m/s) and road roughness levels (A, B, and C) has been investigated, utilizing sensor placement S7. The sampling frequency is 200 Hz, and measurement noise is 2%. The relative percentage errors are tabulated in Table 3-8.

Table 3-8: The relative error (%) of moving load identification from sensor placement S7

Speed (m/s)	10			20			30			40		
Road roughness	A	B	C	A	B	C	A	B	C	A	B	C
Front axle load	1.1	9.5	12.2	2.2	8.2	-	1.8	7.5	-	0.9	7.2	-
Rear axle load	1.5	6.5	19.6	2.8	9.6	-	2.2	14.3	-	2.4	6.8	-

As can be seen from Table 3-8, the relative percentage errors at each speed increase as road roughness gets tougher, and are slightly affected by speed at each road roughness level. Considering that the road roughness and measurement noise are being generated randomly at each run of the program, and error values can be slightly more or less than these values, it can be said that the method is not sensitive to speed, which is investigated further in the next example and through the experimental studies in the laboratory. Identified loads at speeds 10 m/s and 40 m/s and different road roughness levels can be seen in Figure 3-8 to Figure 3-12. These figures show identified loads are fluctuating around the static values, indicating the accuracy of the method. For more investigation, the average of true loads (F_{true}) and the average of identified loads (F_{id}) have been calculated and compared as reported in Table 3-9.

`

Table 3-9: The error (%) of the average of identified forces via sensor location S7

Speed (m/s)	Roughness	Ave. of front axle load (kN)			Ave. of rear axle load (kN)		
		F_{true}	F_{id}	Error (%)	F_{true}	F_{id}	Error (%)
10	A	98.1	98.9	0.82	99.7	98.8	0.93
	B	98.9	102.8	3.9	99.7	102.4	2.7
	C	99.1	103	0.97	101	102.7	1.7
20	A	98.13	99.6	1.5	100.08	100.02	0.06
	B	98.1	91.9	6.3	101.3	92.2	9.04
30	A	98.6	98.7	0.17	100.06	99.98	0.07
	B	100.3	100.8	0.43	99.1	97.5	1.61
40	A	98.6	98.9	0.38	99.9	98.9	1.05
	B	101.88	101.79	0.09	101.46	103.23	1.7

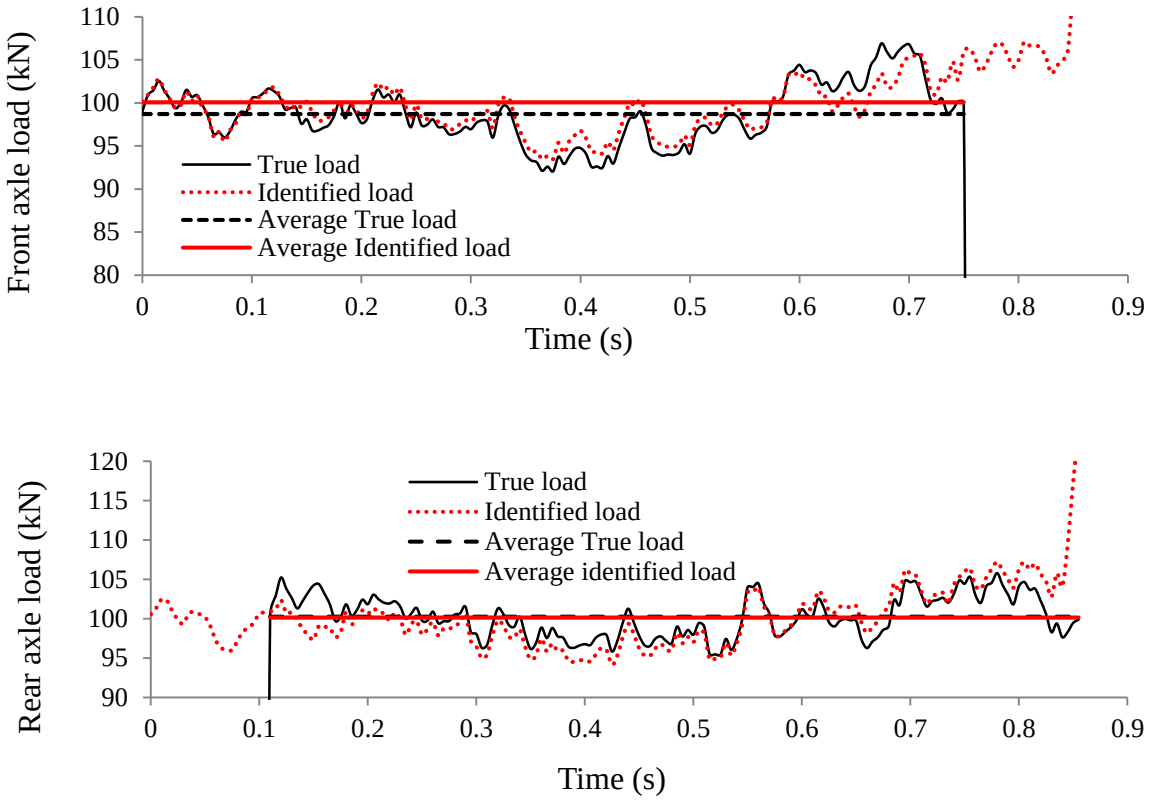

Figure 3-8: Identified results at road roughness level A- speed 40 m/s- 2% noise;

`

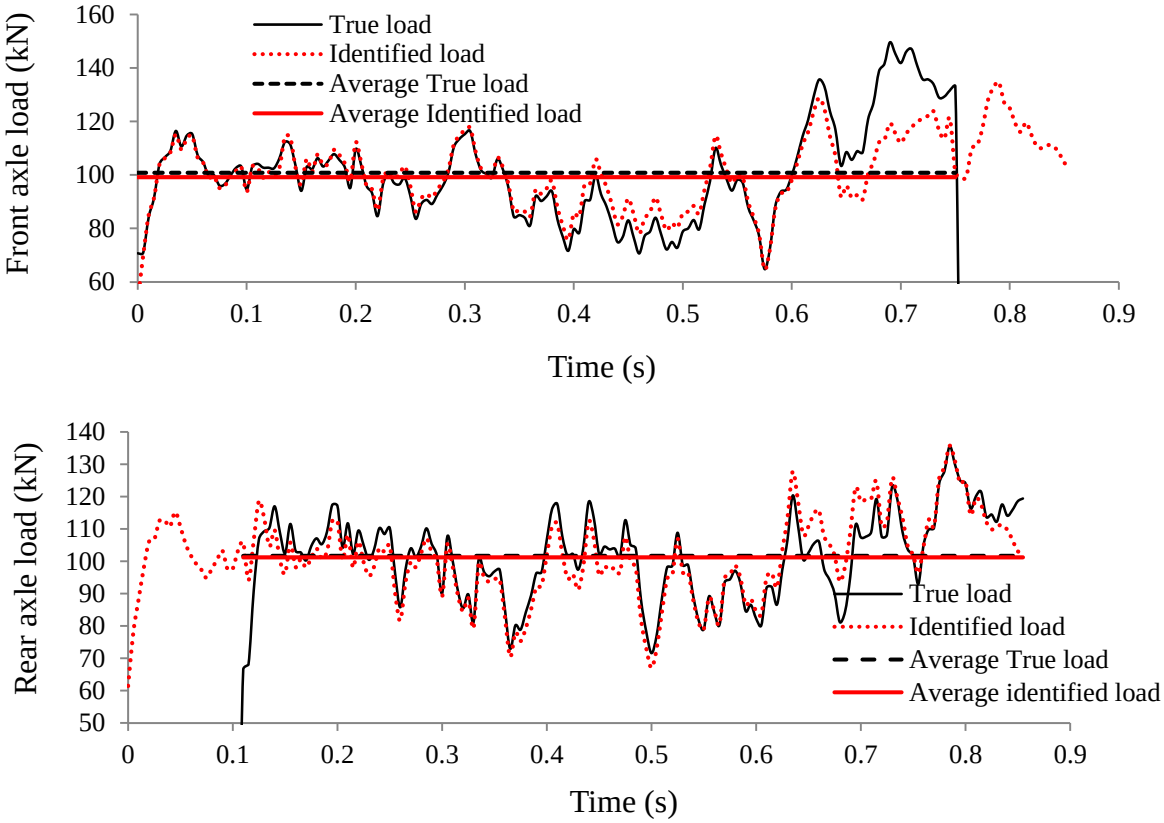

Figure 3-9: Identified loads at road roughness level B- speed 40 m/s- 2% noise;

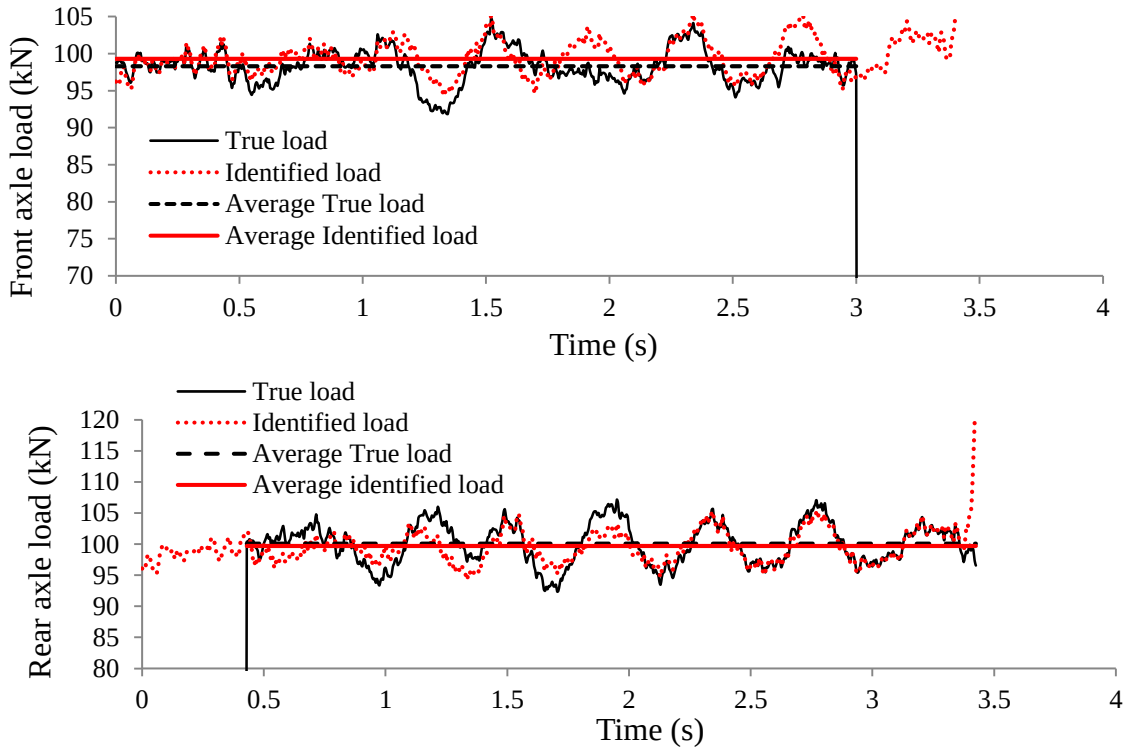

Figure 3-10: Identified loads at road roughness level A- speed 10 m/s- 2% noise;

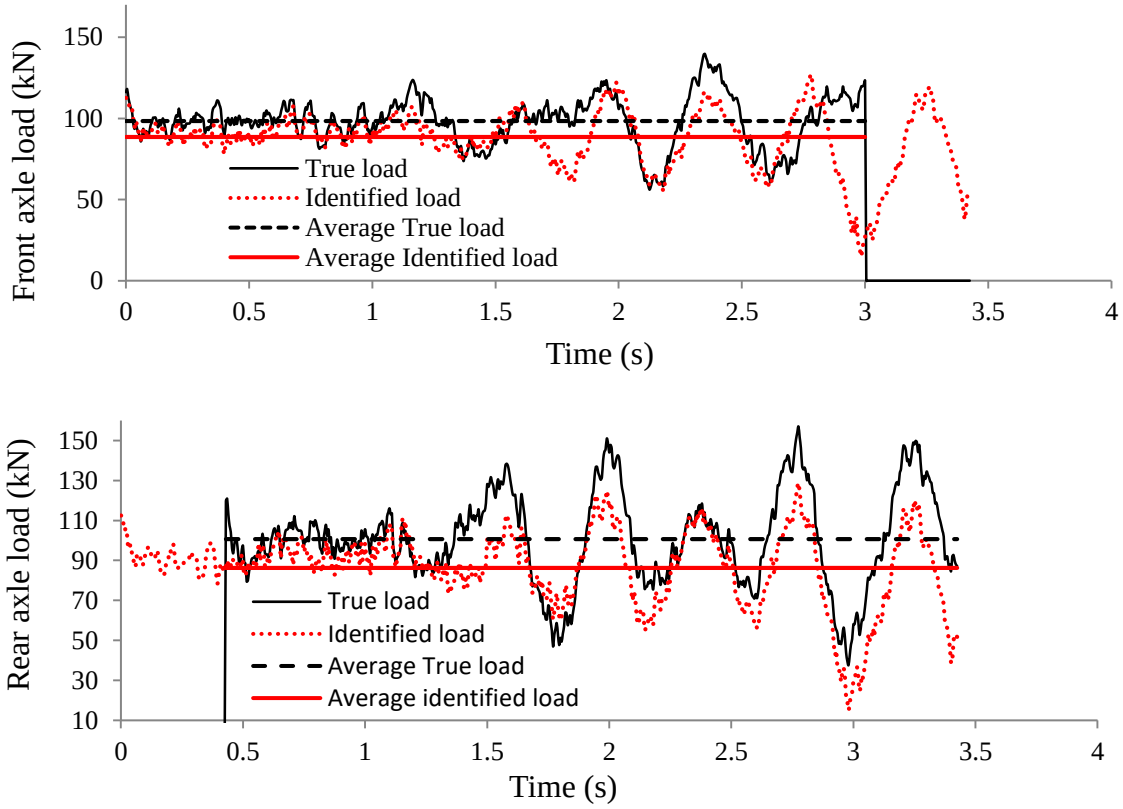

Figure 3-11: Identified loads at road roughness level B- speed 10 m/s- 2% noise;

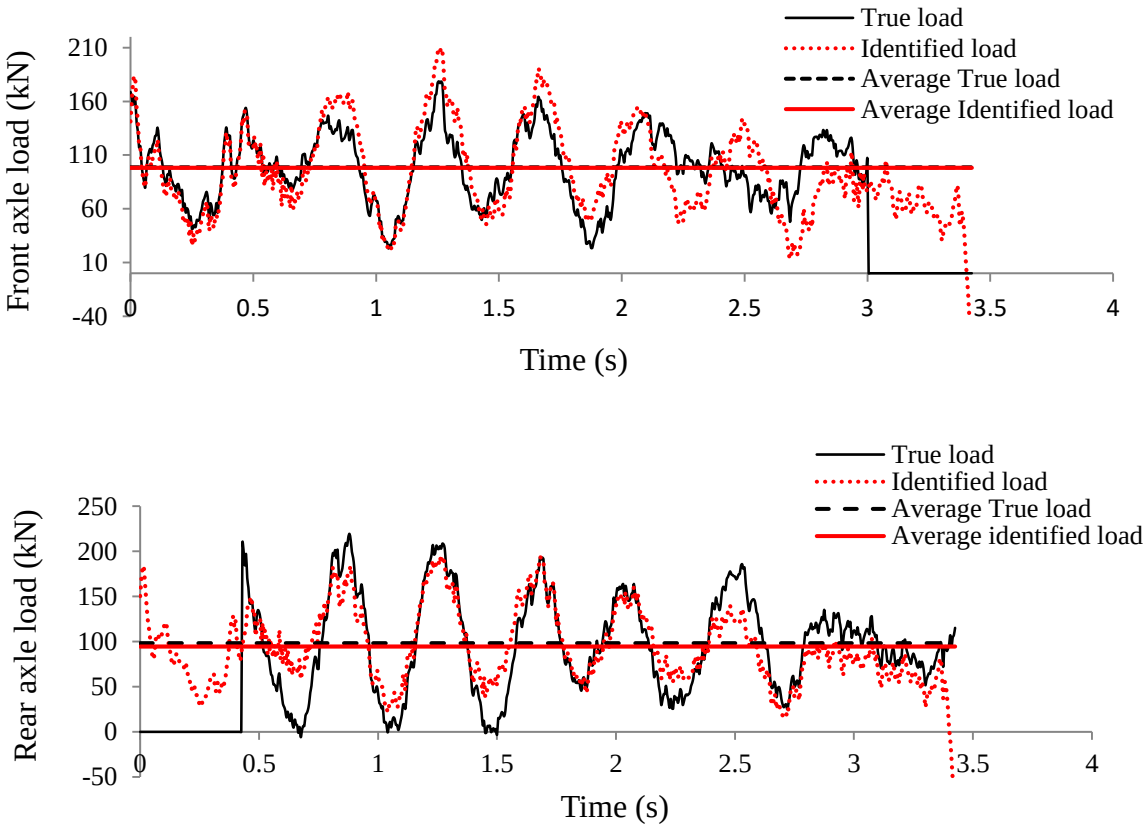

Figure 3-12: Identified loads at road roughness level C- speed 10 m/s- 2% noise;

`

3.5. Numerical example 2: three-span continuous bridge

Most existing studies are not successful when it comes to multi-span continuous bridges. They fail in identifying loads at the instants when a vehicle enters/exits the bridge or passes through the mid-supports (Feng, Sun & Feng 2015; Law, S. S. et al. 2004; Zhu, XQ & Law 2002), and they are not as accurate as for simple span bridges. The application of the proposed method has been studied for a 90 m three-span bridge with spans of 30 m (see Figure 3-13). The bridge is discretised into 45 equally spaced Euler-Bernoulli elements with 91 DOFs and its first five natural frequencies are 3.90, 5.00, 7.30, 15.61, and 17.79 Hz. Other properties of the bridge and the vehicle passing on it are the same as the numerical example 1 (see Table 3-4 and Table 3-5). The time step in this study is 0.005 sec and 6 accelerometers are placed at one-third of each span. The effects of measurement noise, vehicle speed and road surface roughness have been investigated in the following sections.

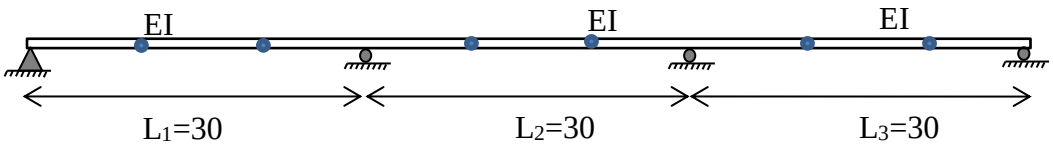

Figure 3-13: Three-span bridge model

3.5.1. The Effect of noise level and vehicle speed

In this section, road roughness level “A” is considered, and the accuracy of the method at different levels of speed (15 m/s, 20 m/s, 30 m/s, and 40 m/s) and noise (0%, 2%, and 5%), is explored. The results are tabulated in Table 3-10 and Figure 3-14 to Figure 3-17.

Table 3-10: Percentage errors of the identified moving loads at different levels of speed and noise

Speed (m/s)	15			20			30			40		
Measurement noise (%)	0	2	5	0	2	5	0	2	5	0	2	5
Front axle load	0.01	3.2	3.4	0.01	2.8	4.8	0.01	2.6	3.1	0.02	2.9	3.6
Rear axle load	0.16	3.5	3.6	0.2	3.6	5.9	0.3	4.6	3.8	0.46	3.8	4.1

`

From the above table, it can be seen that the identification accuracy is slightly affected by adding measurement noise, however, it is not sensitive to increase in the noise level, as well as vehicle speed, and the error values are in the same range.

From Figure 3-14 to Figure 3-17, it can be seen that this method is able to promisingly identify moving loads without disruptions when passing through supports, which is not possible by other methods (Feng, Sun & Feng 2015) and this is a significant improvement in moving load identification. This has been further investigated in the next sections.

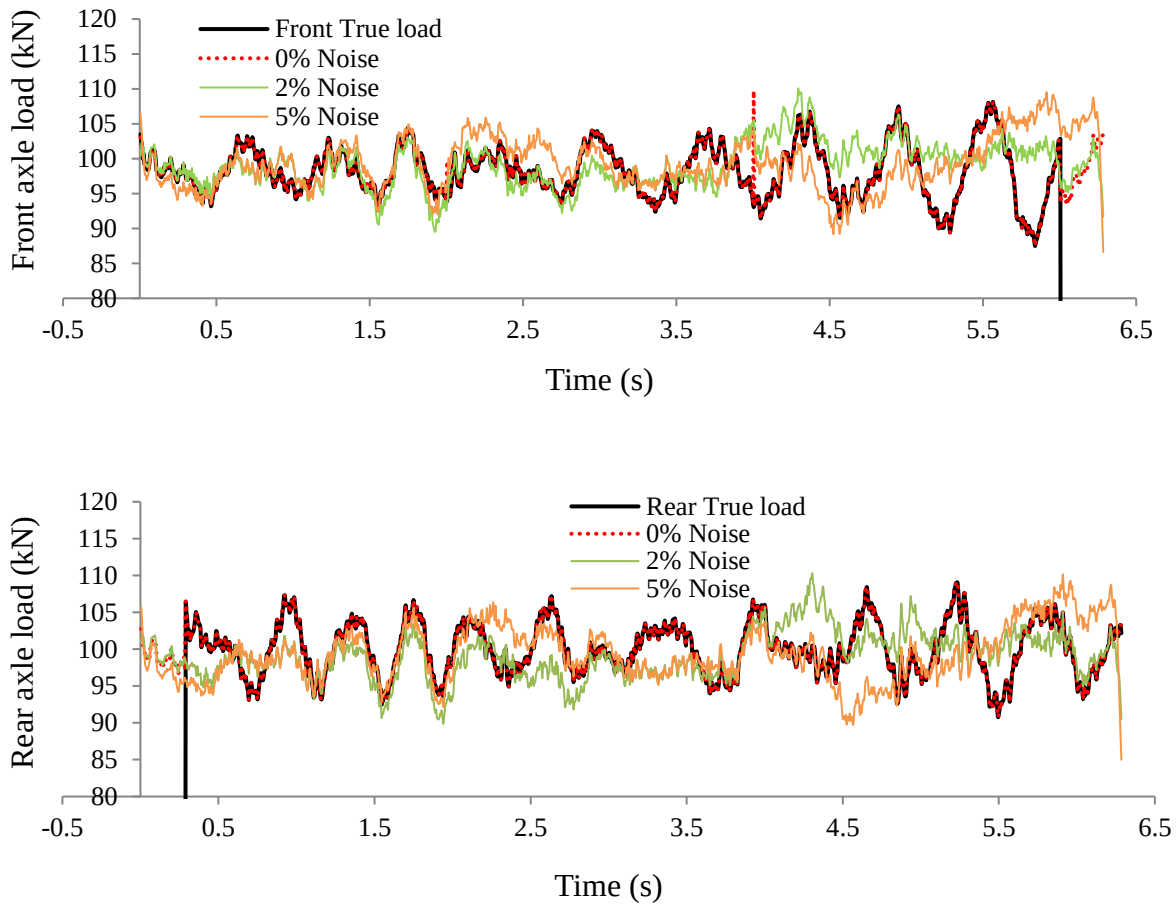

Figure 3-14: Effect of noise on load identification at road roughness level A- speed 15 m/s

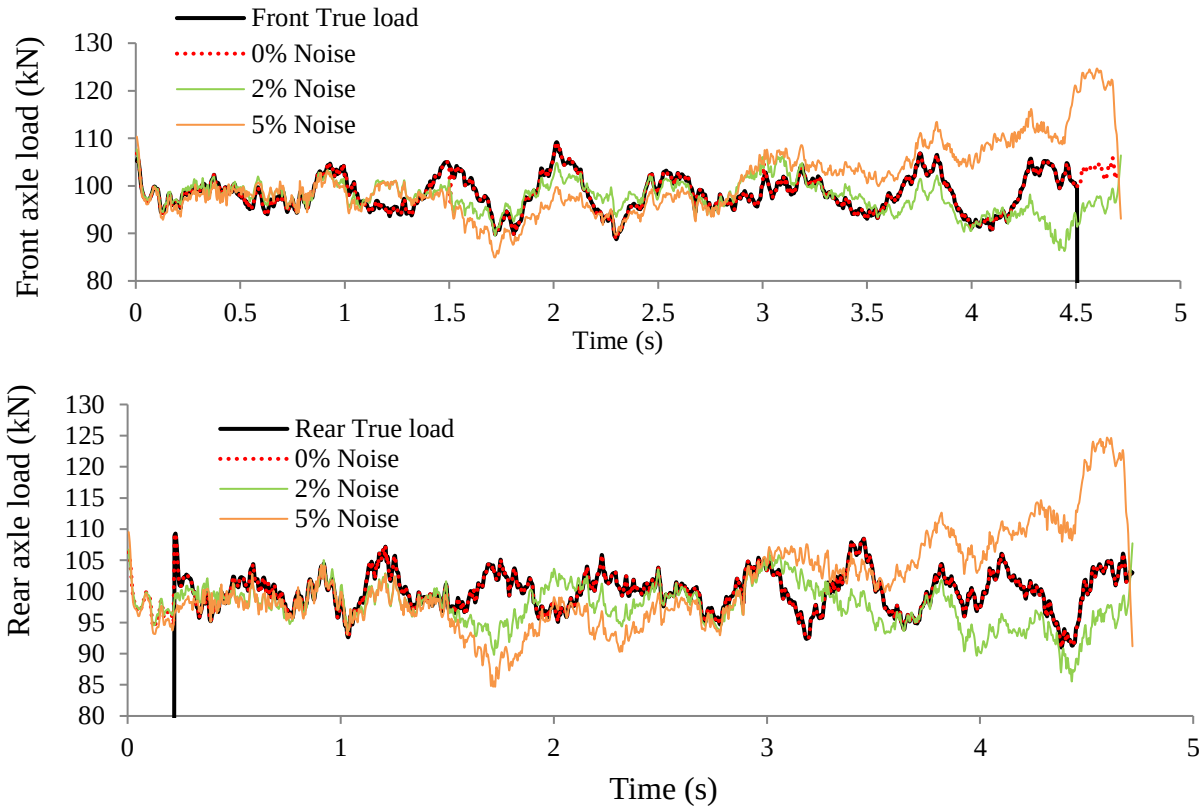

Figure 3-15: Effect of noise on load identification at road roughness level A and speed 20 m/s

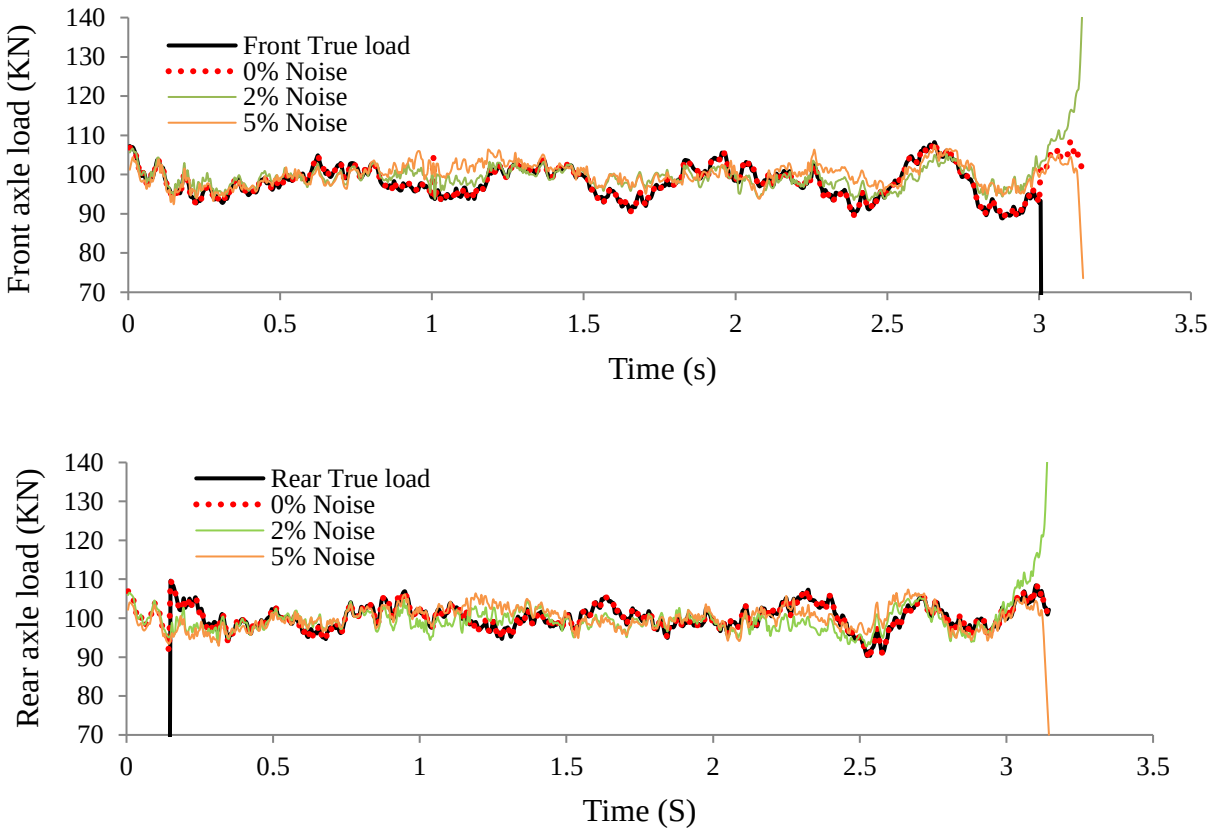

Figure 3-16: Effect of noise on load identification at road roughness level A and speed 30 m/s

`

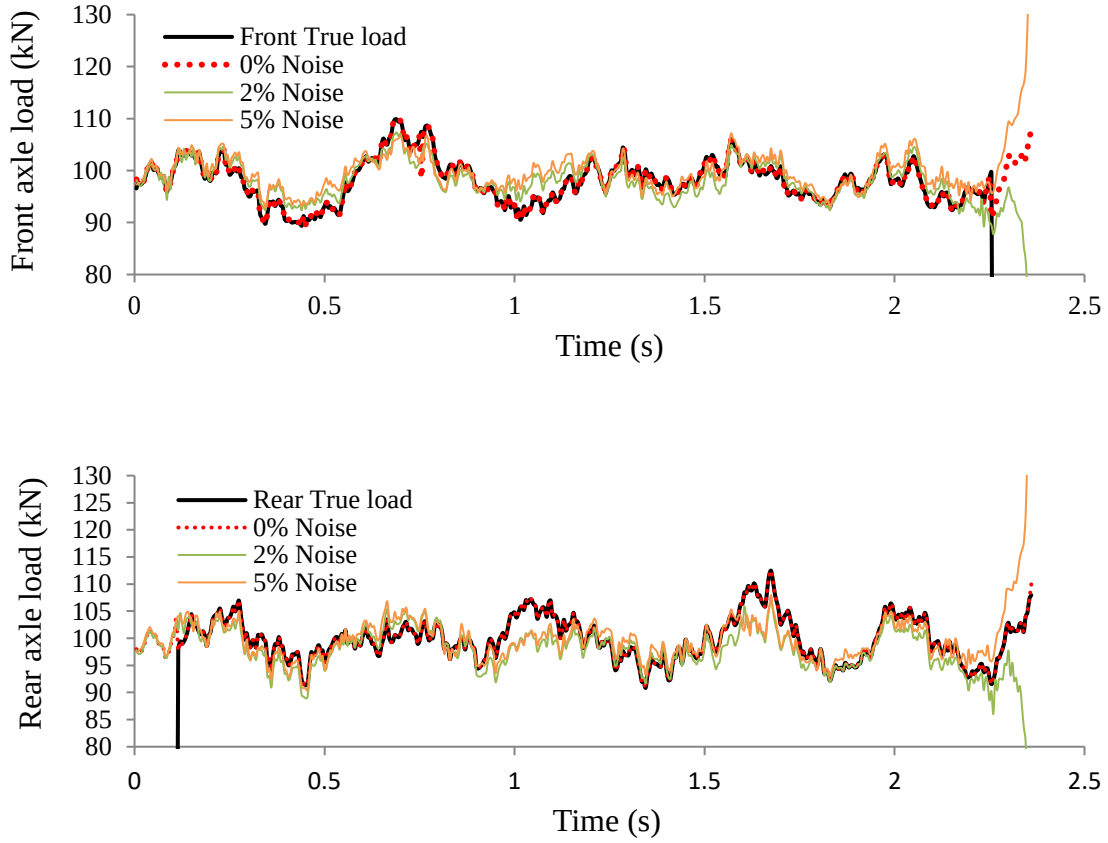

Figure 3-17: Effect of noise on load identification at road roughness level A and speed 40 m/s

3.5.2. The Effect of road roughness level and vehicle speed

In this section, the accuracy of the method at different road roughness levels (A, B, and C) as well as different vehicle speeds (15 m/s, 20 m/s, 30 m/s, and 40 m/s) with and without noise has been investigated, and results are tabulated in Table 3-11 and Table 3-12. It is important to note that since both road roughness and measurement noise are produced by random functions in MATLAB, the error values might not be the same at different runs of the program.

Table 3-11: The relative error (%) of the identified forces at noise 0%

Speed (m/s)	15			20			30			40		
Road roughness	A	B	C	A	B	C	A	B	C	A	B	C
Front axle load	0.01	0.05	0.25	0.01	0.01	-	0.1	0.1	-	0.02	-	-
Rear axle load	0.16	0.15	0.13	0.2	0.21	-	0.4	0.3	-	0.46	-	-

`

Table 3-12: The relative error (%) of the identified forces at noise 2%

Speed (m/s)	15			20			30			40		
Road roughness	A	B	C	A	B	C	A	B	C	A	B	C
Front axle load	3.2	10.8	32.5	2.8	12.7	-	2.6	9.6	-	2.3	-	-
Rear axle load	3.5	11.8	29.2	3.6	18.0	-	4.6	12.4	-	3.4	-	-

According to Table 3-11, when there is not measurement noise, the method is not sensitive to speed and road roughness level, and errors are very close to zero showing the accuracy of the method. However, in the existence of the measurement noise (Table 3-12), the accuracy of the method is affected at road roughness levels “B” and “C”.

To investigate further, the average of the identified loads and true loads has also been compared and results can be seen in Figure 3-18 to Figure 3-27, as well as Table 3-13 and Table 3-14. From Table 3-13 and Table 3-14, it can be concluded that when there is no measurement noise, average identified loads are quite close to average true loads. In existence of 2% measurement noise, there are very small errors, except for the case in which a vehicle is passing the road with surface roughness level “C” at speed 15 m/s, and that is because the excitation frequency is close to the bridge natural frequency.

`

Table 3-13: The error (%) of the average of identified forces with 0% measurement noise

Speed (m/s)	Roughness	Ave. of front axle load (kN)			Ave. of rear axle load (kN)		
		F_{true}	F_{id}	Error (%)	F_{true}	F_{id}	Error (%)
15	A	98.09	98.17	0.09	99.92	99.92	0.00
	B	98.5	98.4	0.06	99.99	99.99	0.00
	C	98.3	98.3	0.02	100.13	100.13	0.00
20	A	98.26	98.36	0.1	99.89	99.89	0.00
	B	98.88	98.90	0.01	100.22	100.23	0.00
30	A	98.32	98.49	0.17	99.89	99.89	0.00
	B	98.46	98.55	0.09	99.53	99.52	0.00
40	A	97.86	98.02	0.16	99.65	99.65	0.00
	B	98.78	98.71	0.07	99.36	99.36	0.00

Table 3-14: The error (%) of the average of identified forces with 2% measurement noise

Speed (m/s)	Roughness	Ave. of front axle load (kN)			Ave. of rear axle load (kN)		
		F_{true}	F_{id}	Error (%)	F_{true}	F_{id}	Error (%)
15	A	98.3	99.4	1.07	99.9	99.1	0.72
	B	98.2	102.1	3.8	100.05	101.8	1.7
	C	97.5	113.8	16.7	99.9	113.5	13.5
20	A	98.2	99.03	0.8	100.01	98.7	1.3
	B	97.5	98.08	0.5	99.2	94.9	4.3
30	A	98.3	99.5	1.2	100.12	100.15	0.02
	B	98.3	99.2	0.9	99.7	100.8	1.02
40	A	98.2	99.1	0.9	100.1	101.2	1.1
	B	99.4	99.7	0.3	98.2	97.5	0.7

`

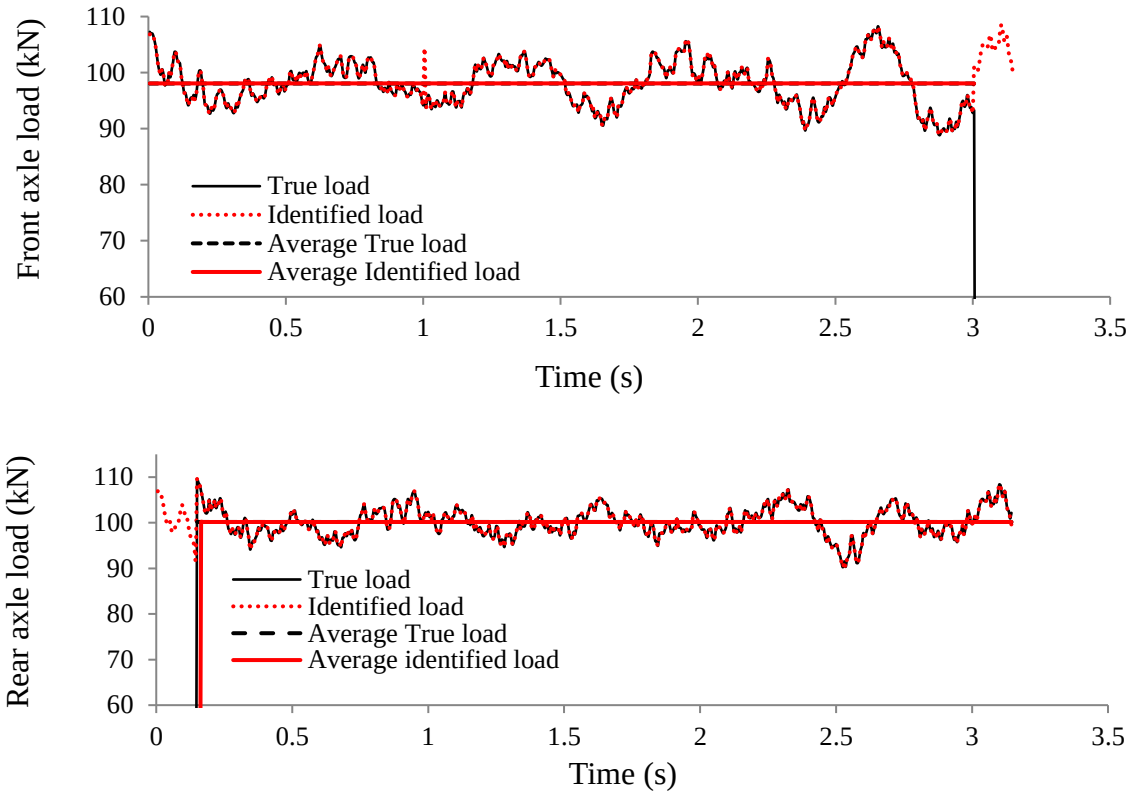

Figure 3-18: Identified loads at road roughness level A- speed 30 m/s- 0% noise;

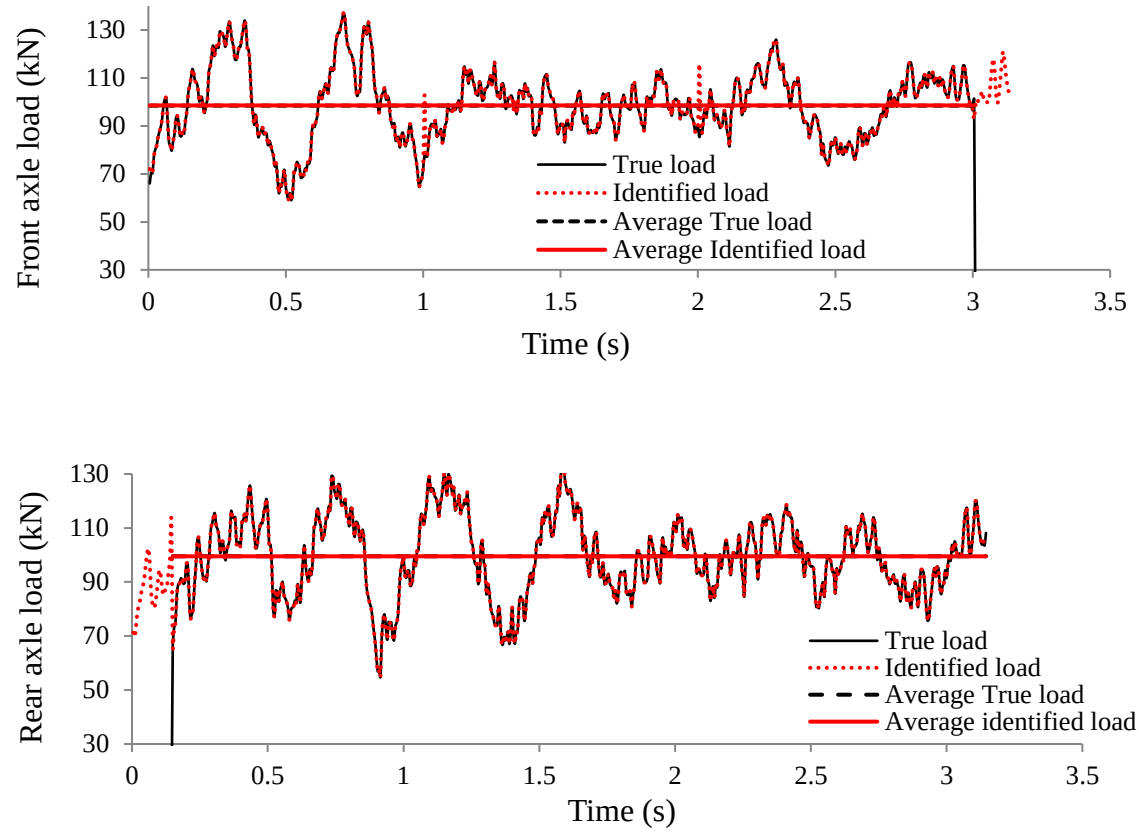

Figure 3-19: Identified loads at road roughness level B- speed 30 m/s- 0% noise;

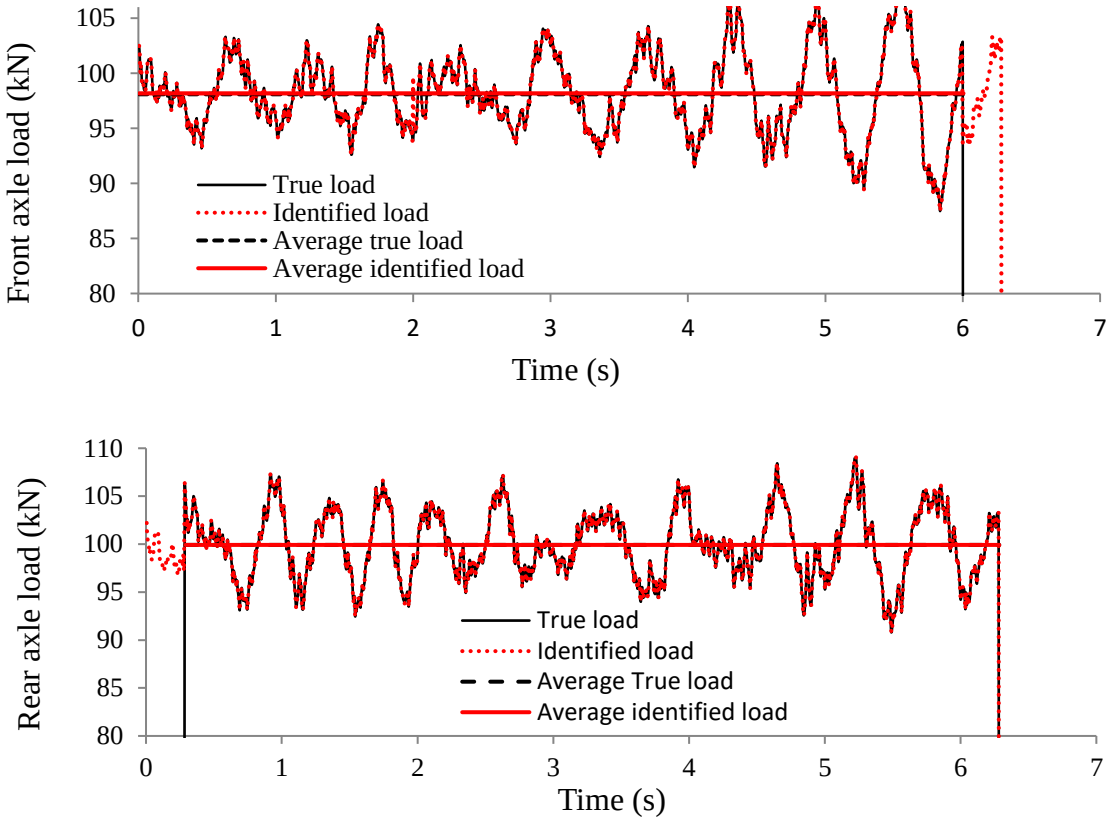

Figure 3-20: Identified loads at road roughness level A- speed 15 m/s- 0% noise;

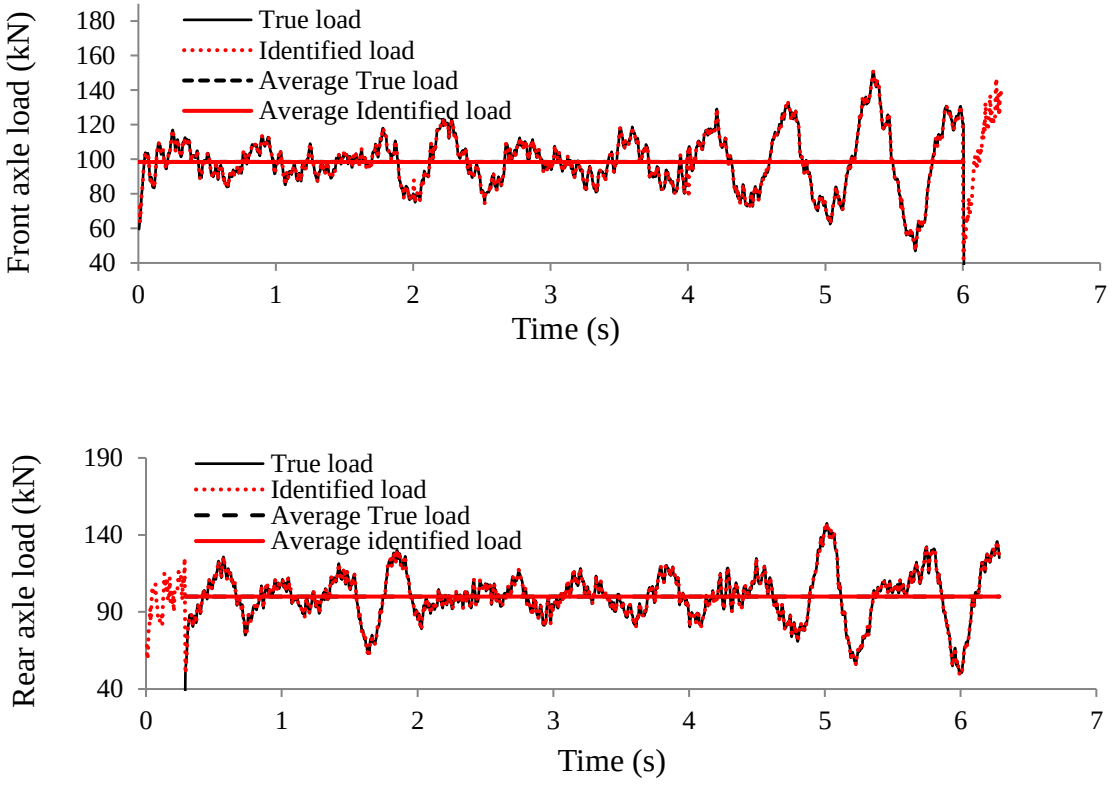

Figure 3-21: Identified loads at road roughness level B- speed 15 m/s- 0% noise;

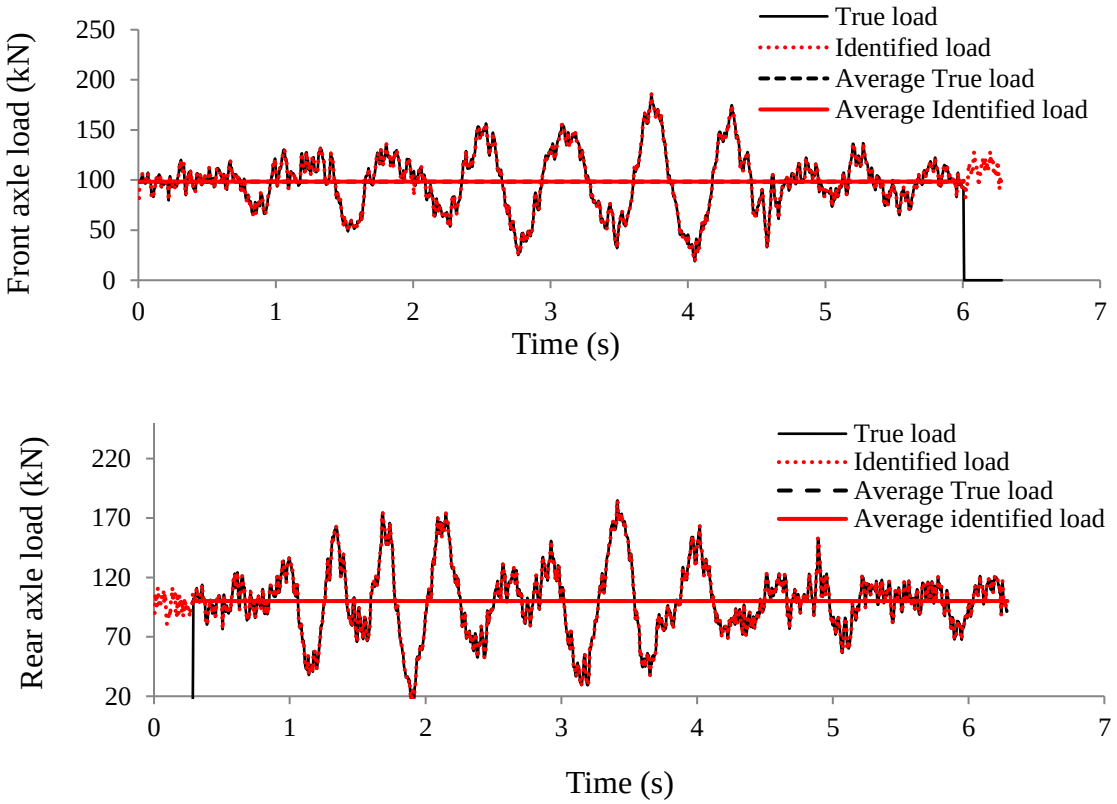

Figure 3-22: Identified loads at road roughness level C- speed 15 m/s- 0% noise;

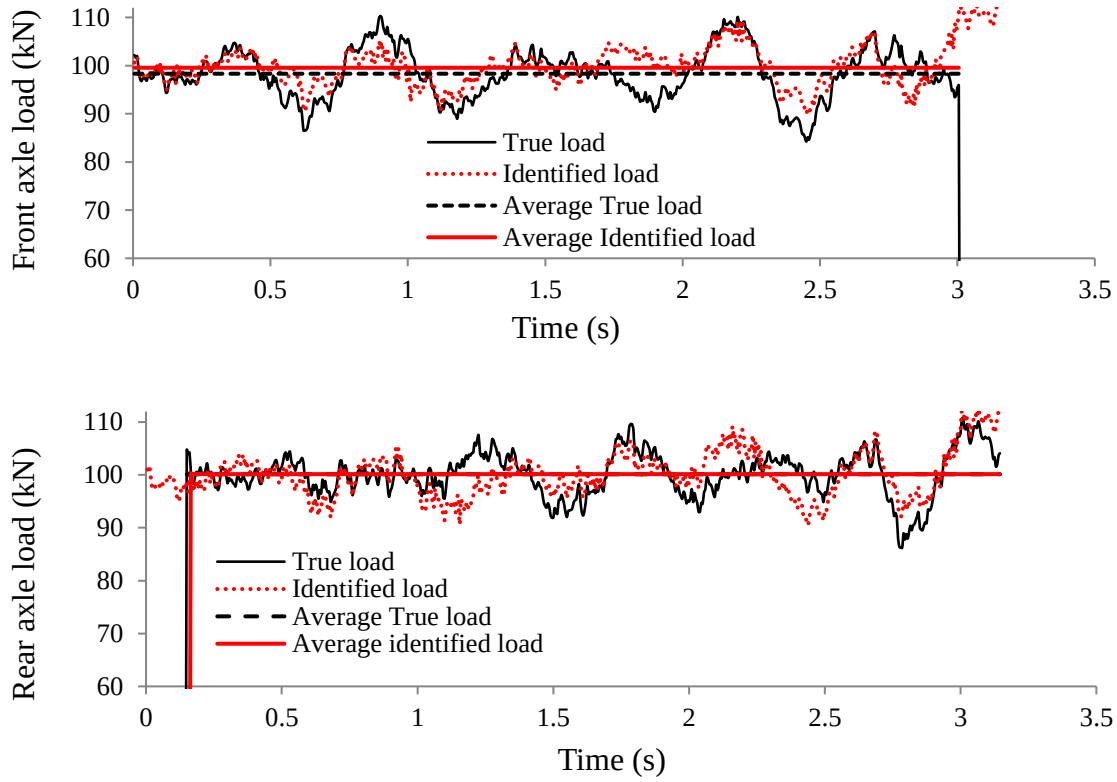

Figure 3-23: Identified loads at road roughness level A- speed 30 m/s- 2% noise;

`

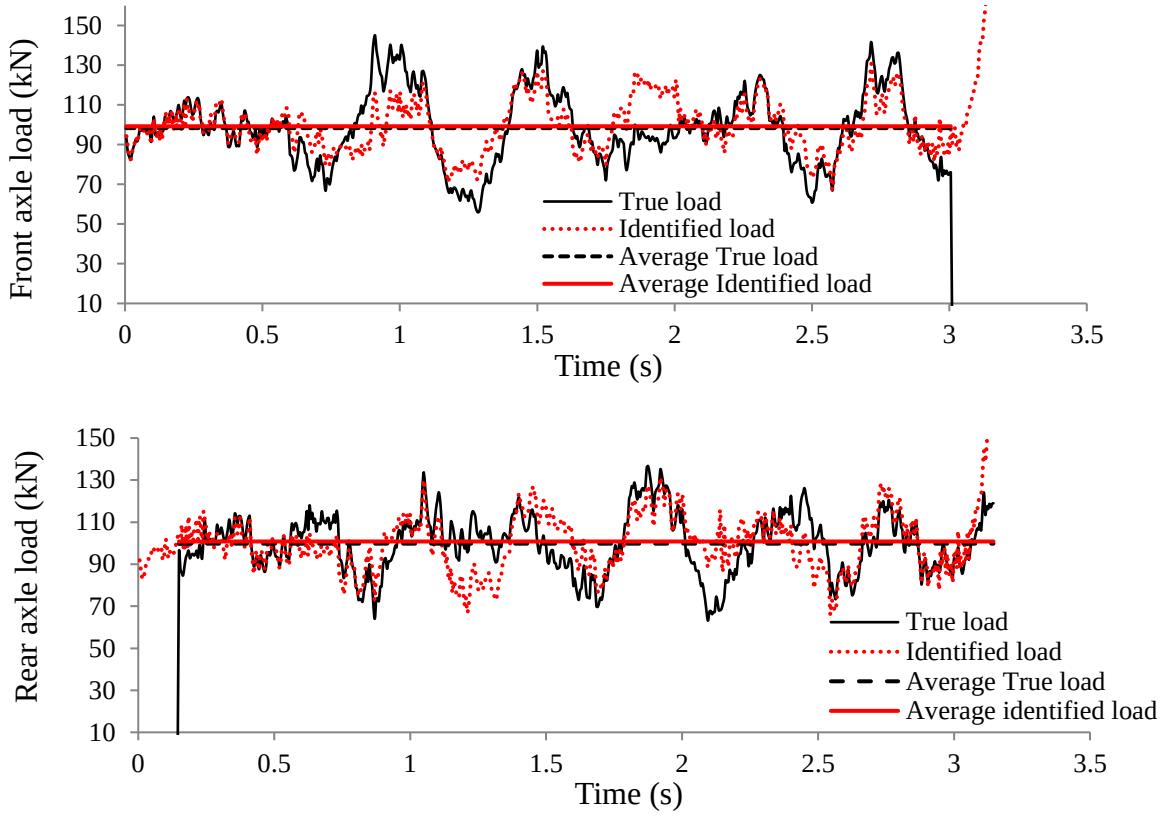

Figure 3-24: Identified loads at road roughness level B- speed 30 m/s- 2% noise;

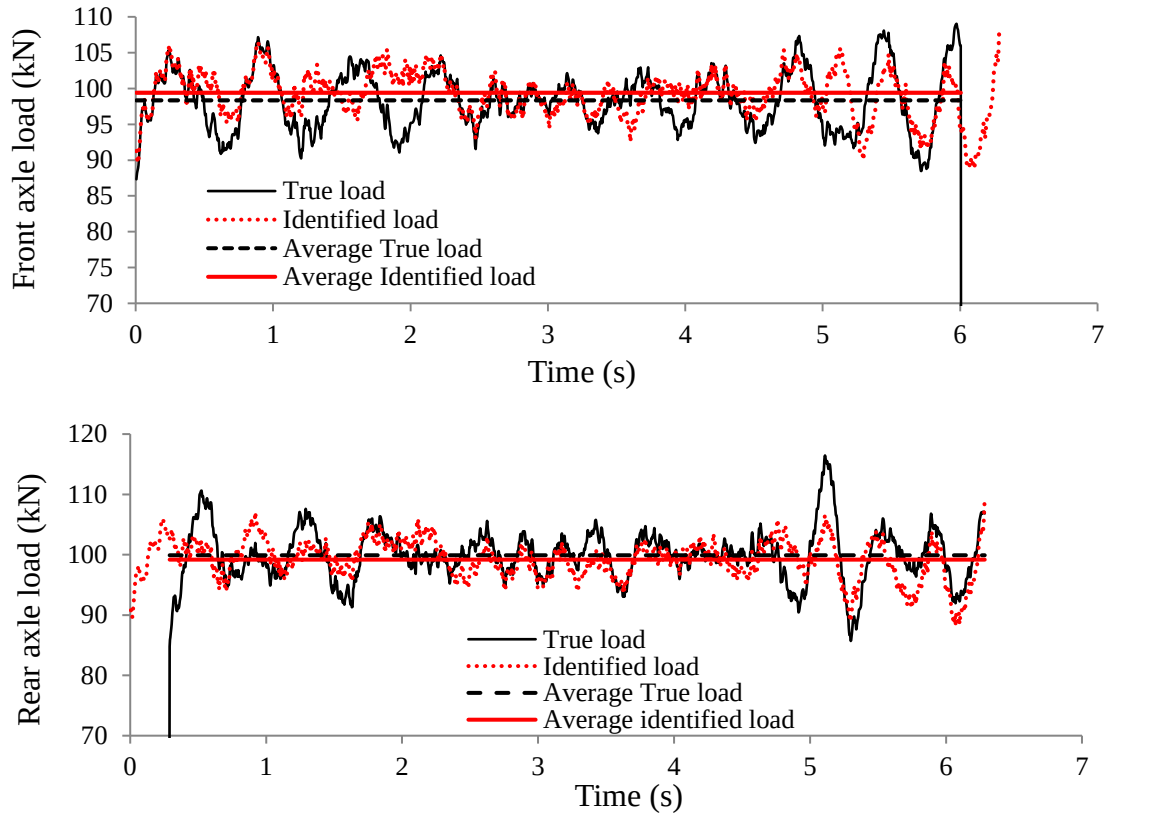

Figure 3-25: Identified loads at road roughness level A- speed 15 m/s- 2% noise;

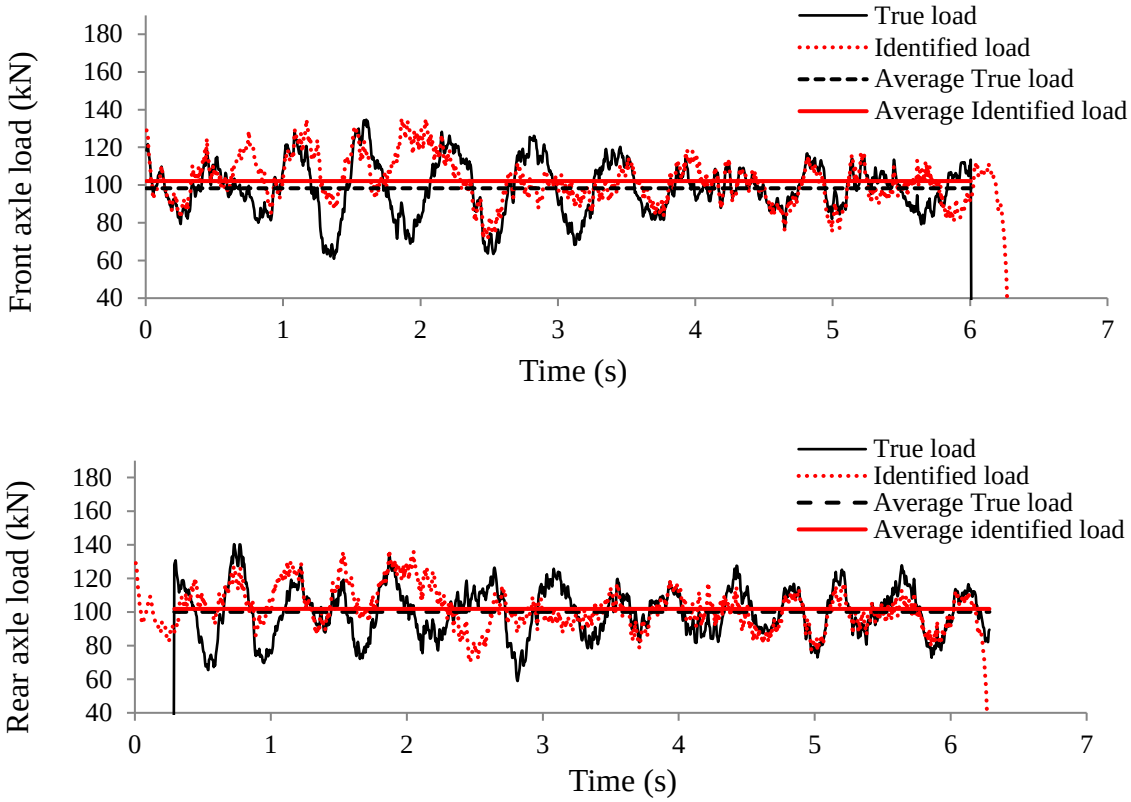

Figure 3-26: Identified loads at road roughness level B- speed 15 m/s- 2% noise;

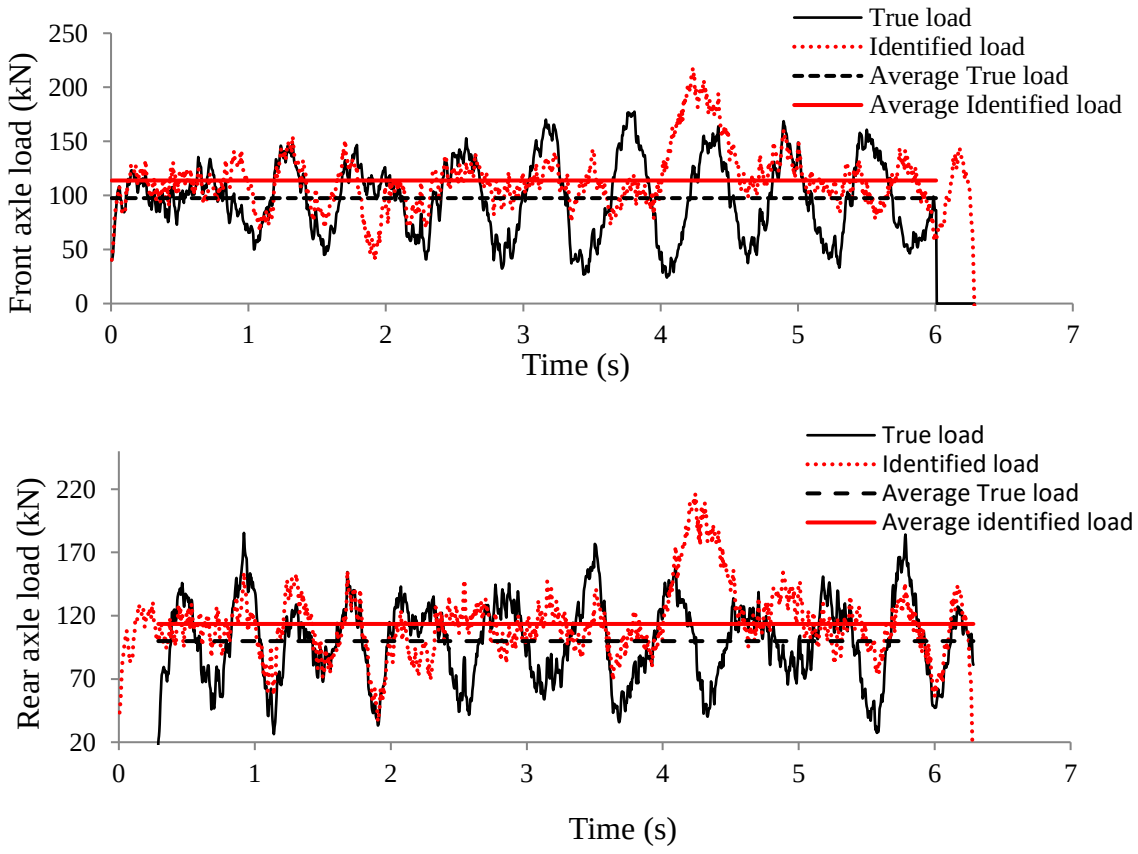

Figure 3-27: Identified loads at road roughness level C- speed 15 m/s- 2% noise;

`

3.6. Conclusion

In this chapter, the explicit form of the Newmark-β method has been applied to identify moving loads passing over a bridge, considering road roughness. Response measurements are simulated by dynamic forward analysis of the vehicle-bridge interaction (VBI) system. The general form of the explicit form of the Newmark-β method is generated to do this. The half-car model vehicle, with four degrees of freedom, is adopted in this study and the Generalized Tikhonov Regularization method is used to provide bounds on the solution.

Results show that the method is not sensitive to sensor placement and a good accuracy can be achieved using three accelerometers. When there is not measurement noise, the proposed method is not sensitive speed, and road roughness, however, when there is measurement noise, the identification accuracy is reduced at road roughness levels “B” and “C”. There is not any constraint to identify moving loads when the road surface level is “A”.

The proposed method is able to identify moving loads without disruptions when passing through the supports which is a significant improvement in moving load identification. Also, it is reliable in estimating the static load of a moving vehicle.

`

`

Chapter 4. Simultaneous identification of bridge structural parameters and moving loads

4.1. Introduction

This chapter describes the simultaneous identification of bridge structural parameters and moving loads based on the Newmark-β method. The formulations of the bridge equation of motion, vehicle model, vehicle-bridge interaction system, and road surface roughness are explained in Chapter 3. Section 4.2 describes the element damage index, sensitivities of dynamic responses, and how it can be used to detect damage. The iterative identification procedure to simultaneously identify moving loads and structural parameters is also described in this section. In section 4.3, numerical analyses of a single-span simply supported bridge are conducted to demonstrate the accuracy and efficiency of the proposed method. The effects of measurement noise, sensor placement, damage location and extension, vehicle speed, and road surface roughness on the accuracy of the method are investigated. In section 4.4, a two-span continuous bridge is studied to check if mid-supports affect the accuracy of the method. Conclusions derived in this chapter can be found in section 4.5.

4.2. Damage Identification formulations

4.2.1 Element Damage Index

The mass matrix of a structure is assumed to remain unchanged as well as decreasing the stiffness matrix of the whole element uniformly due to damage. The flexural rigidity, EI_i of the i^{th} finite element of the beam, becomes $\beta_i EI_i$ when there is damage. The fractional change in stiffness of an element can be expressed as (Zhu and Hao 2007):

$$\Delta \boldsymbol{k}_i = \boldsymbol{k}_i - \widetilde{\boldsymbol{k}}_i = (1-\beta_i)\boldsymbol{k}_i \tag{4-1}$$

where $\boldsymbol{k}_i$ and $\widetilde{\boldsymbol{k}}_i$ are the i^{th} element stiffness matrices of the undamaged and damaged beam, respectively. The value of β_i ranges between 0 and 1, where $\beta_i = 1$ indicates no stiffness loss in the i^{th} element while $\beta_i = 0$ indicates the stiffness of the i^{th} element is completely lost.
The stiffness matrix of the damaged structure is the assemblage of the entire element stiffness matrix $\widetilde{\boldsymbol{k}}_i$

$$\boldsymbol{K} = \sum_{i=1}^{N} \boldsymbol{A}_i^T \widetilde{\boldsymbol{k}}_i \boldsymbol{A}_i = \sum_{i=1}^{N} \beta_i \boldsymbol{A}_i^T \boldsymbol{k}_i \boldsymbol{A}_i \tag{4-2}$$

where $\boldsymbol{A}_i$ is the extended matrix of element nodal displacement that facilitates assembling of global stiffness matrix from the constituent element stiffness matrix.

`

4.2.2. Structural response sensitivities

The sensitivity method can be applied once forces are identified in order to effectively identify any local damage, and thereby quantify the effects of parameter variations on the results calculated. The most important difficulty to consider is the calculation of the sensitivity matrix, and while there are many methods, this study makes use of the direct differentiation method (Abbasnia, Mirzaee & Shayanfar 2015).

Performing differentiation on both sides of Equation 3-5 with respect to the parameter β_i , and assuming Rayleigh damping is used in the system, we have,

$$\boldsymbol{M}\frac{\partial \ddot{\boldsymbol{y}}}{\partial \beta_i}+\boldsymbol{C}\frac{\partial \dot{\boldsymbol{y}}}{\partial \beta_i}+\boldsymbol{K}\frac{\partial \boldsymbol{y}}{\partial \beta_i}=-\frac{\partial \boldsymbol{K}}{\partial \beta_i}\boldsymbol{y}-a_2\frac{\partial \boldsymbol{K}}{\partial \beta_i}\dot{\boldsymbol{y}} \qquad 4\text{-}3$$

where a_2 is the Rayleigh damping co-efficient. The responses of the structure have been calculated from Equation 3-23. The response sensitivities are solved by the explicit form of the Newmark-β method. The initial values of the dynamic responses and the sensitivities are considered equal to zero.

4.2.3. Damage detection applying dynamic response sensitivity analysis

The local damage of the structure can be identified using Taylor series as follows:

$$\ddot{\boldsymbol{X}}^m-\ddot{\boldsymbol{X}}=\frac{\partial \ddot{\boldsymbol{X}}}{\partial \boldsymbol{\beta}}\boldsymbol{\beta} \qquad 4\text{-}4$$

where $\ddot{\boldsymbol{X}}^m$ = measured acceleration responses, $\ddot{\boldsymbol{X}}$ = calculated acceleration responses, $\boldsymbol{\beta}$ = vector of perturbation of the parameter, and $\frac{\partial \ddot{\boldsymbol{X}}}{\partial \boldsymbol{\beta}}$ = acceleration sensitivities. The high order terms due to the changes in the element have been eliminated. Having sensitivities from Equation 4-3, the unknown local changes of the elements can be solved by Equation 4-5. This problem is ill-posed in nature and the standard-form of Tikhonov regularization method is adopted to solve it as follows:

$$\boldsymbol{\beta}=\left(\left(\frac{\partial \ddot{\boldsymbol{X}}}{\partial \boldsymbol{\beta}}\right)^T\frac{\partial \ddot{\boldsymbol{X}}}{\partial \boldsymbol{\beta}}+\lambda^2\boldsymbol{I}\right)^{-1}\left(\frac{\partial \ddot{\boldsymbol{X}}}{\partial \boldsymbol{\beta}}\right)^T(\ddot{\boldsymbol{X}}^m-\ddot{\boldsymbol{X}}) \qquad 4\text{-}5$$

The optimal regularization parameter λ is obtained by the L-curve method.

The structural matrices are updated and sensitivities are recalculated based on the updated matrices. Vector $\boldsymbol{\beta}$ is recalculated until convergence is reached with

`

$$\left\| \frac{\boldsymbol{E}_{k+1} - \boldsymbol{E}_k}{\boldsymbol{E}_{k+1}} \right\| \leq Tol \quad 4\text{-}6$$

$$\left\| \frac{\boldsymbol{X}_{k+1} - \boldsymbol{X}_k}{\boldsymbol{X}_{k+1}} \right\| \leq Tol \quad 4\text{-}7$$

where k is the number of iterations and the tolerance is equal to 10^{-6} in this chapter. The error of damage identification is defined as follows:

$$damage\ identification\ error = \left\| \frac{\boldsymbol{E}_{identified} - \boldsymbol{E}_{true}}{\boldsymbol{E}_{true}} \right\| \times 100\% \quad 4\text{-}8$$

Moving load identification error can be obtained by:

$$Identified\ Load\ Error = \left\| \frac{\boldsymbol{F}_{id} - \boldsymbol{F}_{real}}{\boldsymbol{F}_{real}} \right\| \times 100\% \quad 4\text{-}9$$

The implementation procedure of the simultaneous identification of structural parameters and moving loads is as follows:

Step 1: Conduct a dynamic measurement of the structure and guess the initial value of EI.

Step 2: Obtain the matrix of system Markov parameters, **H**, from Equation 3-21.

Step 3: Identifying moving loads from Equation 3-22.

Step 4: Compute the responses of the structure from Equation 3-18.

Step 5: Compute structural response sensitivities from Equation 4-3.

Step 6: Calculate structural parameters perturbation from Equation 4-5.

Step 7: Update the Finite element model.

Step8: Repeat Steps 2-6 until the convergence condition is met.

4.3. Numerical Example I: Simply supported single span bridge

The vehicle-bridge system explained in section 3.4. is used to demonstrate the applicability and effectiveness of the proposed algorithm. The time step is 0.005 seconds in the simulation. The finite element model (FEM) of the bridge includes 15 Euler-Bernoulli beam elements, with 16 nodes. Each node has two degrees of freedom, rotation and vertical. The bridge mass information and damping ratios are assumed to be known.

The effects of damage properties, sensor placement, road surface roughness, vehicle speed, and measurement noise have been investigated. It should be noted that no prior knowledge is required of the road roughness and vehicle information for the proposed method to be applied, with the exception of the axle spacing and speed, which can both be easily obtained by the optical sensors installed at the entry and exit locations of the bridge. The system

`

processor used in this study is an Intel® Core ™ i7-4790 CPU @ 3.60 GHz and the installed memory (RAM) is 32.0 GB.

4.3.1. A numerical verification of the proposed method

Here, a detailed study of the effects of damage location and its extension on the accuracy of the identification results is carried out. Seventeen different damage scenarios are investigated, as shown in Table 4-1. The vehicle moves over the bridge at speed 40 m/s, and the road surface roughness is assumed to be "A" (according to chapter 3). Measured accelerations have been simulated by a forward analysis of the vehicle-bridge interaction system using the Newmark-β method. Full sensor placement is used. Noise is not considered here. Convergence tolerance is applied as 10^{-6}.

Two types of damage can be seen in Table 4-1. In single damage cases, only one element of the bridge is damaged at a time to study the effect of different damage levels. Elements 8, 10, 12, and 15 are considered for this research. By having different damage elements, the effect of the damage location is studied. Scenarios 16 and 17, including two damaged elements, are intended to investigate the efficiency of the method when there are multiple damaged elements. The percentage error of identified loads (I.L.), reconstructed response (Rec. Acc.), and damage identification error (D.I.), as well as the total time and the number of iterations (N.I.) to converge, are tabulated in Table 4-2. Identified stiffness reduction for each type of damage is shown in Figures 5.2-5.6. Scenario #16 is fixed for further studies in this research.

Table 4-1: Different damage scenarios

Damage scenario	Damage type	Damage location	Reduction in elastic modulus (%)	Noise
#1	Single	Element 8	60	Nil
#2			50	
#3			40	
#4			30	
#5			20	
#6			10	
#7	Single	Element 10	50	Nil
#8			30	
#9			10	

`

#10	Single	Element 12	50	Nil
#11			30	
#12			10	
#13	Single	Element 15	50	Nil
#14			30	
#15			10	
#16	Multiple	Elements 8 and 10	20	Nil
#17			10	

In reality, both true loads and structural parameters are unknown, so it is not possible to quantify accuracy by Equations 4-9 and 4-8. In this case, responses can be reconstructed by inputting the identified moving loads and structural parameters into Equation 3-22. This has two benefits; one of which is to check the accuracy of identification and the other being to predict dynamic structural responses such as acceleration at locations where sensors are unavailable or difficult to install. The error of reconstructed responses can be calculated from Equation 4-10.

$$\text{Reconstructed Response Error} = \left\| \frac{\text{Reconstructed } X - X}{X} \right\| \times 100\% \qquad 4\text{-}10$$

where X is the assembled measured acceleration vector. Here, the acceleration responses are used. The results are tabulated in Table 4-2. Furthermore, the number of iterations (N.I.) and the total time to meet the convergence value are recorded in the table.

Table 4-2: The results obtained from different damage scenarios

Damage scenario	Total time hr:min:sec	N.I.	I.L. error (%)		D.I. error (%)	Rec. Acc. error (%)
			Front	Rear		
#1	1:00:42	4518	0.33	1.01	0.44	0.15
#2	1:06:39	4136	0.21	0.91	0.36	0.12
#3	0:23:06	1688	0.06	0.78	0.07	0.02
#4	0:25:54	1971	0.13	0.78	0.03	0.00
#5	0:24:05	1705	0.05	0.76	0.03	0.01
#6	0:31:54	2402	0.03	0.79	0.08	0.03
#7	00:34:50	2677	0.1	0.83	0.2467	0.06
#8	00:40:08	3013	0.01	0.78	0.0653	0.02

`

#9	00:21:06	1574	0.15	0.86	0.1549	0.05
#10	00:50:06	3440	0.05	0.77	0.0749	0.02
#11	00:26:27	1962	0.02	0.76	0.0419	0.01
#12	00:26:26	1928	0.08	0.82	0.0498	0.02
#13	00:25:58	2017	0.07	0.83	0.1154	0.05
#14	00:26:32	1798	0.07	0.77	0.0528	0.01
#15	00:13:51	1094	0.07	0.77	0.0461	0.02
#16	00:28:22	2273	0.1	0.85	0.2004	0.06
#17	00:27:23	1868	0.09	0.86	0.1513	0.04

Table 4-2 indicates that moving loads are identified with less than 1% error in all cases. In all damage scenarios, acceleration has been reconstructed with less than 0.2% error. Therefore, this method can be used to predict acceleration at nodes that are not accessible to be measured directly by accelerometers. The damage identification error in all cases is less than 0.5%. Identified stiffness reduction of damage scenarios #1 to #17 is shown in Figure 4-1 to Figure 4-5. Damaged elements are detected and quantified precisely. The identified stiffness reduction of all intact elements is very close to zero, which shows the accuracy of the simulation. Results show that the method is robust and not sensitive to different damage locations and extensions. In the study by O'Brien et.al. (2015), the method is sensitive to damage location and it can be identified well only if it is close to the centre of the beam.

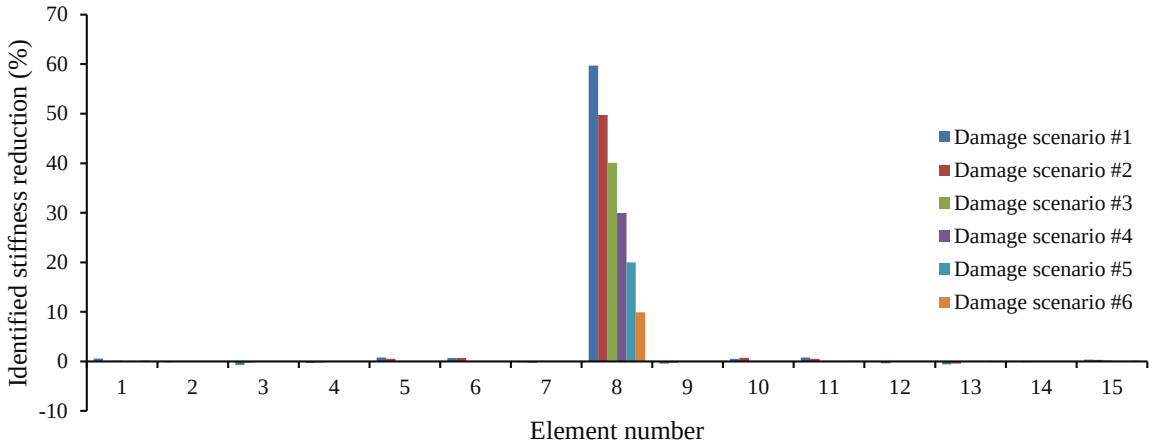

Figure 4-1: Accuracy of the method for different levels of damage in element 8

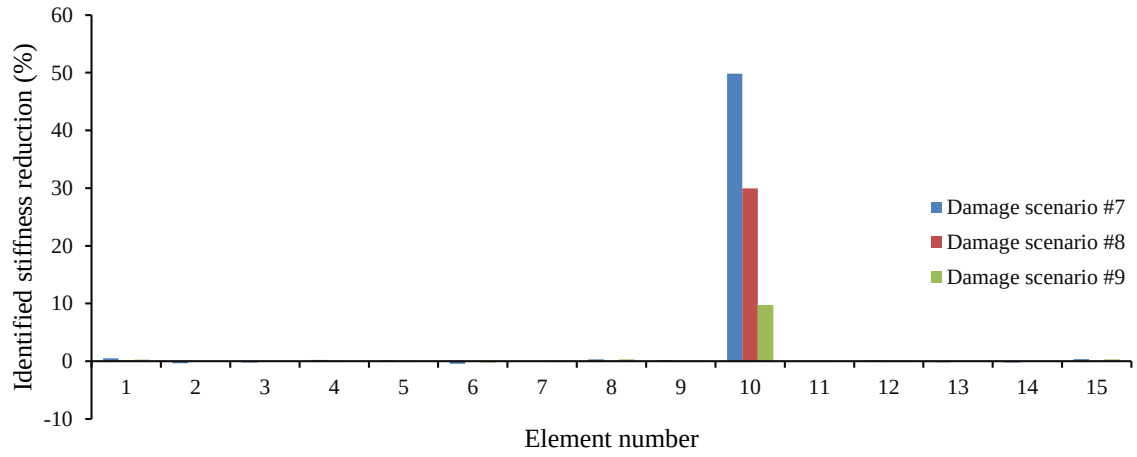

Figure 4-2: Accuracy of the method for different levels of damage in element 10

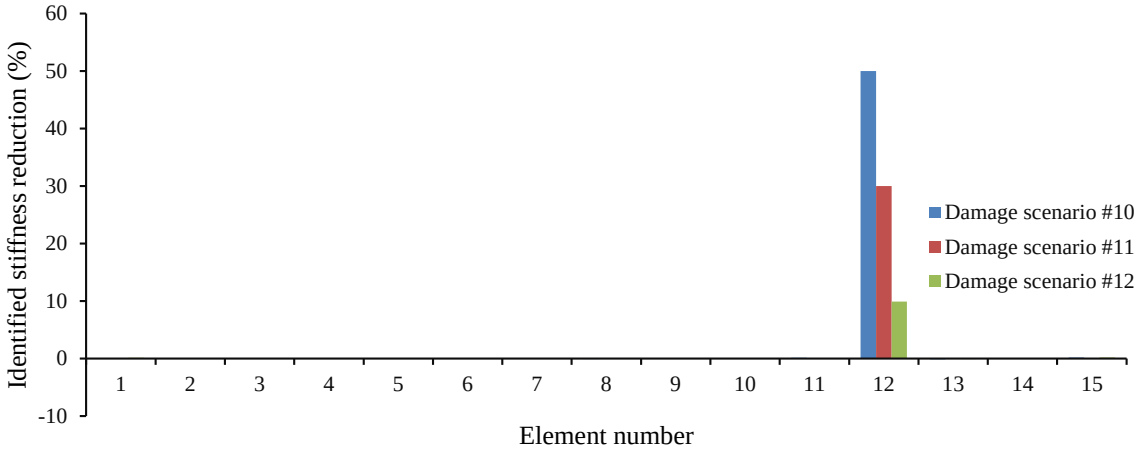

Figure 4-3: Accuracy of the method for different levels of damage in element 12

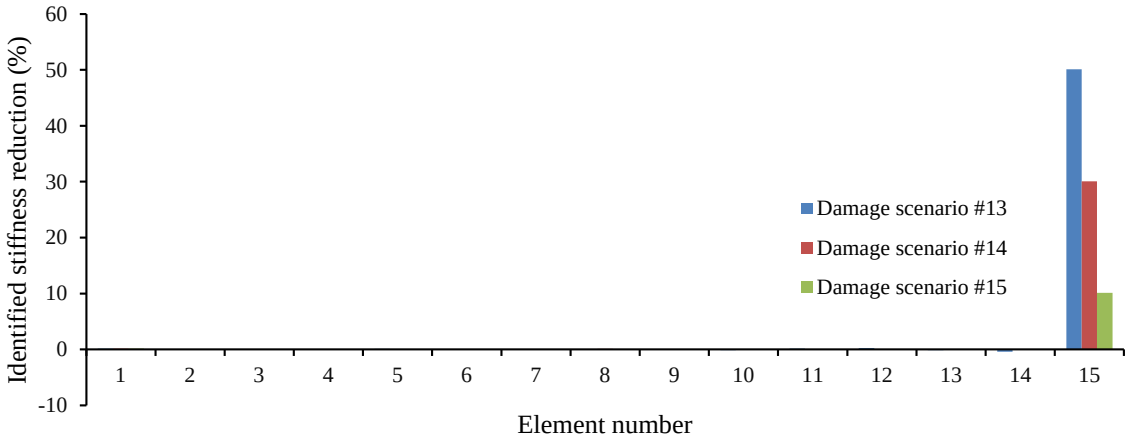

Figure 4-4: Accuracy of the method for different levels of damage in element 15

`

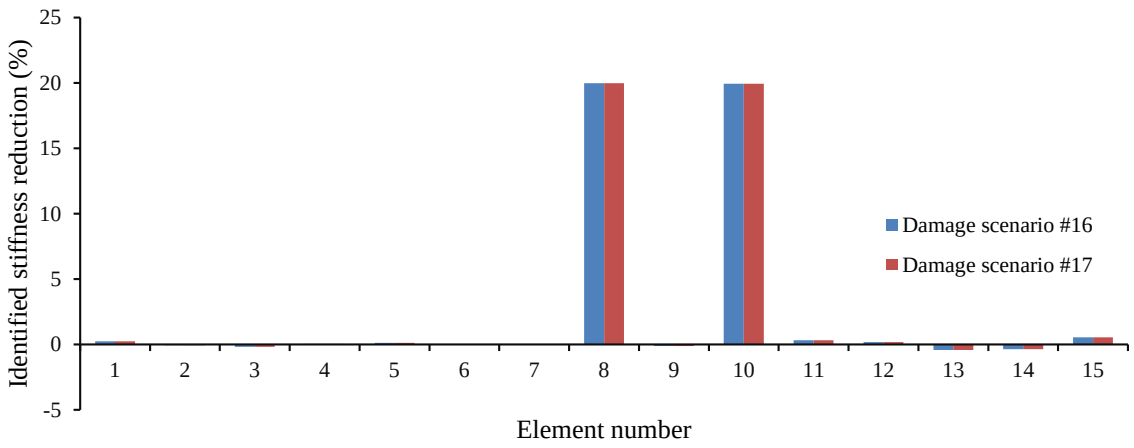

Figure 4-5: Accuracy of the method for different levels of damage in elements 8 and 10

4.3.2. Effect of sensor placements

In the last section, a full sensor placement was used to examine the accuracy and robustness of the method for different damage locations and extensions. Now, as tabulated in Table 4-3, the effect of 5 different sensor placements has been investigated. Sensors are approximately equally spaced.

In this section, the vehicle moves over the bridge at a speed of 40 m/s. The road surface roughness is assumed to be "A". Damage scenario #16 is applied here. Measured accelerations have been simulated by a forward analysis of the vehicle-bridge interaction system using the Newmark-β method. Noise is not considered, and convergence tolerance is applied as 10^{-6}. The percentage error of identified loads (I.L.), reconstructed response (Rec. Acc.), and damage identification error (D.I.), as well as the total time and the number of iterations (N.I.) to converge, are tabulated in Table 4-4.

Table 4-4 shows that all five cases of sensor placement are able to identify moving loads and structural parameters with less than 1% percent error and to reconstruct acceleration with less than 0.08% error. In this aspect this method is superior to that proposed by Zhu and law (2007), needing full sensor placement, and the method studied by O'Brien (2015) which is effective only when the sensor is close to the damage zone. Identified stiffness reduction by these sensor placements is shown in Figure 4-6. Damage has been detected and quantified very precisely and identified stiffness reduction in intact elements is very close to zero, which demonstrates the accuracy of the simulation. Sensor placement S3 with the least number of sensors is associated with the most computation time. Here, considering both computation time and number of sensors, sensor placement of the case with 6 accelerometers is the optimized one. However, in reality there might be some limitations due to accessible locations or budget,

`

then 3 or 5 sensors could be sufficient as well. Case S6 is fixed for further studies in this research.

Table 4-3: Different sensor placements

Case number	Number of sensors	Nodes with accelerometers
S14	14	All nodes except supports
S3	3	5, 9,13
S4	4	4, 7, 10, 13
S5	5	3, 6, 8, 11, 14
S6	6	3, 5, 7, 10, 12, 14

Table 4-4: Identification results by different sensor placements

Sensor placement	Total time hr:min:sec	N.I.	I.L. error (%)		D.I. error (%)	Rec. Acc. Error (%)	Noise
			Front	Rear			
S3	1:23:57	6373	0.06	0.78	0.0743	0.00	0%
S4	00:39:39	3224	0.82	0.13	0.54	0.07	
S5	00:53:14	4046	0.88	0.04	0.12	0.03	
S6	00:25:37	2307	0.08	0.86	0.2061	0.05	
S14	00:28:22	2273	0.1	0.8	0.2004	0.06	

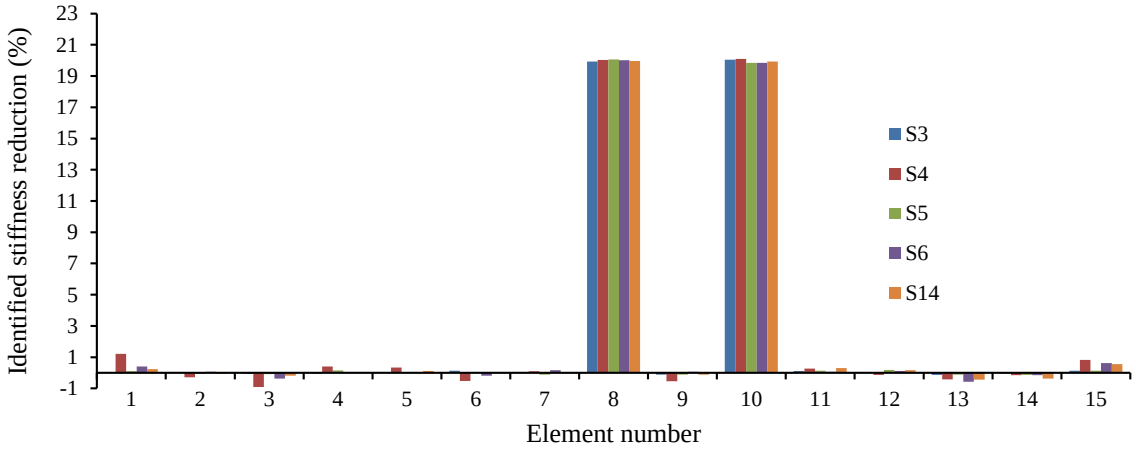

Figure 4-6: Effect of different sensor placements on identifying damage

4.3.3. Effect of vehicle speed and road surface roughness

In this section, the effect of vehicle speed and road surface roughness is studied. Four different vehicle speeds, namely, 15 m/s, 20m/s, 30 m/s, and 40 m/s and three different classes

`

of road roughness, namely, A, B, and C are considered. Noise is not considered here; it will be studied in the next section. Measured accelerations have been simulated by a forward analysis of the vehicle-bridge interaction system using the Newmark-β method. Sensor placement S6 and damage scenario #16 have also been applied. Convergence tolerance is applied as 10^{-6}. Identification results are tabulated in Table 4-5. Most of the existing studies for simultaneous identification of moving loads and structural parameters have not investigated the effect of vehicle speed or road surface roughness (Abbasnia, Mirzaee & Shayanfar 2015; Feng, Sun & Feng 2015; Zhang, Qingxia et al. 2013; Zhang, Qingxia, Jankowski & Duan 2010a, 2010b).

According to the results, at speeds of 20 m/s and above, the damage is detected and quantified very precisely at all road roughness levels. At speed 15 m/s, some of the intact elements are identified as damaged elements. This might be because the bridge is not excited enough at this speed. At each type of road roughness, computation time increases as speed decreases, reaching its maximum value when road roughness is "C" and speed is 15 m/s.

Identified front and rear loads at a speed of 15 m/s and at different road roughness types are shown in Figure 4-7 and Figure 4-8 respectively. As can be seen, even in the worst case of moving load identification, speed 15 m/s and road roughness "C", loads are identified reasonably. Identified stiffness reduction at different road roughness levels and vehicle speeds is shown in Figure 4-9. Each red horizontal line shows the location and extent of a damage. As shown in Figure 4-10, the predicted acceleration values at the mid-span point closely match the true time histories.

Table 4-5: Identification results at different road roughness and vehicle speed

Roughness	Speed (m/s)	Total time hr:min:sec	N.I.	I.L. error (%)		D.I. error (%)	Rec. Acc. Error (%)
				Front	Rear		
A	15	07:42:07	5014	1.99	1.44	1.9436	0.27
	20	4:31:36	5370	1.08	0.89	0.8486	0.17
	30	1:22:51	3622	0.02	0.63	0.1078	0.02
	40	00:25:37	2307	0.08	0.86	0.2061	0.05
B	15	09:09:30	6474	4.65	5.89	2.88	0.39
	20	06:37:27	7673	2.93	1.11	0.84	0.22
	30	1:19:41	3571	1.36	1.11	0.3807	0.11
C	15	10:37:47	7595	5.95	4.73	2.53	0.41
	20	06:37:37	7812	2.57	1.71	0.62	0.11

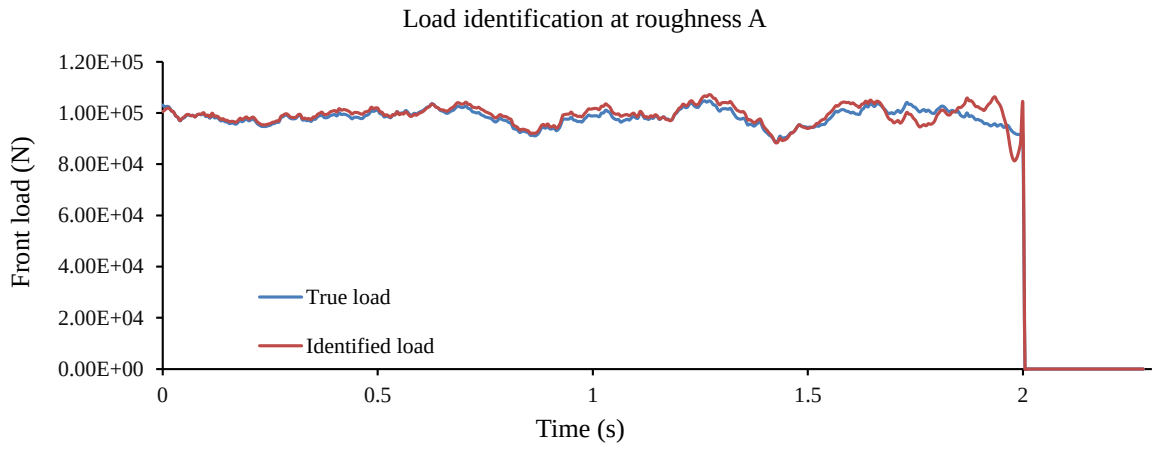

(a)

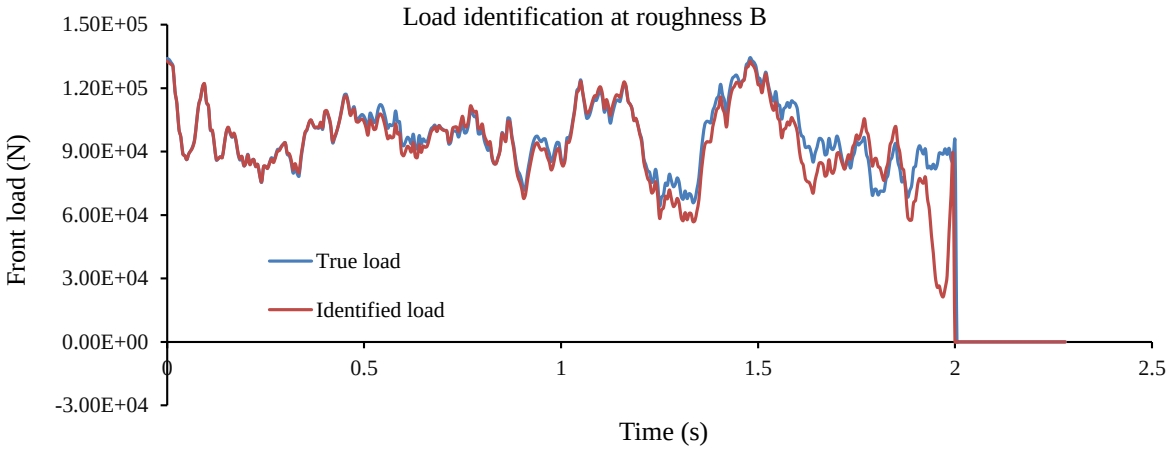

(b)

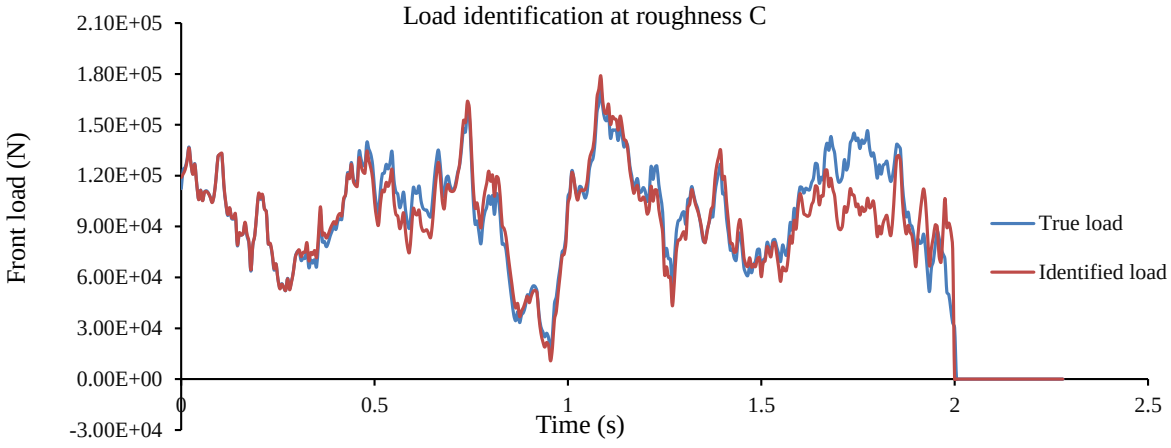

(c)

Figure 4-7: Front load identification at roughness A, B, and C (speed 15 m/s)

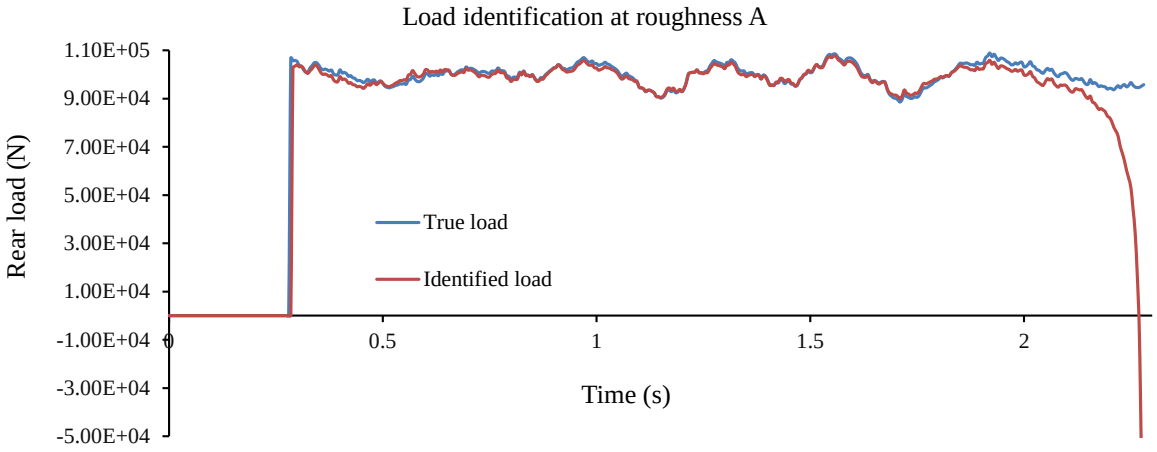

(a)

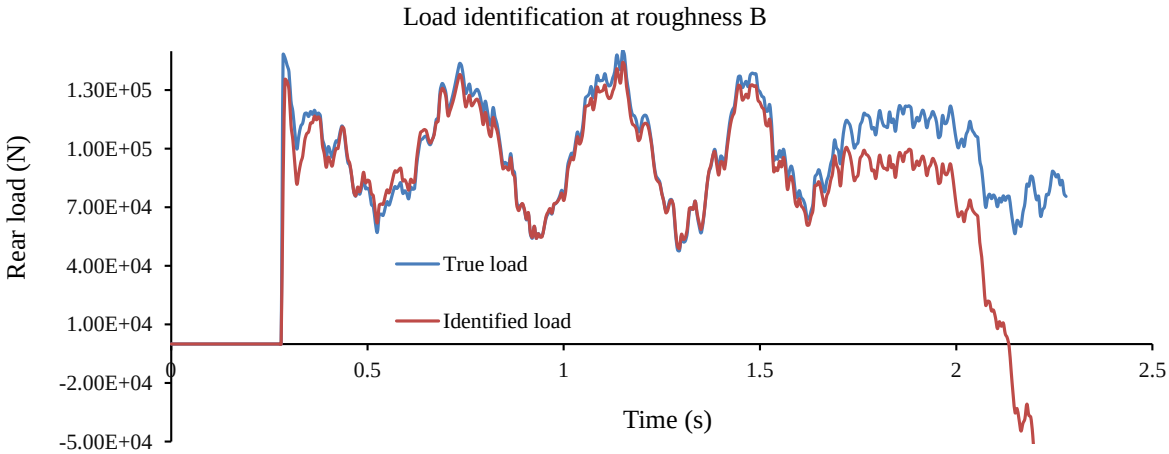

(b)

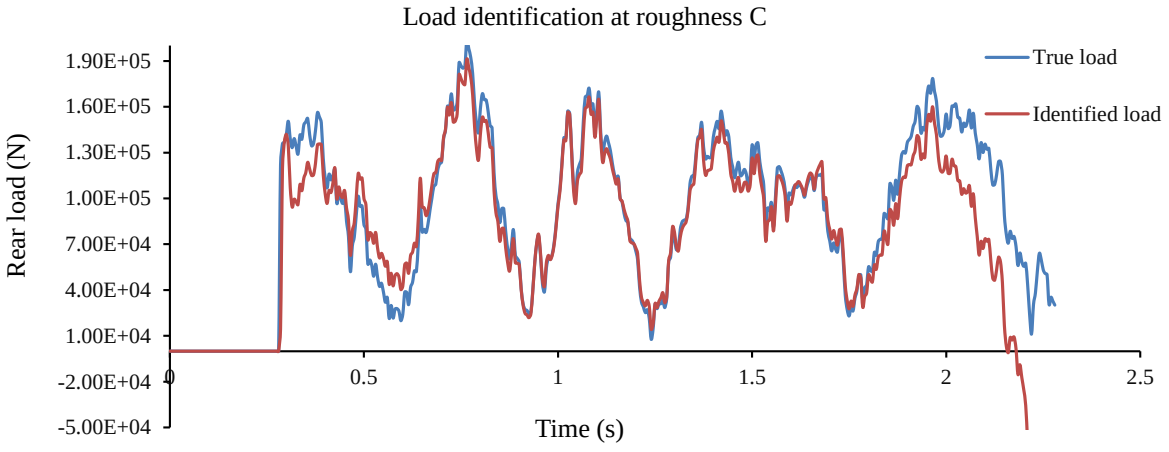

(c)

Figure 4-8: Rear load identification at roughness A, B, and C (speed 15 m/s)

`

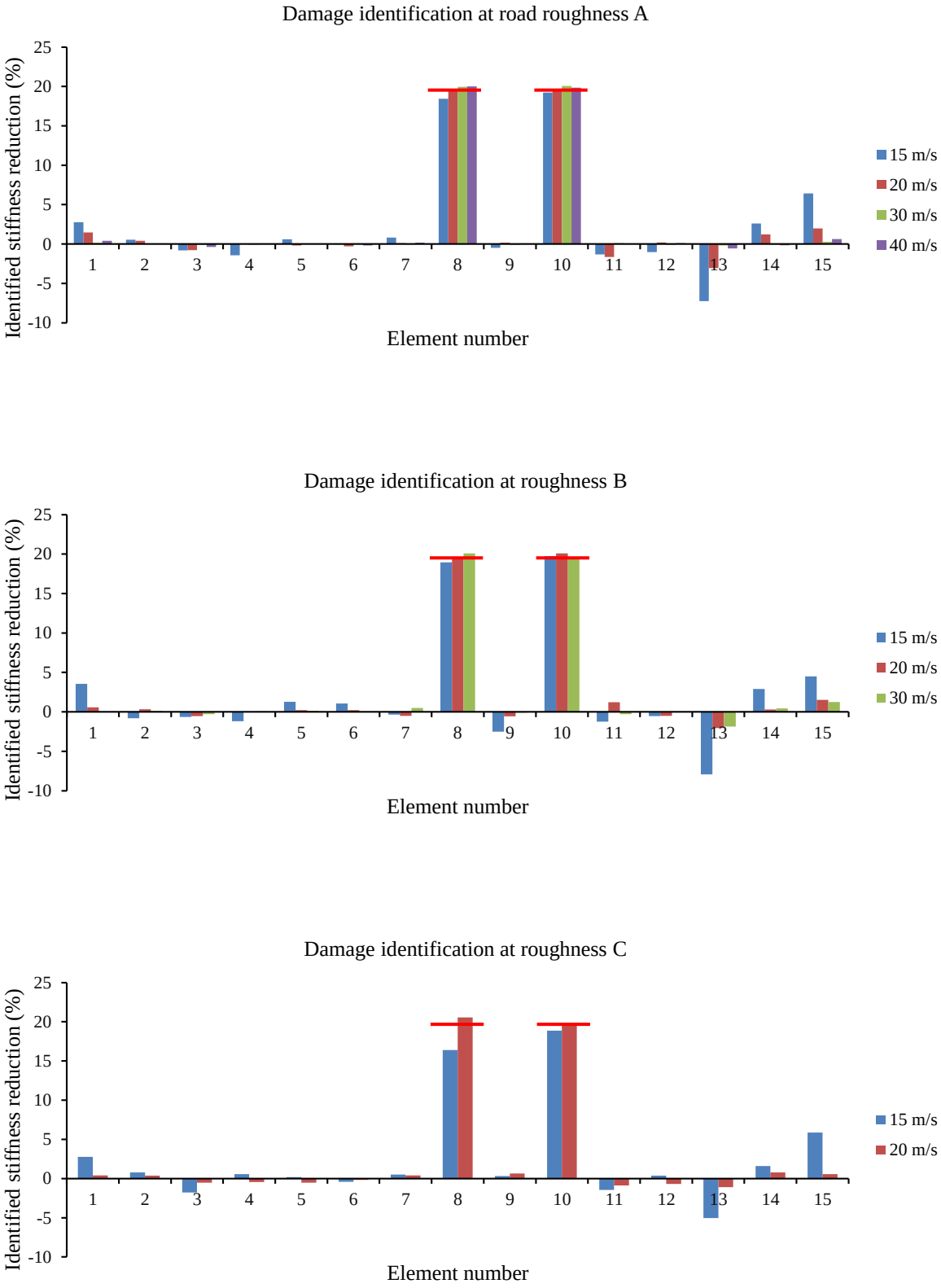

Figure 4-9: Effect of speed at road roughness A, B, and C (0% noise)

`

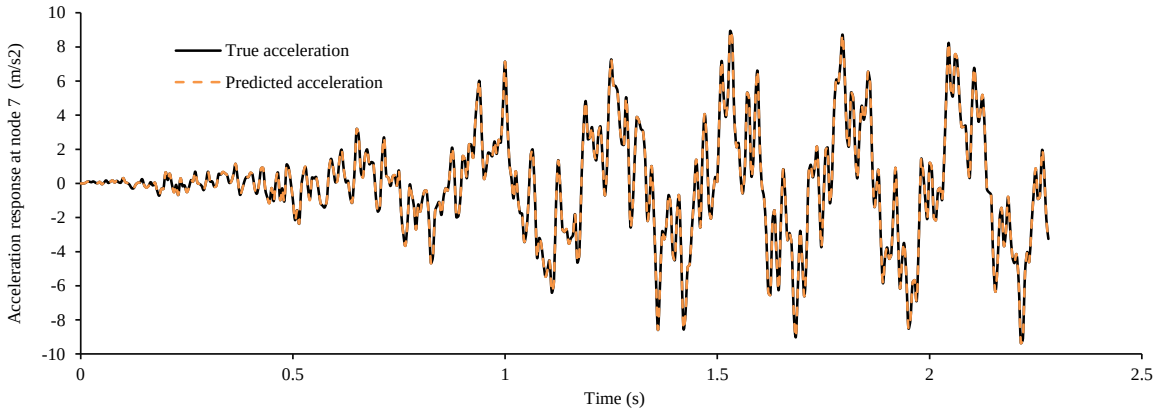

Figure 4-10: True and predicted acceleration time histories at 0% noise (speed 15 m/s and roughness C)

4.3.4. Effect of measurement noise

In the previous sections, investigations were carried out without considering noise. Here, the effect of noise on the accuracy of the method is now explored. To account for the effect of measurement noise, the calculated responses are polluted with white noise to simulate the polluted measurement as follows:

$$y = y_{real} + E_p std(y_{real}) N_{oise} \quad 4\text{-}11$$

Where y is a vector of polluted response, y_{real} is the vector of real responses, E_p represents noise level, and N_{oise} is a standard normal distribution vector with zero mean and unit standard deviation. It is notable that the effect of noise can be figured out more realistically by the experimental study in the lab. The results of the experimental study are presented in chapter 6.

In this section, the road surface roughness is assumed to be "A" and the efficiency of the method at vehicle speed 40 m/ and three different noise levels (1%, 5%, and 10%) is studied. Measured accelerations have been simulated by a forward analysis of the vehicle-bridge interaction system using the Newmark-β method. Sensor placement S6 is used and damage scenario #16 is applied.

Identification results are tabulated in Table 4-6. As can be seen, the moving load identification errors are in the same range at different measurement noise levels, however, damage identification errors and reconstructed responses errors are considerably affected by adding to the measurement noise level. Identified moving loads at vehicle speed 40 m/s are shown in Figure 4-11. Without noise, moving loads closely match the true loads, showing the accuracy of the method.

`

Identified stiffness reduction at speed 40 m/s can be seen in Figure 4-12. According to the figure, without noise, damaged elements are detected correctly without false positives or negatives at other elements, or the false values are too small to be considered. Damage is quantified very close to 20% at both elements 8 and 10. At a 1% noise level, the damage identification result is very close to that without noise. With the increase in measurement noise, damaged elements are still detected correctly and their extension is quantified close to true values, however, some false positives and negatives in other elements are arisen. The reason is that the damage identification technique studied here is based on moving load identification which is affected by noise, especially at a 10% noise level.

Table 4-6: Identification results at different noise levels and vehicle speed- road roughness A

Roughness-Speed (m/s)	Total time hr:min:sec	N.I.	I.L. error (%)		D.I. error (%)	Rec. Acc. Error (%)	Noise
			Front	Rear			
A-40	00:32:50	3404	1.91	1.10	0.45	0.82	1%
	00:18:50	1660	1.27	2.25	1.6747	4.08	5%
	00:26:41	2725	2.01	2.31	5.38	8.46	10%

`

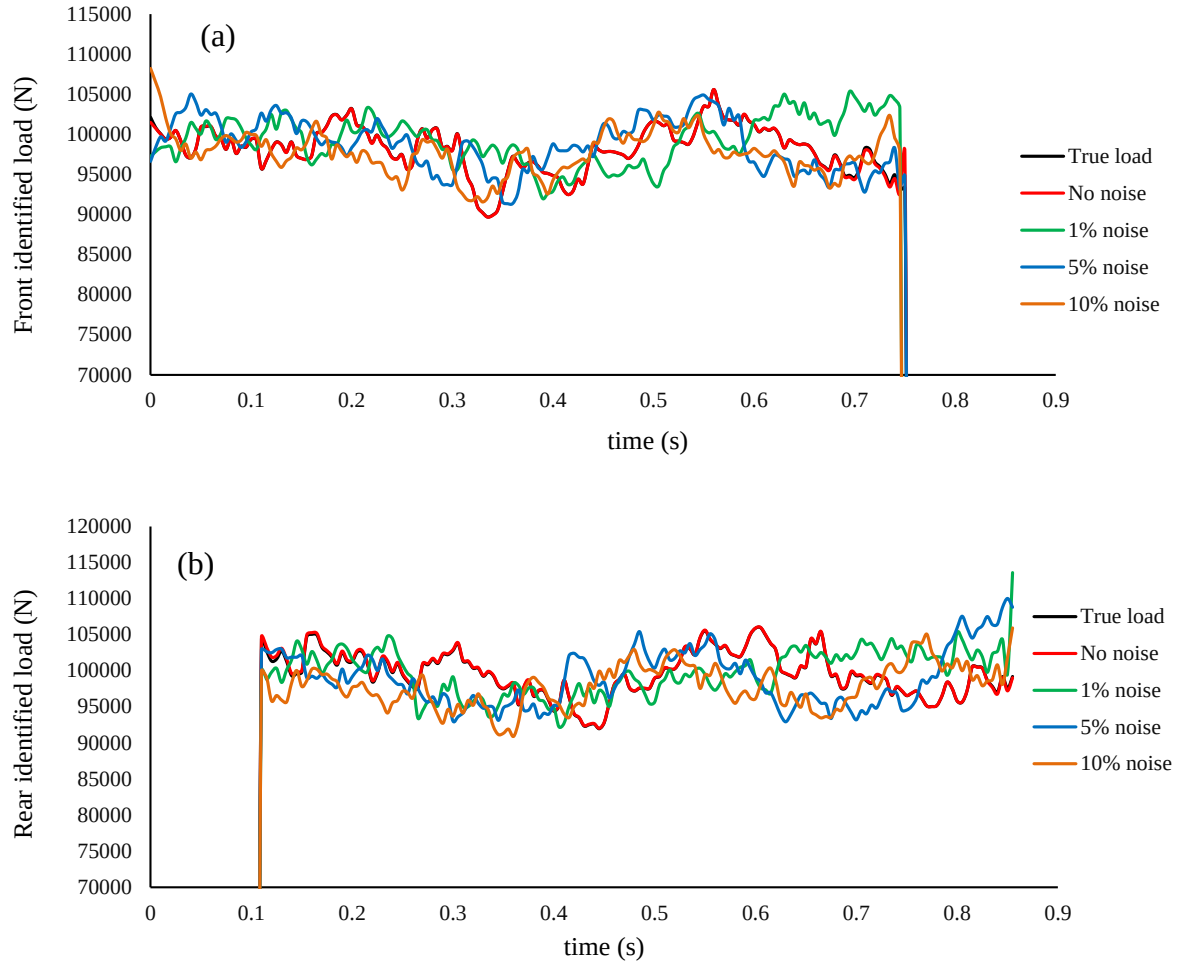

Figure 4-11: Effect of noise on moving load identification at speed 40 m/s; a: front load, b: rear load

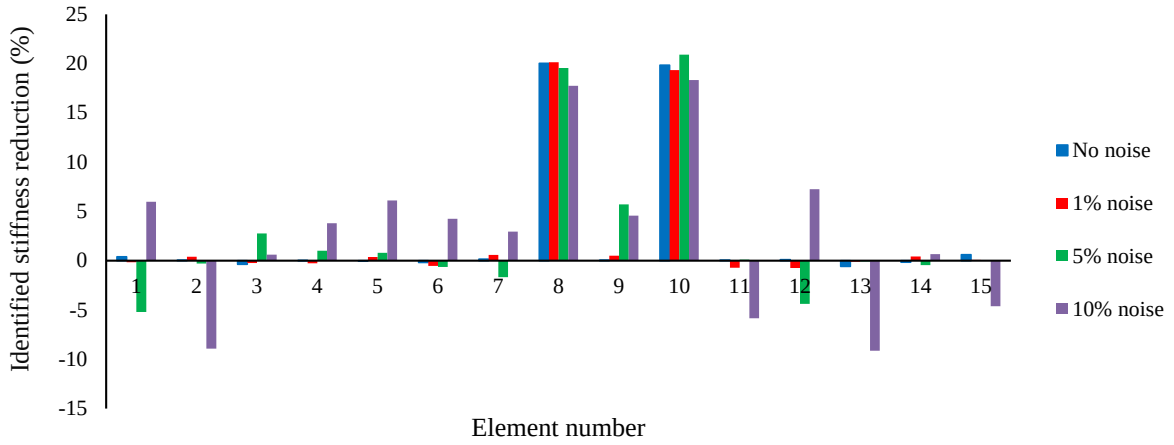

Figure 4-12: Effect of noise on damage identification at speed 40 m/s

`

4.4. Numerical Example II: Two-span continuous bridge

In this section, the application of the method for a two-span continuous bridge, with spans of 15 m (see Figure 4-13), is numerically investigated.

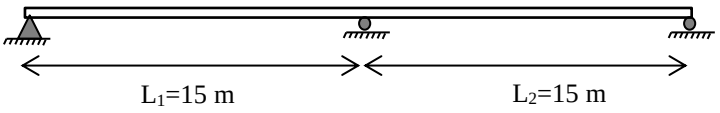

Figure 4-13: Two-span continuous bridge

The vehicle and bridge parameters for the two-span continuous bridge remain the same as for the simply supported bridge previously analysed. The same discretisation and sensor location S6 are applied. The time step is 0.005s. Elements 8 and 10 are assumed to have a 20% reduction in the stiffness of the whole element.

Identification errors have been tabulated in Table 4-7. Comparing this new model with the single span simply supported bridge, it can be seen that identification errors fall in the same range and very close to each other, showing that the method is not sensitive to the type of bridge. Figure 4-14 shows the identified stiffness reduction of the elements of the bridge. It shows that damaged elements are detected and quantified well at 5% noise, although some intact elements are detected as damaged elements, as well. The proposed method by Abbasnia (2015) is sensitive to noise greater than 1.4% and damage cannot be detected beyond this point.

Figure 4-15 shows the predicted acceleration matches completely with the simulated acceleration measurement. Figure 4-16 shows the identification evolution process of structural parameters with 5% noise. Figure 4-17 shows the identified moving loads at 5% noise, as can be seen moving loads are successfully identified at supports. In the proposed method by Feng et al. (2015), load identification errors exist over mid supports, in the presence of noise.

Table 4-7: Identification results for a two-span continuous bridge

Roughness	Speed (m/s)	Total time hr:min:sec	N.I.	I.L. error (%)		D.I. error (%)	Rec. Acc. Error (%)	Noise
				Front	Rear			
A	40	00:28:03	2375	2.81	2.3	3.61	4.2	5%

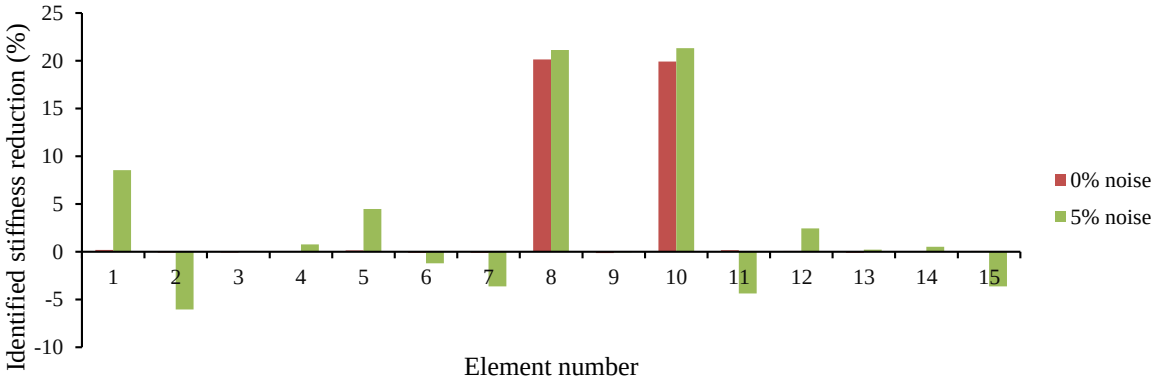

Figure 4-14: Effect of noise on damage identification of a two-span continuous bridge

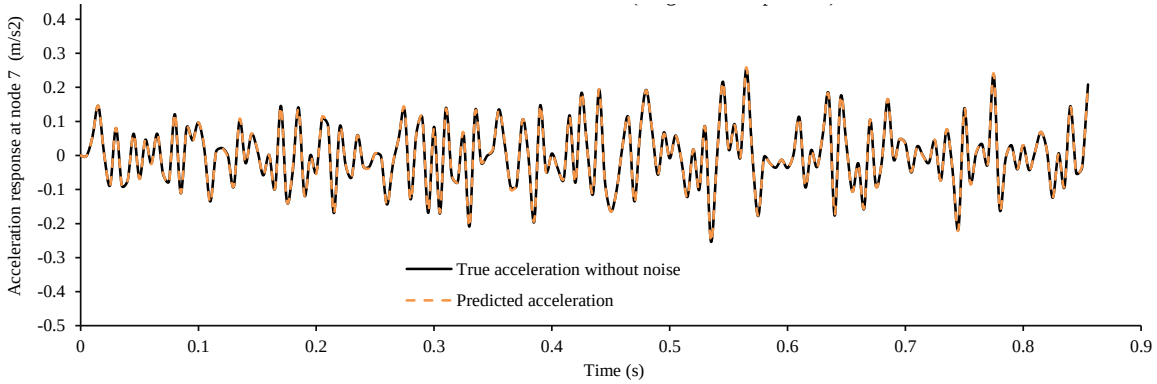

Figure 4-15: True and predicted acceleration time histories at 5% noise

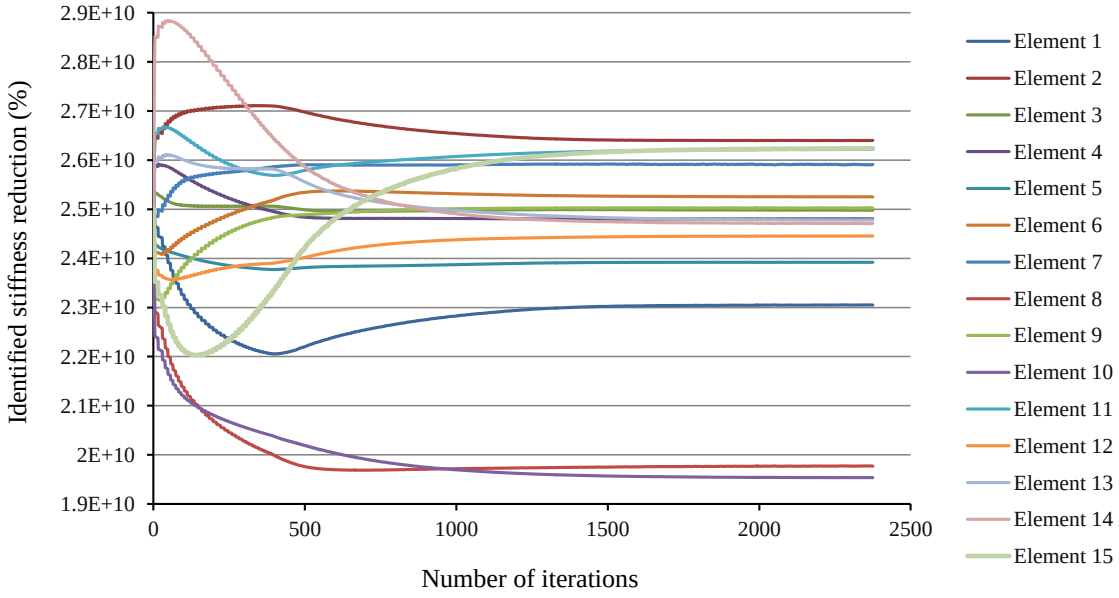

Figure 4-16: Identification evolution process for structural parameters at 5% noise

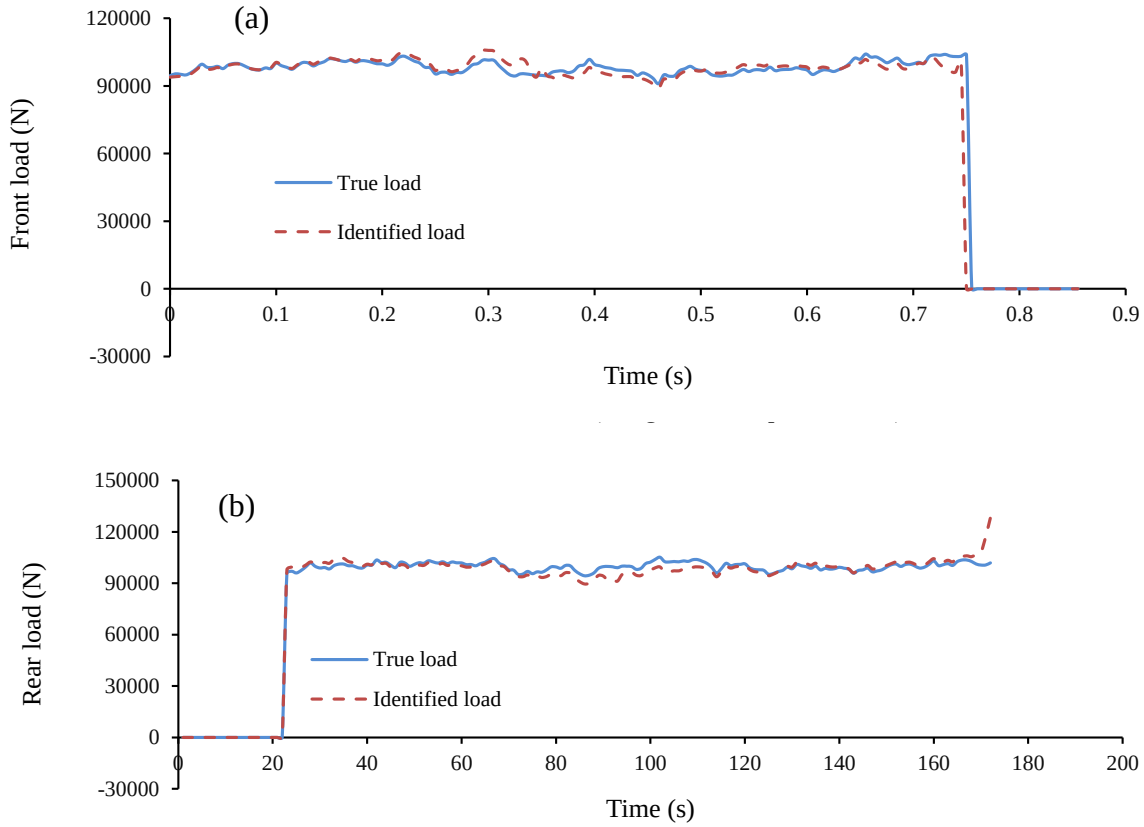

Figure 4-17: Load identification at 5% noise; a) front load, b) rear load

4.5. Summary

In this chapter, a numerical study of simultaneous identification of moving loads and structural parameters based on the explicit form of the Newmark-β method has been carried out. The Generalized Tikhonov regularization technique is used to solve the ill-posed problem and the GCV method is used to find the optimal parameter λ. The method is verified by a single-span simply supported beam and a two-span continuous beam. The effects of damage location, sensor placements, measurement noise, vehicle speeds, and road surface roughness on the accuracy of the method were investigated. Acceleration responses were reconstructed by inputting the identified moving loads and structural parameters in the equation of motion of the bridge to check the accuracy of the method.

Results indicate that the method is able to detect all levels of damage with at least three sensors, and it is not sensitive to the location of the sensors. The number and location of the sensors can be determined based on the accessibility of the locations, client budget and time. Moving loads and damages can be identified at different speed and roughness levels, and higher accuracy is achieved when speed is higher than 15 m/s, which might be because of stronger excitations. Measurement noise level more than 5% can affect the results and reduce the

`

accuracy of damage detection. At 10% noise, there are many false positives and negatives at other intact elements.

`

`

Chapter 5. Substructural condition assessment of bridge structures subject to moving loads

5.1. Introduction

Generally, most domain substructure methods are developed and verified for structures under non-moving loads, or require the entire interface force measurements (Koh, C. G., Hong & Liaw 2003; Yun & Bahng 2000; Yun & Lee 1997). Furthermore, most existing techniques are commonly formulated by state-space method (Law, S, Pinghe & Li 2014; Law, S. S. & Yong 2011; Law, S. S., Zhang & Duan 2010; Li, Jun & Hao 2014; Li, J., Law & Ding 2012; Tee, Koh & Quek 2009; Trinh & Koh 2012), suffering from the errors of discretization and sampling ratio. Liu et al. (2014) developed and verified the explicit form of the Newmark-β method for a force identification of a full scale structure under a non-moving load. It is shown to be superior to the state-space method. Liu et al. (2015) showed this superiority for interface force identification of substructures while the structure is under a non-moving load. Here, load identification is formulated by the explicit form of the Newmark-β method and damage identification of the target substructure is carried out based on the identified loads. The effect of uncertainties such as road roughness, vehicle speed, and measurement noise, which lack in existing studies, has also been investigated.

In section 5.2, the equation of motion of a target substructure when the bridge is subject to a moving vehicle is explained. Substructures are not isolated from the remaining structure and interface forces between substructures have to be applied as dynamic forces to substructures. The formulation of interface force identification with the Newmark-β method is developed in section 5.3. Local damage is simulated as a reduction in element stiffness, and damage detection is carried out by model updating based on the response sensitivity method, explained in section 5.5. Two scenarios of substructure damage identification are studied, the first of which (Scenario A) requires the intact finite element model (FEM) of the whole structure and the second being a scenario (Scenario B) in which the FEM of the whole structure is unknown but the intact FEM of the target substructure is available. The implementation procedures for these two scenarios are explained in section 5.6. Also, in section 5.6, a numerical verification of these two scenarios is carried out on a 30 m long simply supported bridge. The effects of vehicle speed, road surface roughness, and measurement noise, as well as that of sensor placement on the damage detection of three different substructures with different damage locations are studied. The chapter is summarized in section 5.7.

`

5.2. Substructural dynamic equation of motion

Several substructures can be identified when dividing the structural system, with one substructure selected as a target for evaluation here. This target substructure may be either vulnerable to damage or of high importance. Figure 5-1 shows the division of the structure into three substructures linked at the interface DOFs. Based on this sub-division of the structure, Equation 3-5 can be rewritten as Equation 5-1, shown below (Koh, C. G., Hong & Liaw 2003).

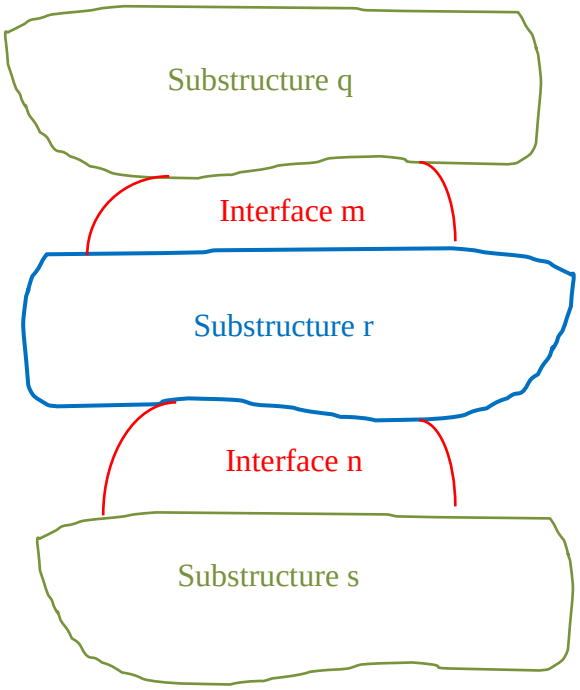

Figure 5-1: substructures division

$$\begin{bmatrix} \mathbf{M}_{qq} & \mathbf{M}_{qm} & \mathbf{0} & \mathbf{0} & \mathbf{0} \\ \mathbf{M}_{mq} & \mathbf{M}_{mm} & \mathbf{M}_{mr} & \mathbf{0} & \mathbf{0} \\ \mathbf{0} & \mathbf{M}_{rm} & \mathbf{M}_{rr} & \mathbf{M}_{rn} & \mathbf{0} \\ \mathbf{0} & \mathbf{0} & \mathbf{M}_{nr} & \mathbf{M}_{nn} & \mathbf{M}_{ns} \\ \mathbf{0} & \mathbf{0} & \mathbf{0} & \mathbf{M}_{sn} & \mathbf{M}_{ss} \end{bmatrix} \begin{Bmatrix} \ddot{\mathbf{y}}_q \\ \ddot{\mathbf{y}}_m \\ \ddot{\mathbf{y}}_r \\ \ddot{\mathbf{y}}_n \\ \ddot{\mathbf{y}}_s \end{Bmatrix} + \begin{bmatrix} \mathbf{C}_{qq} & \mathbf{C}_{qm} & \mathbf{0} & \mathbf{0} & \mathbf{0} \\ \mathbf{C}_{mq} & \mathbf{C}_{mm} & \mathbf{C}_{mr} & \mathbf{0} & \mathbf{0} \\ \mathbf{0} & \mathbf{C}_{rm} & \mathbf{C}_{rr} & \mathbf{C}_{rn} & \mathbf{0} \\ \mathbf{0} & \mathbf{0} & \mathbf{C}_{nr} & \mathbf{C}_{nn} & \mathbf{C}_{ns} \\ \mathbf{0} & \mathbf{0} & \mathbf{0} & \mathbf{C}_{sn} & \mathbf{C}_{ss} \end{bmatrix} \begin{Bmatrix} \dot{\mathbf{y}}_q \\ \dot{\mathbf{y}}_m \\ \dot{\mathbf{y}}_r \\ \dot{\mathbf{y}}_n \\ \dot{\mathbf{y}}_s \end{Bmatrix} +$$
$$\begin{bmatrix} \mathbf{K}_{qq} & \mathbf{K}_{qm} & \mathbf{0} & \mathbf{0} & \mathbf{0} \\ \mathbf{K}_{mq} & \mathbf{K}_{mm} & \mathbf{K}_{mr} & \mathbf{0} & \mathbf{0} \\ \mathbf{0} & \mathbf{K}_{rm} & \mathbf{K}_{rr} & \mathbf{K}_{rn} & \mathbf{0} \\ \mathbf{0} & \mathbf{0} & \mathbf{K}_{nr} & \mathbf{K}_{nn} & \mathbf{K}_{ns} \\ \mathbf{0} & \mathbf{0} & \mathbf{0} & \mathbf{K}_{sn} & \mathbf{K}_{ss} \end{bmatrix} \begin{Bmatrix} \mathbf{y}_q \\ \mathbf{y}_m \\ \mathbf{y}_r \\ \mathbf{y}_n \\ \mathbf{y}_s \end{Bmatrix} = \begin{Bmatrix} \mathbf{N}_q\mathbf{F}_{\mathbf{int}q} \\ \mathbf{N}_m\mathbf{F}_{\mathbf{int}m} \\ \mathbf{N}_r\mathbf{F}_{\mathbf{int}r} \\ \mathbf{N}_n\mathbf{F}_{\mathbf{int}n} \\ \mathbf{N}_s\mathbf{F}_{\mathbf{int}s} \end{Bmatrix} \quad \text{5-1}$$

Where **M**, **C**, and **K** are mass, damping and stiffness matrices, respectively; $\mathbf{y}$, $\dot{\mathbf{y}}$, and $\ddot{\mathbf{y}}$ are the nodal displacement, velocity, and acceleration vectors, respectively. The subscript ‘r’ denotes

`

internal DOFs of the target substructure, subscripts ‘q’ and ‘s’ denote the internal DOFs of the remaining substructures on the two sides. Subscripts ‘m’ and ‘n’ denote interface DOFs of the target substructure with the remaining substructures. The matrix N is a transformation matrix that distributes interaction forces ($\boldsymbol{F}_{int}$) to equivalent nodal forces (see section 3.2.3).

The equation of motion of the target substructure can be extracted from the above equation as follows:

$$[\mathbf{0}\ \ \boldsymbol{M}_{rm}\ \ \boldsymbol{M}_{rr}\ \ \boldsymbol{M}_{rn}\ \ \mathbf{0}]\begin{Bmatrix}\ddot{\boldsymbol{y}}_q\\ \ddot{\boldsymbol{y}}_m\\ \ddot{\boldsymbol{y}}_r\\ \ddot{\boldsymbol{y}}_n\\ \ddot{\boldsymbol{y}}_s\end{Bmatrix}+[\mathbf{0}\ \ \boldsymbol{C}_{rm}\ \boldsymbol{C}_{rr}\ \boldsymbol{C}_{rn}\ \mathbf{0}]\begin{Bmatrix}\dot{\boldsymbol{y}}_q\\ \dot{\boldsymbol{y}}_m\\ \dot{\boldsymbol{y}}_r\\ \dot{\boldsymbol{y}}_n\\ \dot{\boldsymbol{y}}_s\end{Bmatrix}+ [\mathbf{0}\ \ \boldsymbol{K}_{rm}\ \boldsymbol{K}_{rr}\ \ \boldsymbol{K}_{rn}\ \ \mathbf{0}]\begin{Bmatrix}\boldsymbol{y}_q\\ \boldsymbol{y}_m\\ \boldsymbol{y}_r\\ \boldsymbol{y}_n\\ \boldsymbol{y}_s\end{Bmatrix}=\boldsymbol{N}_r\boldsymbol{F}_{int_r} \quad 5\text{-}2$$

Letting subscript ‘z’ show interface DOFs (i.e. m and n included), the above equation can be rewritten as follows (Koh, C. G., Hong & Liaw 2003):

$$\boldsymbol{M}_{rr}\ddot{\boldsymbol{y}}_r+\boldsymbol{C}_{rr}\,\dot{\boldsymbol{y}}_r+\boldsymbol{K}_{rr}\boldsymbol{y}_r=\boldsymbol{N}_r\boldsymbol{F}_{int_r}-(\boldsymbol{M}_{rz}\ddot{\boldsymbol{y}}_z+\boldsymbol{C}_{rz}\,\dot{\boldsymbol{y}}_z+\boldsymbol{K}_{rz}\boldsymbol{y}_z) \quad 5\text{-}3$$

The right-hand-side of the above equation can be treated as “input” of the target substructure. $\boldsymbol{N}_r\,\boldsymbol{F}_{int_r}$ is the interaction force between the target substructure and vehicle, and $-(\boldsymbol{M}_{rz}\ddot{\boldsymbol{y}}_z+\boldsymbol{C}_{rz}\,\dot{\boldsymbol{y}}_z+\boldsymbol{K}_{rz}\boldsymbol{y}_z)$ is the vector of interface forces associated with interface DOFs. When the vehicle is moving out of the target substructure, $\boldsymbol{N}_r\,\boldsymbol{F}_{int_r}$ is equal to zero and vanishes, which is the case being studied in this chapter.

5.3. Interface force identification based on the explicit form of Newmark-β method

In this research, it is assumed that the vehicle is moving out of the target substructure r, therefore $\boldsymbol{N}_r\,\boldsymbol{F}_{int_r}$ is equal to zero and vanishes from Equation 5-3. Since the structure of the Equation 5-3 is similar to that for a full structure, substructural force identification can be performed in the same way. Following the equation below:

$$\boldsymbol{L}_{sub}\boldsymbol{P}_{sub}=-(\boldsymbol{M}_{rz}\ddot{\boldsymbol{y}}_z+\boldsymbol{C}_{rz}\,\dot{\boldsymbol{y}}_z+\boldsymbol{K}_{rz}\boldsymbol{y}_z) \quad 5\text{-}4$$

then the displacement, velocity, and acceleration of the target substructure at time t_i can be obtained from Equation 5-5 similar to a full structure (see section 3.3.1) as

$$\begin{bmatrix}(\boldsymbol{y}_r)_i\\ (\dot{\boldsymbol{y}}_r)_i\\ (\ddot{\boldsymbol{y}}_r)_i\end{bmatrix}=\sum_{j=0}^{i-1}\begin{bmatrix}\boldsymbol{A}_{dr}\ \boldsymbol{A}_{vr}\ \boldsymbol{A}_{ar}\\ \boldsymbol{B}_{dr}\ \boldsymbol{B}_{vr}\ \boldsymbol{B}_{ar}\\ \boldsymbol{C}_{dr}\ \boldsymbol{C}_{vr}\ \boldsymbol{C}_{ar}\end{bmatrix}^{j}\begin{bmatrix}\boldsymbol{A}_{0r}\\ \boldsymbol{B}_{0r}\\ \boldsymbol{C}_{0r}\end{bmatrix}\boldsymbol{L}_{sub}(\boldsymbol{P}_{sub})_{i-j}+\begin{bmatrix}\boldsymbol{A}_{dr}\ \boldsymbol{A}_{vr}\ \boldsymbol{A}_{ar}\\ \boldsymbol{B}_{dr}\ \boldsymbol{B}_{vr}\ \boldsymbol{B}_{ar}\\ \boldsymbol{C}_{dr}\ \boldsymbol{C}_{vr}\ \boldsymbol{C}_{ar}\end{bmatrix}^{i}\begin{bmatrix}(\boldsymbol{y}_r)_0\\ (\dot{\boldsymbol{y}}_r)_0\\ (\ddot{\boldsymbol{y}}_r)_0\end{bmatrix} \quad 5\text{-}5$$

where

`

$$\boldsymbol{A}_{0r} = \left(\widehat{\boldsymbol{K}}_r\right)^{-1}, \boldsymbol{A}_{dr} = \left(\widehat{\boldsymbol{K}}_r\right)^{-1}\left[\frac{1}{\beta\Delta t^2}\boldsymbol{M}_{rr} + \frac{\gamma}{\beta\Delta t}\boldsymbol{C}_{rr}\right],$$

$$\boldsymbol{A}_{vr} = \left(\widehat{\boldsymbol{K}}_r\right)^{-1}\left[\frac{1}{\beta\Delta t}\boldsymbol{M}_{rr} + (\frac{\gamma}{\beta} - 1)\boldsymbol{C}_{rr}\right],$$

$$\boldsymbol{A}_{ar} = \left(\widehat{\boldsymbol{K}}_r\right)^{-1}\left[(\frac{1}{2\beta} - 1)\boldsymbol{M}_{rr} + \frac{\Delta t}{2}(\frac{\gamma}{\beta} - 2)\boldsymbol{C}_{rr}\right],$$

$$\boldsymbol{B}_{0r} = \frac{\gamma}{\beta\Delta t}\left(\widehat{\boldsymbol{K}}_r\right)^{-1}, \qquad \boldsymbol{B}_{dr} = \frac{-\gamma}{\beta\Delta t}\widehat{\boldsymbol{K}}_r{}^{-1}\boldsymbol{K}_r,$$

$$\boldsymbol{B}_{vr} = \frac{\gamma}{\beta\Delta t}\widehat{\boldsymbol{K}}_r{}^{-1}\left[\left(\frac{\beta\Delta t}{\gamma} - \Delta t\right)\boldsymbol{K}_{rr} + \frac{1}{\gamma\Delta t}\boldsymbol{M}_{rr}\right],$$

$$\boldsymbol{B}_{ar} = \frac{\gamma}{\beta\Delta t}\widehat{\boldsymbol{K}}_r{}^{-1}\left[\left(\frac{\beta\Delta t^2}{\gamma} - \frac{\Delta t^2}{2}\right)\boldsymbol{K}_{rr} + (\frac{1}{\gamma} - 1)\boldsymbol{M}_{rr}\right],$$

$$\boldsymbol{C}_{0r} = \frac{\gamma}{\beta\Delta t^2}\widehat{\boldsymbol{K}}_r{}^{-1}, \boldsymbol{C}_{dr} = \frac{-1}{\beta\Delta t^2}\widehat{\boldsymbol{K}}_r{}^{-1}\boldsymbol{K}_r, \boldsymbol{C}_{vr} = \frac{-1}{\beta\Delta t^2}\widehat{\boldsymbol{K}}_r{}^{-1}(\boldsymbol{C}_{rr} + \Delta t\boldsymbol{K}_{rr})$$

$$\boldsymbol{C}_{ar} = \frac{\gamma}{\beta\Delta t^2}\widehat{\boldsymbol{K}}_r{}^{-1}\left[(\gamma - 1)\Delta t\boldsymbol{C}_{rr} - \beta\Delta t^2(\frac{1}{2\beta} - 1)\boldsymbol{K}_{rr}\right]$$

$$\widehat{\boldsymbol{K}}_r = \boldsymbol{K}_{rr} + \frac{1}{\beta\Delta t^2}\boldsymbol{M}_{rr} + \frac{\gamma}{\beta\Delta t}\boldsymbol{C}_{rr}$$

Letting vector $\boldsymbol{x}_{rr} \in \boldsymbol{R}^{n_s \times 1}$ denote the output of the substructure r, we can write

$$\boldsymbol{x}_r = \boldsymbol{R}_{ar}\ddot{\boldsymbol{y}}_r + \boldsymbol{R}_{vr}\dot{\boldsymbol{y}}_r + \boldsymbol{R}_{dr}\boldsymbol{y}_r \qquad 5\text{-}6$$

where $\boldsymbol{R}_{ar}, \boldsymbol{R}_{vr}$ and $\boldsymbol{R}_{dr} \in \boldsymbol{R}^{n_s \times N}$ are the influence matrices for the measured acceleration, velocity, and displacement, respectively, n_s is the dimension of the measured responses and N is the number of degrees of freedom of the target substructure. Letting $\boldsymbol{R}_r = [\boldsymbol{R}_{dr}\ \boldsymbol{R}_{Vr}\ \boldsymbol{R}_{ar}]$, Equation 5-6 can be represented as:

$$\begin{aligned}\boldsymbol{x}_r(t_i) = \sum_{j=0}^{i-1} & \boldsymbol{R}_r \begin{bmatrix} \boldsymbol{A}_{dr} & \boldsymbol{A}_{vr} & \boldsymbol{A}_{ar} \\ \boldsymbol{B}_{dr} & \boldsymbol{B}_{vr} & \boldsymbol{B}_{ar} \\ \boldsymbol{C}_{dr} & \boldsymbol{C}_{vr} & \boldsymbol{C}_{ar} \end{bmatrix}^j \begin{bmatrix} \boldsymbol{A}_{0r} \\ \boldsymbol{B}_{0r} \\ \boldsymbol{C}_{0r} \end{bmatrix} \boldsymbol{L}_{sub}(\boldsymbol{P}_{sub})_{i-j} + \\ & \boldsymbol{R}_r \begin{bmatrix} \boldsymbol{A}_{dr} & \boldsymbol{A}_{vr} & \boldsymbol{A}_{ar} \\ \boldsymbol{B}_{dr} & \boldsymbol{B}_{vr} & \boldsymbol{B}_{ar} \\ \boldsymbol{C}_{dr} & \boldsymbol{C}_{vr} & \boldsymbol{C}_{ar} \end{bmatrix}^i \begin{bmatrix} (\boldsymbol{y}_{sub})_0 \\ (\dot{\boldsymbol{y}}_{sub})_0 \\ (\ddot{\boldsymbol{y}}_{sub})_0 \end{bmatrix}\end{aligned} \qquad 5\text{-}7$$

Assuming zero initial conditions of the structure and let

$$\boldsymbol{H}_{kr} = \boldsymbol{R}_r \begin{bmatrix} \boldsymbol{A}_{dr} & \boldsymbol{A}_{vr} & \boldsymbol{A}_{ar} \\ \boldsymbol{B}_{dr} & \boldsymbol{B}_{vr} & \boldsymbol{B}_{ar} \\ \boldsymbol{C}_{dr} & \boldsymbol{C}_{vr} & \boldsymbol{C}_{ar} \end{bmatrix}^j \begin{bmatrix} \boldsymbol{A}_{0r} \\ \boldsymbol{B}_{0r} \\ \boldsymbol{C}_{0r} \end{bmatrix} \qquad 5\text{-}8$$

Equation 3-20 can then be rewritten in the matrix form in the time duration from t_1 to t_{tt} as

$$\boldsymbol{X}_{sub} = (\boldsymbol{H}_{sub})_L\, \boldsymbol{F}_{sub} \qquad 5\text{-}9$$

where tt is the number of time instants and

`

$$\boldsymbol{X}_{sub} = \begin{bmatrix} \boldsymbol{x}_r(t_1) \\ \boldsymbol{x}_r(t_2) \\ \vdots \\ \boldsymbol{x}_r(t_{tt}) \end{bmatrix}, (\boldsymbol{H}_{sub})_L = \begin{bmatrix} \boldsymbol{H}_0 & \boldsymbol{0} & \dots & \boldsymbol{0} \\ \boldsymbol{H}_1 & \boldsymbol{H}_0 & \dots & \boldsymbol{0} \\ \vdots & \vdots & \ddots & \vdots \\ \boldsymbol{H}_{tt-1} & \boldsymbol{H}_{tt-2} & \dots & \boldsymbol{H}_0 \end{bmatrix},$$

and $\boldsymbol{F}_{sub} = \begin{bmatrix} \boldsymbol{L}_{sub}\boldsymbol{P}_{sub}(t_1) \\ \boldsymbol{L}_{sub}\boldsymbol{P}_{sub}(t_2) \\ \vdots \\ \boldsymbol{L}_{sub}\boldsymbol{P}_{sub}(t_{tt}) \end{bmatrix}$

$\boldsymbol{X}_{sub}$ is the assembled measured responses from the target substructure, $\boldsymbol{F}_{sub}$ is the assembled unknown forces at interface DOFs, and $(\boldsymbol{H}_{sub})_L$ is known as the Hankel matrix which is constant here. Provided that $(\boldsymbol{H}_{sub})_L$ can be identified in Equation 5-9, $\boldsymbol{F}_{sub}$ can be determined from measured $\boldsymbol{X}_{sub}$.

5.4. Response sensitivity of substructure

It is assumed that the mass matrix of the structure remains unchanged and the stiffness matrix of the whole element decreases uniformly with damage. The flexural rigidity, $EI_i$of the i^{th} finite element of the substructure, becomes $\beta_i EI_i$ when there is damage. The fractional change in stiffness of an element can be expressed as (Zhu and Hao 2007):

$$(\Delta\boldsymbol{k}_{sub})_i = (\boldsymbol{k}_{sub})_i - \left(\widetilde{\boldsymbol{k}}_{sub}\right)_i = (1-\beta_i)(\boldsymbol{k}_{sub})_i \qquad 5\text{-}10$$

where $(\boldsymbol{k}_{sub})_i$ and $\left(\widetilde{\boldsymbol{k}}_{sub}\right)_i$ are the i^{th} element stiffness matrices of the undamaged and damaged substructure, respectively. The value of β_i ranges between 0 and 1, where $\beta_i = 1$ indicates no stiffness loss in the i^{th} element while $\beta_i = 0$ indicates the stiffness of the i^{th} element is completely lost.

The stiffness matrix of the damaged substructure is the assemblage of the entire element stiffness matrix $\left(\widetilde{\boldsymbol{k}}_{sub}\right)_i$

$$\boldsymbol{K}_{sub} = \sum_{i=1}^{N} (\boldsymbol{A}_{sub})_i^T \left(\widetilde{\boldsymbol{k}}_{sub}\right)_i (\boldsymbol{A}_{sub})_i = \sum_{i=1}^{N} \beta_i (\boldsymbol{A}_{sub})_i^T (\boldsymbol{k}_{sub})_i (\boldsymbol{A}_{sub})_i \qquad 5\text{-}11$$

where $(\boldsymbol{A}_{sub})_i$ is the extended matrix of element nodal displacement that facilitates assembling of global stiffness matrix from the constituent element stiffness matrix.

Similar to the full-structure, response sensitivities of the target substructure can be obtained by performing differentiation to both sides of Equation 5-3 with respect to β_i , and assuming Rayleigh damping in the system as:

$$\boldsymbol{M}_{rr}\frac{\partial \ddot{\boldsymbol{y}}_r}{\partial \beta_i} + \boldsymbol{C}_{rr}\frac{\partial \dot{\boldsymbol{y}}_r}{\partial \beta_i} + \boldsymbol{K}_{rr}\frac{\partial \boldsymbol{y}_r}{\partial \beta_i} = -\frac{\partial \boldsymbol{K}_{rr}}{\partial \beta_i}\boldsymbol{y}_r - a_2\frac{\partial \boldsymbol{K}_{rr}}{\partial \beta_i}\dot{\boldsymbol{y}}_r \qquad 5\text{-}12$$

`

where a_2 is the Rayleigh damping co-efficient. Once the external forces are identified from Equation 5-9, the responses of the substructure can be calculated from Equation 5-5. The response sensitivities, $\frac{\partial \ddot{\boldsymbol{y}}_r}{\partial \beta_i}$, $\frac{\partial \dot{\boldsymbol{y}}_r}{\partial \beta_i}$, $\frac{\partial \boldsymbol{y}_r}{\partial \beta_i}$ are then obtained from Equation 5-12 using the explicit form of the Newmark-β method. The initial values of the dynamic responses and the sensitivities are considered equal to zero.

5.5. Substructural damage identification procedure

Two scenarios for substructural damage detection are studied, in the first one of which (Scenario A), the intact finite element model (FEM) of the whole structure is available. In this scenario moving loads passing through the bridge structure are identified from Equation 3-22, and then structural responses are obtained. Having substructural response, external forces at interface DOFs of the substructure can be calculated from Equation 5-4 . In the second scenario (Scenario B), the FEM of the whole structure is unknown but the intact FEM of the target substructure is available. In this scenario interface forces of the substructure are treated as external loads and identified by the explicit form of the Newmark-β method from Equation 5-9. By having external forces at interface DOFs of the substructure, structural damage can be identified through procedures explained in sections 5.5.1 and 5.5.2.

5.5.1. Scenario A when the FEM of the whole structure is available

Step 1: Conducting the dynamic measurements in the structure and guessing the initial EI.

Step 2: Obtaining the mass, stiffness and damping matrices of the full structure.

Step 3: Obtaining matrix $\boldsymbol{H_L}$ of the full-structure from Equation 3-23.

Step 4: Identifying moving loads from Equation 3-22.

Step 5: Calculating structural responses of the bridge via Equation 3-18.

Step 6: Obtaining the mass, stiffness and damping matrices of the target substructure.

Step 7: Calculating interface forces acting at interface DOFs of the substructure from Equation 5-4.

Step 8: Calculating substructural response sensitivities of the substructure by forward analysis of Equation 5-12.

Step 9: Identifying the perturbation of substructural parameters from Equation 4-4.

Step 10: Updating the substructural parameters.

Step 11: Repeating steps 6 to 10 until the convergence is met with Equation 4-6.

Step 12: Updating full-structure finite element and repeating steps 1 to 12 for more accurate results.

`

5.5.2. Scenario B when only the FEM of the target substructure is available

Step 1: Conducting the dynamic measurements in the substructure and guessing the initial EI.

Step 2: Obtaining the mass, stiffness and damping matrices of the target substructure.

Step 3: Obtaining matrix $(\boldsymbol{H}_{sub})_{\mathrm{L}}$ of the substructure and identifying substructural external forces from Equation 5-9.

Step 4: Calculating substructural responses from Equation 5-3.

Step 5: Calculating substructural response sensitivities from Equation 5-12.

Step 6: Identifying the perturbation of substructural parameters from Equation 4-4.

Step 7: Updating the substructural parameters and repeating steps 2 to 7 until the convergence is met with Equation 4-6.

5.6. Numerical verification of the proposed method

The example explained in section 3.4 is used to investigate the robustness of the method at Scenarios A and B for a list of parameters as follows:

- Does the target substructure need a full sensor placement?
- Is it necessary to have sensors installed very close to the damage's location?
- Is it necessary to have sensors installed at specific locations? Not all bridges are fully accessible to install sensors.
- Do the size and boundary conditions of the substructure affect the accuracy?
- What is the impact of discretization on the substructure condition assessment?
- Is the method reliable at different road surface conditions, vehicle speeds, and measurement noise levels?

In the assessment process of scenario A, moving loads are identified using the whole length of measurement time history, which means when the front wheel enters the bridge and rear wheel leaves the bridge. However, to detect and quantify substructural damaged elements, only the part of measurement time history in which the vehicle is moving out of the substructure is considered. This period starts when the front wheel enters the bridge and ends before the front load reaches the interface node. The advantage of this approach is that unknown moving loads vanish from damage detection formulations, reducing computation time effectively.

In Scenario B, the finite element model of the whole structure is not available and interface forces should be identified as a type of external force acting on the target substructure. Similar to Scenario A, only the interval of measurement time history in which the vehicle is moving out of the substructure is considered, and unknown moving loads have vanished from

`

the equation of motion of the target substructure. This interval starts when the front wheel enters the bridge and ends before the front load reaches the interface node.

Acceleration measurements are used, simulated by forward analysis of the vehicle-bridge interaction system using the explicit form of the Newmark-β method. Accelerometers measure acceleration in a vertical direction only. The calculated responses are polluted with white noise to simulate the polluted measurement as follows:

$$y = y_{real} + E_p std(y_{real}) N_{oise} \quad 5\text{-}13$$

where y is a vector of polluted response, y_{real} is the vector of real responses, E_p is a noise level, and N_{oise} is a standard normal distribution vector with zero mean and unit standard deviation.

5.6.1. The effect of sensor placement

Three different substructures are studied, namely: Substructure case #I, Substructure case #II, and Substructure case #III. For each case, the effect of sensor placement is investigated. Different sensor placements will vary in the number of sensors existing at boundary nodes and mid nodes. To study the effect of sensor placement, damage location, and the chosen substructure, other parameters are considered as fixed. The vehicle moves over the bridge from left to right at a speed of 40 m/s. The road surface roughness is assumed to be "A". The finite element model of the beam is divided into 15 elements and 16 nodes, each with two degrees of freedom. The sampling frequency rate is 200 Hz. In this study the impact of noise has not been considered.

5.6.1.1. Substructure "case #I"

The finite element model of the bridge and the target substructure in case #I is shown in Figure 5-2. The target substructure, in this case, starts at node 8 and ends at node 13, including 5 elements, 6 nodes, and 12 degrees of freedom. Nodes 8 and 13 are interface nodes shown with green colour, each associated with two unknown interface forces- rotational and vertical. The substructure geometrical boundary condition is free-free. Local damage is assumed to be a 20% reduction in the elemental stiffness of elements 8 and 10. These two elements are shown by two circles in the figure. Damaged element 8 is the boundary element in the substructure. This element has the potential to affect the accuracy of damage detection, and the impact is investigated. This substructure includes one-third of the whole structure.

Eight different sensor placements (S.P.) are studied in this case as listed in Table 5-1, (N.S. stands for the number of sensors). These sensor placements are selected in order to

`

determine if the target substructure needs a full sensor placement, or needs sensors installed either close to the damaged elements or any other specific location. According to the table, sensor placement number 1 has 6 sensors, the maximum number of sensors possible here, but this does not mean full sensor placement. This is discussed in section 5.6.2. The mid-nodes in sensor placement number 3 and the boundary nodes in sensor placement number 5 are not covered with accelerometers. The right boundary node in sensor placement number 6 does not have any sensor. Sensor placements number 7 and 8 have fewer than four sensors. In the next sections, this substructure with sensor placement #2 is used to study the effect of other parameters, like: vehicle speed, road roughness, and measurement noise.

Convergence tolerance is applied as 10^{-6}. Damage identification error (D.I. error) and load identification error (L.I. error) are calculated from Equations 4-8 and 4-9 respectively. Damage identification error is calculated considering the substructure elements only. Since in reality, both true loads and true structural parameters are unknowns, it is not possible to quantify accuracy via Equations 4-8 and 4-9. In this case, responses can be reconstructed by inputting the identified moving loads and structural parameters into Equation 5-3. This has two benefits, one of which is to check the accuracy of identifications and another being to predict dynamic structural responses such as acceleration at locations where sensors are unavailable or difficult to install. The error of reconstructed responses (Rec. Acc. Error) can be calculated from Equation 4-10.

$$\text{Re}\,constructed\ \text{Re}\,sponse\ Error = \left\| \frac{\text{Re}\,constructed\ X_{sub} - X_{sub}}{X_{sub}} \right\| \times 100\% \qquad 5\text{-}14$$

Where X_{sub} is the assembled measured acceleration vector in the substructure.

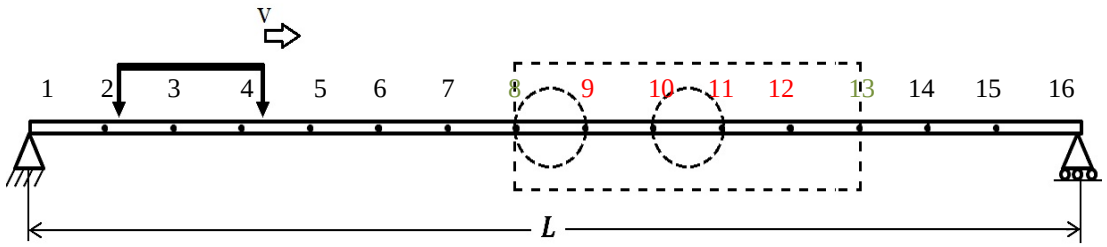

Figure 5-2: Substructure case #I

`

Table 5-1: Sensor placement for substructure case #I

S.P.	N.S.	Node number in the structure															
		1	2	3	4	5	6	7	8	9	10	11	12	13	14	15	16
1	6								*	*	*	*	*	*			
2	4								*		*	*		*			
3	4								*	*			*	*			
4	4								*	*		*		*			
5	4									*	*	*	*				
6	4								*	*	*	*					
7	3								*			*		*			
8	2								*					*			

Results from Scenario A are tabulated in Table 5-2. According to the table, the last four sensor placements could not converge, indicating that the number of sensors should be at least four and it is necessary to have accelerometers at both boundary nodes. Accelerometers measure acceleration in the vertical direction. The first four sensor placements are able to identify moving loads with less than 2.54% error and damage with less than 2.21% error, which is a satisfying result. These results show that boundary nodes need to be installed by sensors, and the best results are obtained when the mid-nodes are installed by sensors, as well. Computation time in all sensor placements is acceptable and increasing the number of sensors can reduce the computation time.

The identified stiffness reduction of the elements, only by the first four successful sensor placements, are shown in Figure 5-3. Each red horizontal line shows the location and extent of a damage. As can be seen, the method is very successful in detecting the damaged elements and quantifying the extent of damage. There are some small false positives and negatives in adjacent elements rooting in smearing effects.

Results from Scenario B are tabulated in Table 5-3. As can be seen, excepting sensor placement #1, there is no ability to converge. According to the table, the load identification error is 0.3%, damage identification error is 0.46% and reconstructing acceleration response error is 0.02%, all of which are satisfactory. Identified stiffness reduction of elements by sensor placement #1 from Scenario B is shown in Figure 5-4. It can be seen that this sensor placement is able to perfectly identify damage in substructure case #I.

`

Table 5-2: Damage identification results – substructure Case #I (Scenario A)

Sensor placement	Number of sensors	Total time hr:min:sec	N.I.	L.I. error (%)		D.I. error (%)	Rec. Acc. Error (%)
				Front	Rear		
1	6	00:03:04	192	1.85	2.54	1.00	0.31
2	4	00:10:59	760	0.45	1.56	0.69	0.35
3	4	00:06:47	349	1.09	1.86	1.92	0.41
4	4	00:06:06	333	1.26	1.99	2.21	0.43
5	4	Could not converge					
6	4	Could not converge					
7	3	Could not converge					
8	2	Could not converge					

Table 5-3: Damage identification results – substructure Case #I (Scenario B)

Sensor placement	Number of sensors	Total time hr:min:sec	N.I.	Interface force error (%)	D.I. error (%)	Rec. Acc. Error (%)
1	6	01:23:25	4871	0.3	0.46	0.02
2	4	Could not converge				
3						
4						
5						
6						
7	3					
8	2					

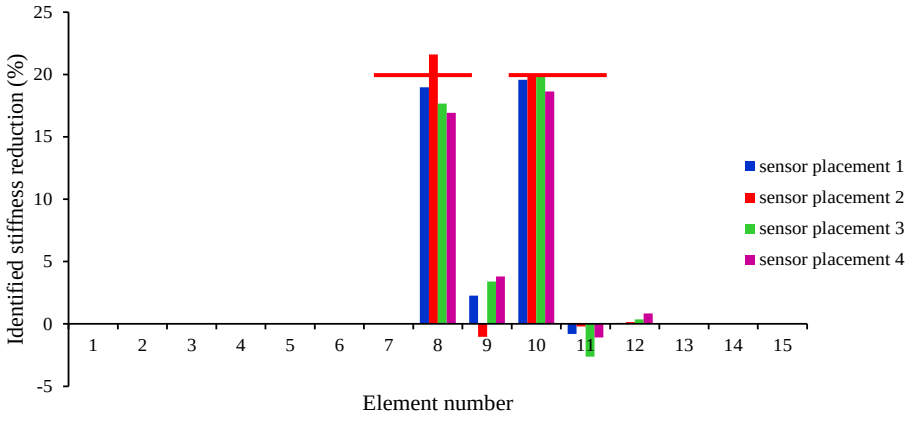

Figure 5-3: The effect of sensor placements on substructure case #I assessment (Scenario A)

`

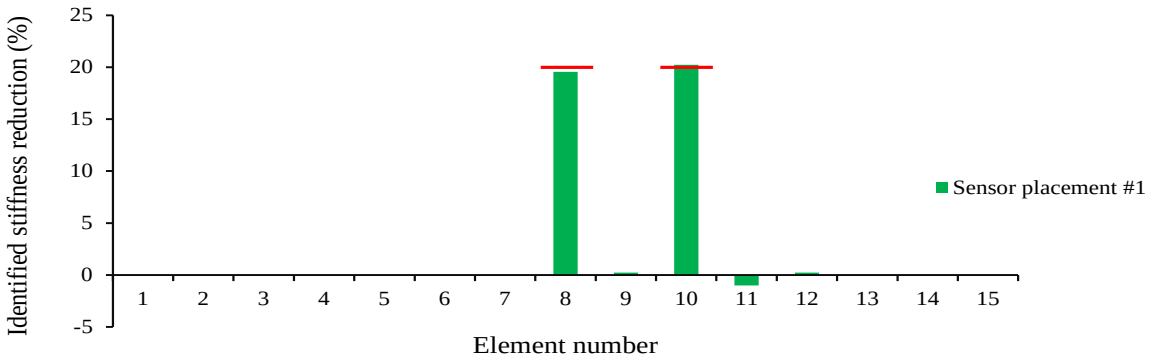

Figure 5-4: The effect of sensor placements on substructure case #I assessment (scenario B)

In comparison with Scenario A, the computation time in Scenario B is increased. Computation time, in this case, is even greater than that for simultaneous identification of full structure parameters and moving loads, for the same beam. It is notable that here a simple 30 m simply supported bridge is being studied, however, this method can effectively save time for bridges with a much higher number of elements and complex structures. So, the increase in computation time does not reduce the value of this method.

5.6.1.2. Substructure "case #II"

Substructure case #II is created by extending the substructure case #I from the right end to include the right-end support (see Figure 5-5). It includes 8 elements, 9 nodes, and 17 degrees of freedom. Node 8 is the interface node associating with two unknown interface forces: rotational and vertical. The substructure geometrical boundary condition is free-pinned. Damage location and extension are the same as in substructure case #I. This substructure includes approximately half of the whole structure.

Twenty different sensor placements are studied for this substructure, as listed in Table 5-4. Sensor placement numbers 1 to 4 include three sensors, numbers 5 to 11 include four sensors, numbers 12 to 17 include five sensors and numbers 18 to 20 include six sensors. The reasons for these sensor placements have been explained in the previous section.

Results from Scenario A are tabulated in Table 5-5 and identified stiffness reduction is shown in Figure 5-6. Each red horizontal line shows the location and extent of a damage. According to the table, the maximum load identification error is 5.16% occurring in sensor placement #14, and the maximum reconstructed acceleration response error is 1.73% occurring in sensor placement #17. According to the results, the proposed method is very promising for moving load identification and reconstructing acceleration responses, even with only three

`

sensors. It does not show any sensitivity to the number and location of sensors, as well as damage location, for moving load identification purposes.

For damage identification, at least four sensors are needed to attain satisfying results. The method is sensitive to sensor location and promising results can be achieved if

- There are at least two accelerometers at the free-end side of the substructure,
- Sensors are distributed as evenly and symmetrically as possible among the boundary nodes and mid nodes.

For example, it is better to have two sensors in the middle of the substructure and two sensors at the right-end of the substructure (sensor placement #19) instead of placing three sensors in the middle of the substructure and one sensor at the right-end of the structure (sensor placement #18).

Optimum results may be achieved even if the above two conditions are not met, however, we are talking about a promising damage detection result. For example, sensor placements #4, #5, #12, #15, and #19, have met the above conditions and have provided satisfying results, while others which have not obeyed the above conditions are not satisfying, except sensor placements #9 and #13.

In comparison with substructure case #I, although there are more elements and unknowns in substructure case #II, the computation time is almost in the same range. For sensor placements meeting the above conditions, the maximum computation time is around 10 minutes for those with four sensors, and it will be half for those with five and six sensors. In general, time is not an issue in the substructure condition assessment, since this method significantly reduces the overall computation time.

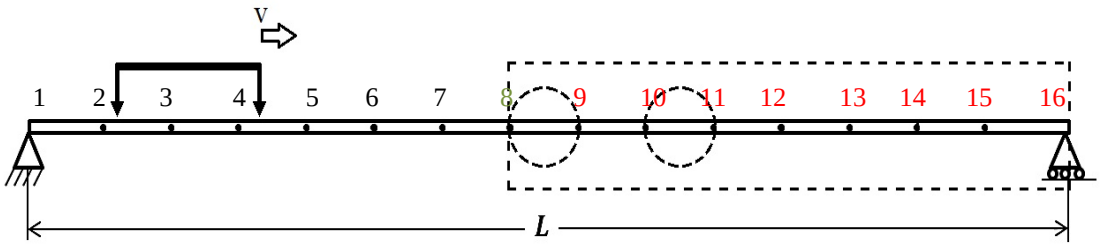

Figure 5-5: Substructure case #II

`

Table 5-4: Sensor placement for substructure case #II

S.P.	N. S.	Sensors location															
		1	2	3	4	5	6	7	8	9	10	11	12	13	14	15	16
1	3								*				*			*	
2												*	*	*			
3											*		*		*		
4									*	*			*				
5	4								*	*			*			*	
6									*	*		*	*				
7									*	*			*	*			
8									*	*					*	*	
9									*	*		*		*			
10									*			*		*		*	
11											*	*	*	*			
12	5								*	*		*		*		*	
13									*			*	*	*		*	
14									*	*		*	*	*			
15									*	*			*		*	*	
16										*		*	*	*		*	
17									*		*		*		*	*	
18	6								*	*		*	*	*		*	
19									*	*		*	*		*	*	
20									*	*	*	*	*	*			

`

Table 5-5: Damage identification results – substructure Case #II (Scenario A)

Sensor placement	Number of sensors	Total time hr:min:sec	N.I.	L.I. error (%)		D.I. error (%)	Rec. Acc. Error (%)
				Front	Rear		
1	3	0:05:41	360	2.66	2.43	32.05	1.49
2		0:14:31	710	1.62	2.54	6.326	0.78
3		Could not converge					
4		0:10:16	487	2.82	2.98	6.36	1.46
5	4	0:10:32	697	2.35	2.13	1.3684	0.63
6		0:03:57	233	0.59	1.96	1.9474	0.59
7		0:04:48	233	2.29	1.88	3.21	0.73
8		Could not converge					
9		0:03:40	262	1.41	2.04	1.38	0.58
10		0:04:12	291	3.11	2.88	10.36	0.99
11		1:15:24	4982	2.23	2.39	3.6316	0.65
12	5	0:05:20	257	1.60	2.09	0.78	0.61
13		0:03:33	245	1.98	1.90	1.6842	0.60
14		0:03:23	221	5.16	3.81	8.26	1.48
15		0:06:18	320	2.05	1.78	2.05	0.70
16		0:05:18	263	4.08	3.10	8.86	1.21
17		0:05:46	374	1.85	1.95	32.9	1.73
18	6	0:05:32	259	2.23	1.89	3.63	0.85
19		0:04:47	245	1.64	2.10	0.59	0.60
20		0:05:42	346	3.41	2.93	9.60	1.50

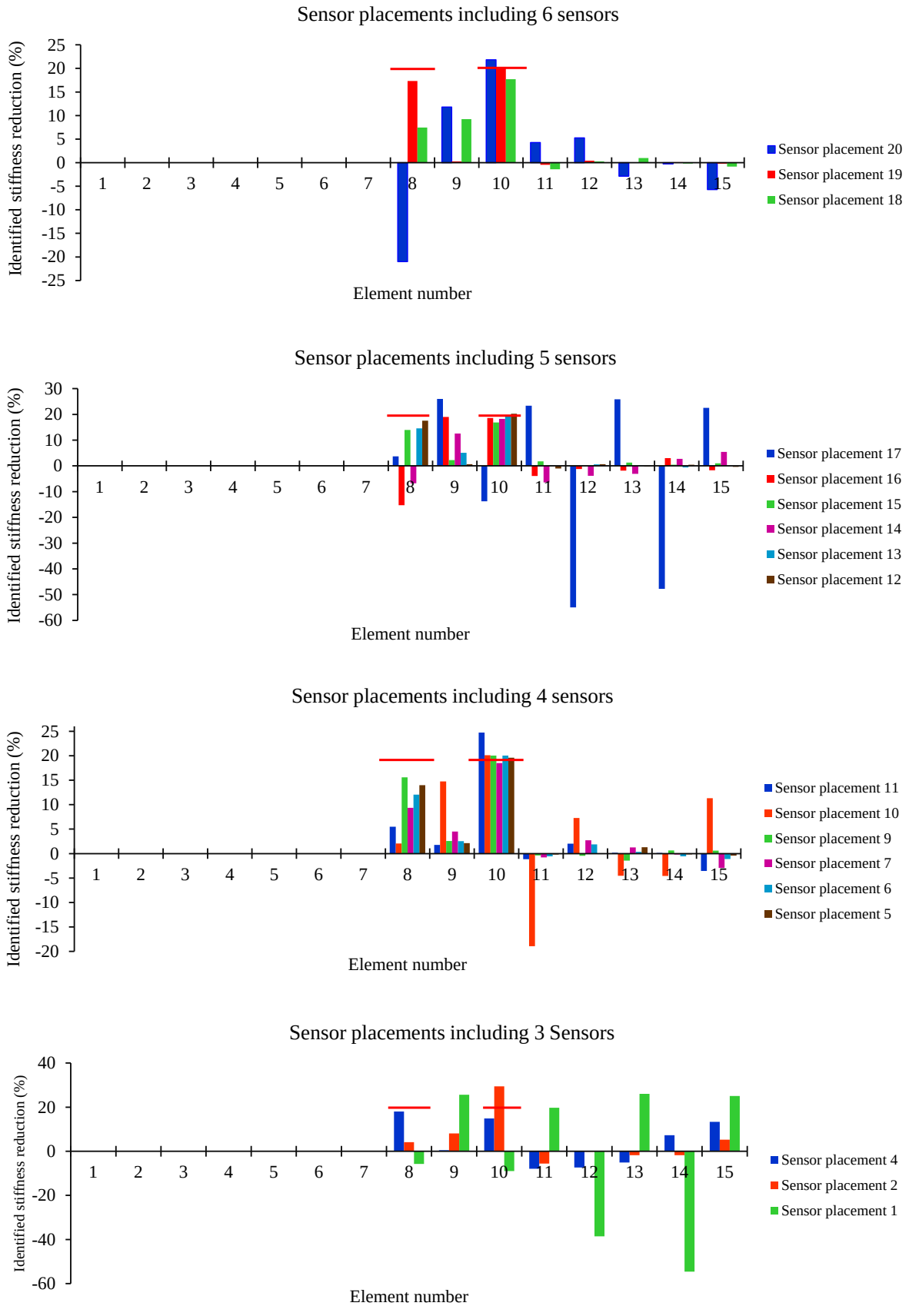

Figure 5-6: Effect of different sensor placements on the assessment of Substructure Case #II

`

Results from Scenario B are tabulated in Table 5-6 and the identified stiffness reduction of elements at different sensor placements is shown in Figure 5-7. Each red horizontal line shows the location and extent of a damage. The maximum error to predict acceleration responses is 0.22% occurring at sensor placement #20.

Through sensor placements including only three sensors, it is not possible to identify damage correctly. Element 8 is not detected and false detection can be seen in other elements. Increasing the number of sensors to four has visibly improved the results. Excepting sensor placements #10 and #11, others are able to identify damaged elements with acceptable accuracy. Boundary nodes in these two sensor placements are either not covered with sensors or the number of sensors is insufficient. Sensor placement #8 is able to perfectly identify damage at damaged elements, however, there are some false positives and negatives at other elements since the mid-nodes are not installed by sensors. Sensor placements #6, #7, and #9 are very successful in identifying damage and they have three characteristics in common which are:

- Having at least four sensors.
- Having at least two sensors at the boundary nodes of the free-end side.
- Having at least two sensors at mid nodes.

As can be seen in Figure 5-7, sensor placements including five or six sensors that have met the above conditions, sensor placements #12, #14, #18, #19, and #20, have provided very accurate results for damage detection. Increasing the number of sensors from four to five or six has not affected the accuracy and computation time notably.

Comparing Scenarios *A* and *B* for damage detection of substructure case #II, it can be seen that the boundary damaged element in Scenario *B* is identified with high accuracy even by four sensors. In Scenario *A*, it is identified with errors, though the error is reduced by increasing the number of sensors. Furthermore, the conditions of Scenario B are easier to meet in practice.

`

Table 5-6: Damage identification results – substructure Case #II (Scenario B)

Sensor placement	Number of sensors	Total time hr:min:sec	NI	Interface force error (%)	DI error (%)	Rec. Acc. Error (%)
1	3	01:16:04	9195	0.9	10.13	0.05
2		01:31:00	11643	0.75	17.22	0.11
3		02:31:02	15978	1.25	39.76	0.02
4		Singularity error				
5	4	00:54:00	6502	0.48	1.65	0.14
6		00:10:46	1262	0.37	1.55	0.15
7		00:30:49	3343	0.32	0.48	0.12
8		00:56:55	6795	0.70	3.83	0.12
9		00:11:10	1304	0.30	0.31	0.13
10		00:56:34	5799	1.12	61.17	2.78
11		02:29:09	18511	1.51	128.66	0.27
12	5	00:08:16	905	0.35	0.44	0.14
13		00:43:06	4607	0.62	3.93	0.16
14		00:16:46	1565	0.25	0.82	0.13
15		Singularity error				
16		Could not converge				
17		00:19:39	1686	0.62	28.4	0.5
18	6	00:06:00	625	0.25	0.23	0.12
19		00:09:18	1001	0.20	0.26	0.17
20		00:09:05	921	0.59	0.81	0.22

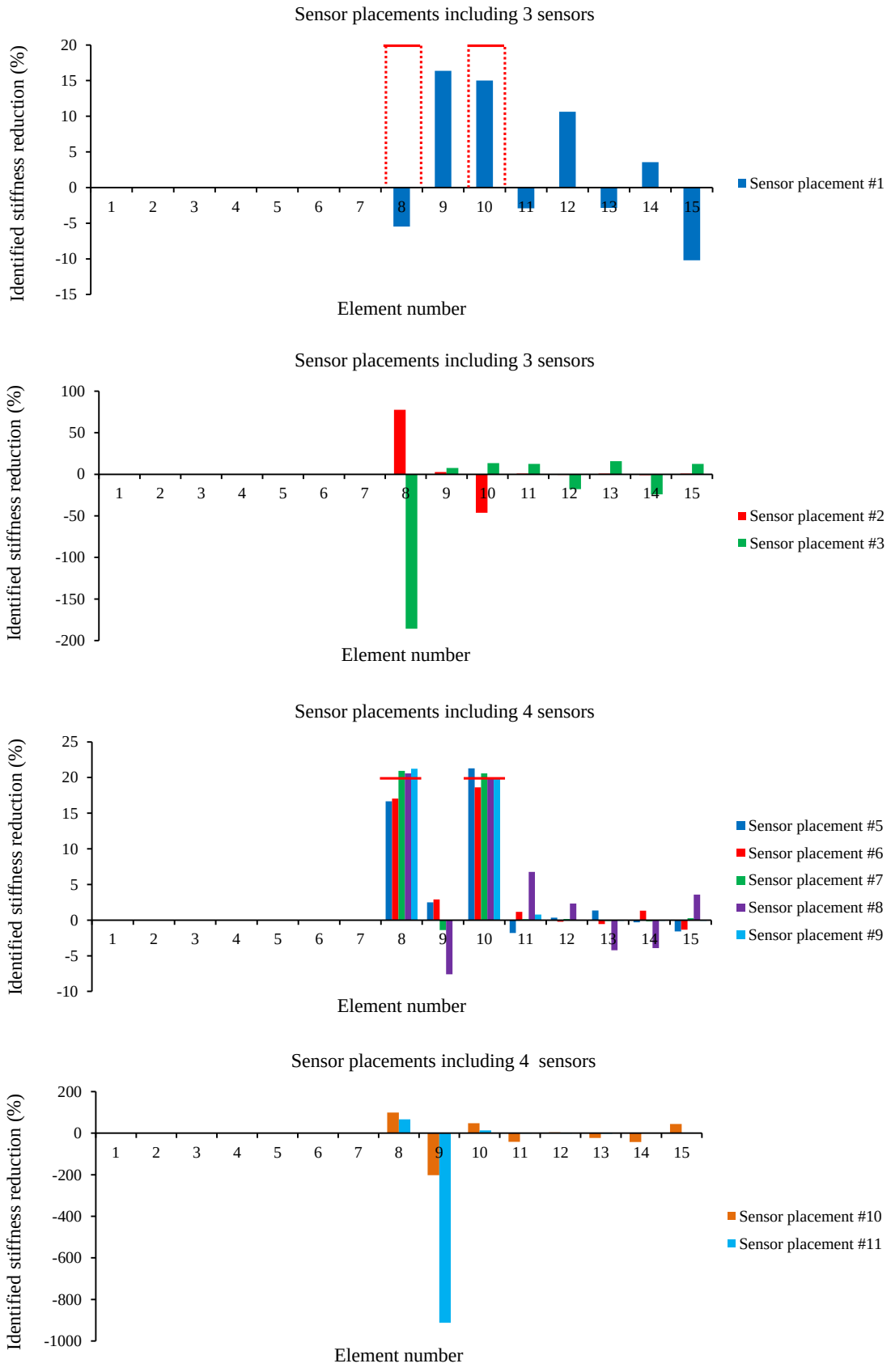

Figure 5-7: The effect of sensor placement on substructure case #II assessment (Scenario B)

`

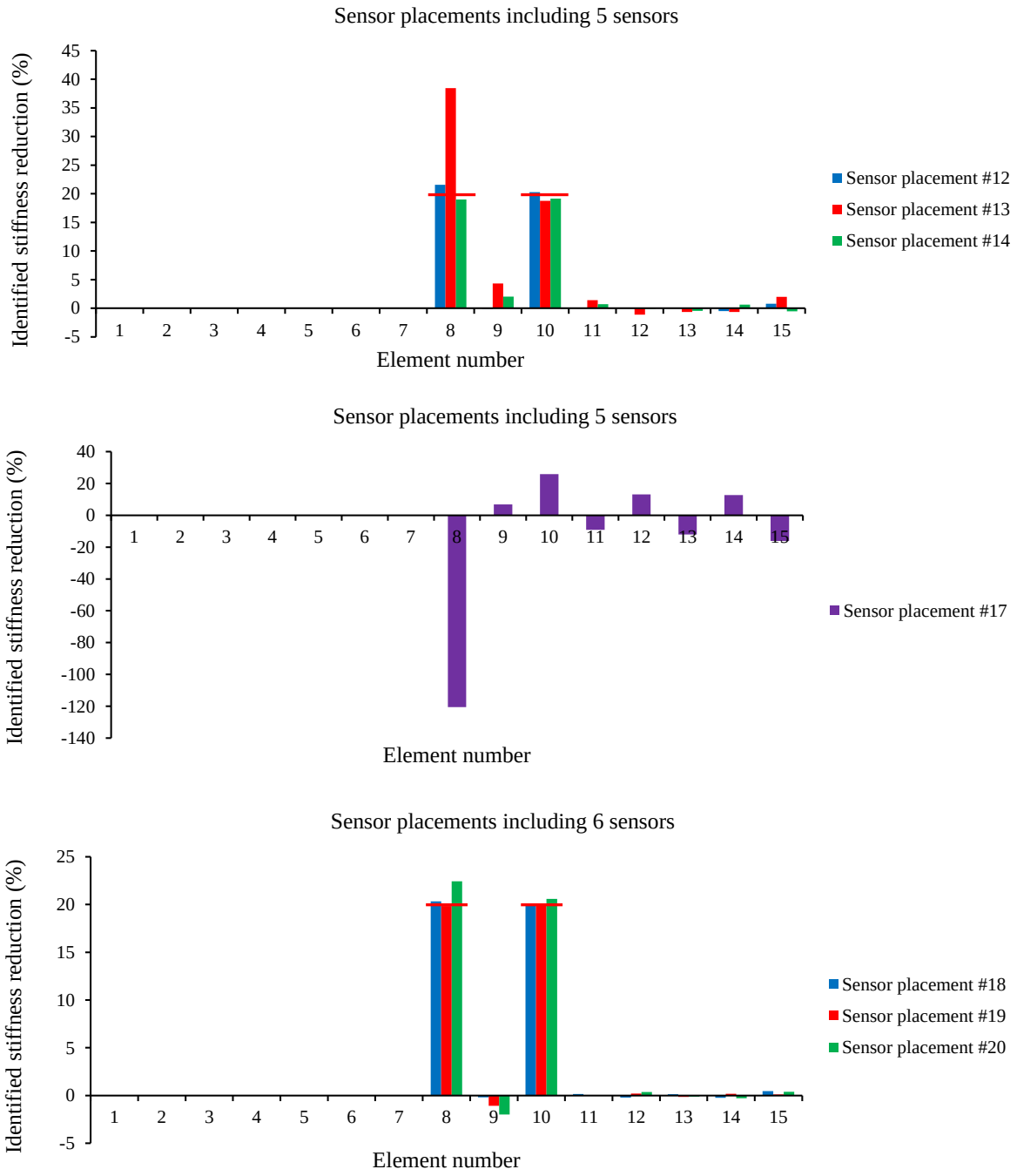

Figure 5-7 (Continue): The effect of sensor placement on substructure case #II assessment (Scenario B)

Comparing substructure cases #I and #II in Scenario B, although substructure case #II includes more elements and unknown structural parameters to identify, it is much less sensitive to the number and location of the sensors and damage can be identified even with four sensors with less computation time. These are due to the free-pinned boundary condition of the

`

substructure where fewer forces need to be identified. In section 5.6.2, it is proven that substructure case #I needs full sensor placement.

Among the four approaches explained for damage detection of elements 8 and 10, substructure case #II using Scenario *B* is the best approach and substructure case #I using Scenario B is the worst approach. Substructures case #I and II in Scenario A are almost at the same level of performance. All of these approaches can be used for damage detection, however, they each involve different costs of time, money and executive issues, and the final decision depends on the client's need.

5.6.1.3. Substructure "case #III"

The finite element model of the bridge and the target substructure is shown in Figure 5-8. The target substructure, in this case, starts at node 11 and ends at node 16, embracing the right-end support. It includes 5 elements, 6 nodes, and 11 degrees of freedom. Node 11 is the interface node associated with two unknown interface forces- rotational and vertical. The substructure geometrical boundary condition is free-pinned. Local damage is assumed to be a 20% reduction in the elemental stiffness of elements 12 and 14. These two elements are shown by two circles in the figure. This substructure is at the end part of the beam including one-third of the whole structure. Four different sensor placements are studied in this case, as listed in Table 5-7. The reasons for these sensor placements have already been explained in the previous sections.

In this substructure, none of the damaged elements are boundary elements. Results of the previous substructures showed that the mid-damaged element is identified better than the boundary damaged element. This is further explored by this substructure. Furthermore, measurement time history length for damage identification is longer in this case.

The results from Scenario ***A*** are tabulated in Table 5-8. According to the table, the maximum load identification error is 2.35%, the maximum damage identification error is 2.5% and the maximum error for the reconstructed acceleration response is 1.85%, which is quite satisfactory. The maximum computation time is 10 minutes which is in the same range as the other two structures. Identified stiffness reduction of elements for each sensor placement is shown in Figure 5-9. Each red horizontal line shows the location and extent of a damage. As can be seen, damage elements are detected and quantified positively in all cases. Among the sensor placements with four sensors, sensor placement #2 has met the conditions previously mentioned and has produced great results. When damage elements are not the boundary

`

elements of the substructure, a high level of accuracy is achieved, otherwise, promising results can be obtained if the above conditions are met.

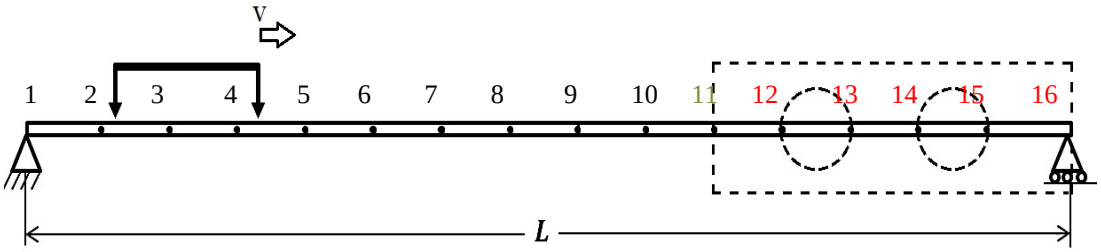

Figure 5-8: Substructure case #III

Table 5-7: Sensor placement for substructure case #III

S.P.	N.S.	Sensor location															
		1	2	3	4	5	6	7	8	9	10	11	12	13	14	15	16
1	5											*	*	*	*	*	
2	4											*	*		*	*	
3													*	*	*	*	
4												*	*	*	*		

Results from Scenario B are tabulated in Table 5-9 and the identified stiffness reduction of elements at different sensor placements is shown in Figure 5-10. Each red horizontal line shows the location and extent of a damage. As can be seen from the picture, sensor placements #1 and #4 have met the conditions mentioned previously and the damage is identified accurately. Although sensor placement #3 does not have a sensor at the free-end of the substructure, it has reliably detected the damage.

Table 5-8: Damage identification results – substructure Case #III (Scenario A)

Sensor placement	Number of sensors	Total time	N.I.	I.L. error (%)		DI error (%)	Rec. Acc. Error (%)
				Front	Rear		
1	5	0:10:00	444	1.23	2.27	2.16	1.85
2	4	0:06:37	439	1.30	2.15	0.90	1.56
3		0:08:06	563	1.60	2.35	1.74	1.23
4		0:08:07	554	1.17	3.21	2.49	1.47

Table 5-9: Damage identification results – substructure Case #III (Scenario B)

`

Sensor placement	Number of sensors	Total time hr:min:sec	N.I.	Interface force error	D.I. error (%)	Rec. Acc. Error (%)
1	5	00:20:26	2266	0.35	1.30	0.30
2	4	Could not converge				
3		00:53:49	6937	0.57	1.69	0.22
4		00:07:44	991	0.46	1.85	0.28

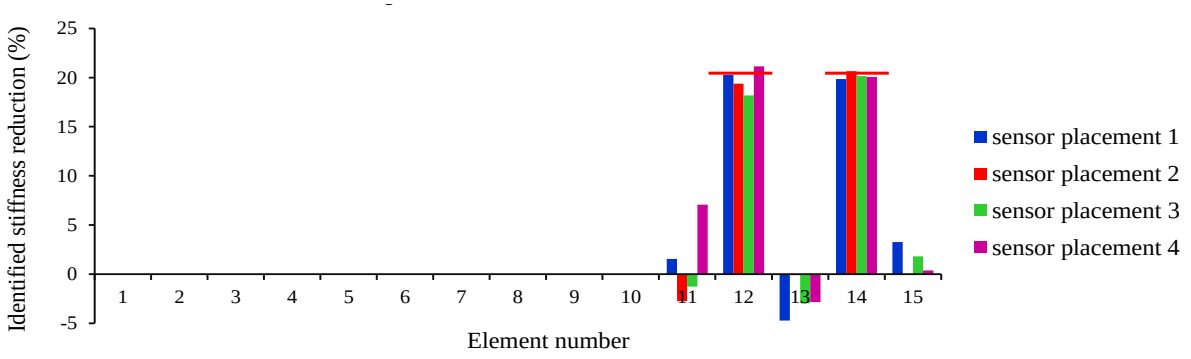

Figure 5-9: The effect of sensor placement on substructure case #III assessment (Scen.A)

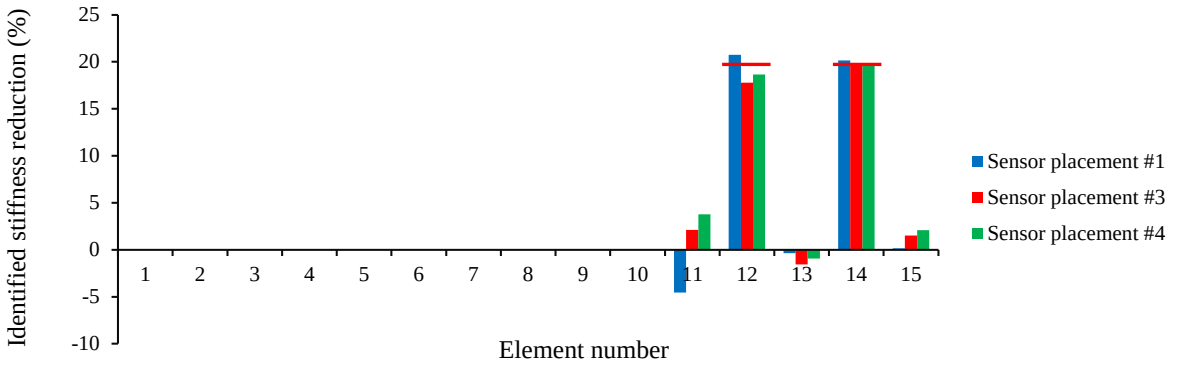

Figure 5-10: The effect of sensor placement on substructure case #III assessment (Scen. B)

5.6.2. The effect of discretization

To find out the effect of discretization on the results of damage detection, the beam is divided into 30 elements. The target substructure includes the length of the beam that substructure case #I includes (see Figure 5-11). The results from the 30 elements-beam (model 1) are compared with the 15-elements beam (model 2). Sensor location is set according to sensor placement #2 of substructure case #I. The vehicle moves over the bridge at a speed of 40 m/s. The road surface roughness is assumed to be "A". The sampling frequency rate is 200 Hz. In this study the impact of noise has not been considered. Convergence tolerance is applied as 10^{-6}.

`

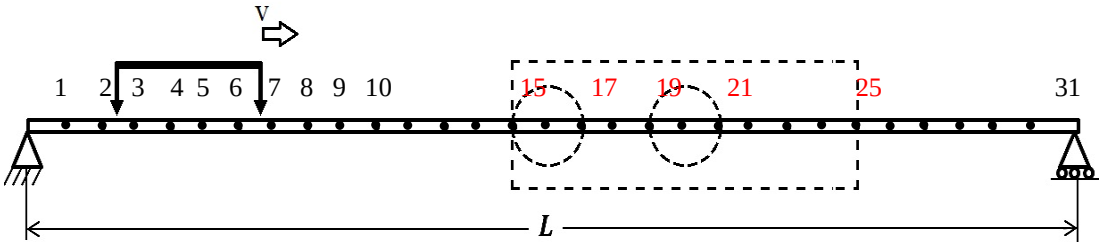

Figure 5-11: Discretization in model 1

Results from Scenario A are tabulated in Table 5-10. Comparing models 1 and 2, finer discretization has increased the computation time remarkably, while the errors of moving load identification, damage identification and reconstructing the acceleration response are in the same range, showing that with the same number of sensors, finer discretization does not improve the accuracy. The identified stiffness of elements by models 1 and 2 are shown in Figure 5-12. As can be seen, both discretizations are able to detect damage locations and extensions perfectly. There are some false positives and negatives in adjacent elements that come from the smearing effect of damaged elements, which is more visible in the model with finer discretization. It is notable that damaged element number 15 in model 1 is the boundary element, which is identified with the most detectable error, showing that quantifying damage in boundary elements is associated with more errors in comparison with other elements. Generally, the accuracy of Scenario ***A*** for damage identification, moving load identification and response prediction is not affected by discretization.

Table 5-10: The effect of discretization on damage detection- Scenario A

Model	Number of elements	Element length	Total time hr:min:sec	N.I.	L.I. error (%)		D.I. error (%)	Rec. Acc. error (%)
					Front	Rear		
1	30	1 m	0:19:07	363	1.55	2.62	2.65	0.28
2	15	2 m	0:03:04	192	1.85	2.54	1.00	0.31

`

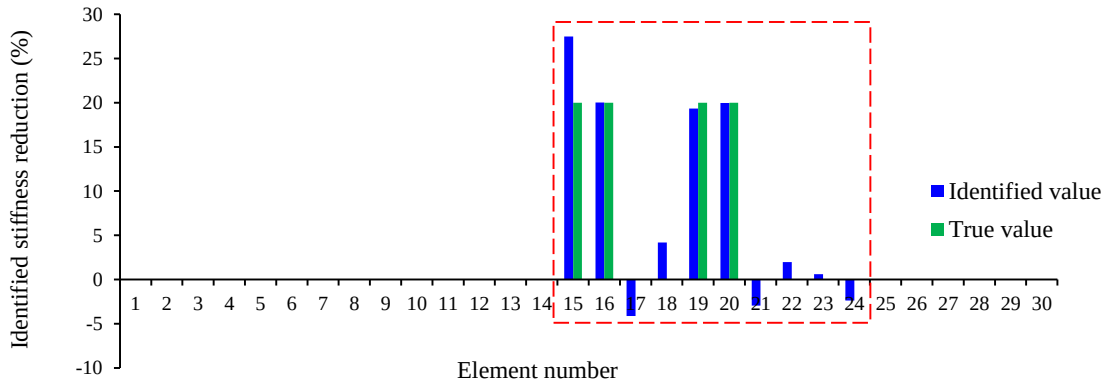

(a)

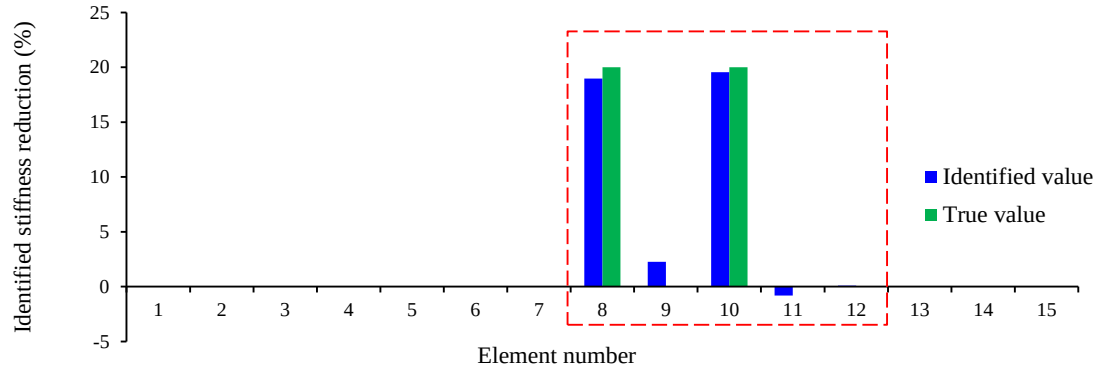

(b)

Figure 5-12: The effect of discretization on substructure case #I assessment (Scenario *A*)
a) model 1: beam with 30 elements b) model 2: beam with 15 elements

Results from Scenario B are tabulated in Table 5-11 and the identified stiffness of elements is shown in Figure 5-13. According to the results and comparing models 1 and 2, model 1 with six sensors fails to identify the damage. This is while interface forces are identified with 0.38% error and acceleration responses are predicted with 0.13% error, showing that identification of interface forces and prediction of acceleration responses are sensitive to discretization and the number of sensors.

Table 5-11: The effect of discretization on damage detection- Scenario B

Model number	Number of elements	Element length	Time duration hr:min:sec	NI	Interface force error	DI error (%)	Rec. Acc. Error (%)
1	30	1 m	00:53:14	2778	0.38 (%)	23.65	0.13
2	15	2 m	01:23:25	4871	0.3(%)	0.46	0.02

`

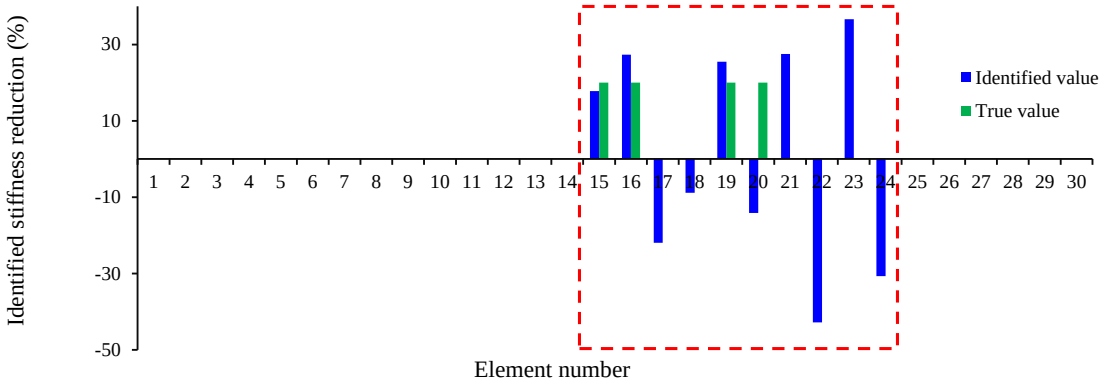

(a)

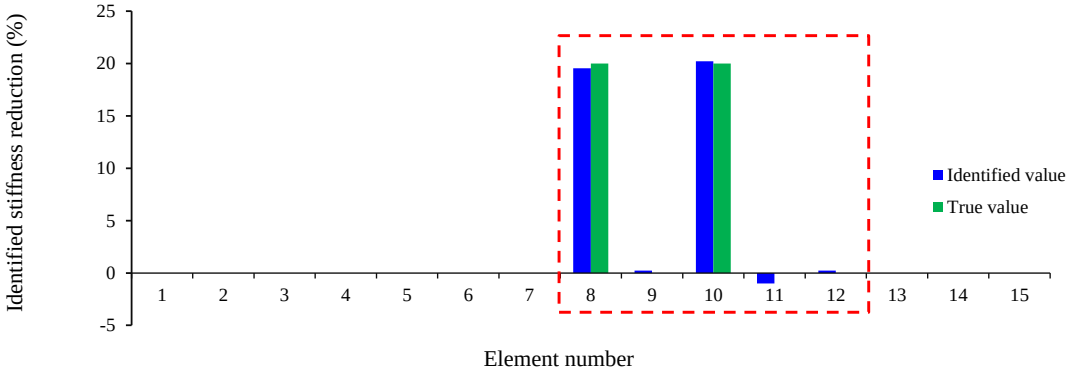

(b)

Figure 5-13: The effect of discretization on substructure case #I assessment (Scenario B)

a) model 1: beam with 30 elements b) model 2: beam with 15 elements

5.6.3. The effect of vehicle speed and road surface roughness

In this section, the effect of vehicle speed and road surface roughness on the damage detection of substructure case #I is investigated. In reality, it is dangerous to drive at high speeds on the roads with higher surface roughness. Considering ride comfort and safety, the maximum vehicle velocity for each level of road roughness is recommended in ISO 8608 (Múčka 2018). The cases which have been investigated are listed in Table 5-12.

Table 5-12: Cases to study the effect of road roughness and vehicle speed

Road surface roughness	Vehicle speed (m/s)			
	15	20	30	40
A	*	*	*	*
B	*	*		
C	*			

`

Results from Scenario ***A*** are tabulated in Table 5-13. According to the table, the proposed method is able to identify moving loads with less than 2% error at road roughness level A, regardless of the vehicle speed. By accurately identifying moving loads, damaged elements are detected and quantified precisely, as well. Identified stiffness of each element at road roughness "A" and at different vehicle speeds are illustrated in Figure 5-14. Each red horizontal line shows the location and extent of a damage. Figure 5-14 shows that the method can be used at different ranges of speed.

Table 5-13: The effect of speed and roughness on damage detection- Scenario A

Roughness	Speed (m/s)	Total time hr:min:sec	N.I.	L.I. error (%)		D.I. error (%)	Rec. Acc. Error (%)	Noise
				Front	Rear			
A	15	00:23:48	271	0.75	1.81	1.3	0.37	0%
	20	00:33:37	624	0.82	1.78	1.4	0.32	
	30	00:06:51	301	0.99	1.95	0.8	0.37	
	40	00:10:59	760	0.45	1.56	1.1	0.35	
B	15	01:13:39	797	6.59	8.26	0.4	0.30	
	20	00:52:13	1113	8.74	9.23	5.74	1.06	
C	15	00:46:58	560	18.95	16.21	9.57	1.08	

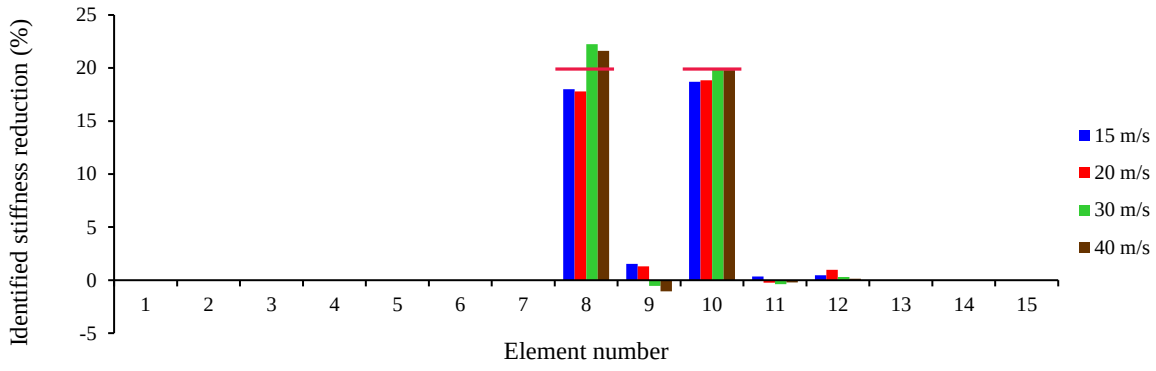

Figure 5-14: Effect of speed at road roughness A (no noise)

`

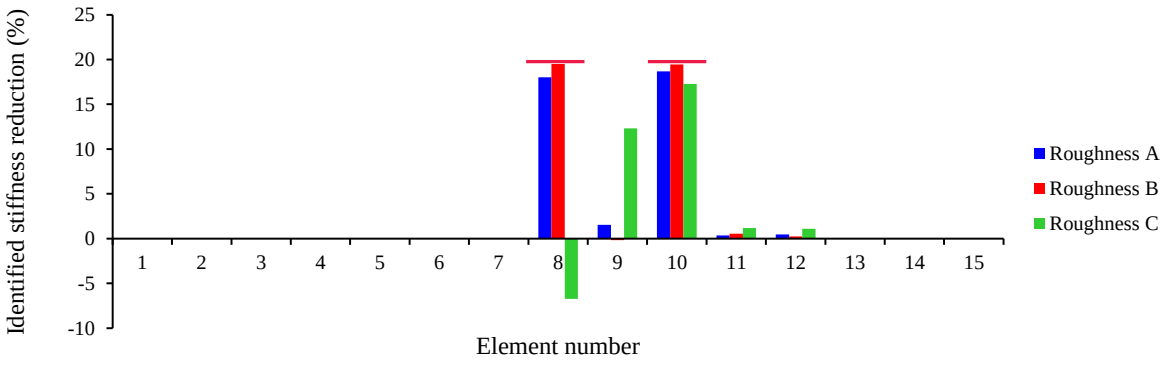

Figure 5-15: Effect of road roughness at speed 15 m/s (no noise)

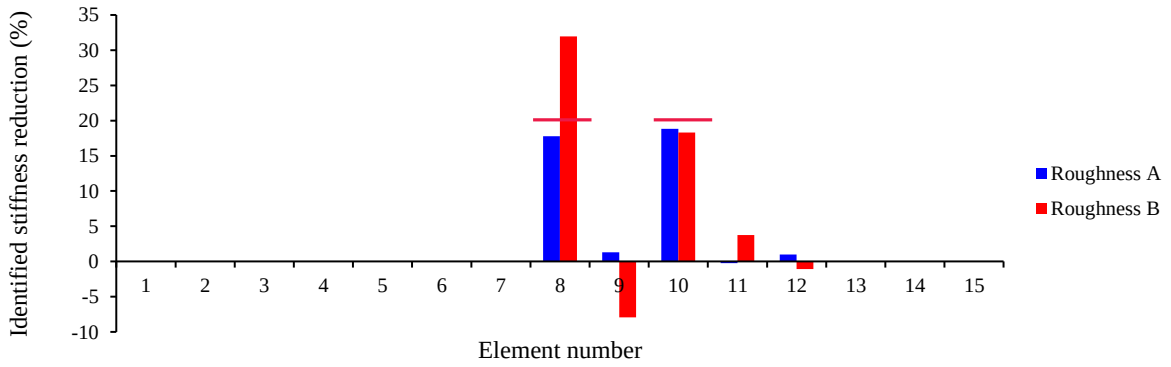

Figure 5-16: Effect of road roughness at speed 20 m/s (no noise)

The effect of road roughness on the identified stiffness reduction at speeds of 15 m/s and 20 m/s is shown in Figure 5-15, and Figure 5-16, respectively. Each red horizontal line shows the location and extent of a damage. As shown in Figure 5-15 (speed 15 m/s), damage is detected and quantified perfectly at road roughness levels A and B. At road roughness level C, the damaged element which is not a boundary element is identified and quantified well, however, the boundary damaged element is not detected correctly and its adjacent element, element number 9 is identified as a damaged element. It was already mentioned that there are some errors in damage identification of boundary elements in substructures with free-free boundary conditions. Figure 5-16 shows that damaged elements are detected perfectly in both levels of road roughness, however when it comes to quantifying the damage, again it is associated with more errors at the boundary damaged element.

`

Generally, the method is reliable for moving loads and damage identification at road roughness levels A and B regardless of the car speed, and it should be used with caution at road roughness level C. Increasing the speed at higher roughness levels not only produces higher interaction forces leading to structural damage and a reduction of ride comfort but also does reduce identification accuracy. The maximum error of reconstructed acceleration responses is 1.08% occurring at road roughness level C.

Results from Scenario B are tabulated in Table 5-14. According to the table, at road surface roughness A, the maximum errors of interface force identification, and damage identification are 0.04%, and 1.24%, respectively. Acceleration responses are predicted with the maximum error of 0.05%. Identified stiffness reduction of all elements at road surface roughness A and different speeds can be seen in Figure 5-17. Each red horizontal line shows the location and extent of a damage. Results indicate that the proposed method is very reliable at road roughness A, at all speed ranges. Damaged elements are detected and quantified with high accuracy.

According to Table 5-14, Figure 5-17, Figure 5-18, and Figure 5-19, it can be seen that an increase in the level of road roughness at different speeds neither has affected the accuracy of damage detection nor has influenced the identification of interface forces or prediction of acceleration responses. However, computation time has greatly increased from the speed of 40 m/s to 15 m/s.

It is shown that computation time can be reduced effectively if a shorter interval of the measurement time history is considered in the identification process. The interval of measurement time history including those moments that the front wheel enters the bridge and reaches Node 5 of the structure is considered and results are tabulated in Table 5-15. It can be seen that in this case computation time is almost half that of different speed levels with the same level of identification accuracy.

`

Table 5-14: The effect of speed and roughness on damage detection- Scenario B

Roughness	Speed (m/s)	Total time hr:min:sec	N.I.	Interface force error (%)	D.I. error (%)	Rec. Acc. Error (%)	Noise
A	15	15:01:40	4144	0.01	0.16	0.03	0%
	20	12:07:55	4367	0.02	0.29	0.02	
	30	03:31:27	5368	0.01	0.27	0.04	
	40	01:24:48	5012	0.04	1.24	0.05	
B	15	25:22:28	4413	0.41	1.13	0.06	
	20	17:19:09	4028	0.10	0.17	0.05	
C	15	25:07:41	2933	0.36	0.54	0.05	

Table 5-15: The effect of speed and roughness on damage detection- Scenario B (shorter time history)

Roughness	Speed (m/s)	Total time hr:min:sec	N.I.	Interface force error (%)	D.I. error (%)	Rec. Acc. Error (%)	Noise
A	15	8:15:37	2705	0.02	0.09	0.02	0%
	20	06:52:31	2881	0.03	0.47	0.025	
	30	01:43:21	1846	0.02	0.57	0.04	
	40	00:49:28	2871	0.01	0.21	0.02	

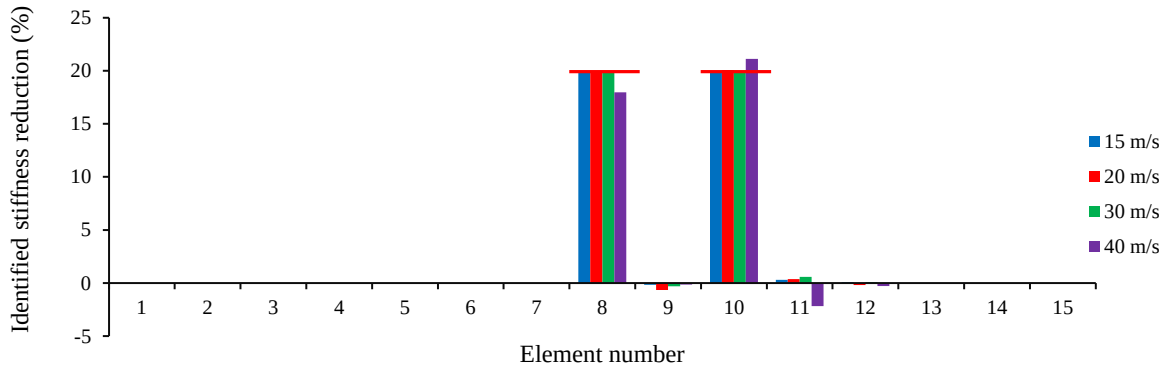

Figure 5-17: Effect of speed on damage identification at road roughness A-no noise

`

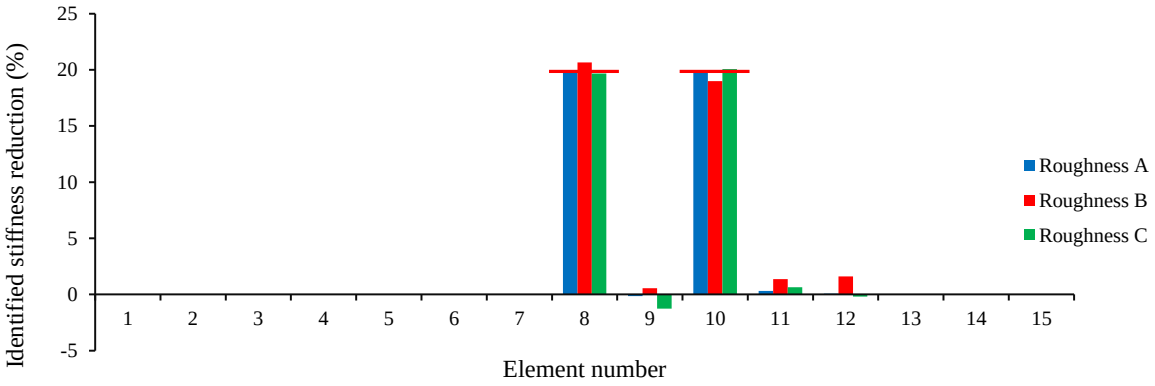

Figure 5-18: Effect of road roughness on damage identification at speed 15 m/s- no noise

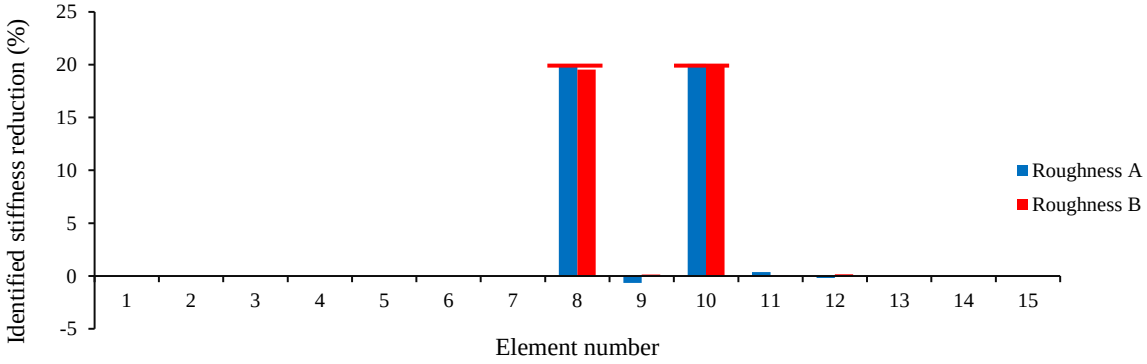

Figure 5-19: Effect of road roughness on damage identification at speed 20 m/s- no noise

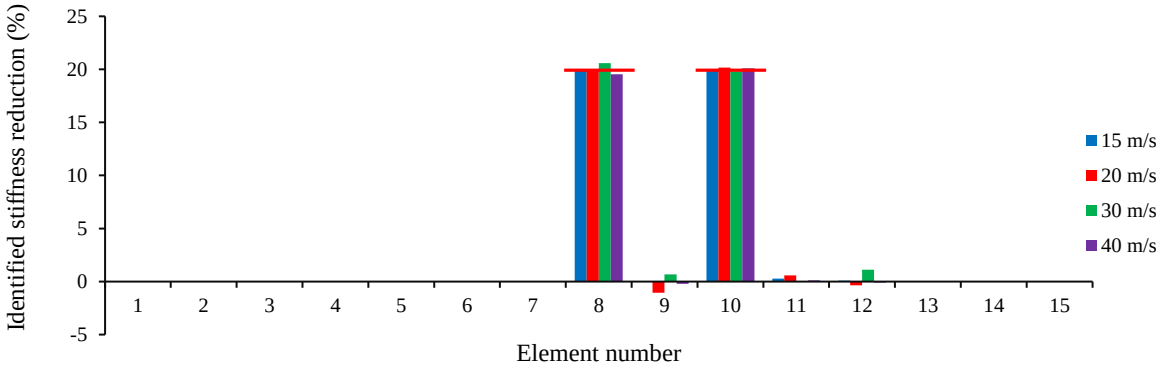

Figure 5-20: Effect of speed on damage identification at road roughness A- no noise (shorter time history)

5.6.4. The effect of measurement noise

In this section, the effect of noise on the assessment of substructure case #I by Scenarios A and B is investigated. The vehicle moves over the bridge at a speed of 40 m/s. The road surface roughness is assumed to be “A”. The finite element model of the beam is divided into 15 elements and 16 nodes, each with two degrees of freedom. The sampling frequency rate is

`

200 Hz. Local damage is assumed to be a 20% reduction in the elemental stiffness of elements 8 and 10.

The effect of noise on damage detection by Scenario A can be seen in Figure 5-21. Each red horizontal line shows the location and extent of a damage. At 0-2% noise, elements 8 and 10 are identified as damaged elements with stiffness reduction values close to 20%, and at noise 3-5% damaged elements are detected with stiffness reduction more than 20% and false positives/ negatives can be seen. Generally, this scenario is reliable when the measurement noise is less than 3%.

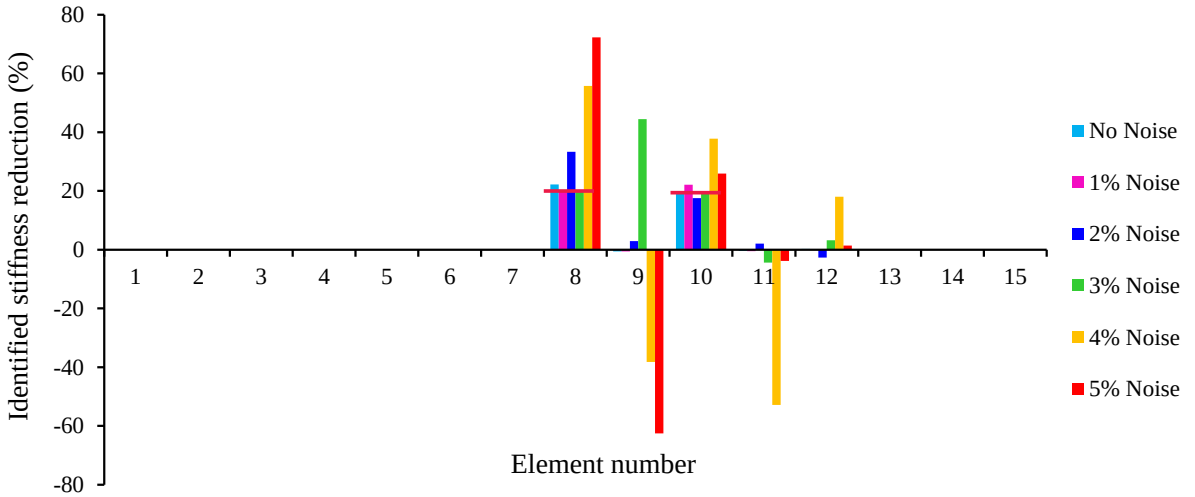

Figure 5-21: Effect of noise on the damage detection at speed 30 m/s- Scenario A

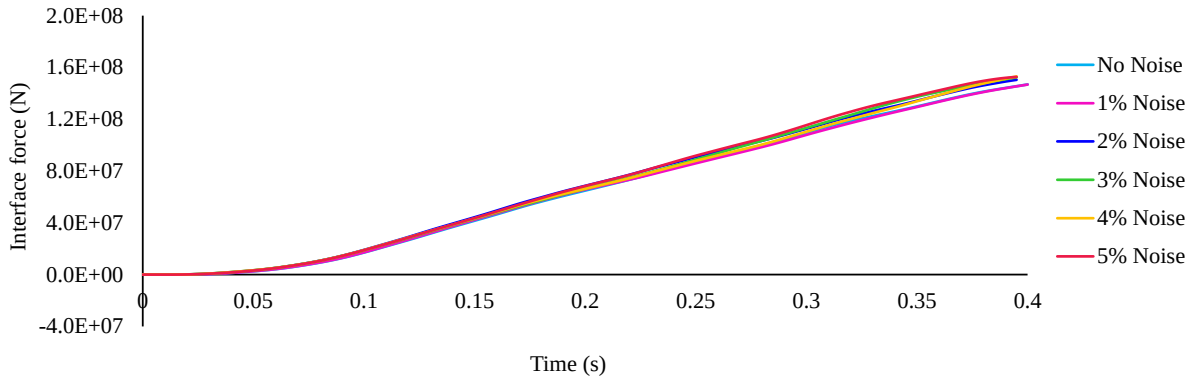

Figure 5-22: Effect of noise on the vertical identified interface force- Scenario A

The effect of noise on the identified vertical interface force and identified moving loads can be seen in Figure 5-22 and Figure 5-23, respectively. As can be seen, noise does not affect

`

the accuracy of the identified interface forces, however, the identified moving loads are affected at 5% and they are identified less than the true loads. The accuracy of the method is confirmed through comparing the results without noise with true ones. Convergence information and calculation accuracy are listed in Table 5-16.

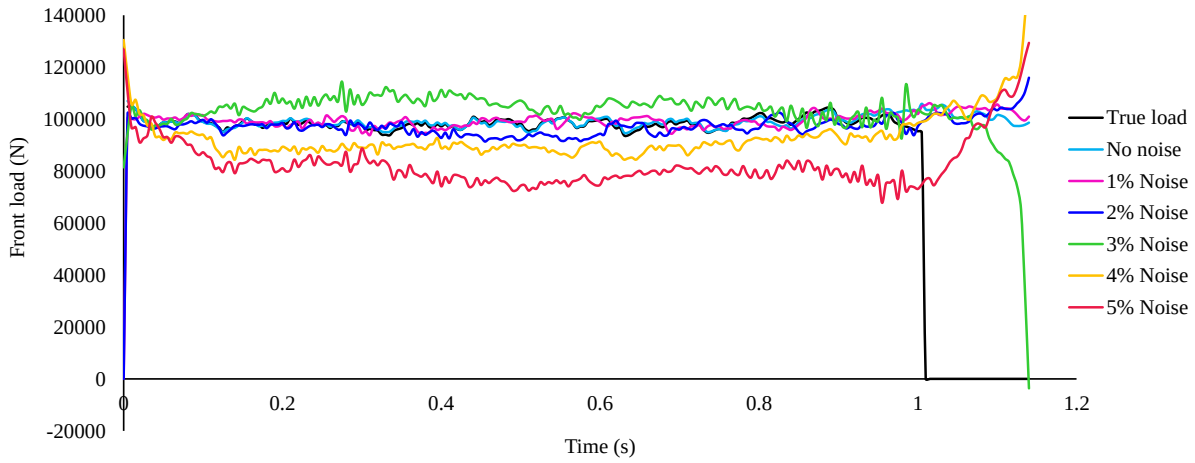

(a)

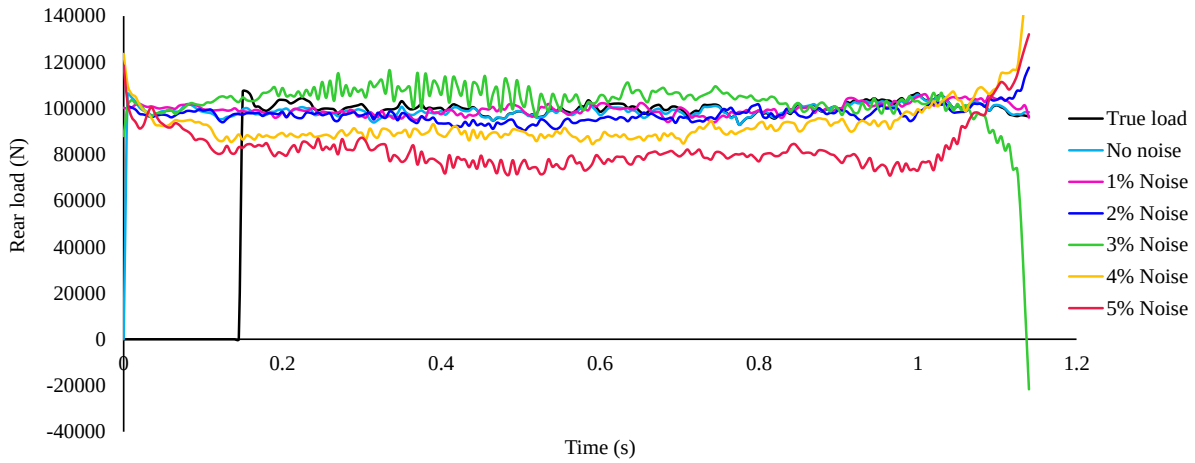

(b)

Figure 5-23: Effect of noise on the identified loads with Scenario A: a) Front load b) Rear load

The effect of noise on damage detection by Scenario B can be seen in Figure 5-24. Each red horizontal line shows the location and extent of a damage. When there is no noise, elements 8 and 10 are detected as damaged elements with stiffness reductions of 19.81% and 19.88%, which are very close to the true values of 20%, confirming the accuracy of the method. With polluted measurements, it can be seen that damaged elements are detected at all levels of noise,

`

however, stiffness reduction values display an error in comparison with the true values and there are some false positives and negatives. Generally, this Scenario is sensitive to measurement noise. This is further investigated by experimental studies.

Table 5-16: Damage identification results - Scenario A

Roughness-Speed	Noise	Total time hr:min:sec	N.I.	L.I. error (%)		D.I. error (%)	Rec. Acc. Error (%)
				Front	Rear		
A-30	0%	00:06:51	301	0.99	1.95	0.77	0.37
	1%	00:01:44	69	0.92	1.83	0.80	1.27
	2%	00:02:53	116	2.75	4.22	5.12	1.97
	3%	00:11:05	396	7.50	6.23	11.47	2.7
	4%	00:05:35	218	8.37	10.66	35.34	6.10
	5%	00:09:19	347	19.48	20.83	27.37	7.54

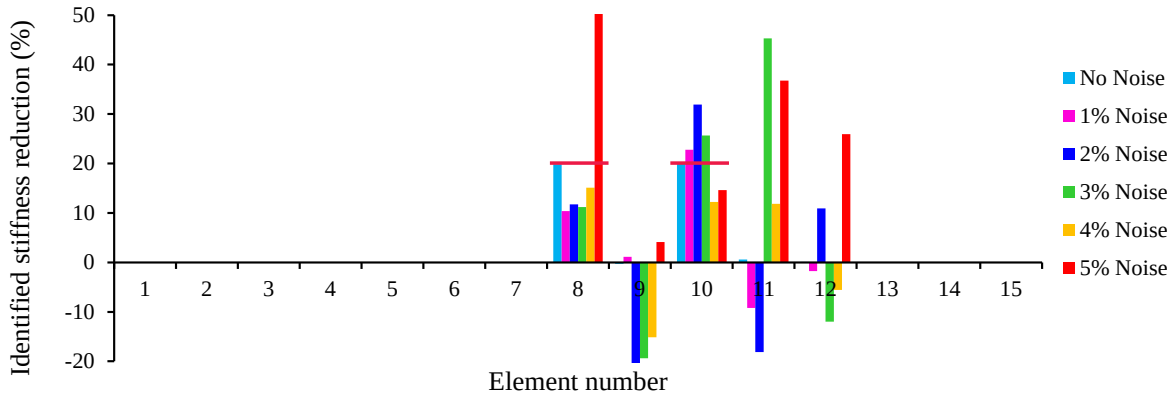

Figure 5-24: Effect of noise on the damage detection at speed 30 m/s- Scenario B

The effect of noise on the identified vertical interface force is illustrated in Figure 5-25. As can be seen, the interface force is not affected considerably by noise, however, the identified interface force in Scenario B is more sensitive to noise when compared to Scenario A and damage detection by Scenario A is more precise. Convergence information and calculation accuracy are listed in Table 5-17.

`

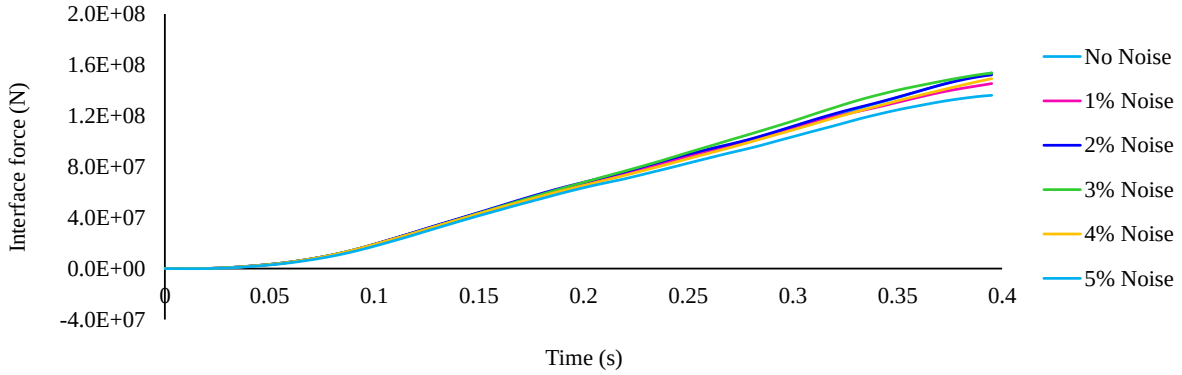

Figure 5-25: Effect of noise on the vertical identified interface force- Scenario B

Table 5-17: Damage identification results - Scenario B

Roughness-Speed	Noise	Total time hr:min:sec	N.I.	F.I. error (%)	D.I. error (%)	Rec. Acc. Error (%)
A-30	0%	03:31:27	5368	0.01	0.27	0.04
	1%	00:41:26	1108	1.16	5.34	0.93
	2%	01:28:08	2191	4.25	15.70	1.97
	3%	02:29:22	3632	4.32	19.74	3.49
	4%	00:42:53	1042	4.51	9.83	3.26
	5%	02:02:37	2957	4.53	27.8	4.75

5.7. Conclusion

A substructure condition assessment of bridge structures under moving vehicles based on the explicit form of the Newmark-β method was proposed in this chapter. Two different Scenarios were studied, namely: Scenario A and Scenario B. In Scenario A, the finite element model of the whole structure was known and in Scenario B only the finite element model of the substructure was known. The effects of the boundary conditions, sensor placements, vehicle speed, road surface roughness, and measurement noise on the accuracy of these two Scenarios were studied and conclusions are listed as follows:

- For Scenario A, good accuracy of damage detection can be achieved with 4 sensors.
- For scenario B, the boundary condition of the target substructure can affect the accuracy of damage detection. When the boundary condition is free-free, it needs at least 6 sensors, however, when one end of the boundary condition is known, good results can be achieved even with 4 sensors.

`

- Scenario A is not sensitive to discretization, but Scenario B is. With proper discretization, Scenario B can provide very promising results.
- Both Scenarios A and B are reliable at different ranges of speed.
- Scenario B can be used at different levels of road roughness. It is not recommended to use Scenario A at road roughness level C.
- Scenario A is reliable to be used at measurement noise less than 3%, however, Scenario B is affected by even 1% measurement noise.

`

`

Chapter 6. Laboratory Experimental study

6.1. Introduction

Experimental studies are performed to validate the proposed techniques for condition assessment of bridge structures under moving loads. In section 6.2, the test set-up is explained and in section 6.3, the results of the modal test on the intact beam are presented. The responses of the beam subject to the moving vehicle are recorded by accelerometers and strain gauges, after which they need to be de-noised and zero shift needs to be removed. The technique performed for signal processing is explained in section 6.4.

In chapter 3 of this thesis, a technique based on the explicit form of the Newmark-β method has been presented to identify moving loads and is then numerically verified. In section 6.5 of the current chapter, experimental studies are carried out to verify the efficiency of the proposed technique at different sensor placements, sampling frequencies, and vehicle speeds in the laboratory.

In chapters 4 and 5 of this thesis, techniques based on the explicit form of the Newmark-β method have been proposed for a full-structure and substructure condition assessment of bridge structures subject to moving loads. The robustness of the proposed techniques has been numerically investigated through studying the effects of measurement noise, sensor placement, vehicle speed, and road surface roughness. These techniques are experimentally verified in section 6.6 of this chapter, and the effects of sampling frequency and vehicle speed are explored.

In section 6.6.1, the proposed technique for simultaneous identification of moving loads and structural damage of the full structure is experimentally verified, and in section 6.6.2, the proposed method for substructural condition assessment is also experimentally validated. Substructural condition assessment is conducted for two Scenarios A and B. In Scenario A (section 6.6.2.1), the finite element model of the whole structure is available, while in Scenario B (section 6.6.2.2), only the finite element model of the target substructure is available. The conclusion of this chapter is then presented in section 6.7.

6.2. Experimental test set-up

A simply supported steel bridge is designed in the laboratory, with the experimental test set up shown in Figure 6-1. Since the whole project is difficult to be shown clearly in one picture, the diagrammatical picture is illustrated in Figure 6-1. The main beam is 3 meters long with a 25×100 mm uniform cross-section and it is simply supported. There are 3 m leading and trailing beams for vehicle acceleration and deceleration. To have a simply supported beam,

`

there should be a gap between the main beam and the other two beams (see Figure 6-2). The details of support, photoelectric sensor, and the gap between the two beams are shown in Figure 6-2. Three photoelectric sensors were equally spaced on the beam to monitor the vehicle entrance/exit and measure its speed. The measured density of the beam is 19.7 kg/m and the initial young's modulus is considered as 210 GPa.

The model vehicle (Figure 6-3) has two axles spacing at 30 cm and running on four steel wheels wrapped by a rubber band. The model is symmetrical and weighs 4.4 kg. A "U" shaped aluminium section is used to guide the vehicle on the beams. The vehicle is pulled along the guide by a string connected to an electrical motor.

Seven strain gauges and accelerometers (see Figure 6-4) are evenly distributed underneath the main beam. Strain gauges are model FLA-5-11-3LJCT and accelerometers are piezoelectric model ICP ®. A 9-slot data acquisition system model NI PXIe-1078 is used to process the signals (Figure 6-5), connected to LabVIEW as a post-processing software.

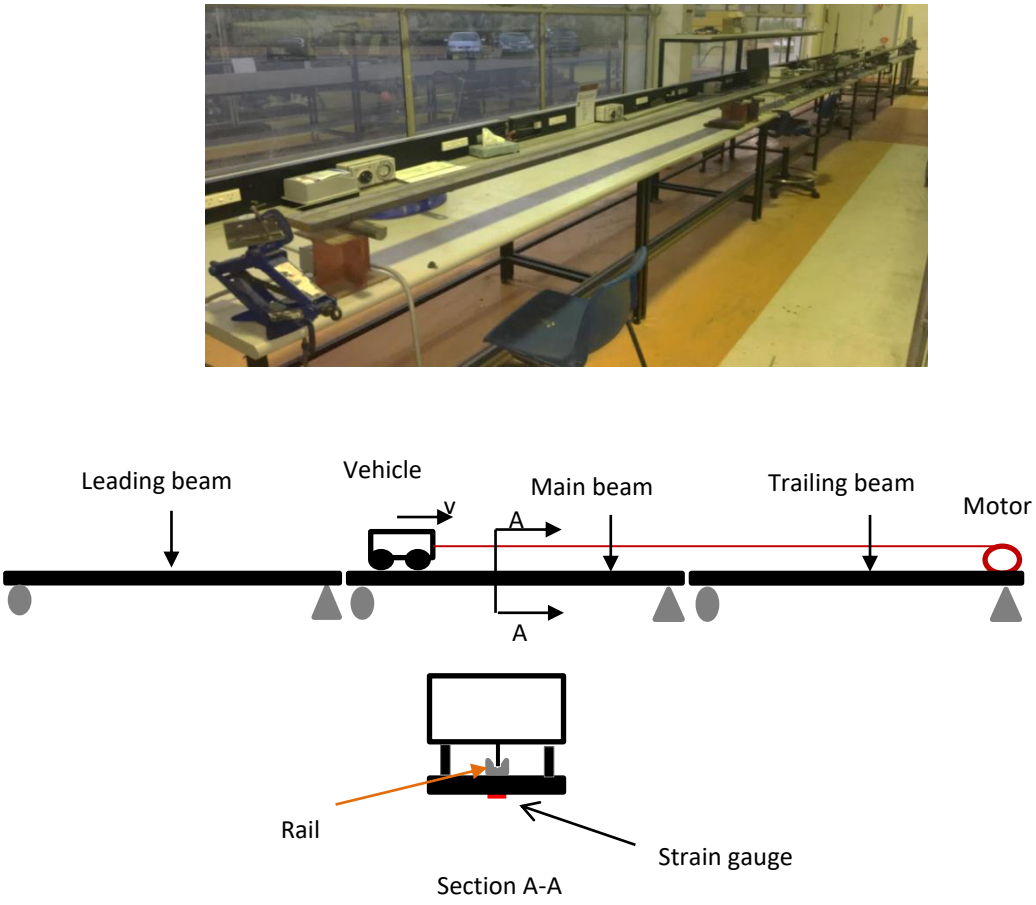

Figure 6-1: Experimental set-up of the vehicle-bridge system

`

Figure 6-2: Details at the left-hand support of the main beam

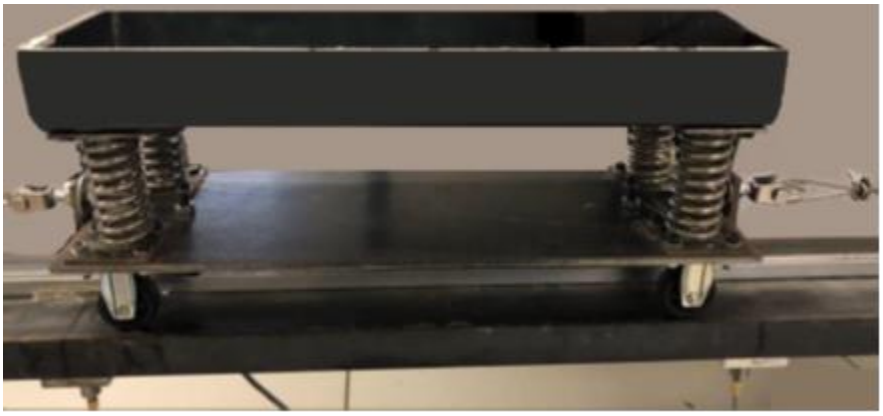

Figure 6-3: The two-axle model vehicle

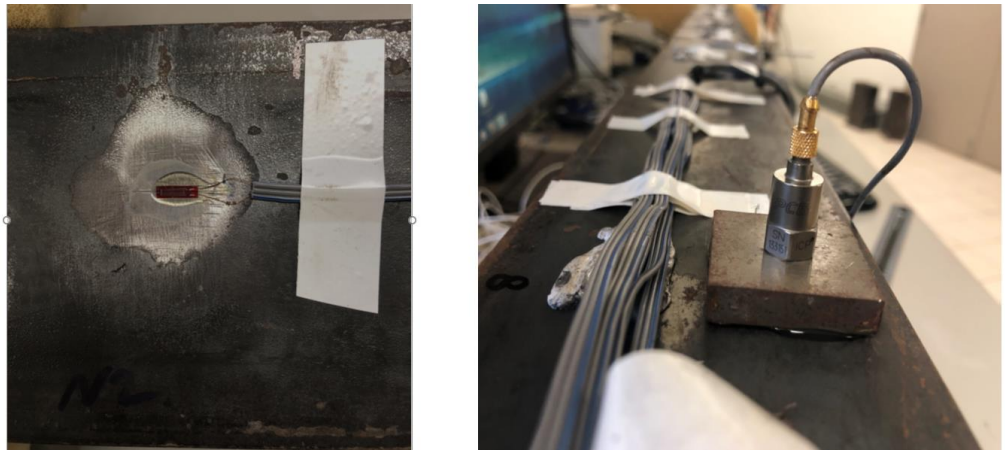

Figure 6-4: Strain gauge and accelerometer - Underneath the beam

`

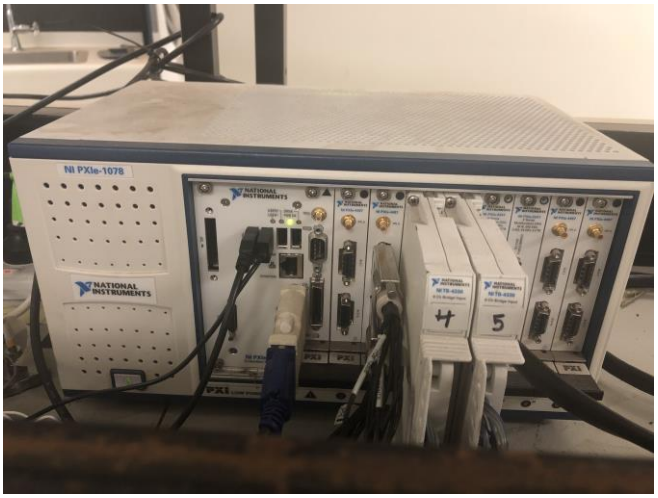

Figure 6-5: Data acquisition system

6.3. Modal test of the beam

To identify the dynamic properties of the steel beam, a modal test is carried out. In the modal test, an impact hammer is used to excite the beam at a certain reference point, and the accelerations of the beam are measured by accelerometers. The impact hammer used to excite the beam is a PCB model 086C41 which is shown in Figure 6-6. The reference point is located at 0.45 L, and the beam responses are measured by two piezoelectric accelerometers at locations 3L/16 and L/2.

The accelerometer installed at location L/2 is able to clearly identify 1st, 3rd, and 5th modes; but not 2nd and 4th modes, since it is located on the node point of these modes. An accelerometer installed at location 3L/16 is able to clearly identify all first five modes. The reference point is chosen at location 0.45 L as none of the first five flexural mode shapes has a node point at location 0.45 L. All these modes are excited through this technique and hence can be identified.

The sampling rate is set at 500 Hz with 35000 time-domain data points being recorded. The impact force curve of the impact hammer is shown in Figure 6-7. The proper impact force has only one peak with maximum amplitude and minimum duration which can excite the main frequencies of the beam. A white tip with mild texture is used for excitation.

`

Figure 6-6: Impact hammer

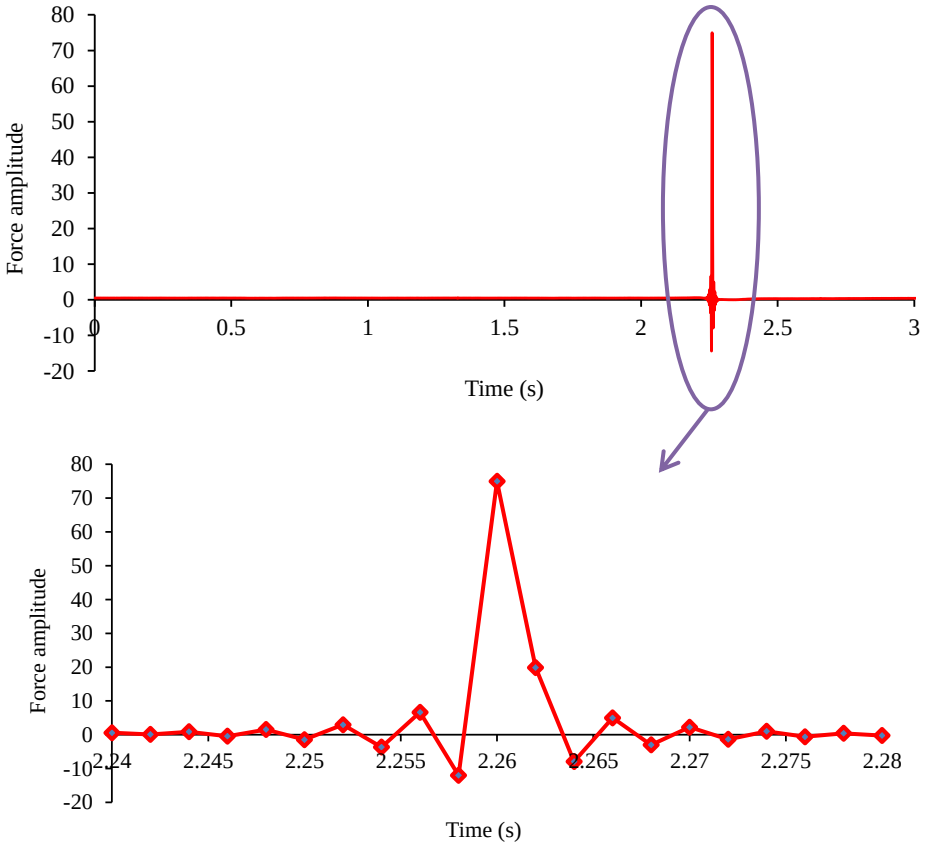

Figure 6-7: Hammer impact force

`

The acceleration time history at location 3L/16 is shown in Figure 6-8. It consists of three parts, namely: before impact, during impact, after impact. The response during the impact force duration is called forced vibration and the response after impact force is called free vibration. To find the first five natural frequencies, sixty seconds of the free vibration signal, including 30000 data points, are considered.

The free vibration signals in the time domain were then converted into the frequency domain using the Fast Fourier Transform (FFT), as illustrated in Figure 6-9. In this figure, distinct frequency peaks are visible describing the first five flexural modes. Some other picks can also be observed, relating to torsional or transversal modes which cannot be precisely identified by the current sensor setup.

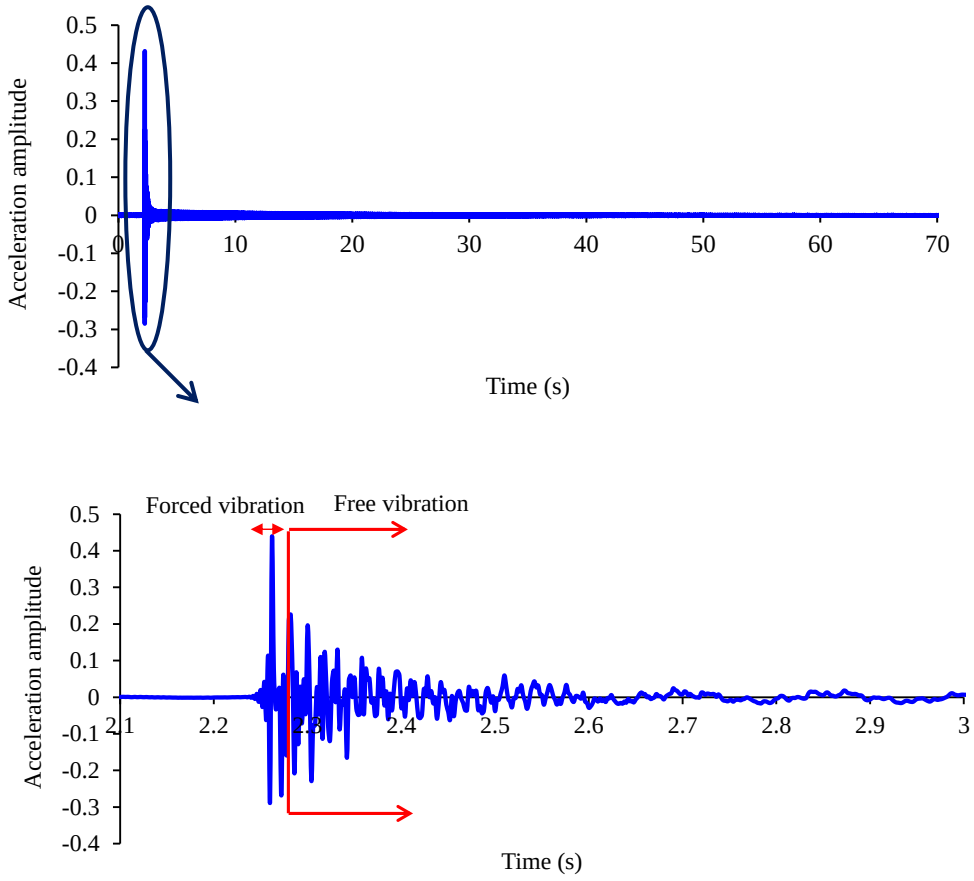

Figure 6-8: Acceleration response at location 3L/16

`

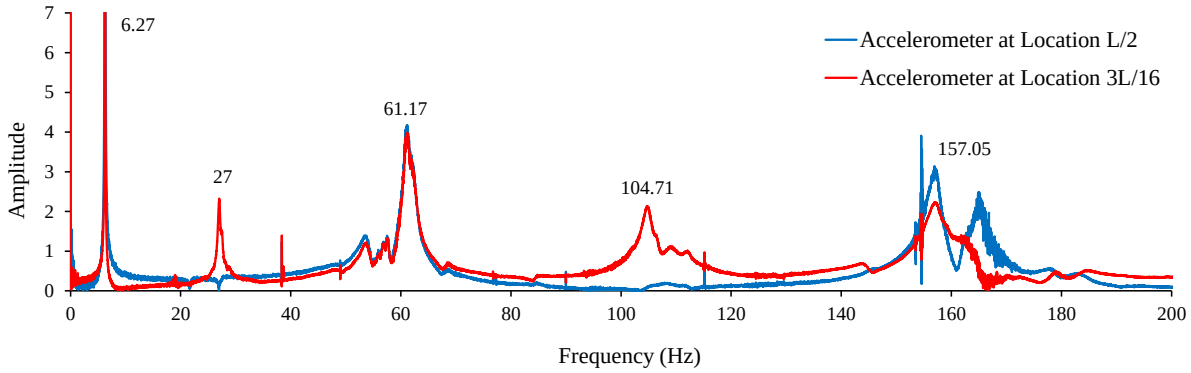

Figure 6-9: FFT of acceleration responses at locations L/2 and 3L/16

The finite element model (FEM) of the bridge beam is created in MATLAB including 8 Euler-Bernoulli beam elements with two degrees-of-freedom at each node. The numerical natural frequencies from the FEM of the beam, experimental ones and the errors between them are tabulated in Table 6-1. The numerical frequencies are found very close to the measured values confirming the accuracy of the model for the simulation.

Table 6-1: Calculated and measured natural frequencies of the test beam (Hz)

Measured	6.27	27	61.17	104.71
Calculated	6.48	25.78	57.38	100.3
Error	3.34%	4.52%	6.19%	4.21%

6.4. Signal processing

To mitigate the effect of measurement noise on the accuracy of the identified loads, the Chebyshev Polynomial is used to smooth measurements as follows:

$$\varepsilon(x,t) = \sum_{i=1}^{N_f} T_i(t) C_i(x) \qquad 6\text{-}1$$

where $\{T_i(t), i = 1,2,3,\dots,N_f\}$ is the generalized orthogonal function (Zhu, XQ & Law 2001b), N_f is the number of terms in the generalized orthogonal function, and $\{C_i(x), i = 1,2,3,\dots,N_f\}$ is the vector of coefficients in the expansion expression. N_f can affect the accuracy of the results, therefore a study is performed to find the best value N_f.

`

6.5. Moving load identification verification

In this section, tests are carried out to verify the proposed method for moving load identification (MLI) when the structure is undamaged. The FEM of the beam is created in MATLAB, including 8 Euler-Bernoulli beam elements. Strain measurements are used as inputs, converted to nodal displacements using the generalized orthogonal function (Zhu, XQ & Law 2001b). The effects of the number of terms in the generalized orthogonal function (N_f), as well as sensor arrangements, sampling frequency, and vehicle speed on the accuracy of the moving load identification are experimentally investigated. To quantify the moving loads' identification accuracy, a percentage error is defined as:

$$\text{Re}constructed\ response\ error = \|\text{Re}sponse_m - \text{Re}sponse_{reconstructed}\|/\|\text{Re}sponse_m\| \times 100\ \% \quad (6\text{-}2)$$

where $\text{Re}sponse_m$ is the experimental response and $\text{Re}sponse_{reconstructed}$ is the reconstructed response at the same point. The reconstructed response can be obtained by inputting the identified loads into the system and calculating the responses of the beam as a forward analysis. The accurately identified moving loads should be able to reconstruct the response very close to the measured one. Another way to check the accuracy of the identified moving load is to compare it with the related static loads of the vehicle. The identified moving loads fluctuate around the static loads of the vehicle model.

6.5.1. The effect of N_f

In this test, the test vehicle is pulled over the beam at an average speed of 27 units (≈ 0.47 m/s). The sampling frequency is set at 200 Hz and strain measurements from seven strain gauges are recorded. The number of master DOFs to convert strains to displacement is considered equal to the number of measured strains. Moving loads are identified by the Tikhonov regularization technique and the optimal regularization parameter is obtained by the L-curve method.

Moving loads are identified with different N_f ranging from 100 to 800, and the error of reconstructed strain at mid-span is calculated and shown in Figure 6-10. The figure shows N_f=283 provides the minimum rating of error (1.75%). In this chapter N_f is optimized for each test separately. In Figure 6-11, the reconstructed strain at mid-span is compared with the measured one when N_f=283, denoting they match very closely.

As N_f is smaller, a bigger range of higher frequencies is omitted resulting in smoother responses and therefore smoother identified loads which are very close to the static axle loads

`

and cannot precisely show the dynamic parts of responses. As N_f is bigger, a lesser range of higher frequencies is omitted, and noise usually appears in high frequencies. Hence, an optimized N_f will remove noise while keeping the dynamic properties of the response. Comparison of the identified moving loads with N_f =283 and N_f =50 is shown in Figure 6-12.

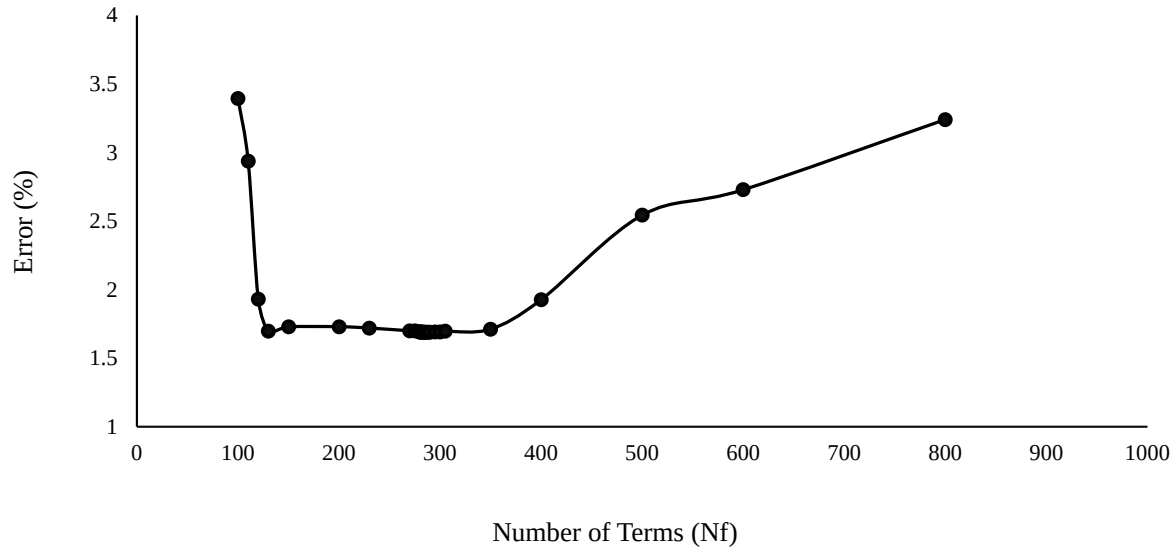

Figure 6-10: The effect of N_f on the error of the reconstructed strain

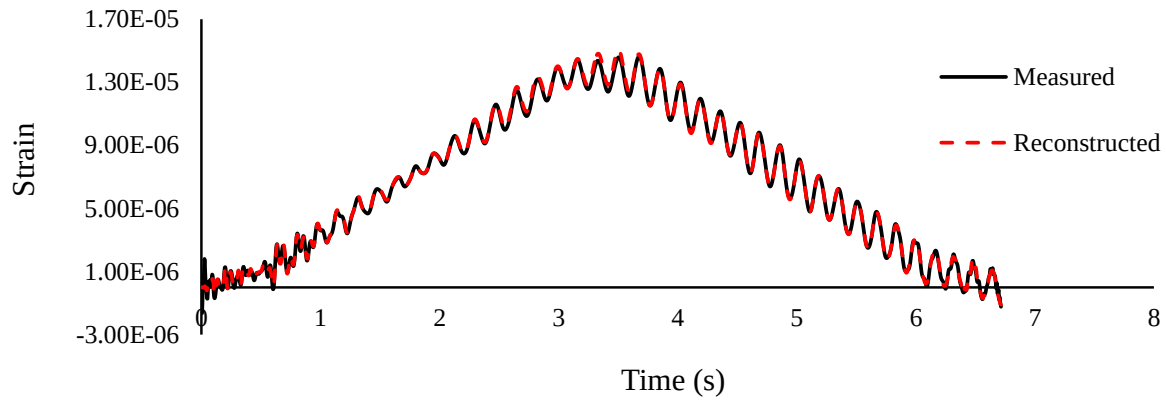

Figure 6-11: Measured and reconstructed strain at mid-span- N_f =283

`

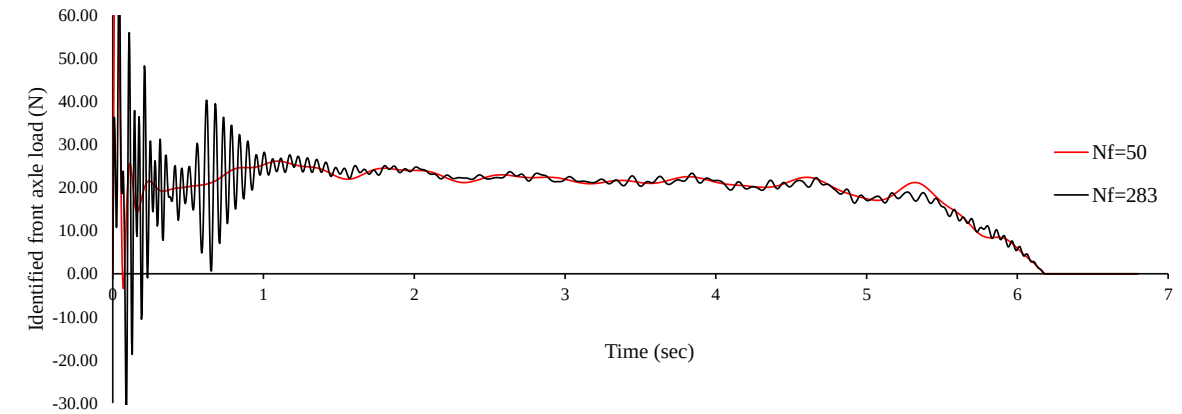

(a)

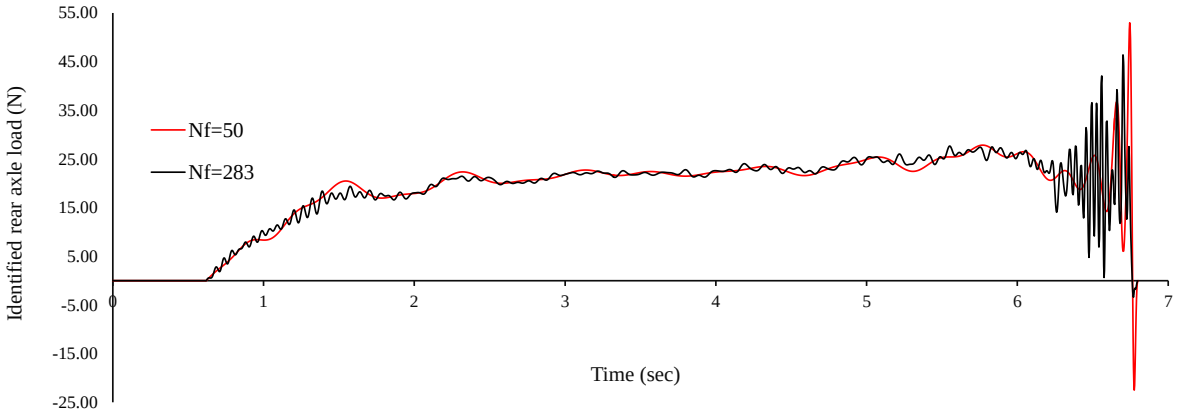

(b)

Figure 6-12: Comparison of the effects of a small N_f and the optimized one on the identified axle loads. (a) Identified front axle load, (b) identified rear axle load

6.5.2. The effect of different measurement arrangements

To investigate the effect of sensor arrangements on identifying moving loads, seventeen different cases are studied as tabulated in Table 6-2. The vehicle is pulled over the beam at an average speed of 27 units (≈ 0.47 m/s), and the sampling frequency is set at 200 Hz.

Strain measurements are smoothed by the Chebyshev polynomial with N_f =283, and are converted into nodal displacements. The Tikhonov regularization method is used to identify moving loads and the optimal regularization parameter is obtained by the L-curve method.

The identified front/rear moving loads from different sensor placements are compared with sensor placement #1 through Figure 6-13 to Figure 6-16. Sensor placement #1 with seven sensors has the least error values for reconstructed strain, therefore it is considered as a reference. Large fluctuations can be seen around 0.625 s and 6.25 s in the identified moving loads time histories, originating from the 1mm-gap between the beams, which produce large

`

impacts when the front/rear axle loads enter/exit the beam. The front/rear axle loads are identified as zero when they are not on the beam, showing the accuracy of the simulation. The pitching motion of the car can be seen in the time histories.

Since the true interaction force is not known to investigate the accuracy of identified axle loads, the strain at mid-span is reconstructed and percentage errors have been calculated and listed in Table 6-3. Furthermore, the average of identified front axle load, identified rear axle load, and resultant identified load when both of the axles are on the beam has been compared with the static axle load (22 N); static weight of the vehicle (44 N) and the identified errors are tabulated in Table 6-3.

Conclusions from Table 6-3 are as follows:

- Moving load identification from 7 strain gauges provides the best accuracy with 1.75% reconstructed strain error.
- At least three strain gauges are required to identify moving loads in such a way that reconstructed strain has less than 5% error.
- It is better to distribute sensors evenly and symmetrically to achieve more accurate results.
- Sensor placements #1, #2, and #9 to #13, having sensors equally spaced, indicate increasing the number of sensors increases the accuracy of moving load identification.

Choosing the best sensor placement depends on budget and customer needs. Here, sensor placement #2 is chosen to investigate the effect of sampling frequency and vehicle speed on identifying the loads moving over the beam at an undamaged state. Front, rear, and resultant identified loads in sensor placement #2 are compared with axle and total static loads of the car as shown in Figure 6-17. It can be concluded that both front and rear identified loads are fluctuating around the static axle values (22 N), and the identified resultant load is fluctuating around the total static weight of the vehicle (44 N).

`

Table 6-2: Sensor arrangements

Case number	Number of sensors	Sensor location						
		L/8	L/4	3L/8	L/2	5L/8	6L/8	7L/8
#1	7	*	*	*	*	*	*	*
#2	3		*		*		*	
#3	3	*			*			*
#4	3			*	*	*		
#5	3	*		*		*		
#6	4	*	*	*	*			
#7	4	*		*	*		*	
#8	4	*	*		*	*		
#9	4	*		*		*		*
#10	5	*	*		*		*	*
#11	5	*		*	*	*		*
#12	5		*	*	*	*	*	
#13	6	*	*	*		*	*	*
#14	1				*			
#15	2			*		*		
#16	2		*				*	
#17	2	*			*			

`

Table 6-3: The percentage error for different sensor arrangements

Case number	Number of sensors	The percentage error (%)			
		Strain at mid-span	Average of identified front axle load	Average of identified rear axle load	Average of resultant identified load
#1	7	1.75	0.09	0.25	0.08
#2	3	2.97	1.03	2.46	0.72
#3	3	4.79	2.33	3.53	2.93
#4	3	4.06	1.66	0.35	0.66
#5	3	2.55	3.77	3.87	0.05
#6	4	4.96	4.10	3.8	0.51
#7	4	2.00	4.15	4.38	0.12
#8	4	3.76	0.03	1.02	0.49
#9	4	2.31	0.51	2.56	1.03
#10	5	2.51	0.53	1.16	0.32
#11	5	1.86	0.28	2.12	0.92
#12	5	1.99	0.32	1.55	0.61
#13	6	1.80	0.36	0.66	0.15
#14	1	10.78	0.31	0.65	0.48
#15	2	5.28	1.70	0.04	0.87
#16	2	11.02	1.74	0.18	0.96
#17	2	9.07	8.82	11.87	1.52

`

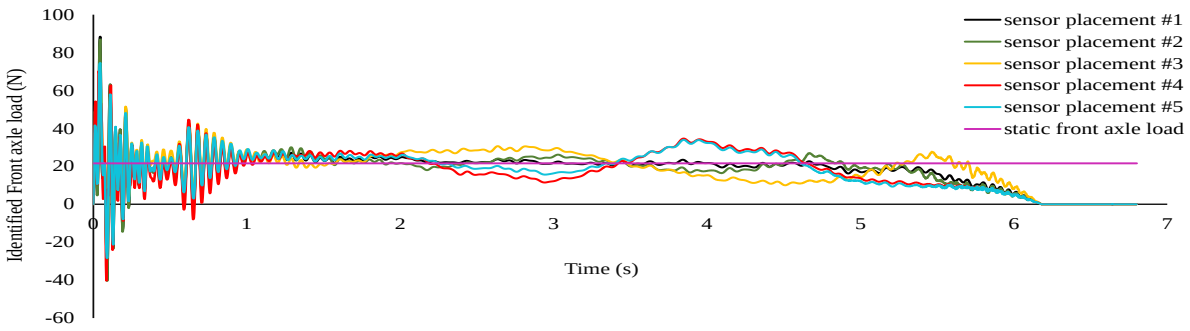

(a)

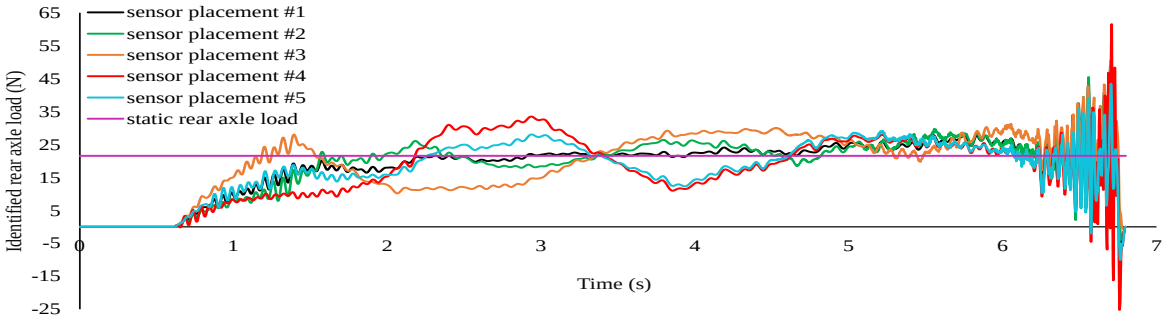

(b)

Figure 6-13: Comparison of the identified loads by sensor placements including 3 sensors and 7 sensors (a) identified front axle load (b) identified rear axle load

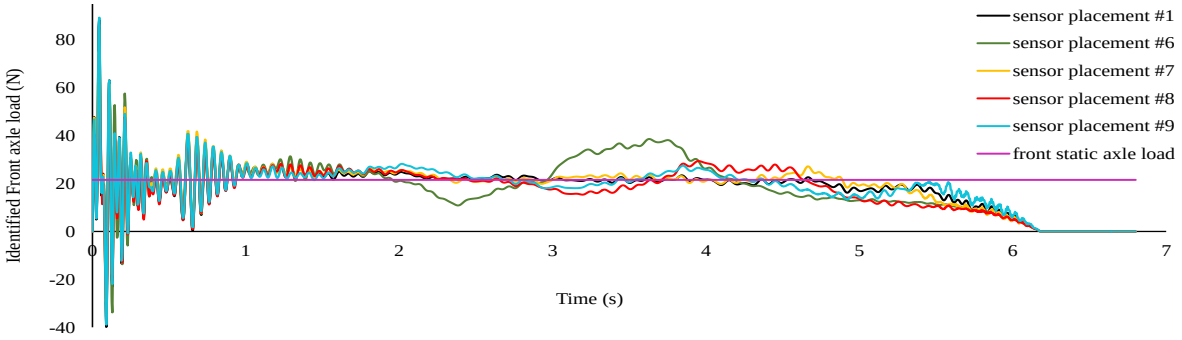

(a)

`

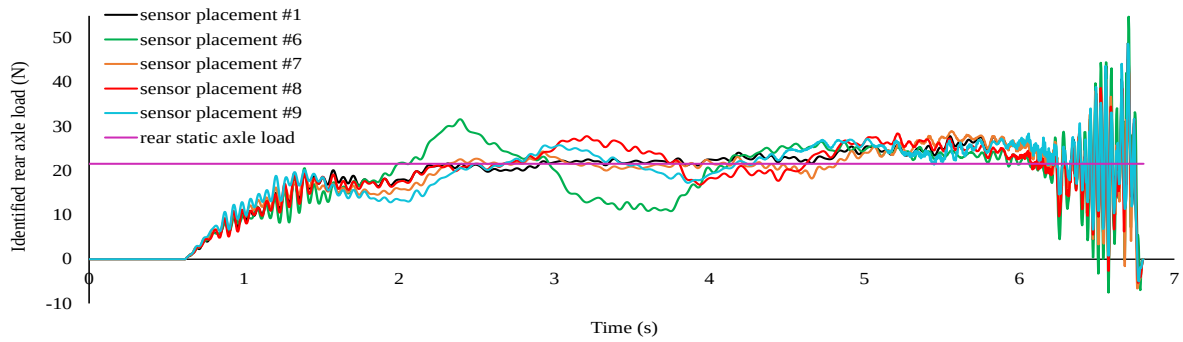

(b)

Figure 6-14: Comparison of the identified loads by sensor placements including 4 sensors and 7 sensors (a) identified front axle load (b) identified rear axle load

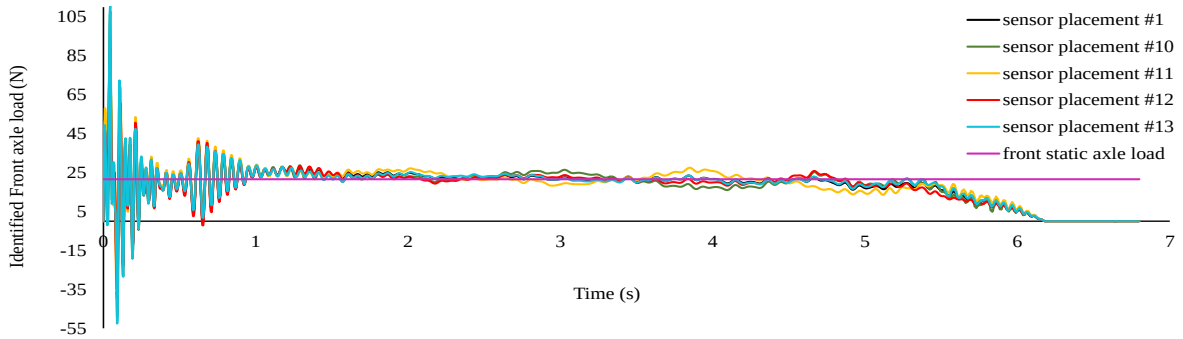

(a)

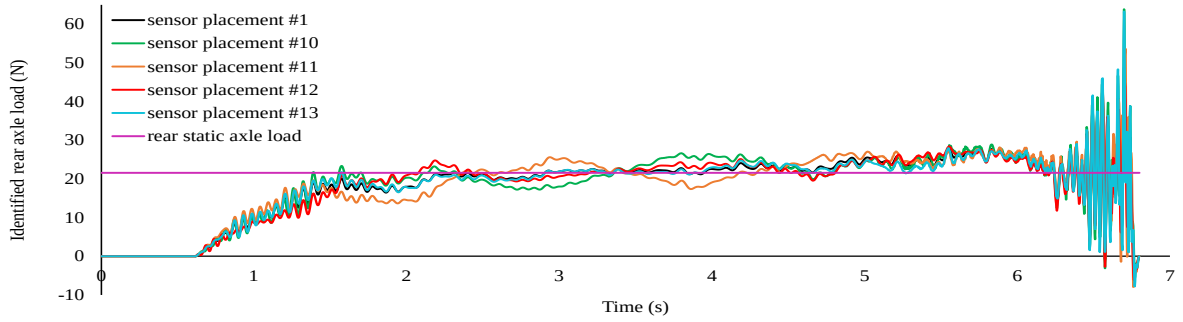

(b)

Figure 6-15: Comparison of the identified loads by sensor placements including 5, 6, and 7 sensors (a) identified front axle load (b) identified rear axle load

`

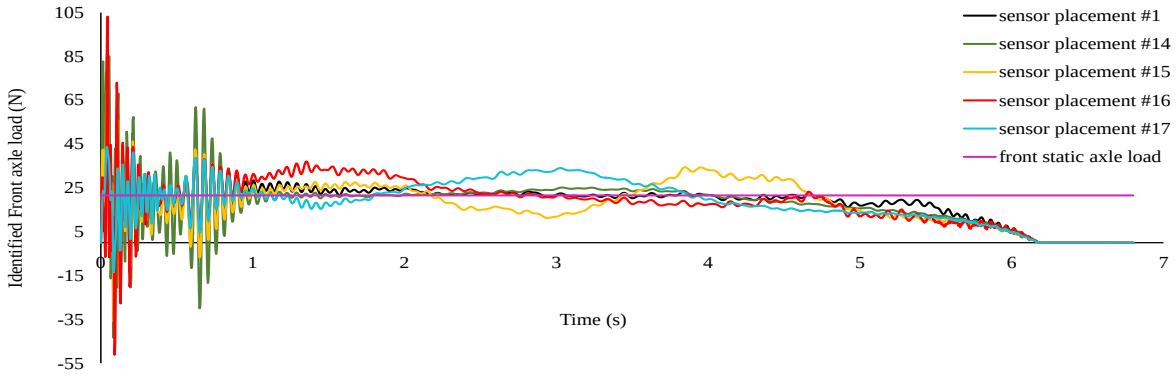

(a)

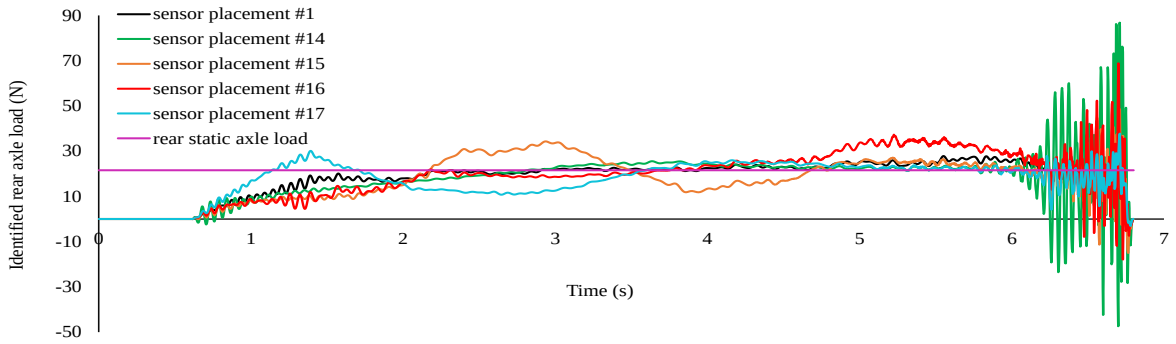

(b)

Figure 6-16: Comparison of the identified loads by sensor placements including 1, 2, and 7 sensors (a) identified front axle load (b) identified rear axle load

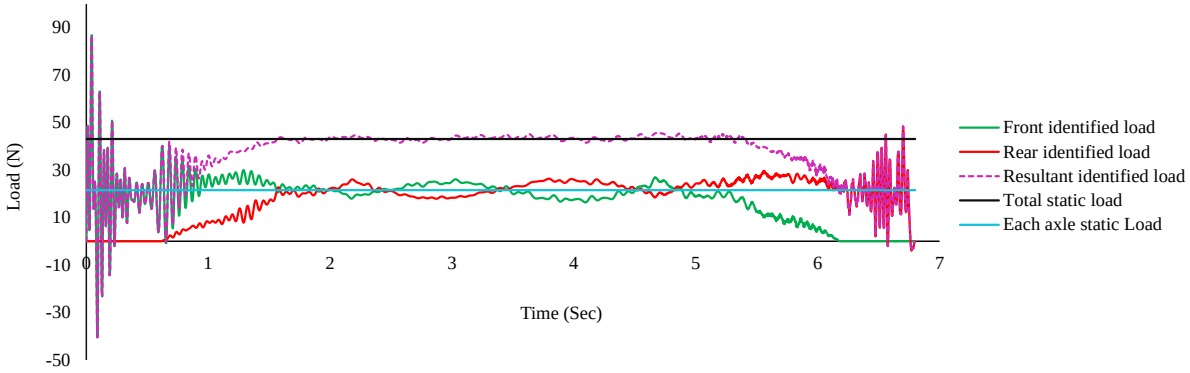

Figure 6-17: Identified front, rear, and resultant load in comparison with the static axle load and static weight of the car (sensor placement #2)

6.5.3. The effect of sampling frequency

In this section, the effect of sampling frequency on the accuracy of the proposed method for moving load identification is investigated. The car is pulled over the bridge at average speeds of 27 units (≈ 0.47 m/s) and 54 units (≈ 0.94 m/s), and the sampling frequency is set at 600 Hz. To analyse the data, sensor placement #2 is used and N_f is considered equal to 283.

`

To study the effect of different sampling frequencies, recorded data is resampled at 300 Hz, 200 Hz, and 100 Hz.

To identify the moving loads, the Tikhonov regularization technique is used and the optimal regularization parameter is obtained by the L-curve method. The identified moving loads at speeds 0.47 m/s and 0.94 m/s at different sampling frequencies are shown in Figure 6-18 and Figure 6-19 respectively. The accuracy is assessed by analysing the reconstructed strain error at mid-span, as well as the difference between the resultant identified load and the static weight of the vehicle, which are tabulated in Table 6-4. According to the results, the method is able to identify the moving loads with high accuracy at all sampling frequency ranges at both low and high speeds. The percentage error of the reconstructed strain at mid-span rises with an increase in car speed and a decrease in sampling frequency, reaching its maximum value (4.61%) at speed 0.94 m/s and sampling frequency 100 Hz.

Table 6-4: The percentage error at different levels of speed and sampling frequency

Sampling Frequency (Hz)	100		200		300		600	
Speed (m/s)	0.47	0.94	0.47	0.94	0.47	0.94	0.47	0.94
Reconstructed strain	3.35	4.61	2.97	3.62	2.5	3.25	2.28	3.16
Average of resultant axle load	0.63	0.3	0.72	0.27	0.6	0.36	0.23	0.09

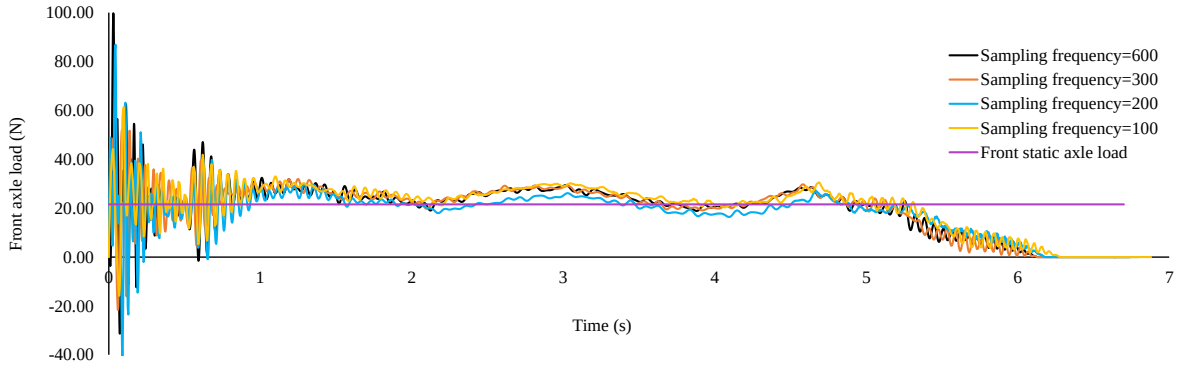

(a)

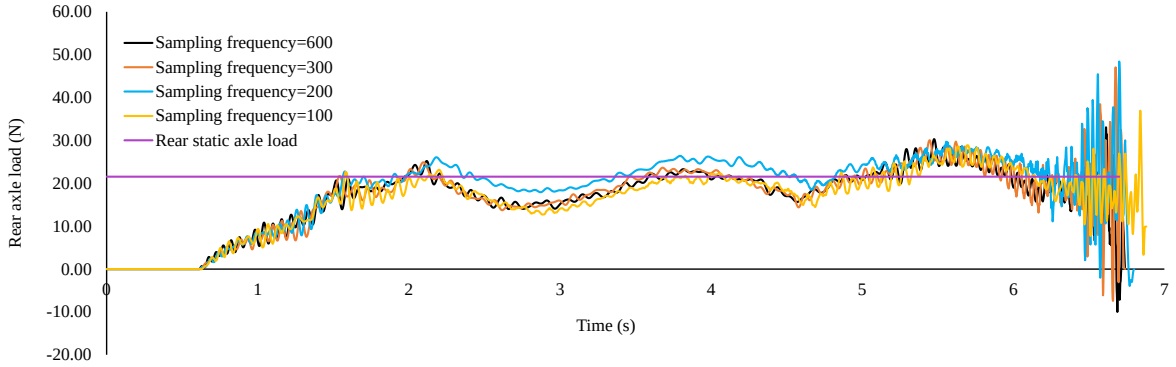

(b)

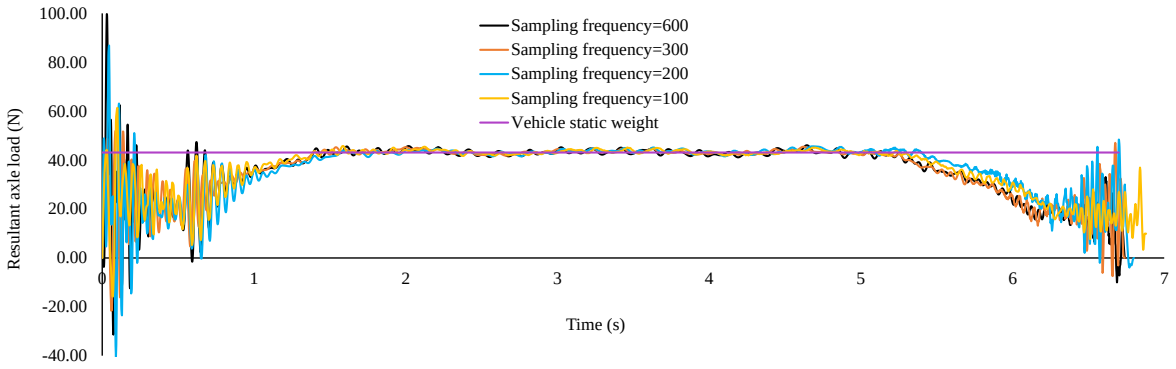

(c)

Figure 6-18: The effect of sampling frequency on the identified loads at speed 0.47 m/s, (a) identified front axle load (b) identified rear axle load (c) Resultant load

`

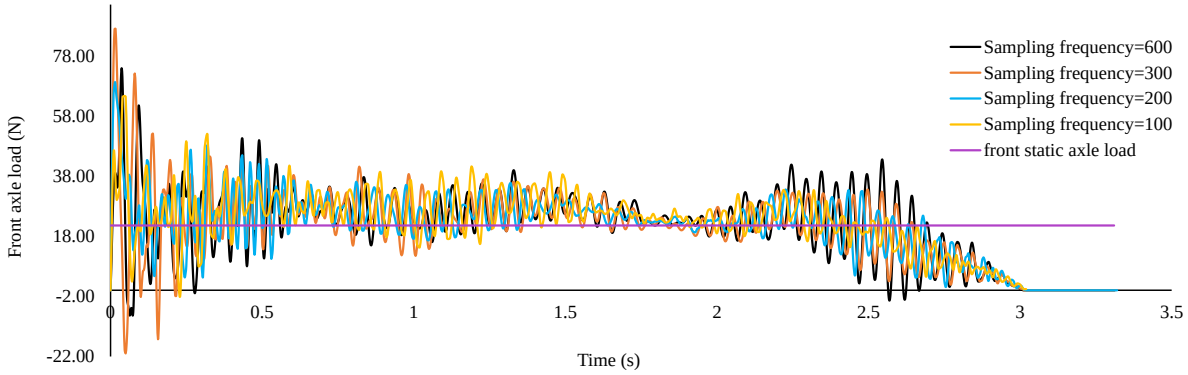

(a)

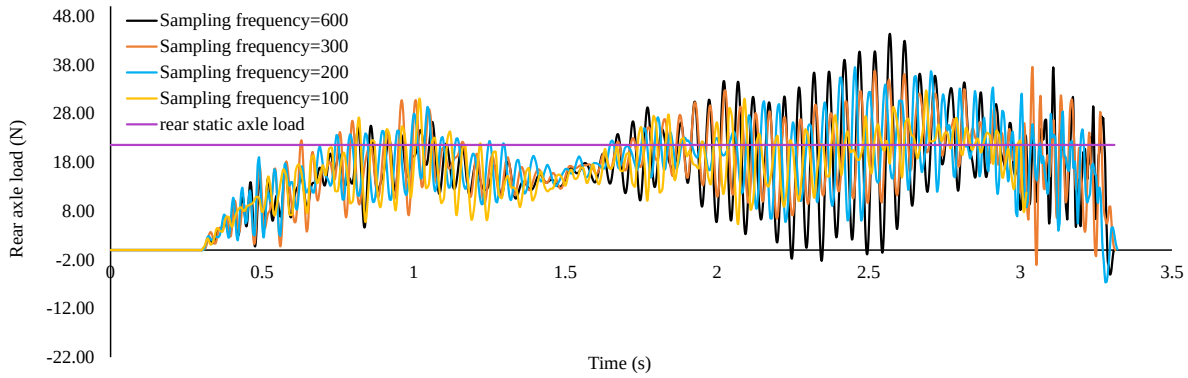

(b)

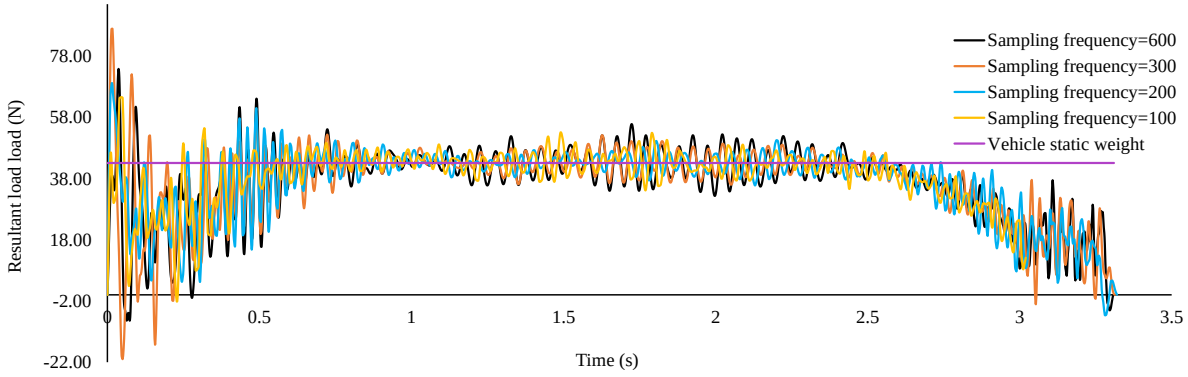

(c)

Figure 6-19: The effect of sampling frequency on the identified loads at speed 0.94 m/s, (a) identified front axle load (b) identified rear axle load (c) Resultant load

`

6.5.4. The effect of vehicle speed

To explore the effect of vehicle speed on the accuracy of moving load identification, the car is pulled over the bridge at speeds of 0.47 m/s, 0.75 m/s, and 0.94 m/s, and the sampling frequency is set at 200 Hz. The electric motor is allowed to work with a minimum speed of 0.47 m/s and a maximum speed of 0.97 m/s. To analyse the data, the Tikhonov Regularization technique is used and the optimal regularization parameter is obtained by the L-curve method, sensor placement #2 is used and N_f is considered equal to 283. Rear, front and resultant identified loads at speeds of 0.47 m/s and 0.94 m/s are shown in Figure 6-18 and Figure 6-19, and at a speed of 0.75 m/s is shown in Figure 6-20 respectively.

The accuracy is assessed by the percentage errors of the reconstructed strain at mid-span and the resultant identified load, which are tabulated in Table 6-5. According to the results, the percentage errors of the reconstructed strain are fluctuation around 3% and the method is not sensitive to vehicle speed. Figures indicate that the amplitudes of interaction loads at a speed of 0.94 m/s are higher than speeds of 0.47 m/s and 0.75 m/s.

Table 6-5: The percentage error at different levels of speed

Speed (m/s)	0.47	0.75	0.97
Strain at mid-span	2.97	2.83	3.62
Average of resultant axle load	0.72	0.07	0.27

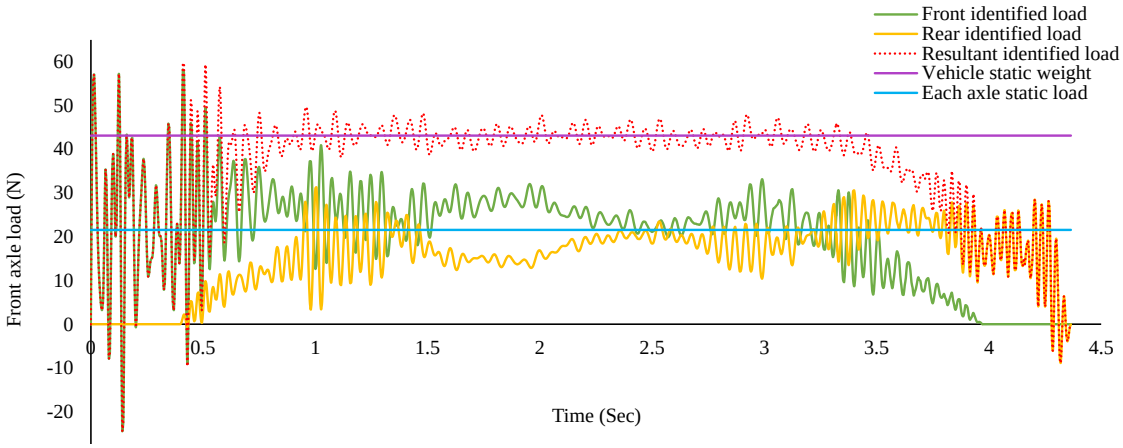

Figure 6-20: Identified front, rear, and resultant load in comparison with the static axle load and static weight of the vehicle (speed: 0.75 m/s)

`

6.6. Structural and substructural condition assessment verification

Tests are carried out to experimentally verify the accuracy of the techniques proposed in chapters 4 and 5 for structural and substructural condition assessment of bridge structures subject to moving loads. The results for structural condition assessment of the bridge where the full structure is assessed simultaneously with moving loads are presented in section 6.6.1. The results of substructural condition assessment where only the target substructure is assessed are discussed in section 6.6.2. In section 6.6.2, the two Scenarios of A and B (see chapter 5) are investigated and results are presented in sections 6.6.2.1 and 6.6.2.2.

Damage is induced at two stages: damage case 1 and damage case 2. Local damage is induced by a band saw removing 1 mm in width of material from the bottom of the beam, across the full width of the beam. The band saw used is illustrated in Figure 6-21. Damage is introduced at two points, both of which are in element 6 of the finite element model of the beam and over the depth of 10 mm and 14 mm, respectively (see Figure 6-22).The bridge beam is modelled in ANSYS and the equivalent reduction in the flexural stiffness of element 6 is obtained using the force-displacement theory. At damage case 1, the equivalent reduction in the flexural stiffness of the damaged element is around 12% and in damage case 2 is around 28.7%.

Figure 6-21: The band saw

`

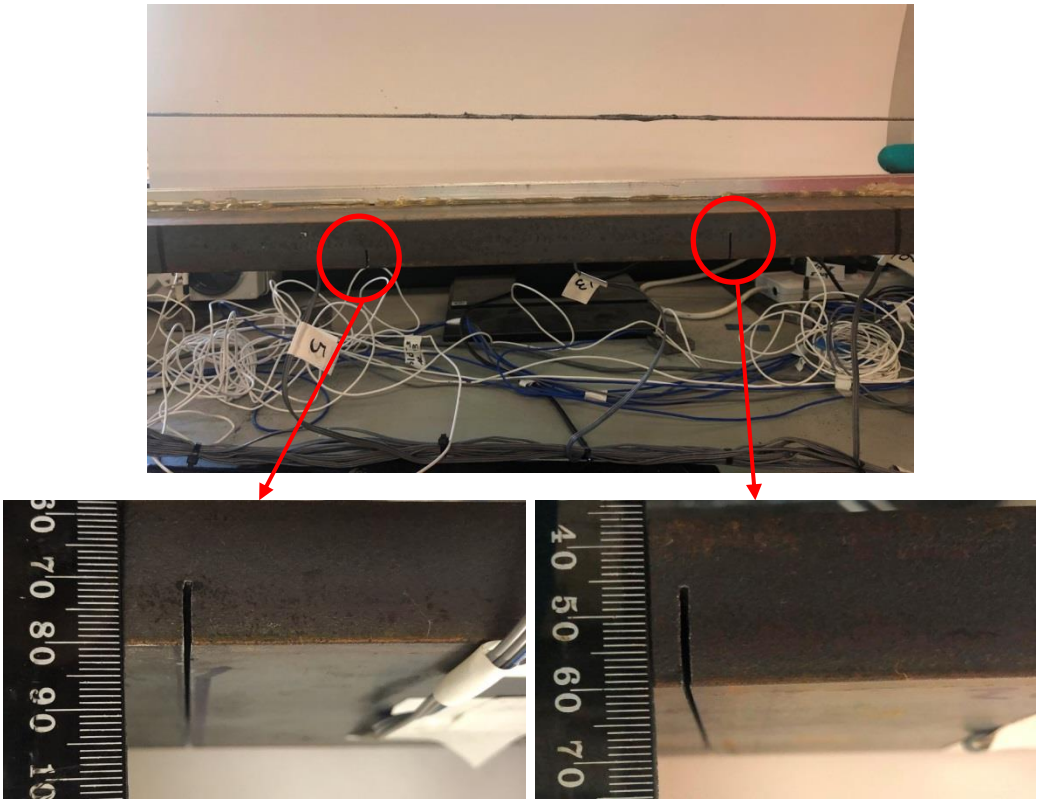

Figure 6-22: The damage induced on the bottom of the beam

Modal tests are carried out before the damage is implemented and at each state of damage to explore the effect of the damage on beam natural frequencies and the first four experimental natural frequencies are tabulated in Table 6-6. As can be seen, the first natural frequency is decreased at each state of the damage. The results are later used to check the accuracy of the methods applied.

Table 6-6: Calculated and measured natural frequencies of the test beam (Hz)

Intact				
Measured	6.27	27	61.17	104.71
Damaged (case 1)				
Measured	6.2	26.4	66.6	99.9
Damage (case 2)				
Measured	6.03	26.5	61.8	102.9

`

6.6.1. Identifying moving loads and structural damage simultaneously

A technique for simultaneous identification of structural damage and moving loads based on the explicit form of the Newmark-β method has been proposed in Chapter 4. The robustness of the method is numerically investigated by studying the effect of measurement noise, vehicle speed, road surface roughness and damage properties for a single span simply supported beam and a multi-span continuous beam. In this section, the proposed method is verified experimentally in the laboratory.

The FEM of the bridge beam is created by MATLAB including eight Euler-Bernoulli beam elements. Strain responses at nodes L/4, L/2, and 6L/8 (sensor placement #2) and acceleration responses at nodes L/8 and 3L/8 are used as inputs. Sensor placement #2 is chosen for strain gauges since it is already investigated for the accuracy of moving load identification and two accelerometers are added to inputs to increase the accuracy in identifying the dynamic aspects of moving loads.

The effect of the sampling rate and vehicle speed on the accuracy of identified moving loads and damage is investigated. The vehicle is pulled on the beam by the electric motor at two average speeds of 0.47 m/s and 0.94 m/s. Responses of the beam are recorded at sampling rates of 200 Hz, 400 Hz, and 800 Hz, and denoising is carried out by applying the Chebyshev polynomial as explained in section 6.4. The best N_f obtained for the mentioned sampling frequencies are 170, 300, and 380, respectively. In this research project, the objective function of the experimental studies of damage detection is to minimize the difference between the measured response and the reconstructed one at the mid-span.

The results of simultaneous identification of damage and moving loads are tabulated in Table 6-7. The total time of calculation rises with the decrease in speed and increase in the sampling frequency, which is the negative point of this method in comparison with the substructural condition assessment technique. The error of the reconstructed strain at mid-span is increased with an increase in speed.

Identified stiffness reduction of structural elements at the two cases of damage when the beam is subject to the moving vehicle at speeds of 0.47 m/s and 0.97 m/s is illustrated in Figure 6-23 to Figure 6-26.

In Figure 6-23 and Figure 6-24, the effect of sampling frequency on identifying damage case 1 at the speeds of 0.47 m/s and 0.94 m/s is shown, respectively. As can be seen in both figures, element six is detected as a damaged element and its extension is quantified reasonably

`

at all sampling frequencies, however, there are large false positives at other elements due to measurement noise and modelling errors of the boundary conditions.

The effect of sampling frequency on damage detection of case 2 at speeds of 0.47 m/s and 0.94 m/s can be seen in Figure 6-25 and Figure 6-26, respectively. Again, element six is detected as a damaged element and the extent of identified stiffness reduction is acceptable close to the true value. Similar to others, there are large false positives in other elements due to measurement noise and modelling errors of boundary conditions.

Natural frequencies at each case of studies are calculated and compared with the measured ones as tabulated in Table 6-8. The calculated natural frequencies are very close to the measured ones showing the accuracy of the method.

Table 6-7: Damage identification results from the simultaneous identification

Damage case	Speed (m/s)	Sampling frequency (Hz)	Total time hr:min:sec	Convergence rate	Reconstructed strain error (%)
1	0.47	200	00:10:19	0.001	2.65
		400	00:51:52	0.001	3.48
		800	02:45:05	0.002	2.99
	0.94	200	00:00:32	0.003	5.55
		400	00:15:16	4.5E-05	10.3
		800	01:05:49	4.0E-05	8.22
2	0.47	200	00:07:15	0.006	3.09
		400	00:52:48	0.001	3.29
		800	04:20:26	0.003	2.33
	0.94	200	00:03:59	8.4E-05	5.35
		400	00:19:55	6.2E-05	6.55
		800	02:19:58	0.006	4.53

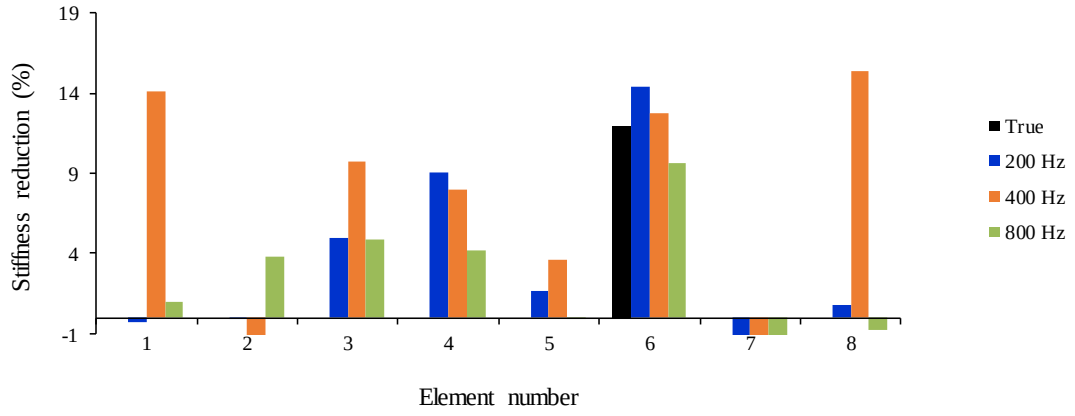

Figure 6-23: The effect of sampling frequency on damage detection at speed of 0.47 m/s - Damage case 1

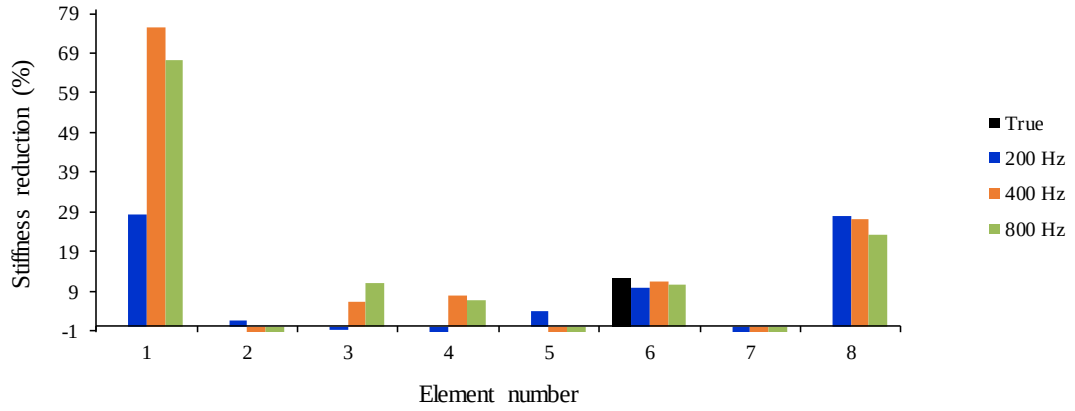

Figure 6-24: The effect of sampling frequency on damage detection at speed of 0.94 m/s - Damage case 1

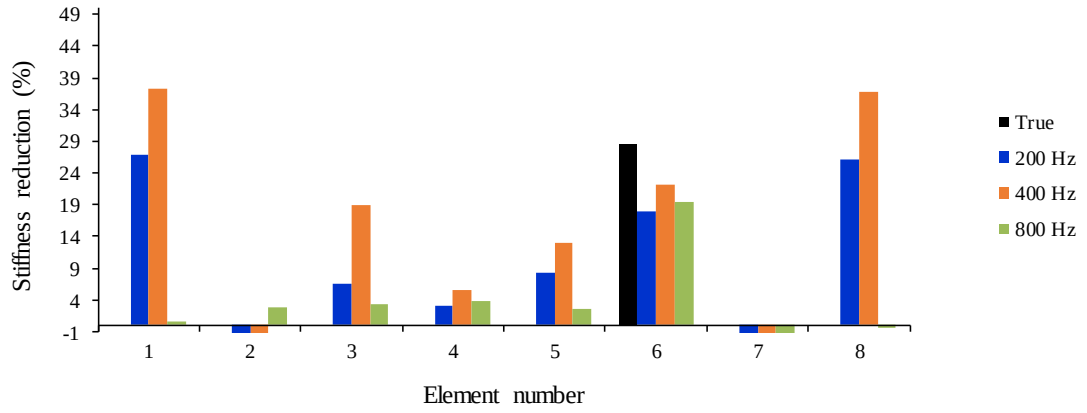

Figure 6-25: The effect of sampling frequency on damage detection at speed of 0.47 m/s - Damage case 2

`

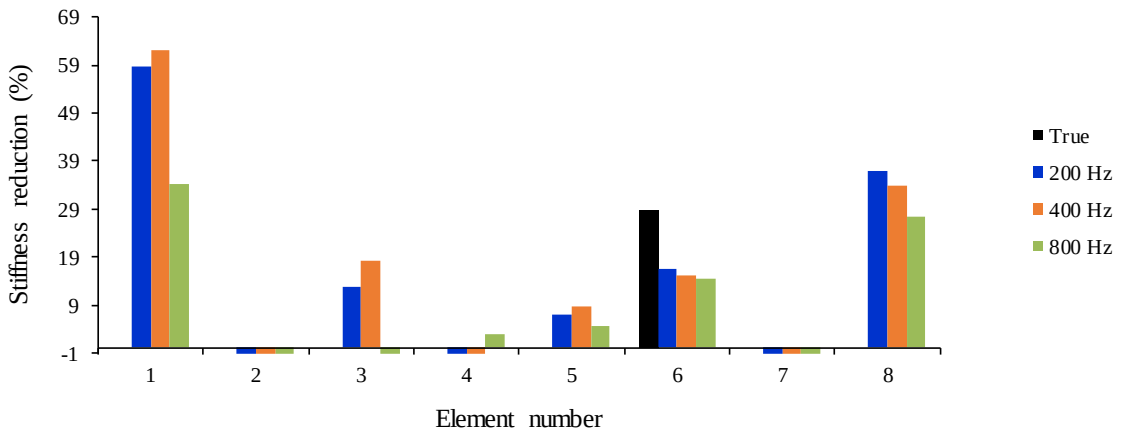

Figure 6-26: The effect of sampling frequency on damage detection at speed of 0.94 m/s - Damage case 2

Table 6-8: Natural frequencies from modal test and numerical studies

Damage case	Speed (m/s)		Sampling frequency (Hz)	Modal frequency (Hz)			
				1st	2nd	3rd	4th
Intact	measured		500	6.3	27	61.2	104.7
	calculated		200	6.4	25.5	57.5	102.4
1	measured		500	6.2	26.4	66.6	99.9
	Calculated	0.47	200	6.2	24.9	56.7	100.3
			400	6.1	24.9	56.6	98.7
			800	6.2	25.06	57.02	101.01
		0.94	200	6.4	25.5	57.1	98
			400	6.4	25.6	53.8	90.3
			800	6.3	25.7	55.8	92.7
2	measured		500	6.03	26.5	61.8	102.9
	Calculated	0.47	200	6.1	24.8	55.9	95.2
			400	5.98	24.4	55.4	93.63
			800	6.2	24.8	56.8	100.2
		0.94	200	6.2	24.96	55.4	92
			400	6.2	25.2	56	91.5
			800	6.3	26.5	56.4	97.5

`

Considering the results of identified stiffness reduction in the two cases of damage, it can be concluded that the accuracy of the method is not affected by speed, sampling frequency, and damage level, but it is affected by the modelling error at the boundary conditions and measurement noise which were discussed in Chapter 4.

The effect of the damage level on the identified moving loads at speeds of 0.47 m/s and 0.94 m/s and at a sampling frequency of 800 Hz can be seen in Figure 6-27 and Figure 6-28. Both the front and rear identified loads are fluctuating around the static axle values (22 N), and the identified resultant load is fluctuating around the total static weight of the vehicle (44 N), showing the accuracy of the method. It can be seen that damage has caused a slight increase in the interaction forces of the vehicle and bridge, which is more visible at the speed of 0.94 m/s in comparison with the speed of 0.47 m/s.

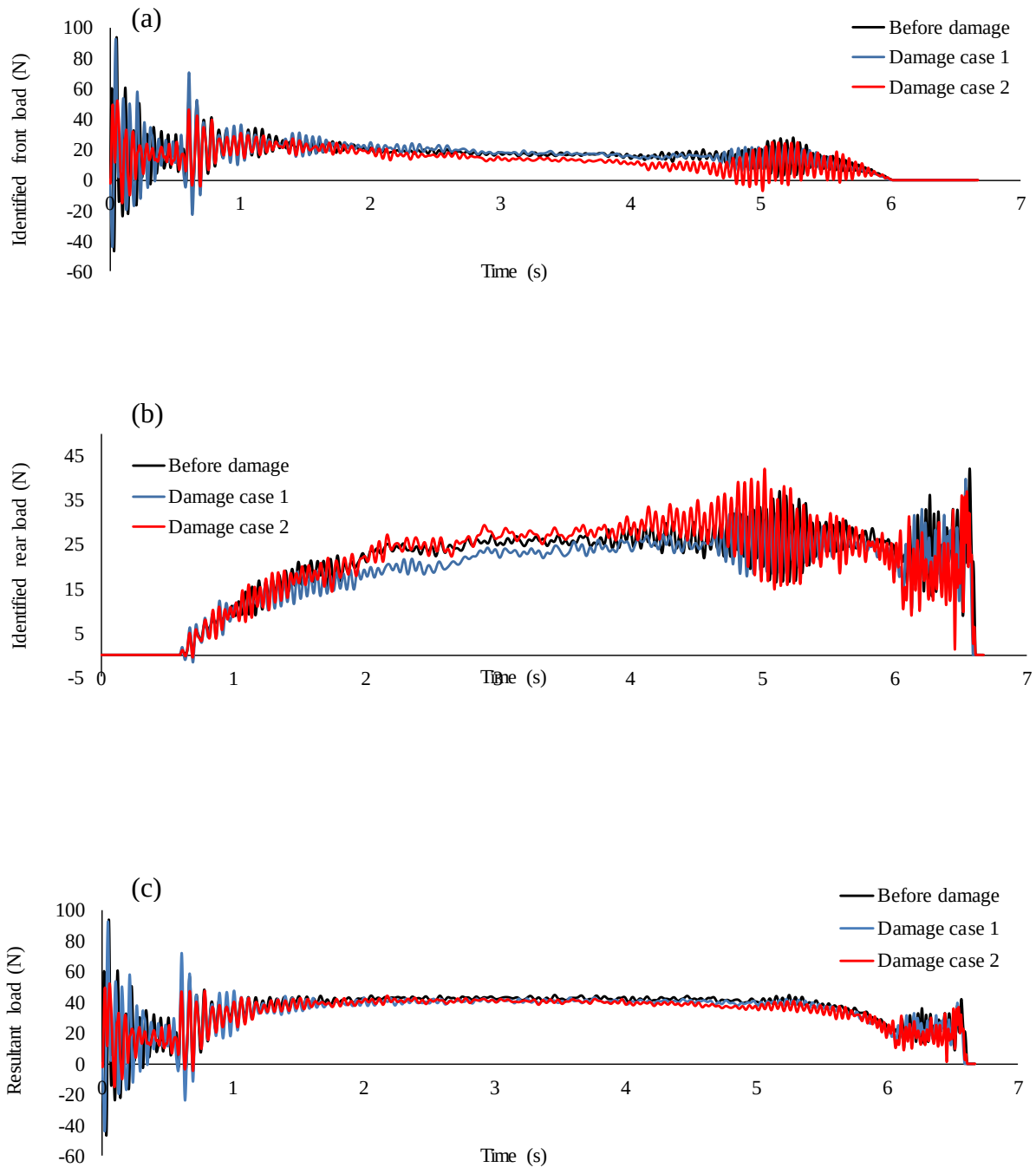

Figure 6-27: The effect of damage on the identified moving loads at speed of 0.47 m/s (sampling frequency 800 Hz); a: front load b: rear load c: resultant load

`

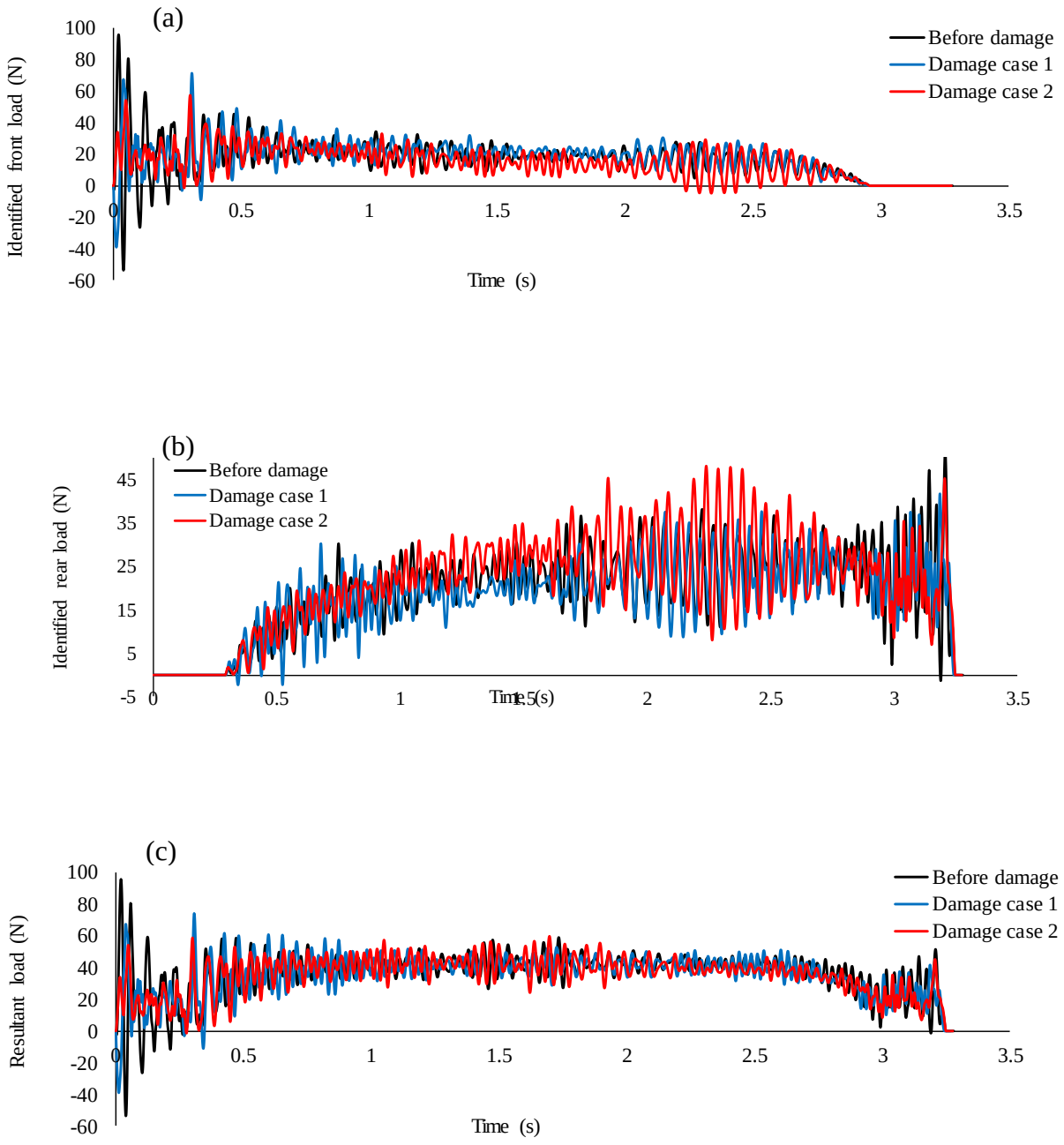

Figure 6-28: The effect of damage on the identified moving loads at speed of 0.94 m/s (sampling frequency 800 Hz); a: front load b: rear load c: resultant load

Measured and reconstructed strain responses at mid-span as well as their difference for two damage cases under two-vehicle speeds at a sampling frequency of 800 Hz are shown in Figure 6-29 to Figure 6-32. The reconstructed response is in a good agreement with the measured one confirming the accuracy of the method.

`

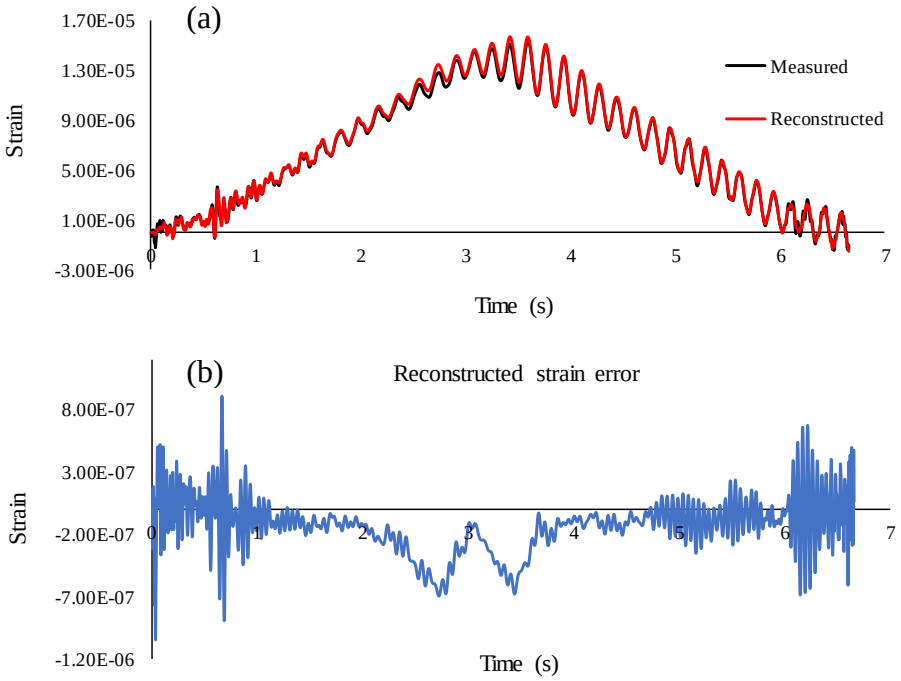

Figure 6-29: a) Measured and reconstructed strain at mid-span b) Error of reconstructed strain (Damage case 1- speed 0.47 m/s- sampling frequency 800 Hz)

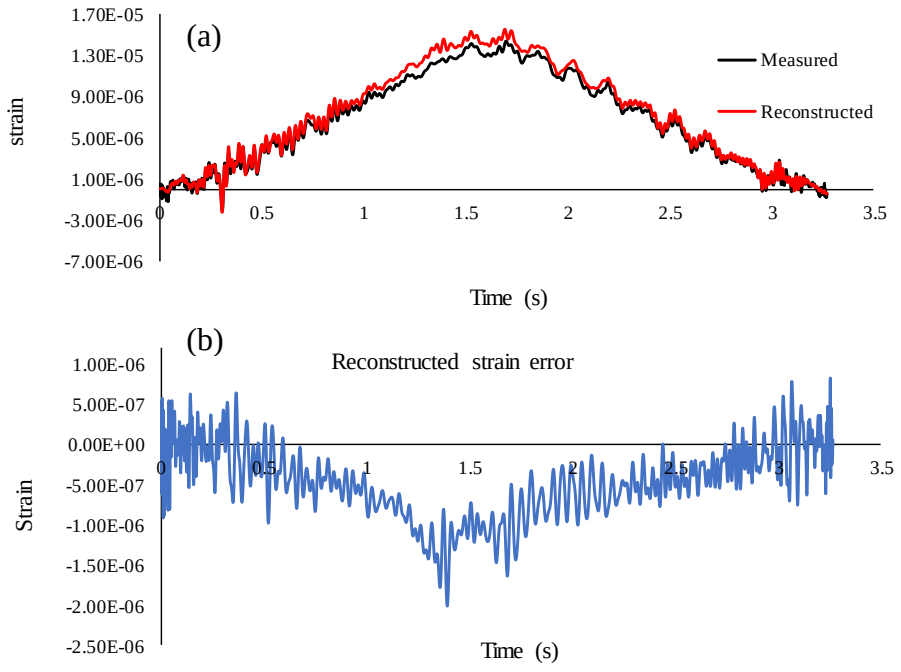

Figure 6-30: a) Measured and reconstructed strain at mid-span b) Error of reconstructed strain (Damage case 1- speed 0.94 m/s- sampling frequency 800 Hz)

`

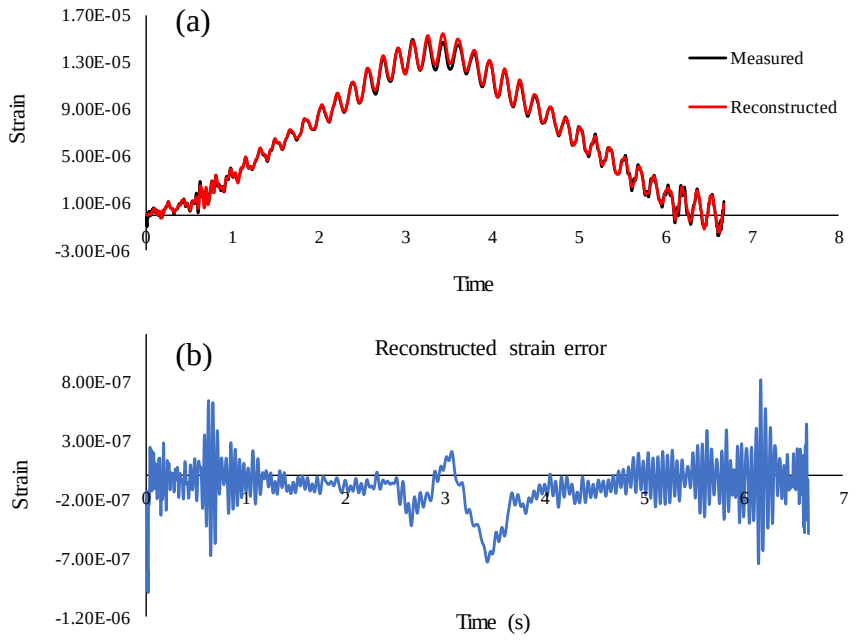

Figure 6-31: a) Measured and reconstructed strain at mid-span b) Error of reconstructed strain (Damage case 2- speed 0.47 m/s- sampling frequency 800 Hz)

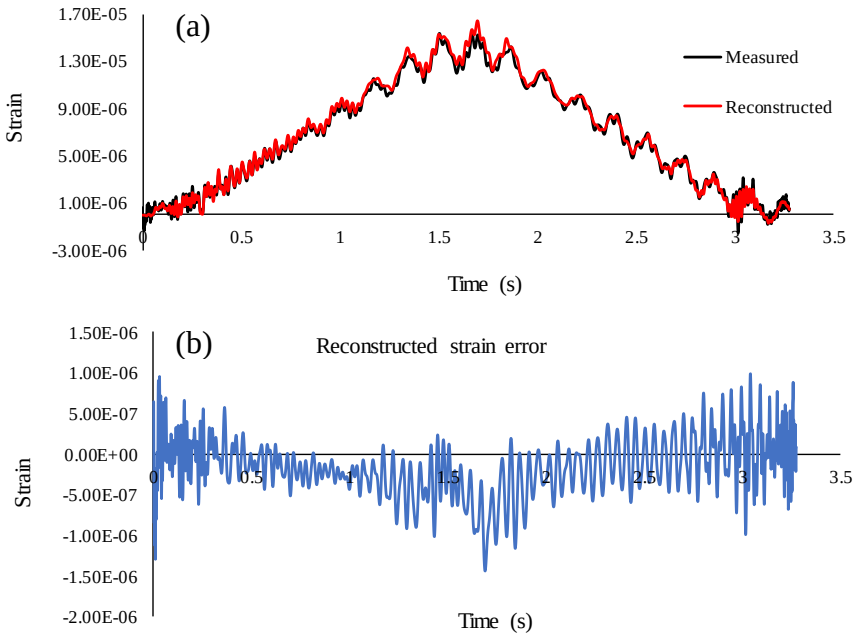

Figure 6-32: a) Measured and reconstructed strain at mid-span b) Error of reconstructed strain (Damage case 2- speed 0.94 m/s- sampling frequency 800 Hz)

`

6.6.2. Substructure condition assessment of the beam

A substructural technique based on the explicit form of the Newmark-β method has been proposed in chapter 5 for condition assessment of bridge structures subject to moving vehicles. The robustness of the method is numerically verified for Scenarios A and B. In this section, the robustness of the proposed technique is experimentally investigated and the effect of vehicle speed, sampling frequency, and damage level is studied for Scenarios A and B (sections 6.6.2.1 and 6.6.2.2). The cases which are studied are similar to the one presented in section 6.6.1.

The FEM of the beam is constructed in MATLAB including 8 Euler-Bernoulli beam elements. The finite element model of the beam and the target substructure are shown in Figure 6-33 and Figure 6-34 respectively. The substructure geometrical boundary condition is free-pinned and it includes 4 elements, 5 nodes, and 9 degrees of freedom. According to the results in section 5.6.1.2, at least four accelerometers are needed for this type of substructure to achieve promising results. Therefore, four accelerometers are installed at nodes 5 to 8 and one strain-gauge is installed at node 5. To identify the static part of the moving loads, at least one strain-gauge is needed. The strain-gauge is installed at the mid-span due to its high signal to noise ratio in comparison with other locations.

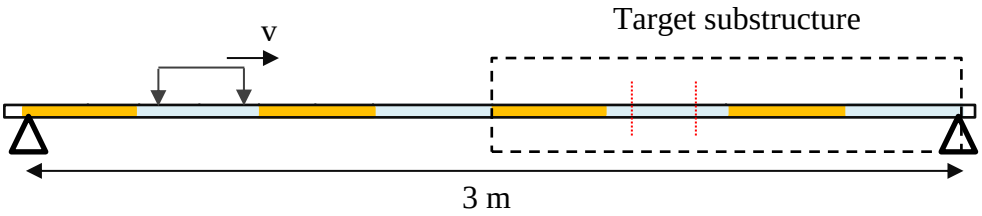

Figure 6-33: Finite element model of the beam subject to moving loads

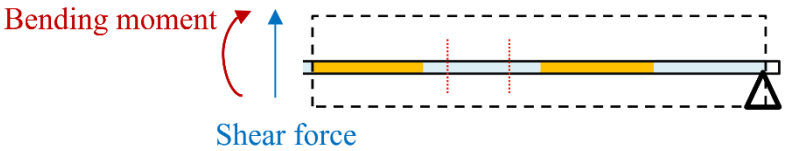

Figure 6-34: Finite element model of the target substructure subject to interface forces

`

6.6.2.1 Scenario A when the FEM of the whole structure is available

When the FEM of the whole structure is available, the procedure explained in section 5.5.1 can be applied to identify moving loads, interface forces, and damage. Results by this technique are tabulated in Table 6-9. In comparison with the condition assessment of the whole structure (Table 6-7), the total time of damage identification is significantly decreased while the error of reconstructed strain is reduced, especially at the speed of 0.94 m/s.

Table 6-9: Substructural damage identification results (Scenario A)

Damage case	Speed (m/s)	Sampling frequency (Hz)	Total time hr:min:sec	Convergence rate	Reconstructed strain error (%)
1	0.47	200	00:01:15	8.90E-07	1.94
		400	00:07:12	6.35E-07	2.12
		800	00:33:29	7.13E-07	2.33
	0.94	200	00:00:13	6.40E-07	2.56
		400	00:01:09	6.55E-07	3.20
		800	00:06:53	8.41E-07	2.85
2	0.47	200	00:01:18	9.13E-07	1.10
		400	00:07:21	3.15E-07	1.59
		800	00:56:52	3.17E-07	2.11
	0.94	200	00:00:13	5.41E-07	1.87
		400	00:01:11	9.82E-07	2.71
		800	00:07:13	5.74E-07	3.84

Natural frequencies of the beam are experimentally measured at three stages, before inducing damage, after inducing damage case 1, and after inducing damage case 2. Furthermore, natural frequencies of the beam at each stage are calculated after structural parameter identification and results are tabulated in Table 6-10. As can be seen, numerical natural frequencies are very close to those measured, showing the accuracy of the method and results.

`

Table 6-10: Natural frequencies from modal test and numerical studies

Damage case	Speed (m/s)		Sampling frequency (Hz)	Modal frequency (Hz)			
				1st	2nd	3rd	4th
Intact	measured		500	6.3	27	61.2	104.7
	calculated		200	6.3	25.4	57	102.8
1	measured		500	6.2	26.4	66.6	99.9
	Calculated	0.47	200	6.3	25.5	57.6	101.1
			400	6.3	25.5	58	101.5
			800	6.3	25.6	58.2	101.3
		0.94	200	6.3	25.6	58.4	100.7
			400	6.3	25.6	58	101
			800	6.3	25.6	58	101.1
2	measured		500	6.03	26.5	61.8	102.9
	Calculated	0.47	200	6.2	25.4	58	98.9
			400	6.3	25.6	58.6	98.4
			800	6.3	25.6	58.8	97.3
		0.94	200	6.3	25.5	58.6	97.8
			400	6.3	25.5	58.4	96.4
			800	6.2	25.4	56.9	99.2

Identified stiffness reduction of substructural elements at the two cases of damage when the beam is subject to the moving vehicle at speeds of 0.47 m/s and 0.94 m/s can be seen in Figure 6-35 to Figure 6-38. The effect of sampling frequency and vehicle speeds on the accuracy of this technique can be seen in these pictures. As can be seen, this method is able to identify element 6 as a damaged element in all cases of damage, speeds and sampling frequencies. There are small false positives and negatives at elements 5 and 7 which are due to measurement noise. In all cases, there is a large false positive at element 8 which is due to a modelling error of the boundary condition. The identified stiffness reduction of element 6 is acceptable and close to the true value in all cases.

In comparison with the damage detection of the whole structure, this technique has significantly improved the results of damage identification by reducing calculation time, reducing false positives and negatives, and increasing the accuracy of identified stiffness reduction of the damaged element.

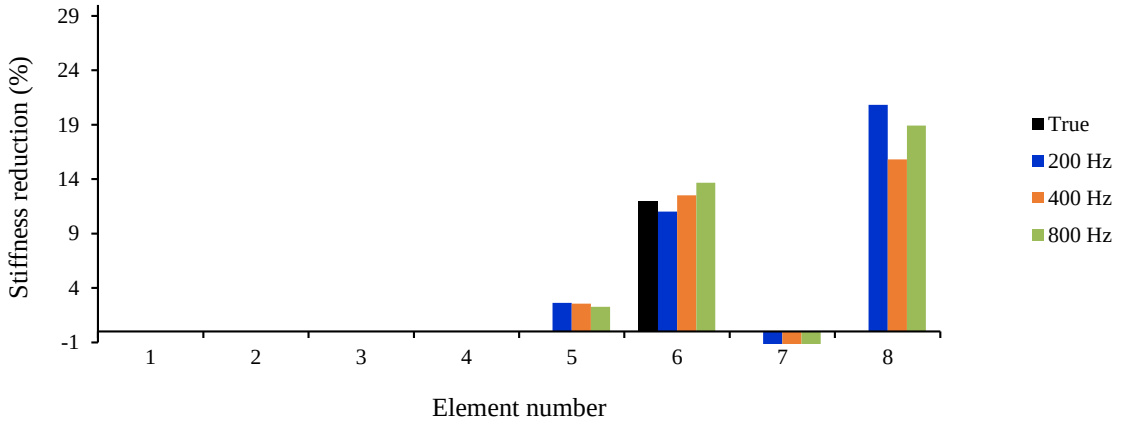

Figure 6-35: The effect of sampling frequency on damage detection at speed of 0.47 m/s - Damage case 1-scenario A

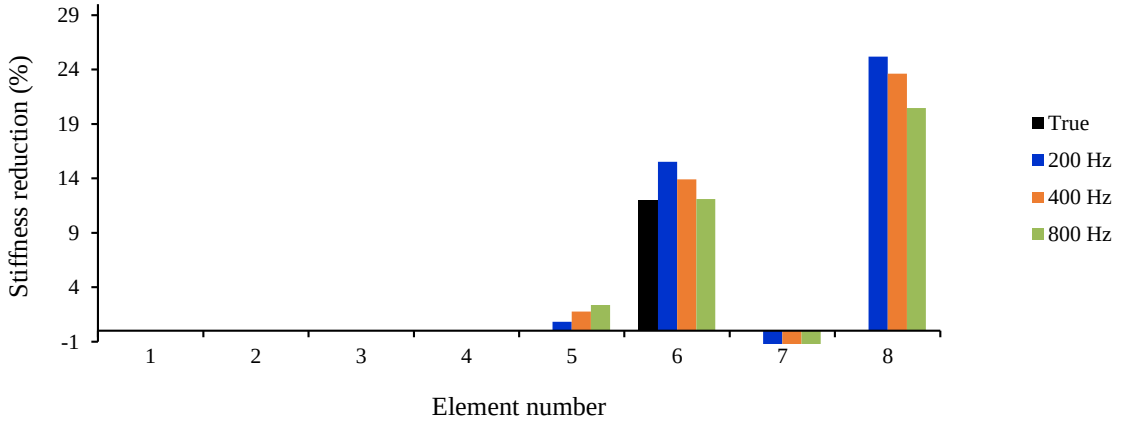

Figure 6-36: The effect of sampling frequency on damage detection at speed of 0.94 m/s - Damage case 1- scenario A

`

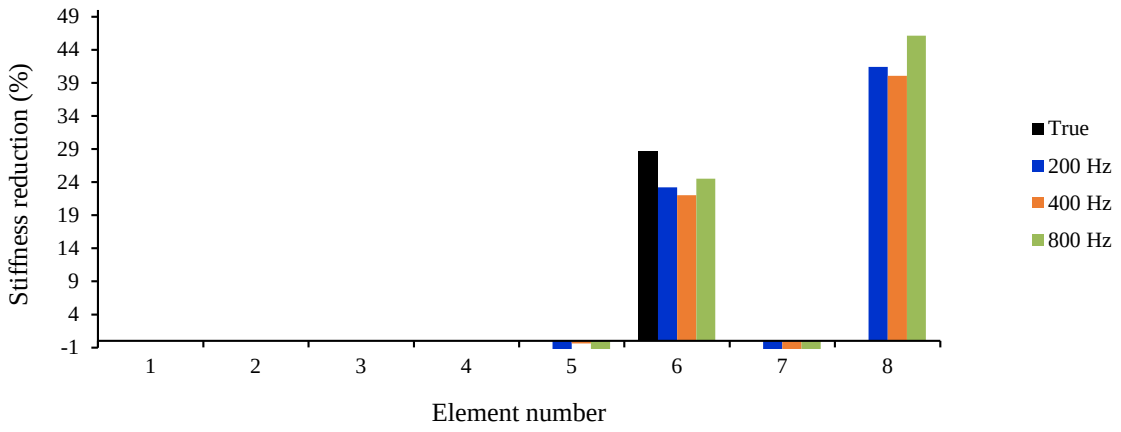

Figure 6-37: The effect of sampling frequency on damage detection at speed of 0.47 m/s - Damage case 2- scenario A

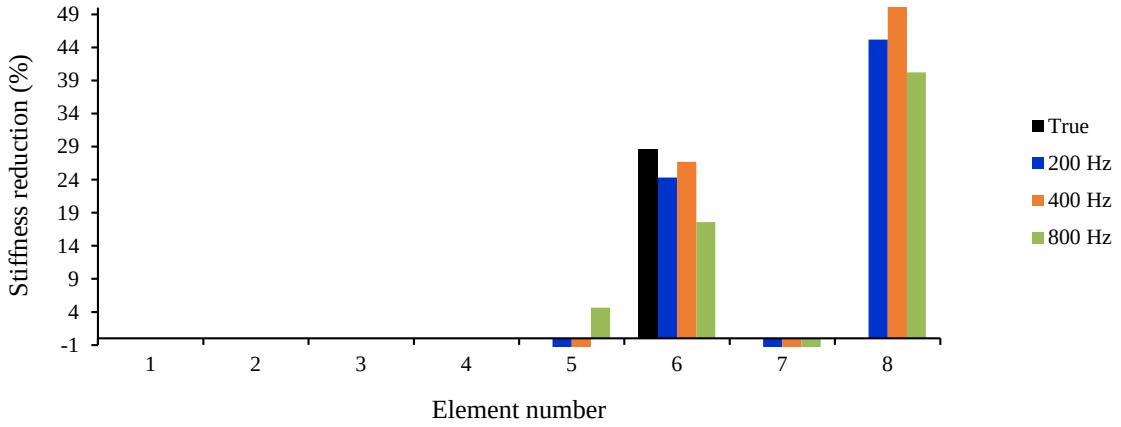

Figure 6-38: The effect of sampling frequency on damage detection at speed of 0.94 m/s - Damage case 2- scenario A

The effect of the damage level on the identified moving loads at speeds of 0.47 m/s and 0.94 m/s at a sampling frequency of 800 Hz can be seen in Figure 6-39 and Figure 6-40, respectively. Both the front and rear identified loads are fluctuating around the static axle values (22 N), and the identified resultant load is fluctuating around the total static weight of the vehicle (44 N), showing the accuracy of the method. It can be seen that damage has caused a slight increase in the interaction forces of the vehicle and bridge when the vehicle is passing over the damaged areas. This increase is more visible at a speed of 0.94 m/s in comparison with a speed of 0.47 m/s.

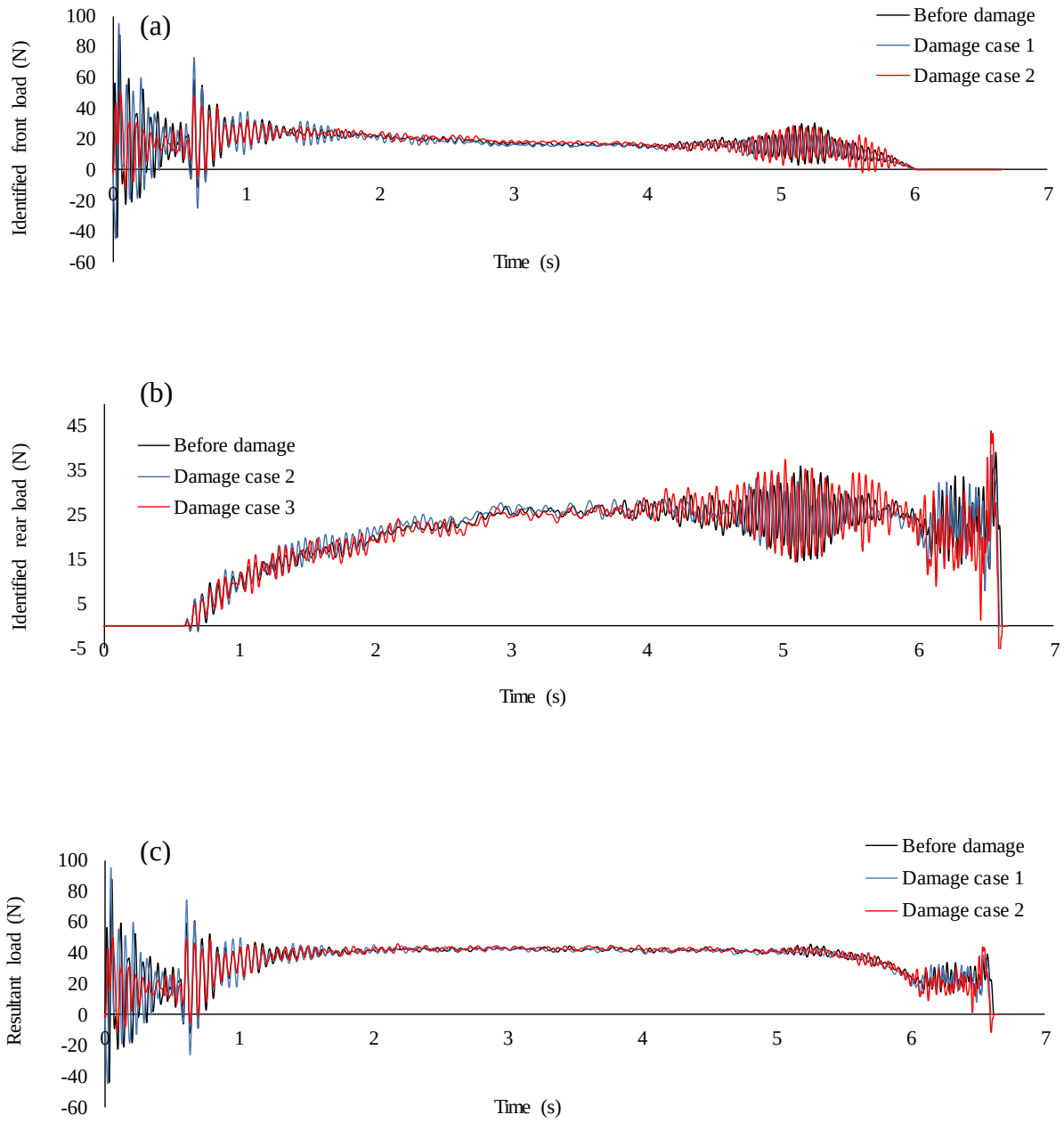

Figure 6-39: Identified moving loads at two damage cases at speed of 0.47 m/s- sampling frequency 800 Hz- scenario A; a: front load b: rear load c: resultant load

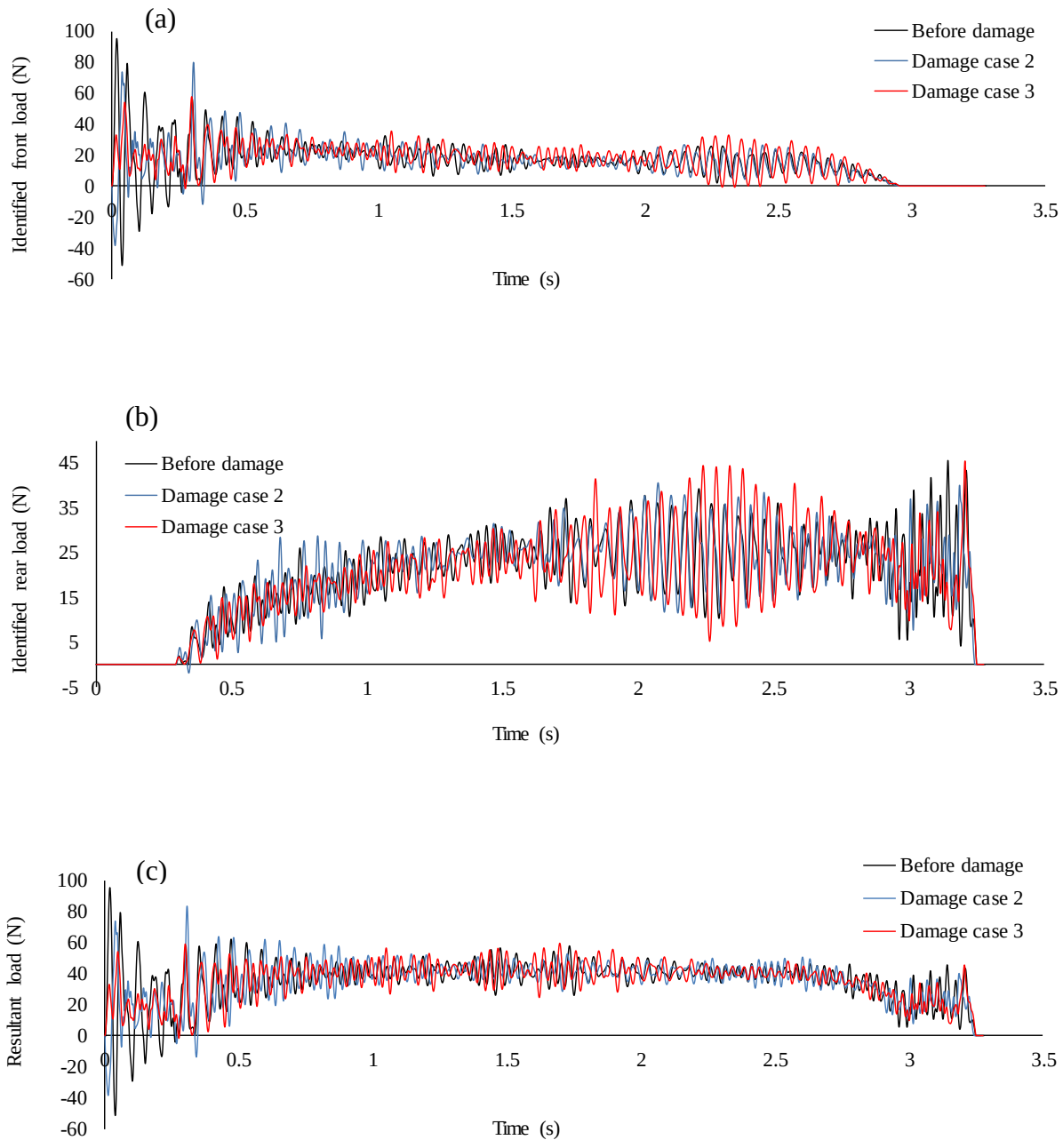

Figure 6-40: Identified moving loads at two damage cases at speed of 0.94 m/s- sampling frequency 800 Hz- scenario A; a: front load b: rear load c: resultant load

`

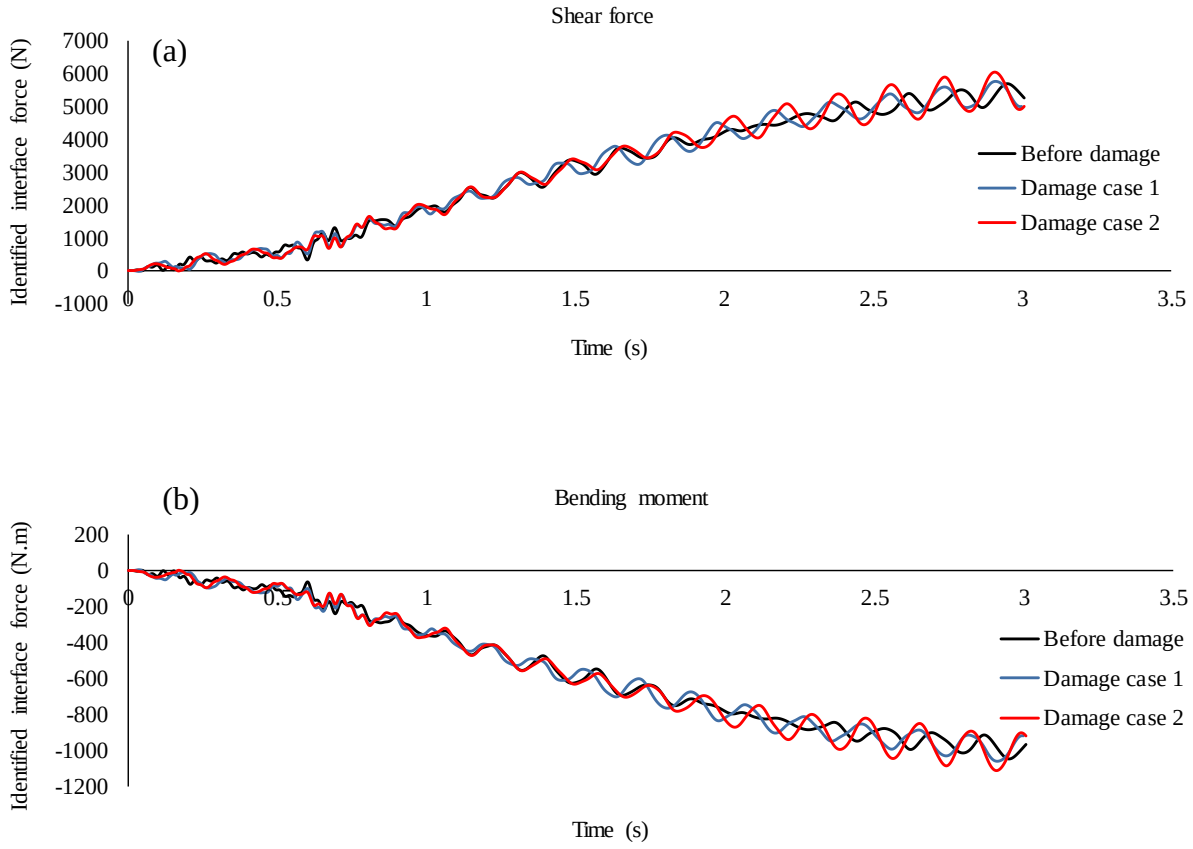

Figure 6-41: Identified interface forces at two damage cases at speed of 0.47 m/s- sampling frequency 800 Hz- scenario A; a: shear force b: bending moment

Structural responses can be obtained by inputting the identified loads into the equation of motion of the beam, and then they can be used to calculate the interface forces. The effect of damage on the interface forces at speeds of 0.47 m/s and 0.94 m/s and at a sampling frequency of 800 Hz can be seen in Figure 6-41 and Figure 6-42. Although damage affects the interaction forces, they are in the same range at different speeds and different states of damage. This is why the assumption made in the calculation of response sensitivity and assuming the sensitivity of substructure external forces to damage is equal to zero has led to acceptable results. Measured and reconstructed strain responses, as well as their difference, are shown in Figure 6-43, showing an optimum agreement.

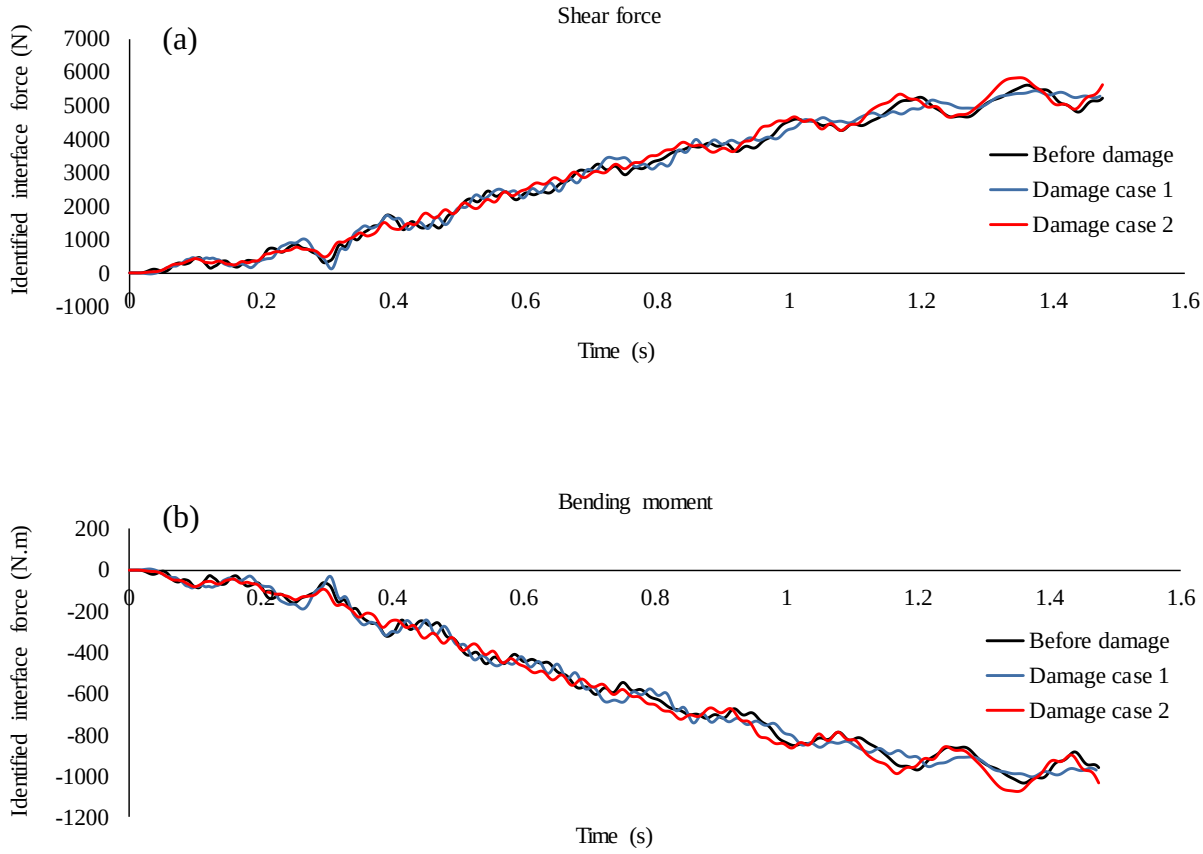

Figure 6-42: The effect of damage on interface forces at speed of 0.94 m/s- sampling frequency 800 Hz- scenario A; a: shear force b: bending moment

`

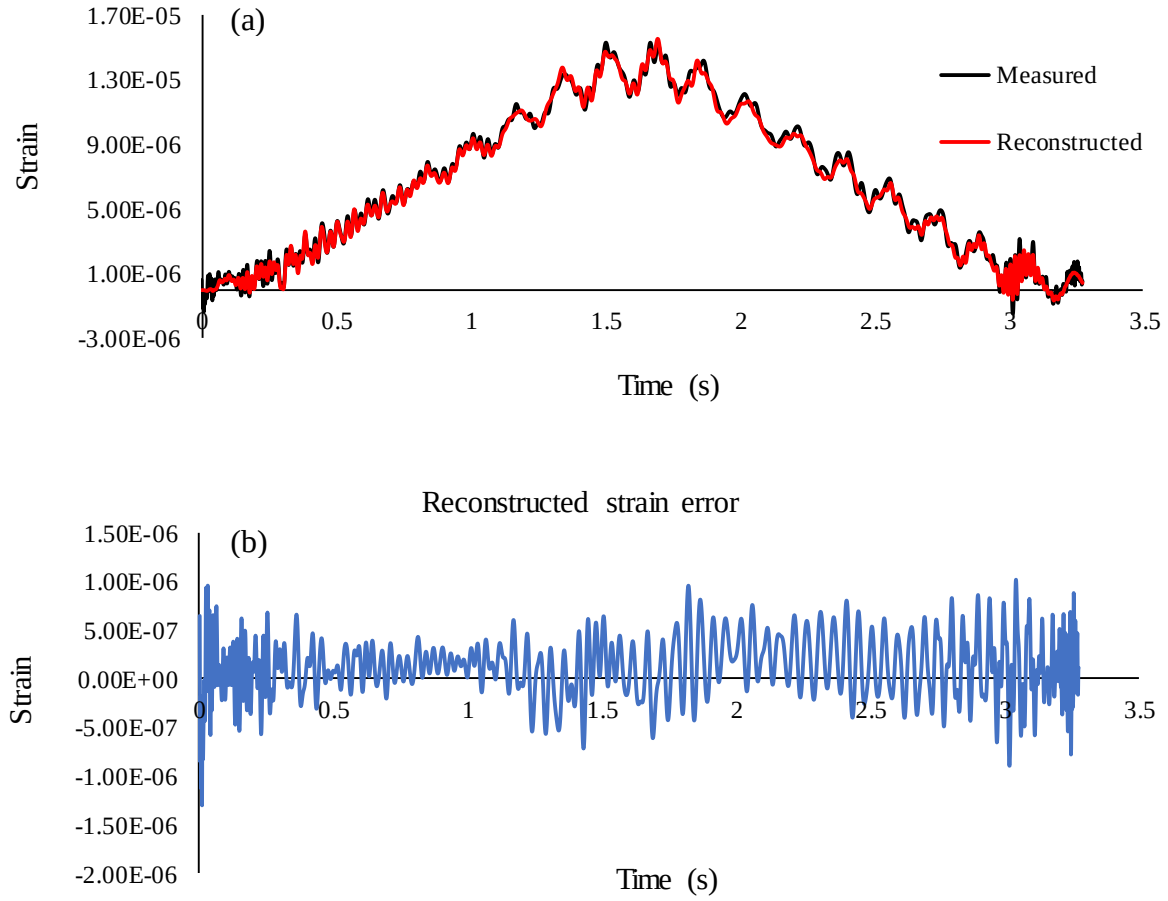

Figure 6-43: a) Measured and reconstructed strain at mid-span b) Error of reconstructed strain (Damage case 2 - speed 0.94 m/s- sampling frequency 800 Hz- scenario A)

6.6.2.2 Scenario B when the FEM of the target substructure is available

When only the FEM of the target substructure is available, the procedure explained in section 5.5.2 can be applied to identify external forces and damage. Results achieved by this technique are tabulated in Table 6-11. As can be seen, the total time of damage identification is greater than Scenario A (Table 6-9), however, it is less than the condition assessment of the whole structure (Table 6-7). The maximum error of reconstructed displacement is 1.27%, demonstrating the accuracy of the method.

Identified stiffness reduction of substructural elements at the two cases of damage when the beam is subject to the moving cart at speeds of 0.47 m/s and 0.54 m/s can be seen in Figure 6-44 to Figure 6-47. The effect of sampling frequency and vehicle speeds on the accuracy of this technique can be seen in these pictures. As can be seen, element 6 is detected as a damaged element in all cases of studies. The extension of damage is quantified close to the true value even at the sampling frequency of 200 Hz.

`

There are small false positives and negatives at elements 5 and 7 which are because of measurement noise. In some of the cases, there is a large false positive at element 8 which roots in the modelling error of the boundary condition. For damage case 1 at a speed of 0.47 m/s and sampling frequency of 200 Hz, for damage case 1 at a speed of 0.94 m/s and all sampling frequencies, for damage case 2 at a speed of 0.94 m/s and sampling frequency of 400 Hz, as well as for damage case 2 at a speed of 0.47 m/s and sampling frequency of 800 HZ, modelling errors of the boundary condition have not lead to a large false positive at element 8, which is an improvement on Scenario A.

Table 6-11: substructural damage identification results (Scenario B)

Damage case	Speed (m/s)	Sampling frequency (Hz)	Total time hr:min:sec	N.I.	Convergence rate	Reconstructed displacement error
1	0.47	200	0:02:45	60	3.14E-05	0.48%
		400	00:20:29	12	5.1E-5	0.55%
		800	01:07:17	10	4.3E-5	0.53%
	0.94	200	00:01:02	11	2.0E-02	1.27%
		400	00:05:32	15	6.2E-04	0.53%
		800	00:42:13	60	3.3E-05	0.61%
2	0.47	200	00:04:20	60	7.1E-05	0.16%
		400	00:07:27	10	8.1E-5	0.19%
		800	00:57:14	11	5.7E-5	0.14%
	0.94	200	00:01:30	60	1.1E-5	0.33%
		400	00:03:59	30	5.13E-05	0.11%
		800	00:23:48	60	2.97E-4	0.26%

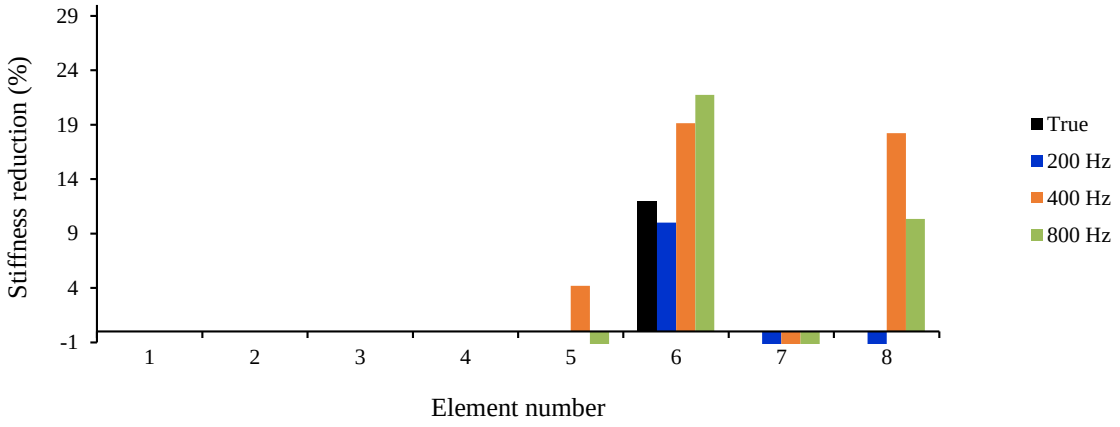

Figure 6-44: Effect of sampling frequency on damage detection at speed of 0.47 m/s - Damage case 1- scenario B

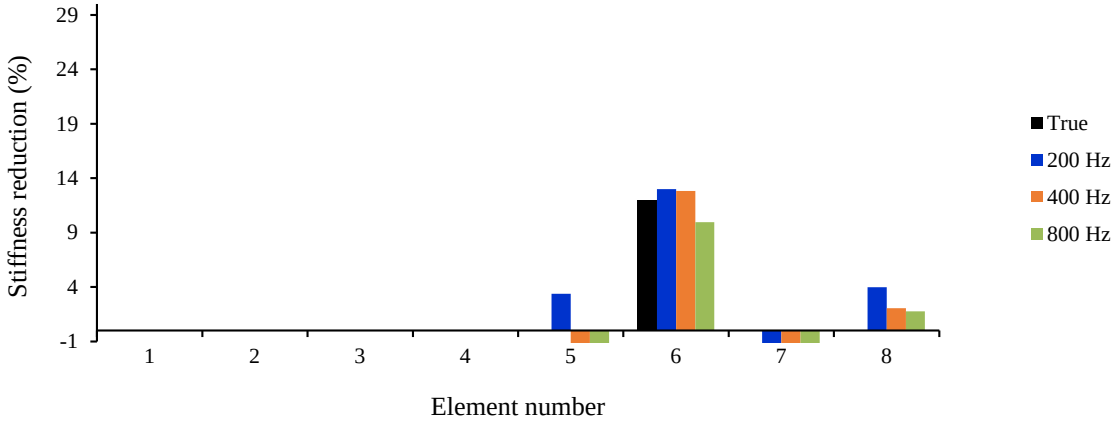

Figure 6-45: Effect of sampling frequency on damage detection at speed of 0.94 m/s - Damage case 1- scenario B

`

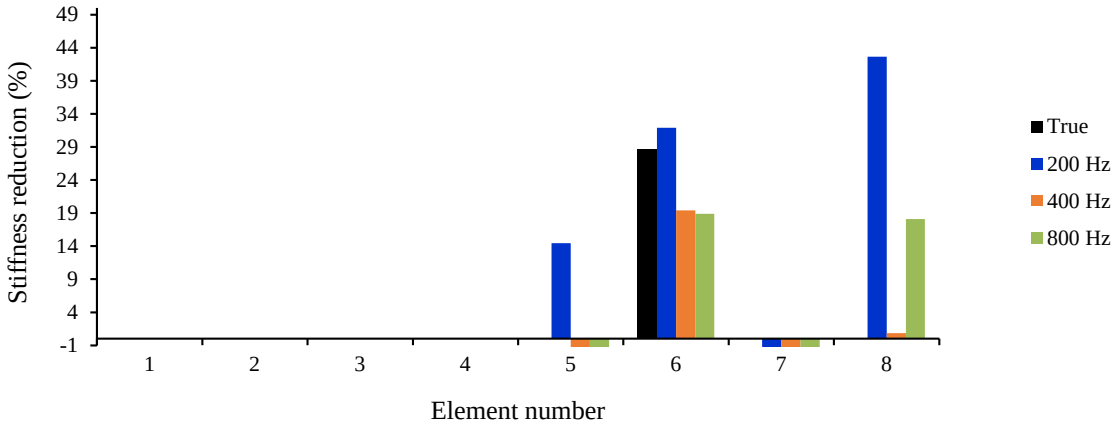

Figure 6-46: Effect of sampling frequency on damage detection at speed of 0.94 m/s - Damage case 2- scenario B

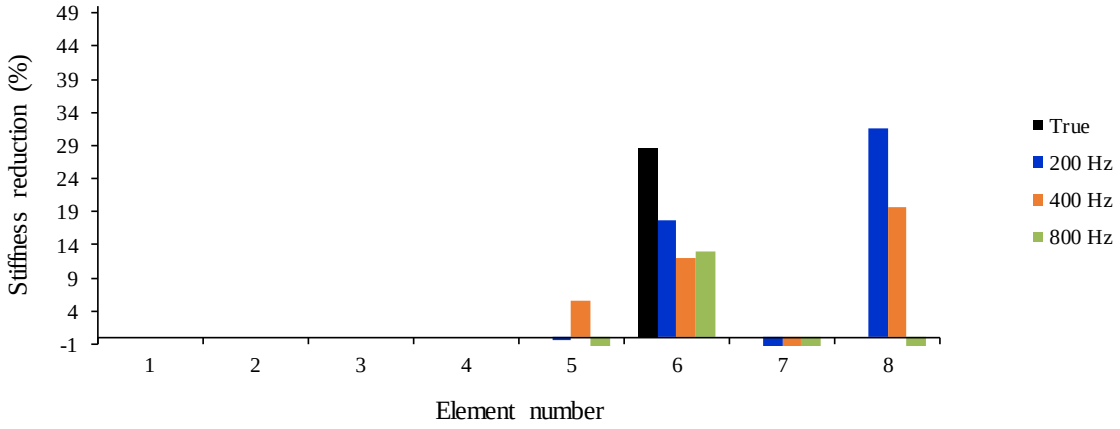

Figure 6-47: Effect of sampling frequency on damage detection at speed of 0.47 m/s - Damage case 2- scenario B

The effect of damage on identified interface forces at speeds of 0.47 m/s and 0.94 m/s and at a sampling frequency of 800 Hz can be seen in Figure 6-48 and Figure 6-49, respectively. Although interface forces are affected by the damage level at a speed of 0.47 m/s, the range of interaction forces is almost similar before damage and after damage. However, the effect of damage on interface forces at a speed of 0.94 m/s in Scenario B is different. Since in the proposed method, the sensitivity of interface loads to damage is assumed zero , and considering Figure 6-49, a shorter sampling period (less than 1.1 s), is studied for damage identification for

`

damage case 2 at a speed of 0.94 m/s, and the results are tabulated in Table 6-12 and Figure 6-50, showing a slight improvement in the results of damage detection.

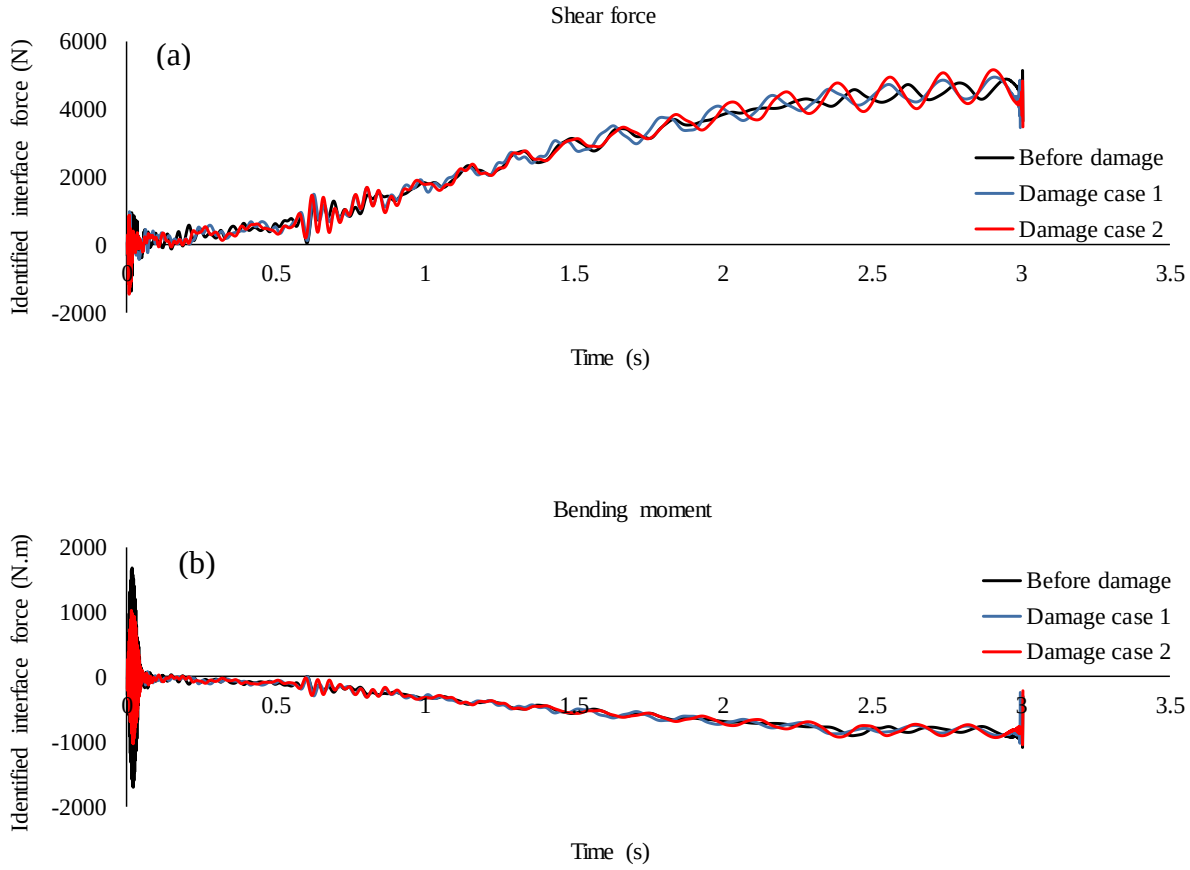

Figure 6-48: Effect of damage on identified interface forces at speed of 0.47 m/s- sampling frequency 800 Hz - scenario B; a: shear force b: bending moment

`

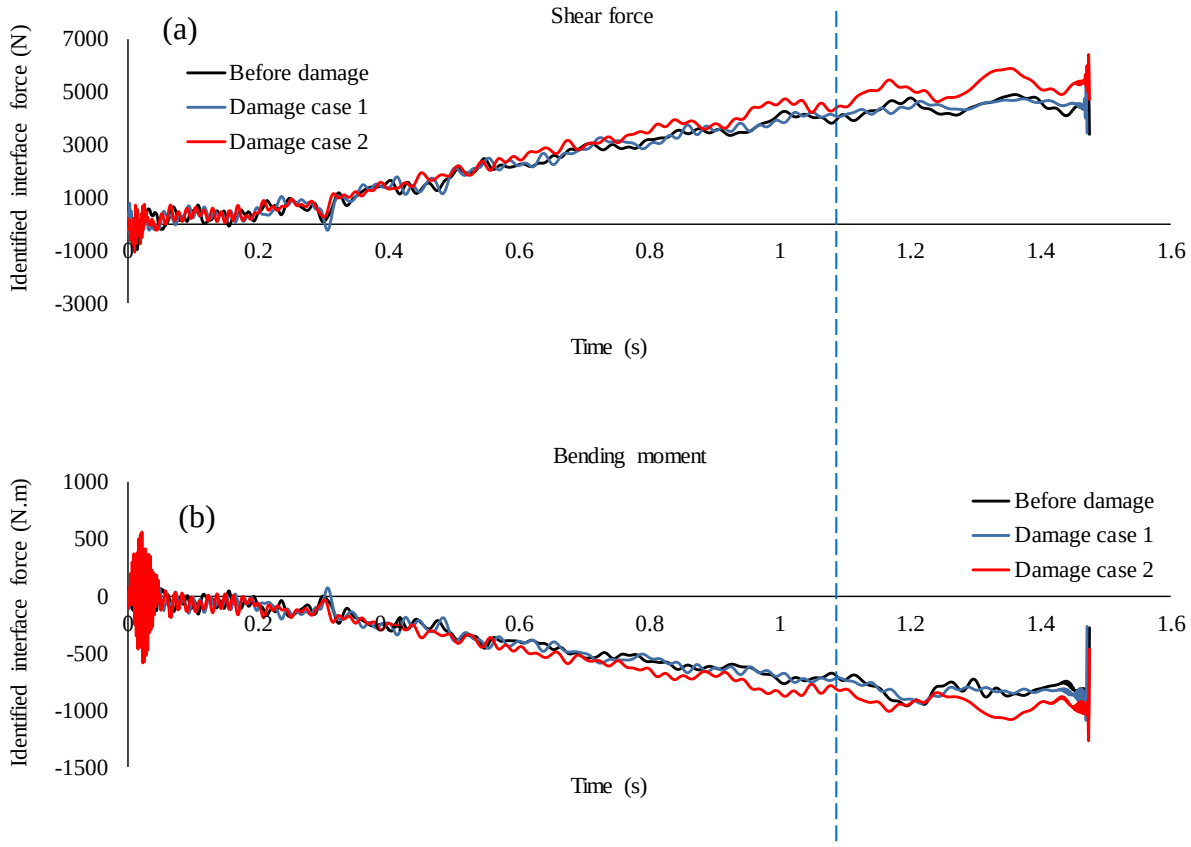

Figure 6-49: Effect of damage on identified interface forces at speed of 0.94 m/s- sampling frequency 800 Hz- scenario B; a: shear force b: bending moment

Table 6-12: Damage identification results with shorter sampling duration

Damage case	Speed (m/s)	Sampling frequency (Hz)	Total time hr:min:sec	N.I.	Convergence rate	Reconstructed displacement error
2	0.94	200	00:00:16	60	0.0088	0.1%
		400	00:00:50	30	8.16E-05	0.14%
		800	00:14:40	60	1.92E-4	0.18%

The effect of including the sensitivity of external loads to damage is not considered in this research and it is recommended for future studies. Measured and reconstructed displacement responses, as well as their difference, are shown in Figure 6-51 and Figure 6-52, respectively, showing that they match closely and the method is accurate.

`

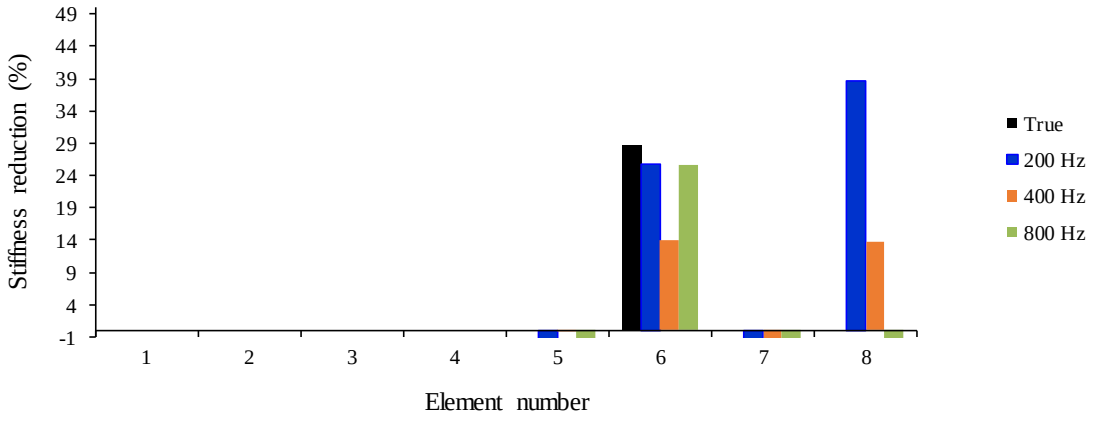

Figure 6-50: Effect of sampling frequency on damage detection at speed of 0.94 m/s - Damage case 2- scenario B

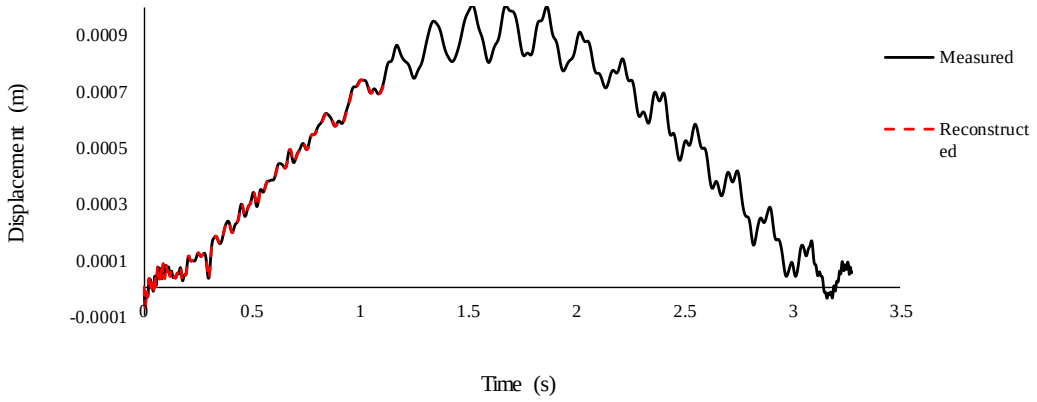

Figure 6-51: Measured and reconstructed displacement response at mid-span (damage case 1- speed 0.94 m/s- sampling frequency 400 Hz- scenario B)

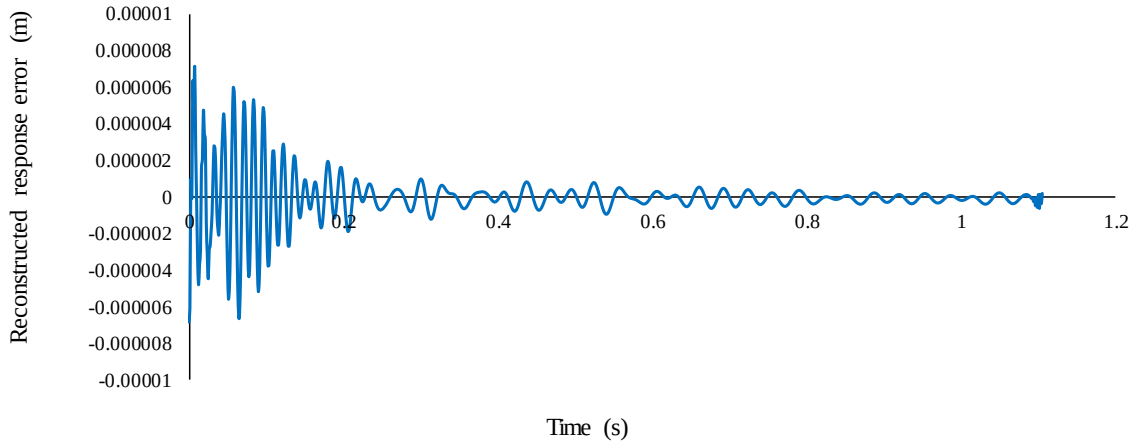

Figure 6-52: The error of reconstructed displacement response at node 5 (damage Scenario 1- speed 0.94 m/s- sampling frequency 400 Hz- scenario B)

`

6.7. Conclusion

Experimental studies have been carried out to verify the proposed techniques for moving load identification in Chapter 3 and the simultaneous identification of moving loads and structural parameters in Chapter 4, as well as the substructural condition assessment of bridge structures subject to moving loads in Chapter 5. A three-meter-long steel simply supported bridge beam was designed in the structural laboratory and a vehicle model pulled by an electric motor through the bridge at a constant speed. Modal tests were conducted before damage and after damage to obtain the natural frequencies and do the finite element model updating by minimizing the difference between experimental natural frequencies and numerical ones. Two instances of local damage were induced in two stages which were different in location and extension.

According to the experimental results, the proposed method is reliable to identify moving loads reasonably at different speed levels and sampling frequencies, whether the moving loads are being identified alone for an intact structure or it is being identified simultaneously with structural parameters. However, when it comes to detect and quantify damaged elements through the simultaneous identification of moving loads and structural parameters, it can be seen that the false positives/ negatives are identified for intact elements and there are very large positives at boundary elements, resulting from the modelling errors of the boundary conditions. As it was concluded by the numerical studies, the accuracy of the method is not changed at different levels of the speed and damage.

Experimental results indicated that the substructural technique- Scenario A for condition assessment provides more accurate results in comparison with the technique for simultaneous identification of moving loads and structural parameters, while reducing computation time significantly. This technique was able to detect the damaged element and the extension of damage very close to the true value in all cases of studies, however, there was a large false positive in the boundary element close to the support, in all cases of studies. As it was concluded in the numerical study, the methods accuracy at different speed and damage levels are same.

Experimental results indicated that the substructural technique- Scenario B for condition assessment is not sensitive to vehicle speed, however, the accuracy of the identified damage is affected by the chosen response time history and its duration. Since, the sensitivity of the internal forces is considered zero, it is better to choose shorter duration from the first moments of the vehicle move. Considering the effect of the internal force sensitivity is recommended for future studies. Same as Scenario A, there are big false positives at the boundary elements,

`

however, the structural stiffness of other elements can be properly identified. The computation time in Scenario B was greater than Scenario A, and it was significantly less than the case the FEM of the whole structure was used in the condition assessment of the structure.

`

`

Chapter 7. Case study: A cable-stayed bridge

7.1. Introduction

Information about the performance of bridge structures can be obtained using laboratory-scale experimentation, analytical and numerical simulations, and full-scale field experimentation. Field experimentation has several advantages since it is free from many assumptions, omissions, and simplifications inherently present in the former two, however, it is generally a more expensive exercise.

For example, the vehicle-bridge interaction is in its true condition during field experiments. Another aspect of in-situ testing is that sensors are exposed to the noisy outdoor testing environment, which presents a challenge to accurately measure data based on the vibration testing data contaminated by noise, especially when the responses are small. The field test provides the ultimate test for the accuracy of results obtained by laboratory experimentation and analytical simulations.

In this research, a 46 m long cable-stayed bridge located near the intersection of Second Avenue at Western Sydney University Werrington Campus and the Great Western Highway in Werrington, NSW (33°45'50.49"S, 150°44'31.14"E), has been chosen as the field full-scaled bridge (Figure 7-1).

In section 7.2 of this chapter, the bridge structure is explained, and in section 7.3 the instrumentation array is presented. The bridge has been modelled in ANSYS and MATLAB and these are explained in sections 7.4 and 7.5, respectively. The procedure of the test is presented in section 7.6, and the extracted data is discussed in section 7.7. Identification results are explained in section 7.8., while section 7.9 presents the conclusion of this chapter.

7.2. Bridge structure

The layout of the beams and the overall bridge dimensions are presented in Figure 7-2 to Figure 7-5. These figures have been extracted from the drawing series by Bruce James & Partners and Hughes Trueman Ludlow project # D1091, July 1990. The bridge deck is composite with a thickness of 0.16 m, consisting of a series of equally spaced lateral beams joined by four I-beam longitudinal girders. Each lateral beam is supported by two stays or a series of 4 pedestal bearings. The longitudinal span of the bridge is 45.5 m with a width of 5 m. The A-shaped steel tower is approximately 33 m high, when measured from the base level. It has a non-prismatic cross-section, starting with a rectangular section of 700 mm by 800 mm at the base and 500 mm by 800 mm at the uppermost level. The 2 by 8 cables are provided to support the bridge. Both the longitudinal and transverse girders have universal beam

`

(410UB54) cross-sectional properties. All cables are super grade circular bars with a diameter of 38 mm. The first three natural frequencies measured by the hammer test on-site are 2.0Hz, 3.7Hz and 5.7Hz. It is notable that there is a roundabout at the south end of the bridge (Figure 7-1) which limits options for choosing test vehicle types and speed. This will be discussed more in the following sections.

7.3. Instrumentation array

The data monitoring systems were installed by EngAnalysis Pty Ltd and CSIRO's Data61 in July 2016 and consist of:

-31 accelerometers including tri-axial accelerometer at top of the suspension mast,

-31 channels of strain gauges,

-1 temperature sensor,

-3 optical sensors to indicate vehicle or pedestrian presence.

The map of accelerometer locations and directions is presented in Figure 7-6. The accelerometers are distributed along the deck at all intersections between the lateral and longitudinal girders with the exceptions of the beams adjacent to the two abutments. They are low-noise Silicone Design accelerometers and measure accelerations of up to 62 g with an output noise of 10mg/Hz and sensitivity of 2000 mV/g. The signal conditioning and data logging system is an HBM Quantum-X data acquisition system. The acceleration time histories of the bridge are continuously measured at a sampling frequency of 600 Hz. The map of strain gauge locations is presented in Figure 7-7. The section of bridge between girders G6 and G7 has a higher density of strain gauges than most other locations within the bridge.

Figure 7-1: The cable-stayed bridge (pictures from google map)

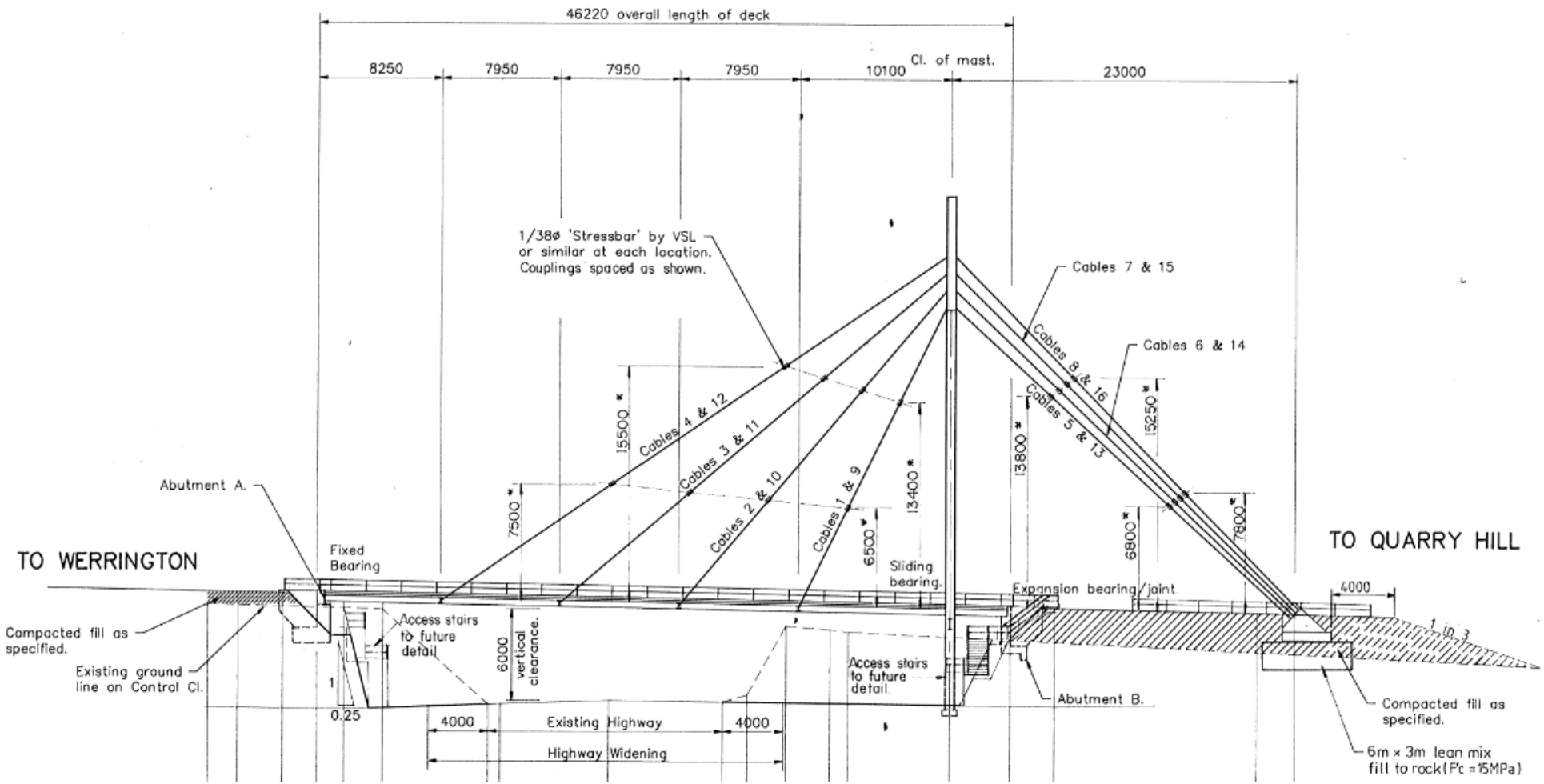

Figure 7-2: Lateral chainage looking east towards bridge (drawing series by Bruce James & Partners and Hughes Trueman Ludlow)

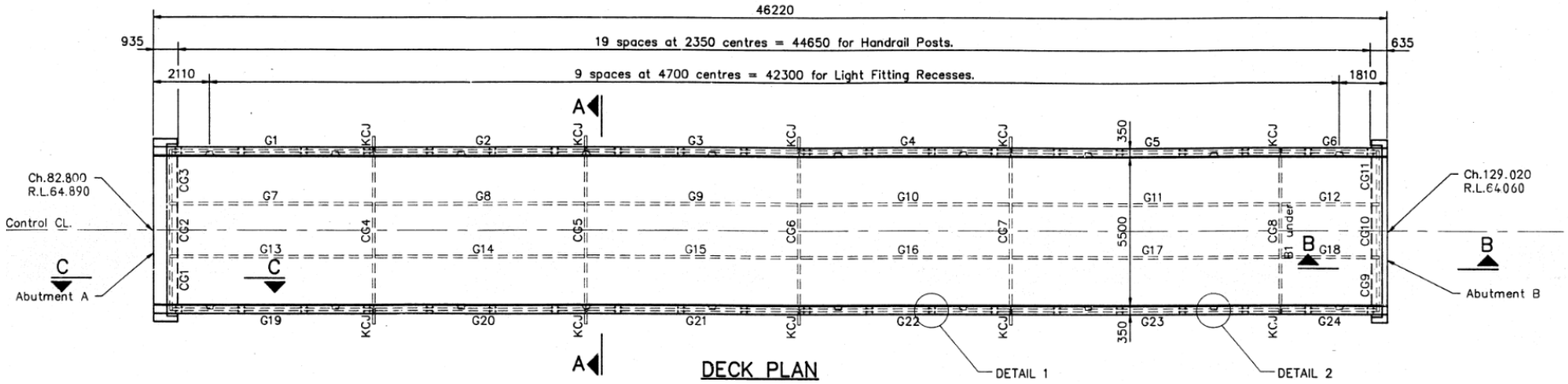

Figure 7-3: Deck plan (drawing series by Bruce James & Partners and Hughes Trueman Ludlow)

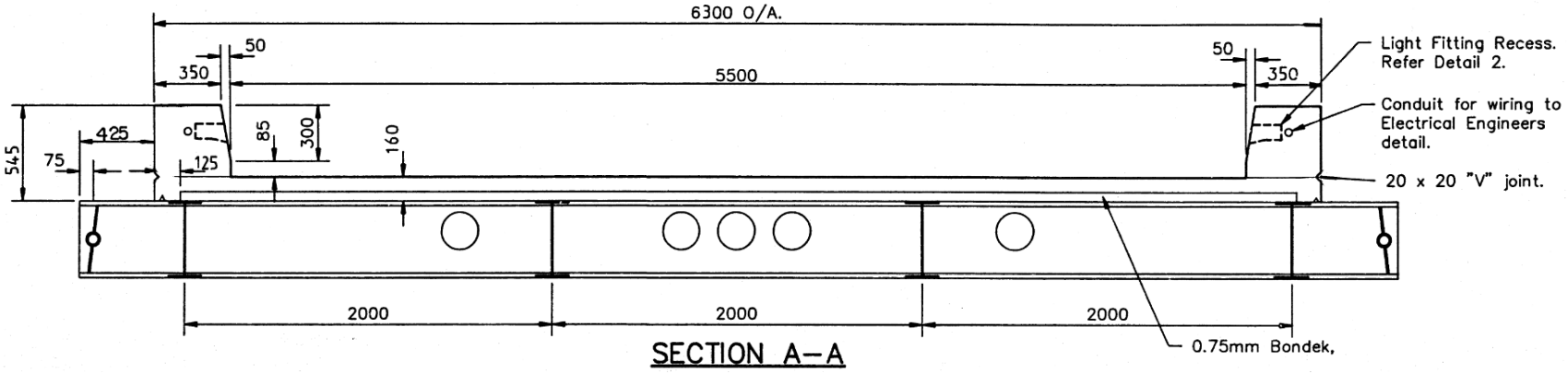

Figure 7-4: Transverse elevation of the lateral beam (drawing series by Bruce James & Partners and Hughes Trueman Ludlow)

`

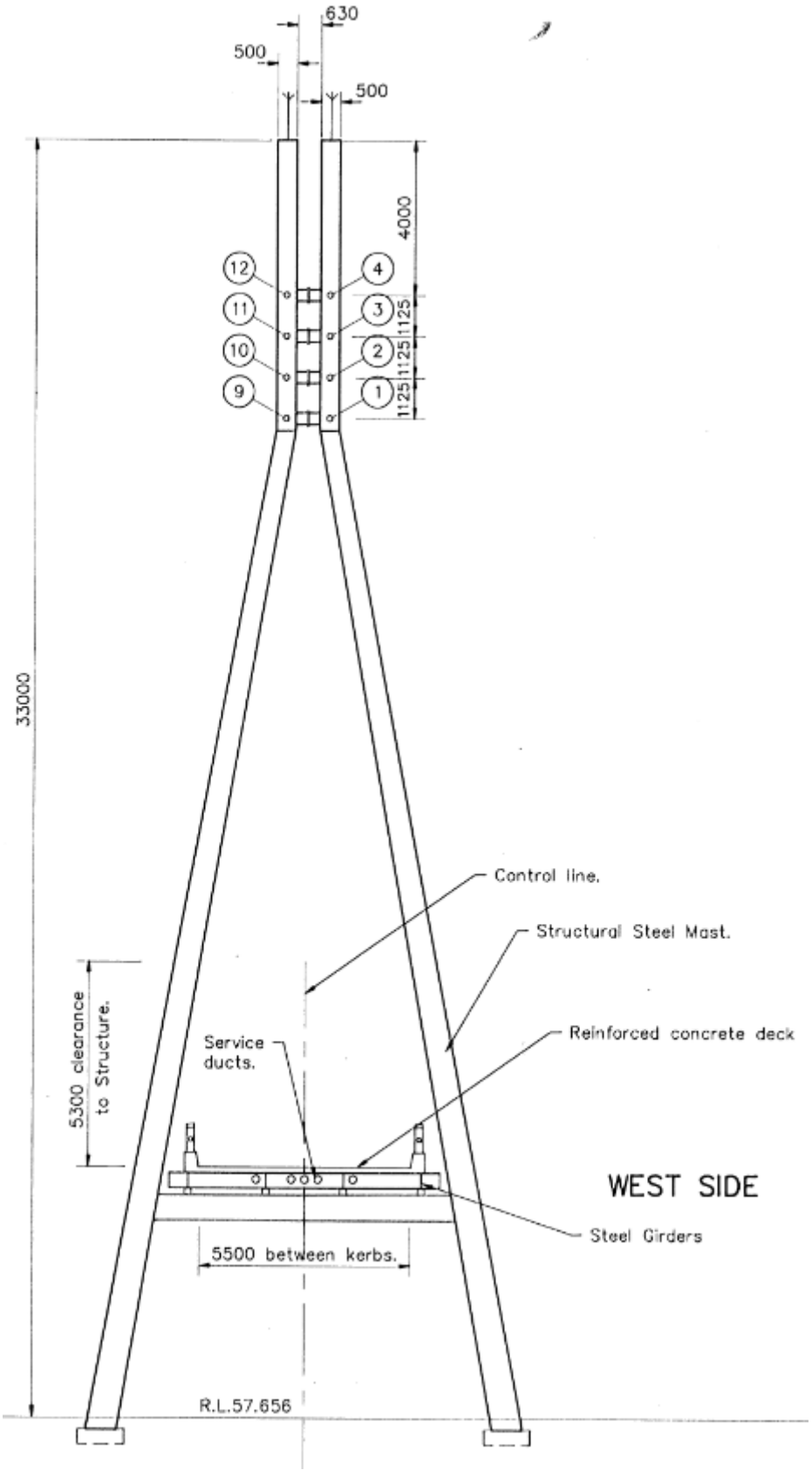

Figure 7-5: Side elevation looking toward the tower of the bridge (drawing series by Bruce James & Partners and Hughes Trueman Ludlow)

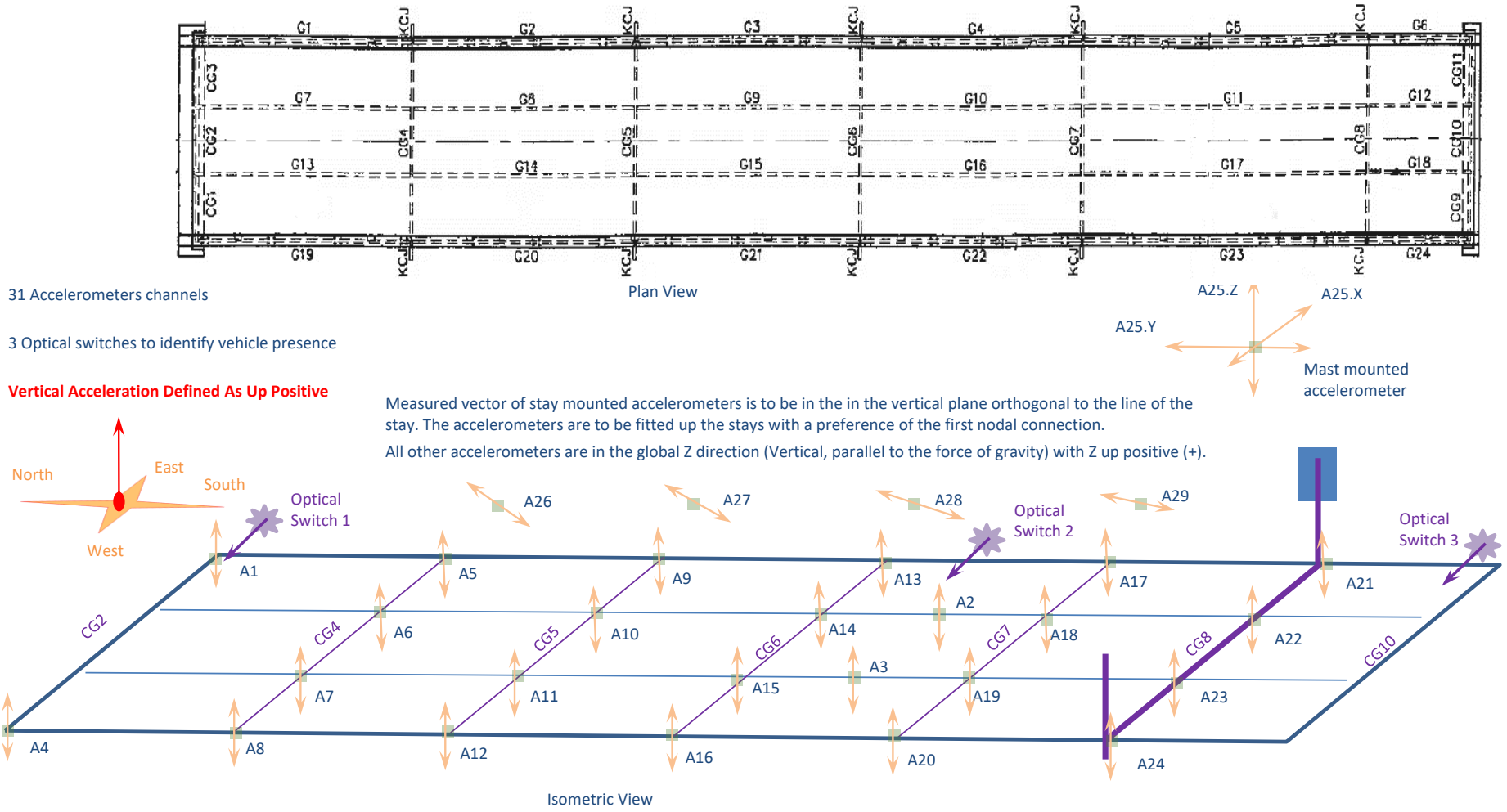

Figure 7-6: Overview of accelerometer locations from above looking through the deck

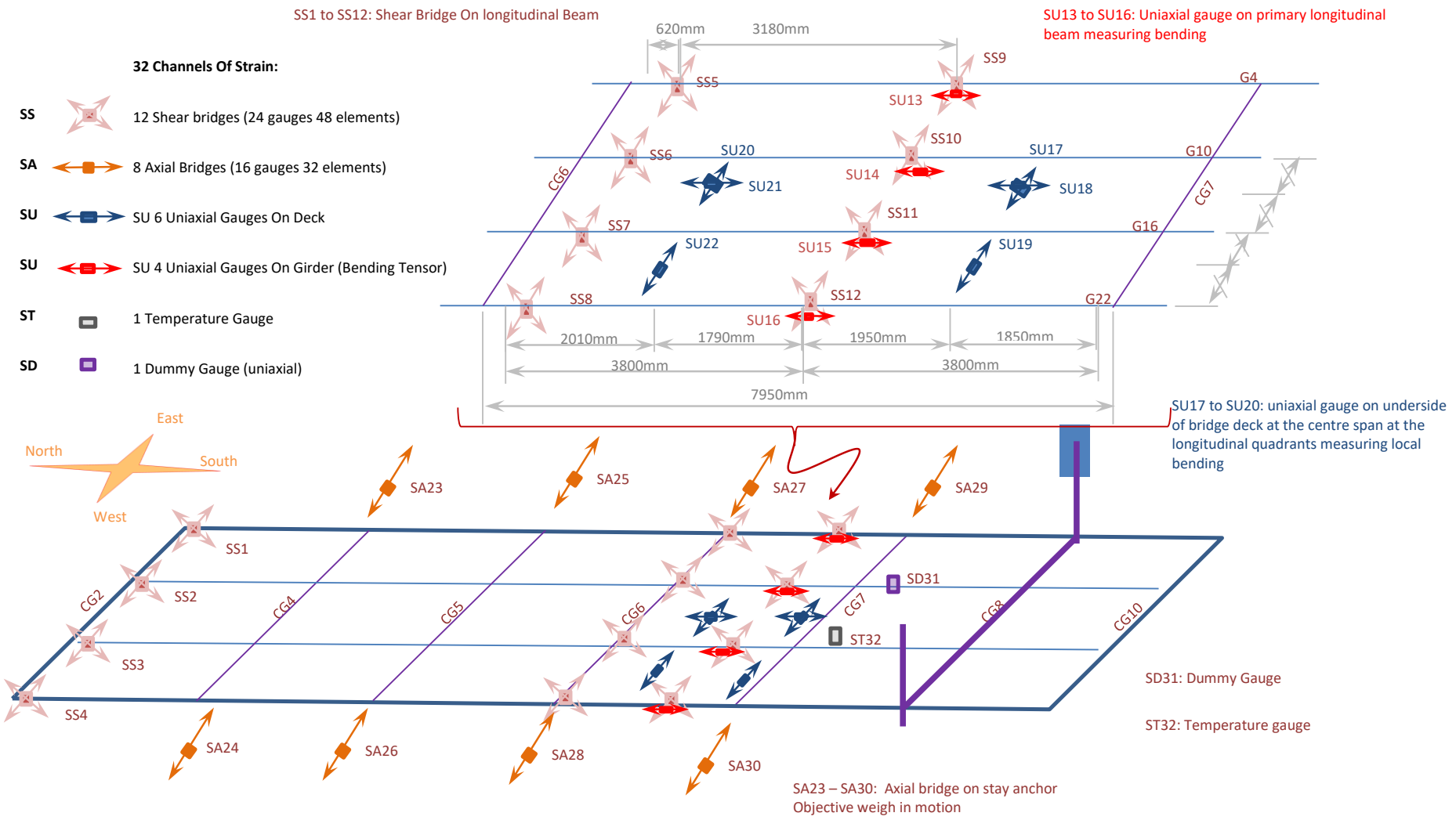

Figure 7-7: Overview of strain gauge locations from above looking through the deck

7.4. Finite element model of the bridge in ANSYS

At the first stage, a 3-D model of the bridge is created in Solidworks (Figure 7-8), this model is then imported to ANSYS (Figure 7-9).

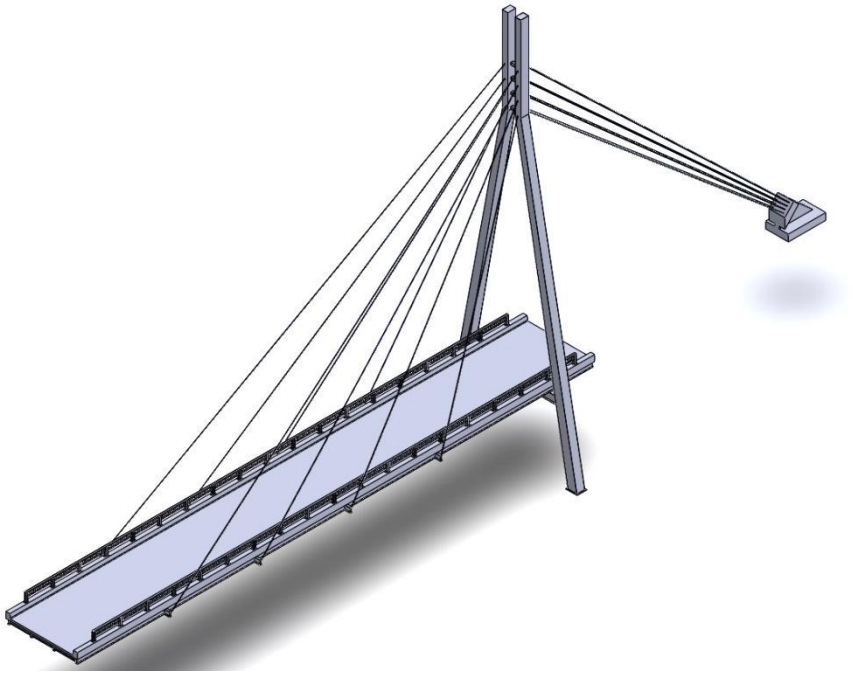

Figure 7-8: Bridge model in Solidworks

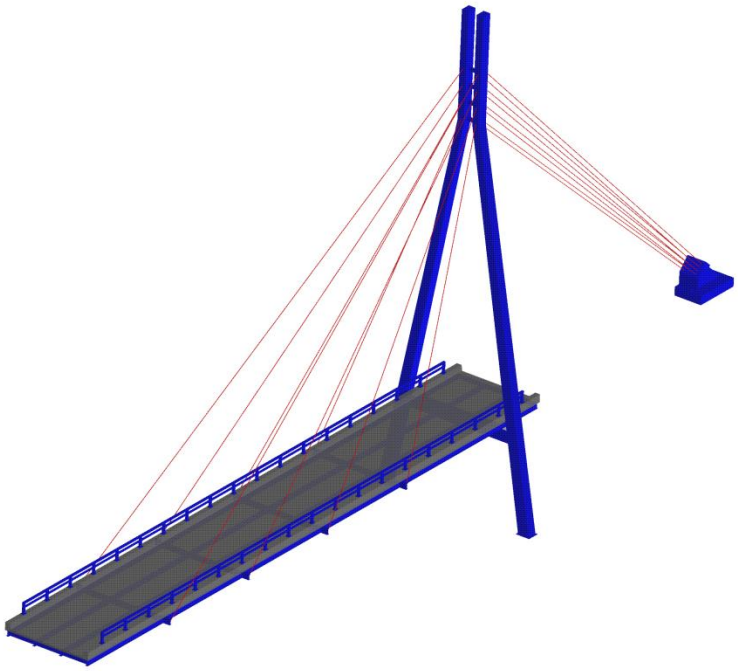

Figure 7-9: Bridge model by ANSYS

The model contains steel girders, cables, handrails, tower, a concrete slab, and a concrete anchor. Three types of elements and three types of materials are used to model the bridge in ANSYS as detailed in Table 7-1:

Table 7-1: Types of elements and materials used to model the bridge

Element Name	Element type	Material type	Element length (m)
Steel girders	SOLID187	1*	0.1
Steel cables	SOLID185	3*	5
Steel handrails	SOLID187	1*	0.1
Steel tower	SOLID187	1*	0.1
Concrete slab	SOLID65	2*	0.1
Concrete anchor	SOLID187	1*	0.5

* Different types of materials are defined as follows:

Material type 1: Modulus of elasticity: 200 GPa- Poisson's ratio: 0.3- Density: 7850 (kg/m^3)

Material type 2: Modulus of elasticity: 17 GPa- Poisson's ratio: 0.15- Density: 2500 (kg/m^3)

Material type 3: Modulus of elasticity175 GPa- Poisson's ratio 0.3- Density: 7850 (kg/m^3)

The first 12 natural frequencies derived by ANSYS are listed in Table 7-2 and the related mode shapes are shown in Figure 7-10 (a to l). The modal analysis run took 5 minutes. The system processor used in this study is Intel® Core ™ i7-4790 CPU @ 3.60 GHz and the installed memory (RAM) is 32.0 GB. Since the focus in this research is on a 2D model, frequencies and mode shapes in the vertical direction (Y) are of importance. From Figure 7-10 (a to l), it can be seen that the first three simulated frequencies in the Y direction on the concrete slab are 1.9 Hz (mode 1), 3.68 Hz (mode 4), and 6.02 Hz (mode 12). Other frequencies are in lateral directions, torsional or related to cables and tower vibrations. The natural frequencies measured on-site through hammer tests are 2.0 Hz, 3.7 Hz and 5.7 Hz, which were measured by SAHM group at CIE-Western Sydney University.

Table 7-2: Frequencies of the bridge derived from ANSYS analysis

Mode number	Frequency	Mode number	Frequency	Mode number	Frequency
1	1.90	5	4.60	9	5.04
2	3.27	6	4.64	10	5.49
3	3.62	7	4.79	11	5.62
4	3.68	8	4.81	12	6.02

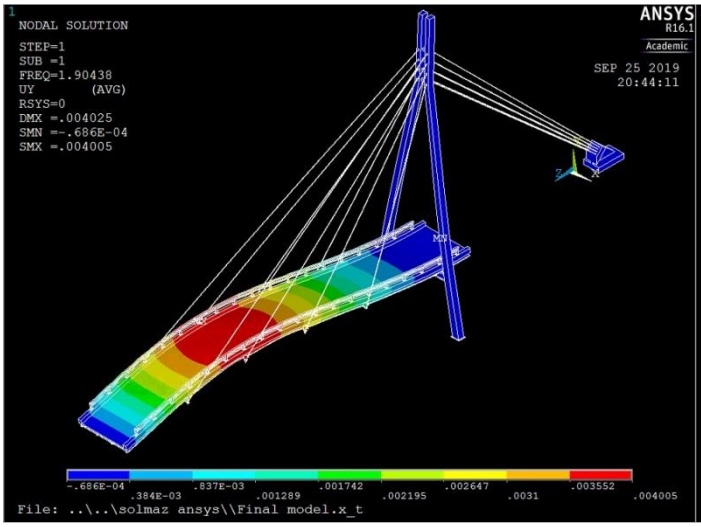

a) Mode 1- Frequency 1.9 Hz

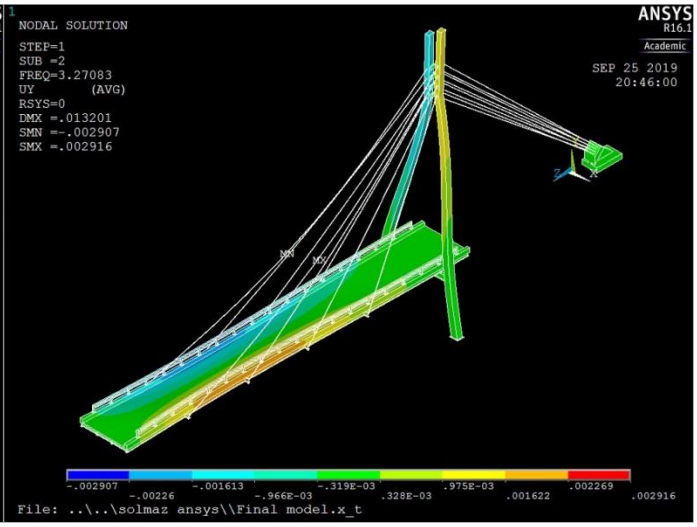

b) Mode 2- Frequency: 3.27 Hz

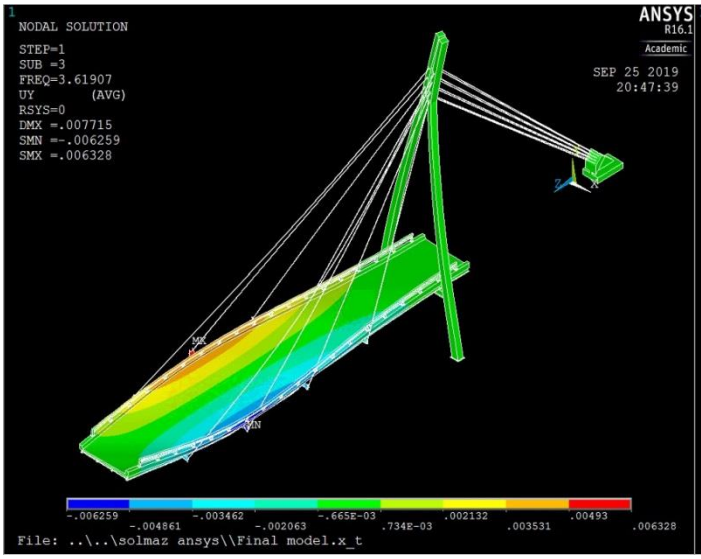

c) Mode 3- Frequency 3.62 Hz

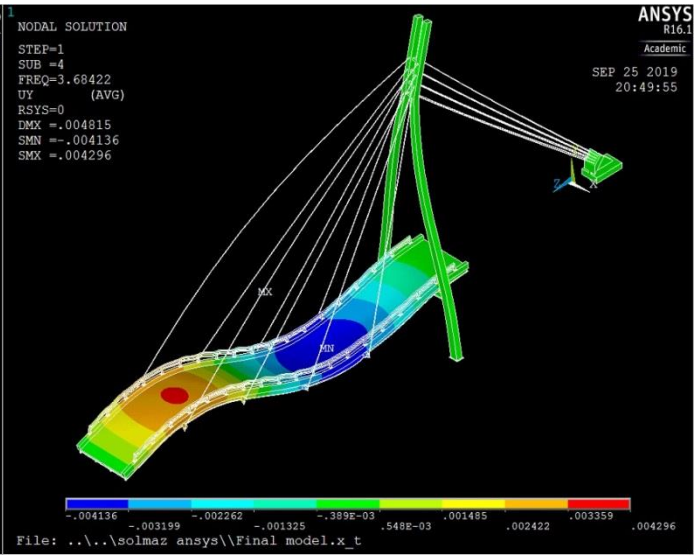

d) Mode 4- Frequency: 3.68 Hz

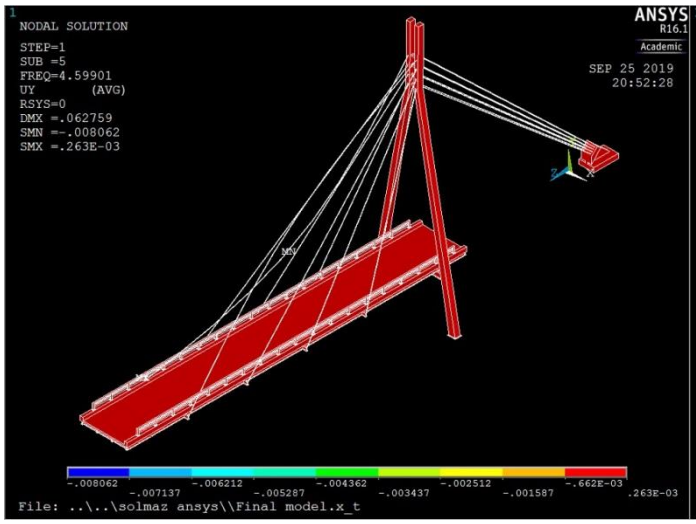

e) Mode 5- Frequency: 4.6 Hz

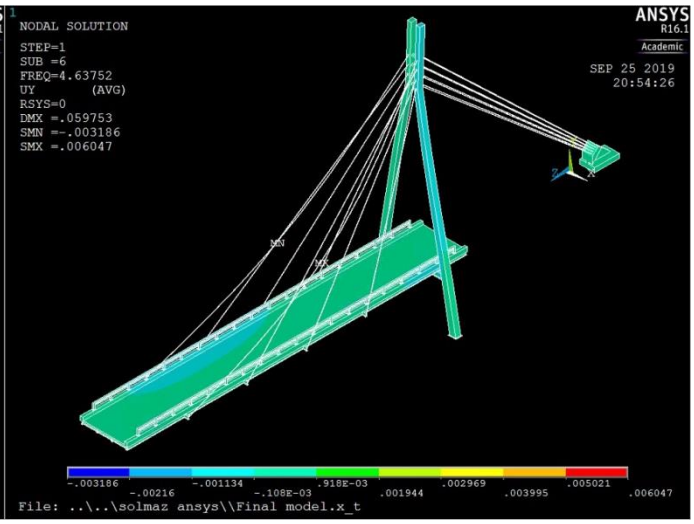

f) Mode 6- Frequency: 4.64 Hz

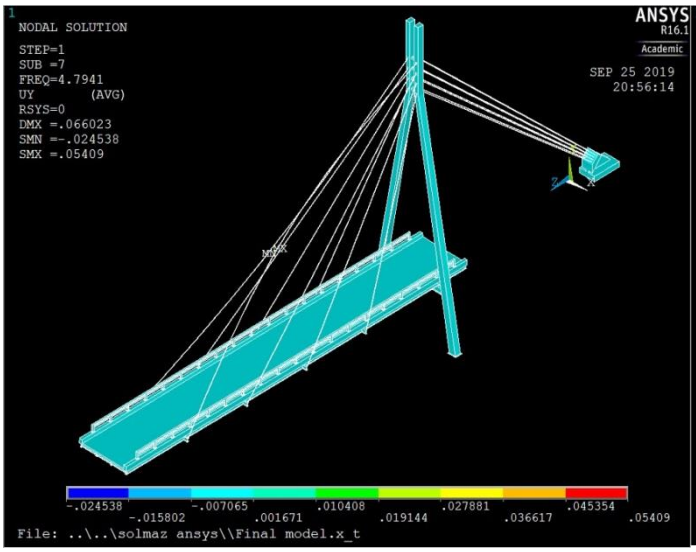

g) Mode 7- Frequency: 4.79 Hz

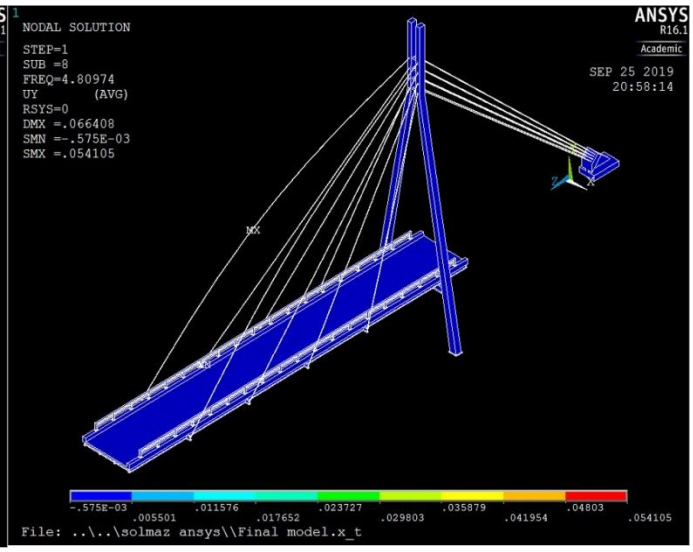

h) Mode 8- Frequency: 4.81 Hz

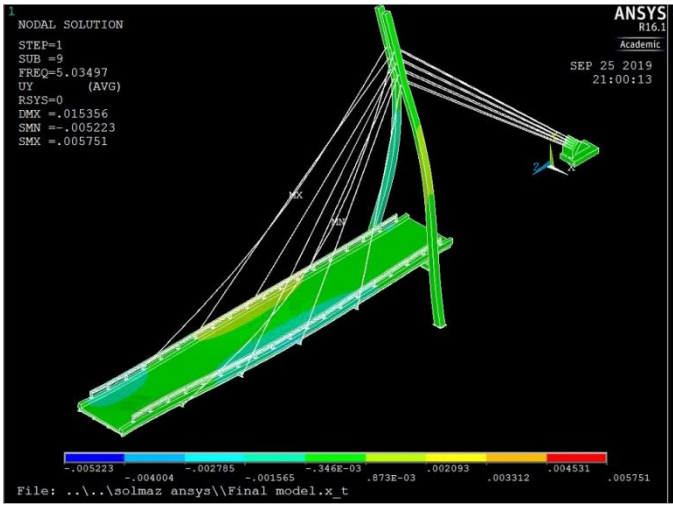

i) Mode 9- Frequency: 5.04 Hz

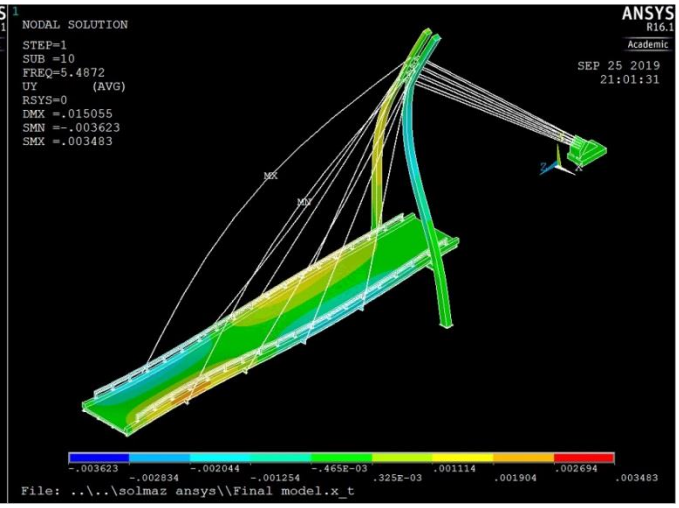

j) Mode 10- Frequency: 5.49 Hz

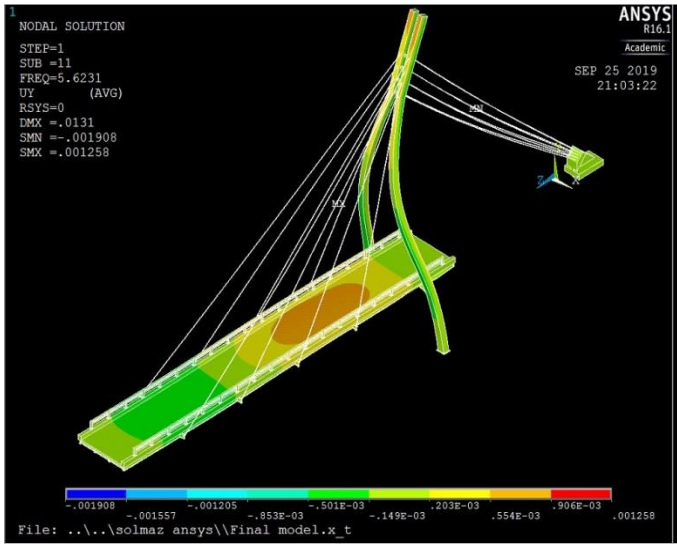

k) Mode 11- Frequency: 5.62 Hz

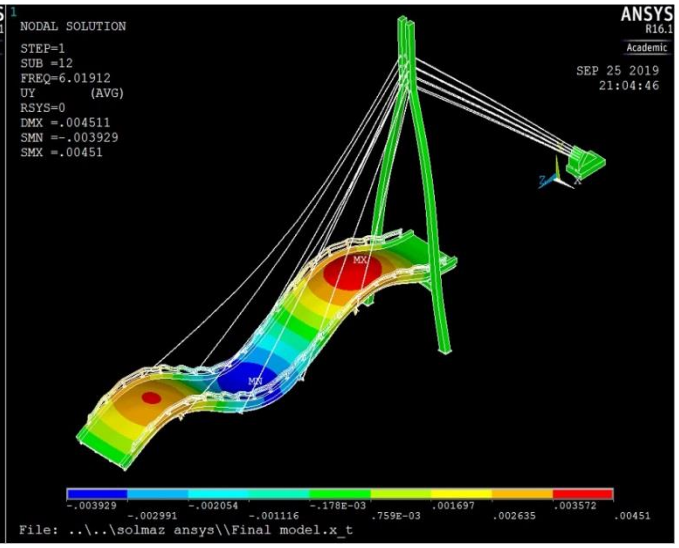

l) Mode 12- Frequency: 6.02 Hz

Figure 7-10: Figures “a” to “l” are the first 12 mode shapes of the bridge by ANSYS

7.5. Finite element model of the bridge in MATLAB

The 2D numerical model of the bridge is constructed in MATLAB. It has 46 nodes, 43 beam-column elements, 8 cable elements, and 131 degrees of freedom (see Figure 7-11). The deck of the bridge is modelled as a simply supported beam. The tower and deck have been modelled by Euler-Bernoulli beam elements with three degrees-of-freedom at each node. The mast base support is modelled as fixed support, in which all degrees of freedom are restrained.

Two nodes are defined at the intersection of the tower and deck to define their connection properly. These two nodes have a same vertical displacement but can have different rotation and horizontal movements. The cables are modelled by bar elements using the same nodes. The vehicle moves from north to south of the bridge (Figure 7-6). Damping ratio of all modes is considered as 1.5% of critical.

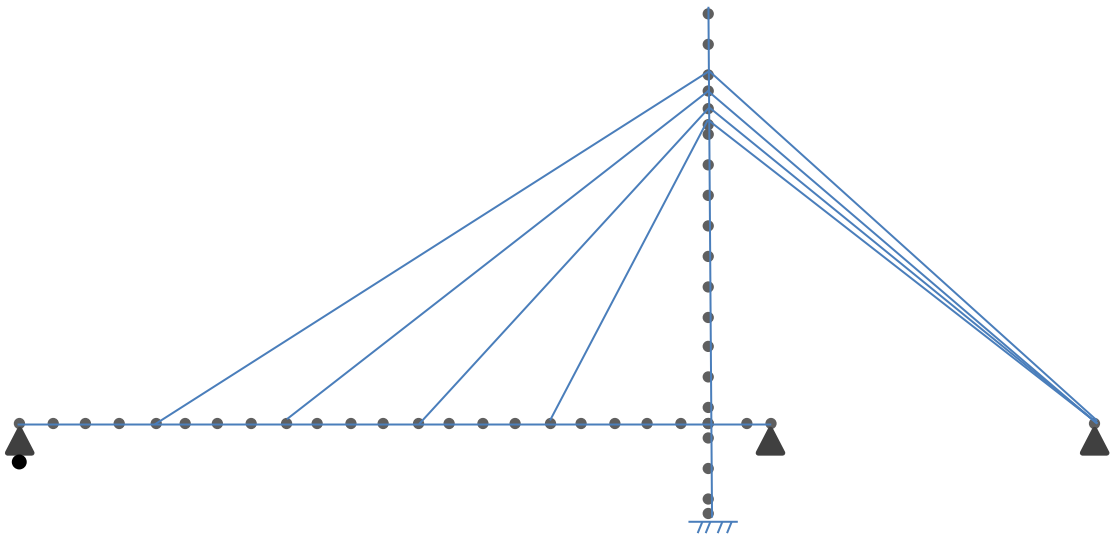

Figure 7-11: Nodes in the finite element model of the bridge

Three discretization types of finite element models are studied and their frequencies are compared with experimental frequencies of the bridge and numerical ones from ANSYS to find the best model. The results are tabulated in Table 7-3. These three types are different in their element length. In the first one, the element length is approximately 0.5 m, for the second one it is approximately 1 m and for the last one is approximately 2 m. The elements length at cables connection positions are a bit different with other elements lengths for precise modelling.

As can be seen from the table, discretization type does not affect the results significantly, however smaller beam elements lead to a larger computation time. Hence, a 2 m beam element is adopted. The natural frequencies derived by MATLAB closely match the natural frequencies derived by ANSYS. There are some small errors between the first three natural frequencies for numerical models and the experimental model, namely, 4.5%, 0.5%, 5.2%, respectively. These values are deemed quite reasonable since there are some uncertainties in the experimental tests and some construction unknowns which affect numerical modelling. The first three mode shapes can be found in Figure 7-12, they closely match the results from ANSYS.

Table 7-3: Natural frequencies of the bridge

Beam element lengths	0.5 m	1 m	2 m	Numerical natural frequency (Hz) (ANSYS)	Experimental natural frequency
Mode number	Numerical natural frequency (Hz) (MATLAB)				
1	1.910	1.908	1.904	1.904	1.996
2	3.686	3.685	3.683	3.684	3.659
3	6.043	6.043	6.042	6.019	5.737

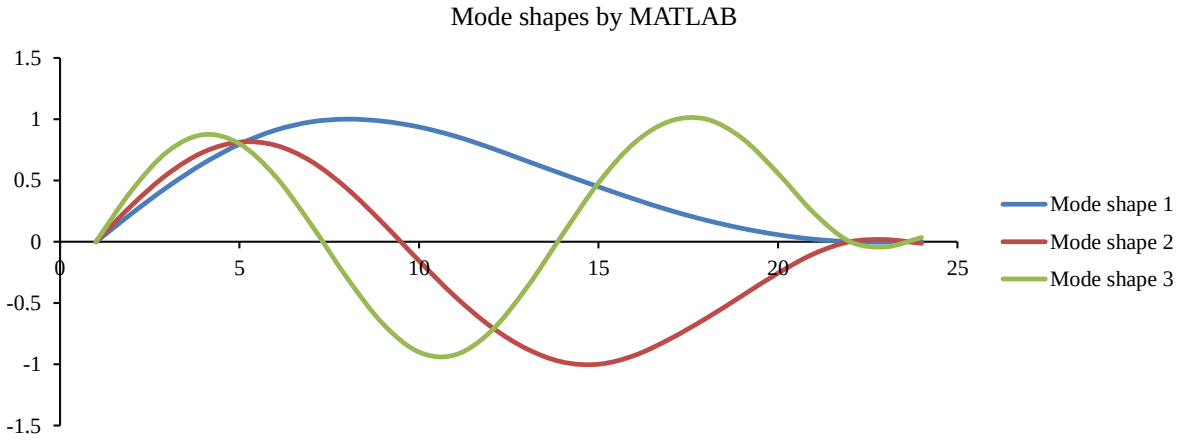

Figure 7-12: The first three mode shapes derived by MATLAB

7.6. Experimental procedure

The test was carried out on Thursday 30-May-2019 and the car was driven from north to south of the bridge at a speed of 42 km/h. Speed was constant and controlled by the vehicle's cruise control functions. The car type was a Mazda 3 (Sedan-Maxx Sport), weighing 1306 kg with an axle distance of 2.7 m (Figure 7-13). It should be noted that the driver and other loads and items in the car weighed approximately 100 kg. Test information is tabulated in Table 7-4.

Due to the presence of a roundabout at the south end of the bridge (Figure 7-1) and the need for constant speed, it was not feasible to have a vehicle with a longer axle distance. Braking, which is necessary before reaching the roundabout, by necessity happens on the bridge for cars with a longer axle distance. This case is out of the scope of this study. For the

same reason, it is not feasible to employ a constant speed of more than 42 km/h. It is notable that the bridge deck is 5 m wide from curb to curb and this leaves significant lateral uncertainty on the location of traffic. It was attempted to drive the car through the longitudinal centreline of the bridge (Figure 7-14) to obtain results with a minimum of errors.

Since the bridge was under operational condition, several cars were moving on the bridge and creating vibration. The test was carried out once the bridge vibration from other cars was sufficiently damped. The test was carried out 5 times. Road surface roughness was of very good quality and is approximated as level A.

In this study, the following assumptions and restrictions have been used for dynamic analysis of the cable-stayed bridge:

- The torsional behaviour caused by eccentric loading of the bridge beam is disregarded,
- Only vertical modes of vibration of the vehicle are considered,
- Longitudinal forces generated by the vehicle are neglected.

Table 7-4: Test information

No.	**Speed**		**Entrance time**		**Exit time**		**explanation**
	km/h	**m/s**	**UTC**	**Sydney**	**UTC**	**Sydney**	
1	42	11.66	22:55:36 Wed. 29/May	8.55 am	22:55:41 Wed. 29/May	8.55 am	Speed was constant by cruise controller

Weights and Capacities

Sedan		Neo Sport	Maxx Sport
Cargo room volume VDA (litres)		408	408
Kerb weight (kg):	Manual	1,258	1,276
	Auto	1,291	1,306
Towing capacity¶ (kg):	Braked	1,200	1,200
	Unbraked	600	600
Tow-ball download maximum (kg)		75	75

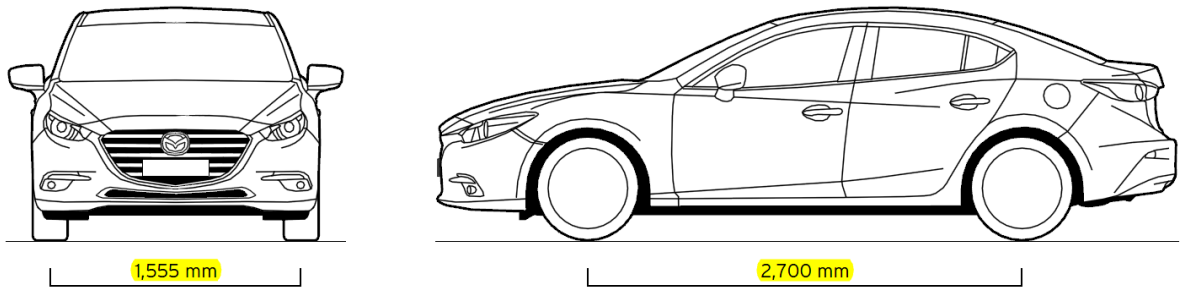

Figure 7-13: Information of the test vehicle (pictures from the digital brochure of Mazda)

Figure 7-14: Reviewing the path of vehicles on the bridge

7.7. Data analysis

At the time of testing, optical sensors were not working properly and they needed to be fixed. The aim of optical sensors is to detect the entrance and exit of the individual vehicle axles. Therefore, an alternate option was used to detect the entrance and exit of the bridge, and that was to use shear strain data at the north end of the bridge. Alamdari et al. (2019) carried out numerous tests on this cable-stayed bridge by different types of the test vehicles and

concluded that shear strain-gauges at the north end of the bridge are able to detect the entrance of individual axles. Unfortunately, however, the cable axial strains and bending strain response of the bridge fail to provide this type of information. Shear strains measured at the mid-span of the bridge can identify the axle groups but are not able to identify individual axles in an axle group of two or three.

Sensor SS2 is located at the north end of the bridge, its 10-minute time history is shown in Figure 7-15. The sampling frequency is 600 Hz; therefore, a 10-minute time history includes 10×60×600 samples or 600 seconds. Multiple picks show the entrance of different vehicles. We know that the pick around 500 seconds relates to the test vehicle. Figure 7-16 shows the shear strain time history recorded by SS2 while the test vehicle is traveling over the bridge. As can be seen, when the front axle enters the bridge, a large fluctuation occurs which is indicated by a red circle. The cruise control is set on 42 km/h (11 m/s), so the total time between the entrance of the front axle load to the bridge and exit of the rear axle load from the bridge is 4.13 sec. The moment when the rear load leaves the bridge is shown with a vertical red line.

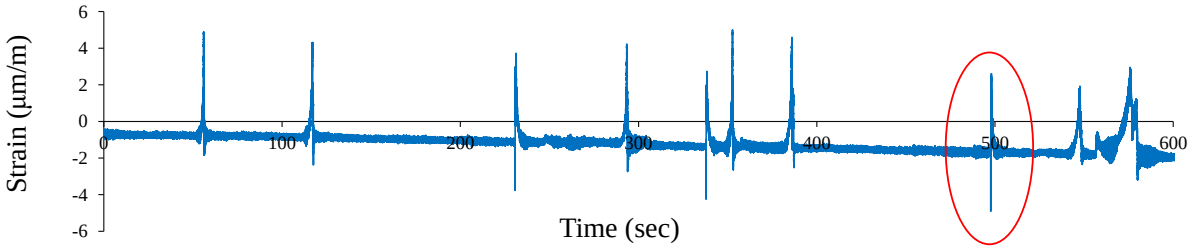

Figure 7-15: Shear strain signal by sensor SS2 (10 min)

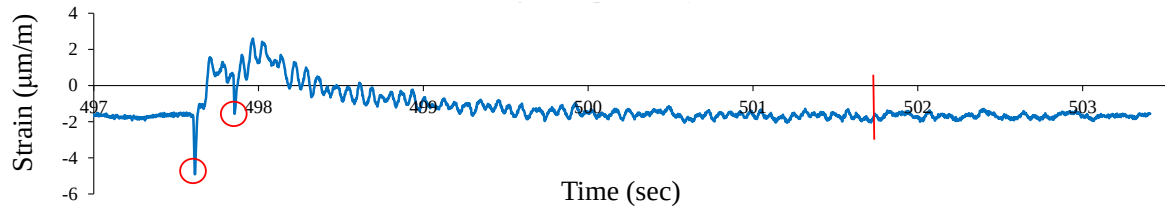

Figure 7-16: Shear strain Signal by sensor SS2 while the car is passing over the bridge

Shear strain time histories of sensors SS6 and SS10, while the test vehicle is passing through the bridge, are shown in Figure 7-17 and Figure 7-18. These sensors are located around mid-span. As can be seen, SS2 is clearer than the other two in showing the entrance of the axles. Information from sensors SS6 and SS10 can be used to approximately check the average speed of the test vehicle.

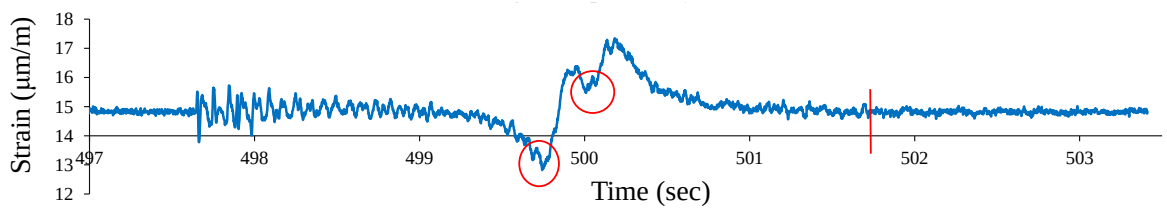

Figure 7-17: Shear strain signal by sensor SS6 while the car is passing over the bridge

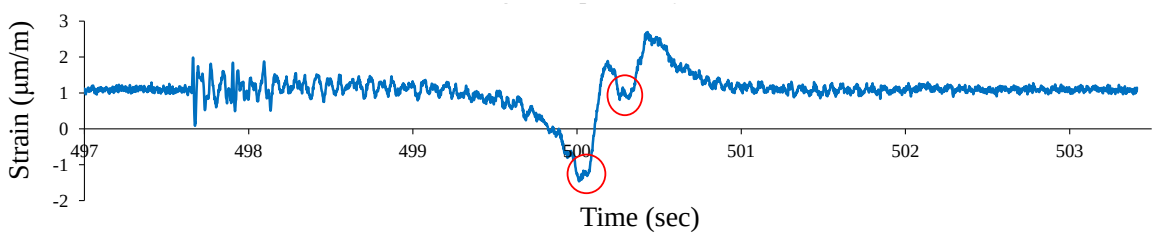

Figure 7-18: Shear strain signal by sensor SS10 while the car is passing over the bridge

Here, in this study, a combination of accelerometers and strain measurements are used. The 10-minute time history of mid-span bending strain is shown in Figure 7-19. Again, picks indicate the number of times different cars have passed over the bridge. We know that the pick around 500 s relates to the test car. Bending strain time history while the test car is passing over the bridge is shown in Figure 7-20. The same thing is true for accelerometer measurements. There is a total of 7 accelerometers, from which signal related to A6 is shown in Figure 7-21 and Figure 7-22. The entrance of the axle loads is obvious in Figure 7-22. Furthermore, it can be seen how bridge induced vibration is damped out when the car leaves the bridge. From the observations, it can be concluded that the entrance of the front and rear axle loads can be identified by all sensors discussed here.

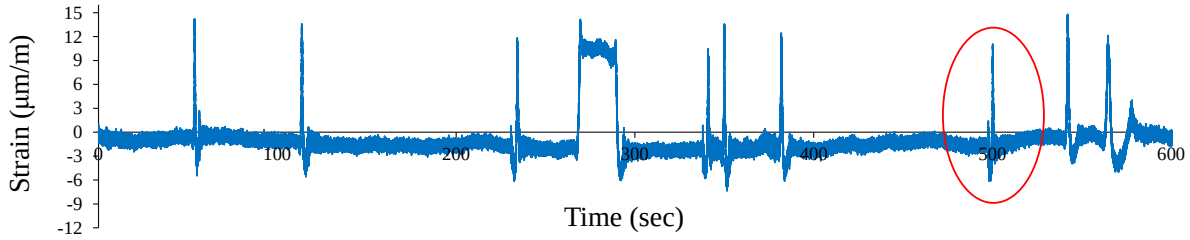

Figure 7-19: Strain signal by sensor SU14 (10 min)

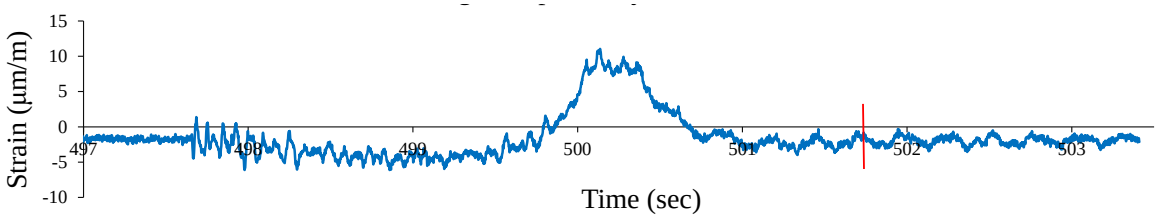

Figure 7-20: Strain signal by sensor SU 14 while the car is passing over the bridge

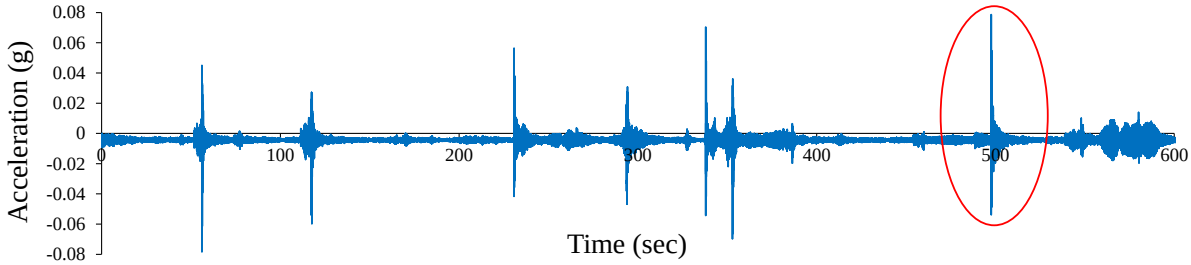

Figure 7-21: Acceleration signal by sensor A6 (10 min)

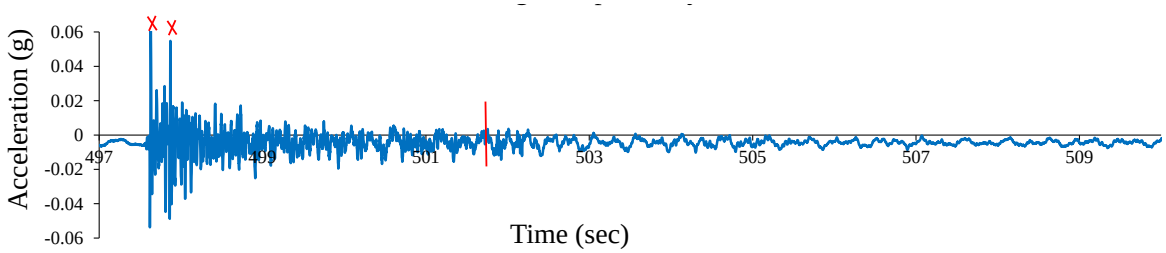

Figure 7-22: Acceleration signal by sensor A6 while the car is passing over the bridge

7.8. Moving load identification results

The combination of 7 accelerometers and 1 strain measurement are used to identify the moving loads passing over the bridge. In the first step, a baseline correction is done for both accelerometers and the strain gauge measurements. Data is analysed by MATLAB. Moving load identification is done based on the Newmark-β method. The generalized Tikhonov regularization is used to bound the results and the GCV method is used to find the optimum regularization parameter λ. Identified front and rear loads are shown in Figures Figure 7-23, a-b.

The front and rear loads are identified very closely. When one of the loads is out of the bridge, it is not identified as zero. This error appears while using accelerometers as the measurements. By the experimental study in the laboratory, where strain measurements were used, this error did not exist. There is a large value at the entrance of the car which is because of a small bump existing at the entrance of the bridge. When the car reaches the end of the bridge, next to the roundabout, braking is inevitable, and this is the reason for the negative value of the identified loads at the last moments.

To check the accuracy of the identified loads, true values are not known, however, the resultant load can be compared with the static load of the vehicle, as shown in Figure 7-23 (c)

Figure 7-23, c. The resultant load is identified very close to the static load and the difference is determined as 5.89%. Another way to check the accuracy of identified loads is to compare the reconstructed strain with the measured one. Here, the strain at the location of sensor SU14 is reconstructed by inputting the identified loads into the equation of motion of the bridge. The results can be seen in Figure 7-24.

It can be seen from Figure 7-24 that the reconstructed strain and the measured strain do not match perfectly. To study this more, it is assumed that vehicle weight is approximately equally divided between the two axles, and axles are moving on a smooth surface without any roughness. Then the moving masses-bridge interaction equation is solved as a forward problem by the Newmark-β method to calculate bridge responses subjected to moving masses. By having displacement responses, strains can be calculated. The calculated strain is called static strain. The static strain at the location of sensor SU14 is compared with the measured and reconstructed ones as shown in Figure 7-24.

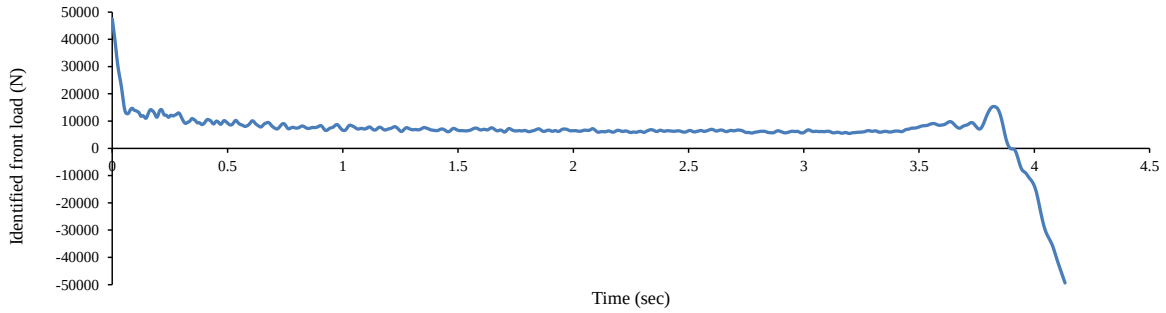

(a)

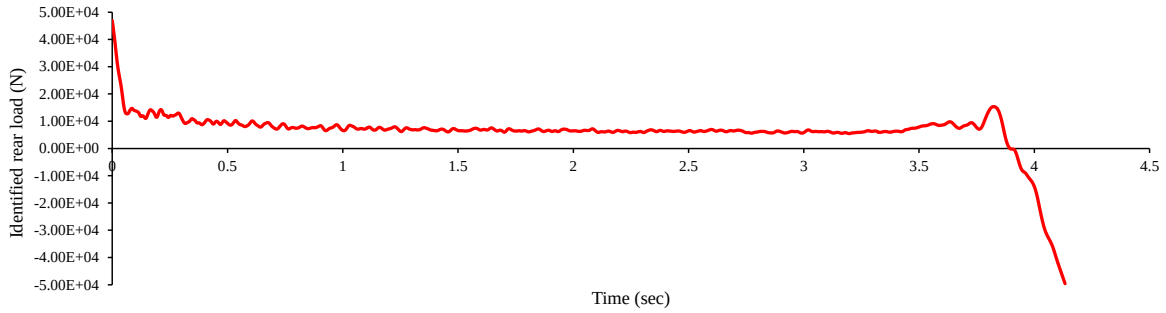

(b)

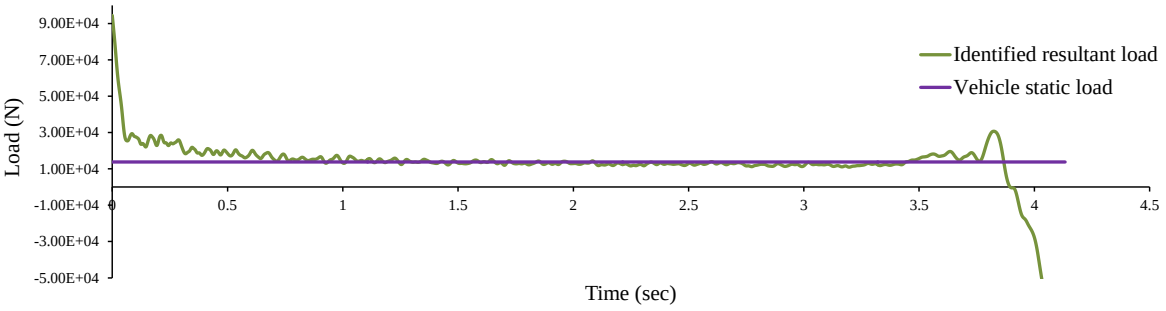

(c)

Figure 7-23: Identified loads, a) Front load b) Rear load c) comparing resultant load with the vehicle static load

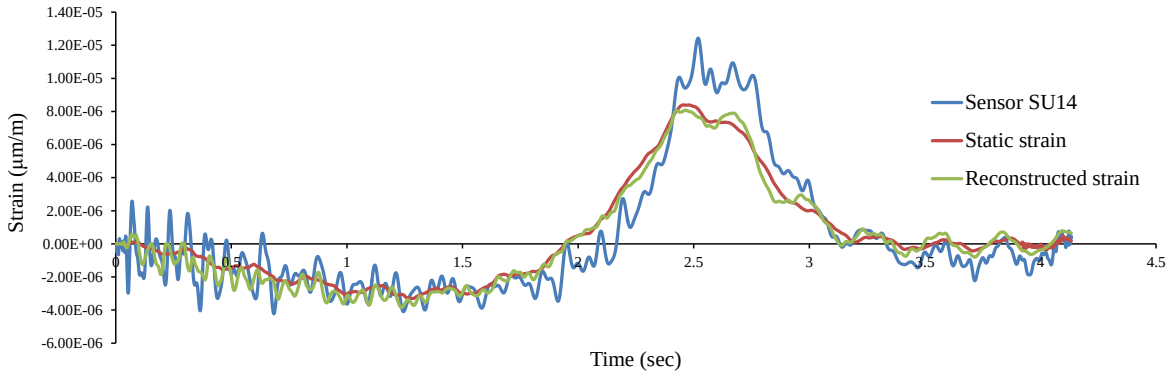

Figure 7-24: Comparing the reconstructed strain with the measured strain and the static strain

It can be seen that reconstructed strain overlaps the static strain, indicating that with the existing sensor measurements, dynamic interactions are not identified correctly and only the static part of the interaction loads has been identified. Existing studies have concluded that a large number of accelerometers are needed to identify the moving loads, and in comparison with strain measurements, they are more sensitive to sampling frequencies (Law, S. S. & Zhu 2011; Zhu, XQ & Law 2001a, 2001b). From the results, it can be seen that the number of accelerometers installed on this bridge is insufficient and installing a few more strain gauges is suggested here. On this bridge, only one strain gauge is installed under the girder and on the longitudinal direction, which is enough for quantifying the static load but not the dynamic one.

Although in numerical studies, a limited number of accelerometers are providing promising results, an experimental study is different and includes uncertainties that are not considered in numerical studies. This is the reason why experimental verification is of high importance and value.

Negotiations are underway to install more strain gauges for further studies, however, considering high expenses associated with sensors, their installation equipment, traffic management, and safety issues, more studies should be carried out to decide the number and location of the sensors before installation.

7.9. Conclusion

The proposed technique for moving load identification has been verified by a field study. A 46 m long cable-stayed bridge located near the intersection of Second Avenue at Western Sydney University Werrington Campus and the Great Western Highway in Werrington, NSW (33°45'50.49"S, 150°44'31.14"E), was chosen as the field full-scaled bridge. This bridge was fitted with accelerometers, strain-gauges, a temperature sensor, and optical sensors. The finite element model of the bridge was created using ANSYS and MATLAB, and calibrated with the experimental model. The car type was a Mazda 3 (Sedan-Maxx Sport) and it was driven at a constant speed of 42 km/h. The static load of the car has been identified very well, however, to identify dynamic parts of the moving loads more sensors are needed to be installed, which is currently under negotiation.

Chapter 8. Conclusions and recommendations

8.1. Conclusions

Condition assessment of bridge structures based on vibration measurements has attracted increasing interest among researchers over the past two decades. In this research program, condition assessment of the bridge structures under moving vehicles has been investigated. A bridge under a moving vehicle is subjected to a type of ambient forced vibration which can be used for assessment, with no need for traffic interruption and extensive experimental arrangements. The dynamic interaction force between vehicles and road surface is a type of external excitations that can be intensified by structural damage, road surface roughness and vehicle speed, and can degrade bridge structures. Therefore, it is of high importance to simultaneously identify moving loads and structural damage while considering road surface roughness. Although there have been extensive attempts to identify moving loads with known structural parameters or detect structural parameters while knowing moving loads, simultaneous identification has not been studied extensively thoroughly.

Most successful studies of simultaneous identification of damage and moving loads, which consider a moving vehicle as an excitation source, have not experimentally studied for the effects of noise and road roughness. Therefore, in this research work, simultaneous identification of moving load and structural damage considering a four-degree-of-freedom model for a moving vehicle was carried out. The effects of uncertainties such as measurement noise, road surface roughness, and the vehicle speed was investigated and the proposed technique was verified both numerically and experimentally. To do simultaneous identification of moving load and structural damage, firstly the identification of moving loads based on the explicit form of the Newmark-β method was proposed and verified, while moving load identification in existing studies is commonly formulated in state space.

For small structures, simultaneous identification of moving loads and structural parameters with the finite element model of the whole structure is reasonable, however, the situation is completely different when it comes to large and complex structures. The identification of structural damage is an inverse and ill-posed problem by nature. When dealing with large and complex structures, accuracy and convergence will become issues to address and the efficiency of the method will be degraded. More response measurements are needed which means more labour, installation difficulties, and expenses. As the number of unknowns increase, this problem will become more challenging. To address this problem, the substructure condition assessment was proposed.

Utilizing the substructure condition assessment technique, the bridge model was split into many substructures. Substructures which are more vulnerable to damage or are of more importance can be chosen as target substructures. A substructure has a considerably smaller number of DOFs in comparison with the whole structure and the number of unknown parameters is also reduced. However, substructures are not isolated from the remaining structure and the interface forces between substructures have to be applied as dynamic forces to substructures.

There are some substructure damage detection approaches which require interface response measurements; however, it is sometimes impossible to measure the interface responses especially when it comes to rotational reactions. Furthermore, domain methods that are commonly developed and verified for structures under non-moving loads, are either sensitive to noise, or lack experimental verification. Furthermore, substructure condition assessment of bridges under moving vehicles considering uncertainties such as road surface roughness and vehicle speed needs more investigation.

In this thesis, moving load identification was formulated by the explicit form of the Newmark-β method and damage identification was conducted based on the identified loads, either for a full structure or for a substructure condition assessment. In this method, strain and acceleration measurements are used as inputs. There is no need for complete measurements at interface nodes as well as no need for interface force measurements. The moving vehicle is unknown and only the location and speed of the vehicle is needed to be known in advance. This project is believed to be among the few studies on condition assessment of bridge structures under moving vehicles considering uncertainties such as noise, vehicle speed, and road surface roughness with numerical and experimental verifications.

The main achievements of this thesis are summarized as follows:

1. **Moving load identification based on the explicit form of the Newmark-β method considering road roughness**

The moving load identification technique is proposed based on the explicit form of the Newmark-β method, taking into account road roughness. Response measurements were simulated by dynamic forward analysis of the vehicle-bridge interaction system. The general form of the explicit form of the Newmark-β method was generated for this purpose. The half-car model vehicle, with four degrees of freedom, was adopted in this study and the Generalized Tikhonov Regularization method was employed to provide bounds on the solution.

Results show that the method is not sensitive to sensor placement and a good accuracy can be achieved using three accelerometers. When there is not measurement noise, the proposed method is not sensitive to noise, speed, and road roughness, however, when there is measurement noise, the identification accuracy is reduced at road roughness levels “B” and “C”. There is not any constraint to identify moving loads when the road surface level is “A”.

The proposed method is able to identify moving loads without disruptions when passing through the supports which is a significant improvement in moving load identification. Also, it is reliable in estimating the static load of a moving vehicle.

2. Simultaneous identification of structural damage and moving loads

A technique was proposed based on the explicit form of the Newmark-β method to identify moving loads and structural damage, simultaneously. The Generalized Tikhonov regularization technique was used to solve the ill-posed problem and the GCV method was used to find the optimal parameter λ. The method was verified by a single-span simply supported beam and a two-span continuous beam. The effects of damage location, sensor placements, measurement noise, vehicle speeds, and road surface roughness, on the accuracy of the method are investigated. Acceleration responses were reconstructed by inputting the identified moving loads and structural parameters in the equation of motion of the bridge to check the accuracy of the method.

Results indicate that the method is able to detect all levels of damage with at least three sensors, and it is not sensitive to the location of the sensors. The number and location of the sensors can be determined based on the accessibility of the locations, client budget and time. Moving loads and damages can be identified at different speed and roughness levels, and higher accuracy is achieved when speed is higher than 15 m/s, which might be because of stronger excitations. Measurement noise level more than 5% can affect the results and reduce the accuracy of damage detection. At 10% noise, there are many false positives and negatives at other intact elements.

3. Substructure condition assessment of bridge structure subject to moving loads

A substructure condition assessment of bridge structures under moving vehicles based on the explicit form of the Newmark-β method was proposed. Two different scenarios were studied: Scenario A and Scenario B. In Scenario A, the finite element model of the whole structure is known and in Scenario B only the finite element model of the substructure is known. The effects of the boundary conditions, sensor placements, vehicle speed, road surface

roughness, and measurement noise on the accuracy of these two scenarios have been studied and conclusions are listed as follows:

- For Scenario A, good accuracy of damage detection can be achieved with 4 sensors.
- For scenario B, the boundary condition of the target substructure can affect the accuracy of damage detection. When the boundary condition is free-free, it needs at least 6 sensors, however, when one end of the boundary condition is known, good results can be achieved even with 4 sensors.
- Scenario A is not sensitive to discretization, but Scenario B is. With proper discretization, Scenario B can provide very promising results.
- Both Scenarios A and B are reliable at different ranges of speed.
- Scenario B can be used at different levels of road roughness. It is not recommended to use Scenario A at road roughness level C.
- Scenario A is reliable to be used at measurement noise less than 3%, however, Scenario B is affected by even 1% measurement noise.

4. Experimental studies in the laboratory

Tests were carried out in the laboratory to verify the proposed techniques. A three-metre-long steel simply supported bridge beam was designed in the structural laboratory and a vehicle model was pulled by an electrical motor along the bridge at a constant speed. Modal tests were conducted before damage and after damage to obtain the natural frequencies and perform finite element model updating by minimizing the difference between experimental natural frequencies and numerical ones. Two instances of local damage have been induced in two stages which are different in location and extent.

According to the experimental results, the proposed method is reliable to identify moving loads reasonably at different speed levels and sampling frequencies, whether the moving loads are being identified alone for an intact structure or it is being identified simultaneously with structural parameters. However, when it comes to detect and quantify damaged elements through the simultaneous identification of moving loads and structural parameters, it can be seen that the false positives/ negatives are identified for intact elements and there are very large positives at boundary elements, resulting from the modelling errors of the boundary conditions. As it was concluded by the numerical studies, the accuracy of the method is not changed at different levels of the speed and damage.

Experimental results indicated that the substructural technique- Scenario A for condition assessment provides more accurate results in comparison with the technique for simultaneous identification of moving loads and structural parameters, while reducing computation time significantly. This technique was able to detect the damaged element and the extension of damage very close to the true value in all cases of studies, however, there was a large false positive in the boundary element close to the support, in all cases of studies. As it was concluded in the numerical study, the methods accuracy at different speed and damage levels are same.

Experimental results indicated that the substructural technique- Scenario B for condition assessment is not sensitive to vehicle speed, however, the accuracy of the identified damage is affected by the chosen response time history and its duration. Since, the sensitivity of the internal forces is considered zero, it is better to choose shorter duration from the first moments of the vehicle move. Considering the effect of the internal force sensitivity is recommended for future studies. Same as Scenario A, there are big false positives at the boundary elements, however, the structural stiffness of other elements can be properly identified. The computation time in Scenario B was greater than Scenario A, and it was significantly less than the case the FEM of the whole structure was used in the condition assessment of the structure.

5. Experimental studies in the field

The proposed technique for moving load identification was verified by a field study. A 46 m long cable-stayed bridge located near the intersection of Second Avenue at Western Sydney University Werrington Campus and the Great Western Highway in Werrington, NSW (33°45'50.49"S, 150°44'31.14"E), was chosen as the field full-scaled bridge. Accelerometers, strain gauges, temperature and optical sensors have all been installed on the bridge. The finite element model of the bridge was created using ANSYS and MATLAB, and calibrated with the experimental model. The car type was Mazda 3 (Sedan-Maxx Sport) and it was driven at constant speed of 42 km/h. The static load of the car has been precisely identified, however, to identify dynamic aspects of the moving loads, more sensors were needed to be installed which can be addressed in future research.

8.2. Recommendations for future studies

Numerical and experimental studies were carried out to explore the efficiency of the proposed techniques for moving load identification as well as full-structure and substructure

condition assessment of bridge structures subject to moving loads. The following recommendations are proposed for consideration in any future studies:

1. It was noted that sensor placement may affect the accuracy of the proposed damage detection techniques which should be further examined. Optimal selection can be considered in future studies.
2. Experimental studies in the laboratory were carried out on a 3 m bridge beam subjected to a moving vehicle. The target substructure studied in this thesis has a free-pinned geometrical boundary condition which includes the support. A modelling error associated with the boundary condition affected the damage detection results in some cases. A longer bridge beam is suggested to be employed in order to conduct studies on a longer target substructure with free-free geometrical boundary condition as well as investigating the effect of sampling duration, and sensor placement on accuracy of the proposed technique.
3. It may be beneficial to study the effect of the sensitivity of external loads to damage in calculating response sensitivities when the bridge is subjected to moving loads.
4. Experimental studies in the laboratory were carried out on a bridge beam. Further research is required to be conducted on a plate-like beam element.
5. The data obtained from the field testing of a 45 m long cable-stayed bridge was used to check the accuracy of the method for moving load identification. It is concluded that more sensors are necessary to improve the accuracy. The proposed techniques can be further verified by more field tests.

References

Abbasnia, R, Mirzaee, A & Shayanfar, M 2015, 'Simultaneous identification of moving loads and structural damage by adjoint variable', *Structural Engineering and Mechanics*, vol. 56, no. 5, pp. 871-97, viewed 01/03/2020.

Agostinacchio, M, Ciampa, D & Olita, S 2014, 'The vibrations induced by surface irregularities in road pavements – a Matlab® approach', *European Transport Research Review*, vol. 6, no. 3, pp. 267-75, viewed 01/03/2020, DOI 10.1007/s12544-013-0127-8.

Alamdari, MM, Ge, L, Kildashti, K, Zhou, Y, Harvey, B & Du, Z 2019, 'Non-contact structural health monitoring of a cable-stayed bridge: case study', *Structure and Infrastructure Engineering*, vol. 15, no. 8, pp. 1119-36, viewed 01/03/2020, DOI 10.1080/15732479.2019.1609529.

American Society of Civil Engineers 2017, *Report Card for American Infrastructure*, viewed 01/03/2020.

Asnachinda, P, Pinkaew, T & Laman, JA 2008, 'Multiple vehicle axle load identification from continuous bridge bending moment response', *Engineering Structures*, vol. 30, no. 10, pp. 2800-17, viewed 01/03/2020, DOI 10.1016/j.engstruct.2008.02.018.

Aster, RC, Borchers, B & Thurber, CH 2005, '5 Tikhonov regularization', in RC Aster, B Borchers & CH Thurber (eds), *International Geophysics*, vol. 90, Academic Press, pp. 89-118.

Brownjohn, JMW 2007, 'Structural health monitoring of civil infrastructure', *Philos. Trans. R. Soc. London, Ser. A*, vol. 365, p. 589, viewed 01/03/2020.

Bu, JQ, Law, SS & Zhu, XQ 2006, 'Innovative Bridge Condition Assessment from Dynamic Response of a Passing Vehicle', *Journal of Engineering Mechanics*, vol. 132, no. 12, pp. 1372-9, viewed 01/03/2020, DOI 10.1061/(ASCE)0733-9399(2006)132:12(1372).

Carden, EP & Fanning, P 2004, 'Vibration based condition monitoring: A review', *Struct. Health Monit.*, vol. 3, p. 355, viewed 01/03/2020.

Catbas, F, Zaurin, R, Gul, M & Gokce, H 2012, 'Sensor Networks, Computer Imaging, and Unit Influence Lines for Structural Health Monitoring: Case Study for Bridge Load Rating', *Journal of bridge engineering.*, vol. 17, no. 4, viewed 01/03/2020, rg.

Cawley, P & Adams, R 1979, 'The Location of Defects in Structures From Measurements of Natural Frequencies', *Journal of Strain Analysis for Engineering Design - J STRAIN ANAL ENG DESIGN*, vol. 14, pp. 49-57, viewed 01/03/2020, DOI 10.1243/03093247V142049.

Chan, CS, Yang, YB, Chen, WF & Yu, HW 2013, 'Experimental study of a hand-drawn cart for measuring the bridge frequencies', *Engineering Structures*, vol. 57, viewed 01/03/2020.

Chan, THT, Law, SS & Yung, TH 2000, 'Moving force identification using an existing prestressed concrete bridge', *Engineering Structures*, vol. 22, no. 10, pp. 1261-70, viewed 01/03/2020, DOI 10.1016/S0141-0296(99)00084-X.

Chan, THT, Yu, L & Law, SS 2000, 'COMPARATIVE STUDIES ON MOVING FORCE IDENTIFICATION FROM BRIDGE STRAINS IN LABORATORY', *Journal of Sound and Vibration*, vol. 235, no. 1, pp. 87-104, viewed 01/03/2020, DOI 10.1006/jsvi.2000.2909.

Chan, THT, Yu, L, Law, SS & Yung, TH 2001, 'MOVING FORCE IDENTIFICATION STUDIES, II: COMPARATIVE STUDIES', *Journal of Sound and Vibration*, vol. 247, no. 1, pp. 77-95, viewed 01/03/2020, DOI 10.1006/jsvi.2001.3629.

Chen, GW, Beskhyroun, S & Omenzetter, P 2014, 'Ambient and forced vibration testing of an eleven-span motorway off-ramp bridge', viewed 01/03/2020.

Chen, S, Xia, H & Zhang, J 2007, 'Review on bridge structural damage identification techniques based on bridge-vehicle coupled vibration analysis', *China Safety Science Journal*, vol. 17, no. 8, pp. 148-55, viewed 01/03/2020.

Chen, Y, Feng, MQ & Tan, C-A 2009, 'Bridge Structural Condition Assessment Based on Vibration and Traffic Monitoring', *Journal of Engineering Mechanics*, vol. 135, no. 8, pp. 747-58, viewed 01/03/2020, DOI 10.1061/(ASCE)0733-9399(2009)135:8(747).

Chen, Y, Tan, C-A, Feng, MQ & Fukuda, Y 2006b, 'A video assisted approach for structural health monitoring of highway bridges under normal traffic', vol. 6174, pp. 61741V-V-18, viewed 01/03/2020.

Chen, Z, Zhu, S, Xu, Y-L, Li, Q & Cai, Q-L 2015, 'Damage Detection in Long Suspension Bridges Using Stress Influence Lines', *Journal of Bridge Engineering*, vol. 20, no. 3, viewed 01/03/2020, DOI 10.1061/(ASCE)BE.1943-5592.0000681.

Curadelli, RO, Riera, JD, Ambrosini, D & Amani, MG 2008, 'damage detection by means of structural damping identification', *Engineering Structures*, vol. 30, no. 12, pp. 3497-504, viewed 01/03/2020.

Daniel, Ľ & Kortiš, J 2017, 'The Comparison of Different Approaches to Model Vehicle-Bridge Interaction', *Procedia Engineering*, vol. 190, pp. 504-9, viewed 01/03/2020, DOI 10.1016/j.proeng.2017.05.370.

Deng, L & Cai, CS 2010, 'Identification of Dynamic Vehicular Axle Loads: Demonstration by a Field Study', *Journal of Vibration and Control*, vol. 17, no. 2, pp. 183-95, viewed 01/03/2020, DOI 10.1177/1077546309351222.

Deng, L & Cai, CS 2011, 'Identification of Dynamic Vehicular Axle Loads: Demonstration by a Field Study', *Journal of Vibration and Control*, vol. 17, no. 2, pp. 183-95, viewed 01/03/2020, DOI 10.1177/1077546309351222.

DeVore, CE 2013, *Damage detection using substructure identification*, ProQuest LLC, University of Southern California, viewed 01/03/2020.

Doebling, SW, Farrar, CR & Prime, MB 1998, 'A summary review of vibration-based damage identification methods', *Shock Vib. Dig.*, vol. 30, p. 91, viewed 01/03/2020.

Doebling, SW, Farrar, CR, Prime, MB & Shevitz, DW 1996, *Damage identification and health monitoring of structural and mechanical systems from changes in their vibration characteristics: A literature review*, LA--13070-MS; Other: ON: DE96012168; TRN: 96:003834 United States 10.2172/249299 Other: ON: DE96012168; TRN: 96:003834 OSTI as DE96012168 LANL English, ; Los Alamos National Lab., NM (United States), viewed 01/03/2020.

Engineers Australia 2010, *Engineers Australia Report Card*, viewed 01/03/2020.

Fan, W & Qiao, P 2011, 'Vibration-based damage identification methods: A review and comparative study', *Struct. Health Monit.*, vol. 10, p. 83, viewed 01/03/2020.

Farrar, CR, Cornwell, PJ, Doebling, SW & Prime, MB 2000, 'Structural Health Monitoring Studies of the Alamosa Canyon and I-40 Bridges', Los Alamos Laboratory viewed 01/03/2020.

Farrar, CR, Duffey, T, Cornwell, PJ & Doebling, SW 1999, 'Excitation methods for bridge structures', viewed 01/03/2020.

Feng, D, Sun, H & Feng, MQ 2015, 'Simultaneous identification of bridge structural parameters and vehicle loads', *Computers & Structures*, vol. 157, pp. 76-88, viewed 01/03/2020, DOI 10.1016/j.compstruc.2015.05.017.

Ferdek, U & Łuczko, J 2016, *Vibration analysis of a half-car model with semi-active damping*, vol. 54.

Fraser, M, Elgamal, A, He, X & Conte, JP 2010, 'Sensor Network for Structural Health Monitoring of a Highway Bridge', *Journal of Computing in Civil Engineering*, vol. 24, no. 1, pp. 11-24, viewed 01/03/2020, DOI 10.1061/(ASCE)CP.1943-5487.0000005.

Gökdağ, H 2013, 'A Crack Identification Approach for Beam-Like Structures under Moving Vehicle using Particle Swarm Optimization', *Materials Testing*, vol. 55, no. 2, pp. 114-20, viewed 01/03/2020.

Golub, GH, Heath, M & Wahba, G 1979, 'Generalized Cross-Validation as a Method for Choosing a Good Ridge Parameter', *Technometrics*, vol. 21, no. 2, pp. 215-23, viewed 01/03/2020, DOI 10.2307/1268518.

Gonz, aacute, lez, A, Dowling, J, rsquo, Brien, E et al. 2012, 'Testing of a Bridge Weigh-in-Motion Algorithm Utilising Multiple Longitudinal Sensor Locations', *Journal of Testing and Evaluation*, vol. 40, no. 6, pp. 961-74, viewed 01/03/2020, DOI 10.1520/JTE104576.

González, A & Hester, D 2013, 'An investigation into the acceleration response of a damaged beam-type structure to a moving force', *Journal of Sound and Vibration*, vol. 332, no. 13, pp. 3201-17, viewed 01/03/2020, DOI 10.1016/j.jsv.2013.01.024.

Gonzalez, A, Obrien, EJ & Mcgetrick, PJ 2012, 'Identification of damping in a bridge using a moving instrumented vehicle', *Journal of Sound and Vibration*, vol. 331, no. 18, pp. 4115-31, viewed 01/03/2020.

González, A, Rowley, C & OBrien, EJ 2008, 'A general solution to the identification of moving vehicle forces on a bridge', *International Journal for Numerical Methods in Engineering*, vol. 75, no. 3, pp. 335-54, viewed 01/03/2020, DOI 10.1002/nme.2262.

Green, M 1995, 'Modal tests methods for bridges: a review', viewed 01/03/2020.

Hancen, PC 2008, *Regularization Tools, A Matlab PAckage for Analysis and Solution of Discrete Ill-Posed Problems*, viewed 01/03/2020.

He, W-Y, Ren, W-X & Zhu, S 2017, 'Baseline-free damage localization method for statically determinate beam structures using dual-type response induced by quasi-static moving load', *Journal of Sound and Vibration*, vol. 400, pp. 58-70, viewed 01/03/2020.

Hester, D & González, A 2012, 'A wavelet-based damage detection algorithm based on bridge acceleration response to a vehicle', *Mechanical Systems and Signal Processing*, vol. 28, pp. 145-66, viewed 01/03/2020, DOI 10.1016/j.ymssp.2011.06.007.

Hoshiya, M & Maruyama, O 1987, 'Identification of Running Load and Beam System', *Journal of Engineering Mechanics*, vol. 113, no. 6, pp. 813-24, viewed 01/03/2020, DOI 10.1061/(ASCE)0733-9399(1987)113:6(813).

Jayalakshmi, V & Rao, AR 2017, 'Simultaneous identification of damage and input dynamic force on the structure for structural health monitoring', *Struct. Multidiscip. Optim.*, vol. 55, no. 6, pp. 2211-38, viewed 01/03/2020, DOI 10.1007/s00158-016-1637-5.

Jie, L & Jun, C 2003, 'A statistical average algorithm for the dynamic compound inverse problem', *Computational Mechanics*, vol. 30, no. 2, pp. 88-95, DOI 10.1007/s00466-002-0369-0.

Kim, C-W & Kawatani, M 2008, 'Pseudo-static approach for damage identification of bridges based on coupling vibration with a moving vehicle', *Structure and Infrastructure Engineering*, vol. 4, no. 5, pp. 371-9, viewed 01/03/2020, DOI 10.1080/15732470701270082.

Kim, CW, Isemoto, R, Mcgetrick, PJ, Kawatani, M & Obrien, EJ 2014, 'Drive-by bridge inspection from three different approaches', *Smart Structures and Systems*, vol. 13, no. 5, pp. 775-96, viewed 01/03/2020.

Kobayashi, Y, Sugiura, K, Yamaguchi, T & Oshima, Y 2008, 'Eigenfrequency estimation for bridges using the response of a passing vehicle with excitation system', in *Bridge Maintenance, Safety Management, Health Monitoring and Informatics - IABMAS '08*, 0 vols, Taylor & Francis.

Koh, CG, Hong, B & Liaw, CY 2003, 'Substructural and progressive structural identification methods', *Engineering Structures*, vol. 25, no. 12, pp. 1551-63, viewed 01/03/2020, DOI 10.1016/S0141-0296(03)00122-6.

Koh, CG, See, LM & Balendra, T 1991, 'Estimation of structural parameters in time domain: A substructure approach', *Earthquake Engineering & Structural Dynamics*, vol. 20, no. 8, pp. 787-801, viewed 01/03/2020, DOI 10.1002/eqe.4290200806.

Koh, CG & Shankar, k 2003, 'Substructural identification method without interface measurement', *Journal of Engineering Mechanics*, vol. 129, no. 7, pp. 769-76, viewed 01/03/2020.

Kong, X, Cai, CS & Kong, B 2015, 'Damage Detection Based on Transmissibility of a Vehicle and Bridge Coupled System', *Journal of Engineering Mechanics*, vol. 141, no. 1, viewed 01/03/2020, DOI 10.1061/(ASCE)EM.1943-7889.0000821.

Kun, L, Law, S & Zhu, X 2015, 'Substructural Condition Assessment Based on Force Identification and Interface Force Sensitivity', *International Journal of Structural Stability and Dynamics*, vol. 15, p. 1450046, viewed 01/03/2020, DOI 10.1142/S0219455414500461.

Law, S, Pinghe, N & Li, J 2014, 'Parallel Decentralized Damage Detection of a Structure with Subsets of Parameters', *AIAA Journal*, vol. 52, viewed 01/03/2020, DOI 10.2514/1.J051716.

Law, SS, Bu, JQ, Zhu, XQ & Chan, SL 2004, 'Vehicle axle loads identification using finite element method', *Engineering Structures*, vol. 26, no. 8, pp. 1143-53, viewed 01/03/2020, DOI 10.1016/j.engstruct.2004.03.017.

Law, SS, Chang, THT, Zhu, QX & Zeng, QH 2001, 'Regularization in moving force identification', *J. Eng. Mech.*, vol. 127, p. 136, viewed 01/03/2020.

Law, SS & Fang, YL 2001, 'MOVING FORCE IDENTIFICATION: OPTIMAL STATE ESTIMATION APPROACH', *Journal of Sound and Vibration*, vol. 239, no. 2, pp. 233-54, viewed 01/03/2020, DOI 10.1006/jsvi.2000.3118.

Law, SS & Li, J 2010, 'Updating the reliability of a concrete bridge structure based on condition assessment with uncertainties', *Engineering Structures*, vol. 32, no. 1, pp. 286-96, viewed 01/03/2020.

Law, SS & Yong, D 2011, 'Substructure methods for structural condition assessment', *Journal of Sound and Vibration*, vol. 330, no. 15, pp. 3606-19, viewed 01/03/2020, DOI 10.1016/j.jsv.2011.03.003.

Law, SS, Zhang, K & Duan, ZD 2010, 'Structural damage detection from coupling forces between substructures under support excitation', *Engineering Structures*, vol. 32, no. 8, pp. 2221-8, viewed 01/03/2020, DOI 10.1016/j.engstruct.2010.03.024.

Law, SS & Zhu, XQ 2009, *Damage models and algorithms for assessment of structures under operating conditions*, CRC Press, Taylor & Francis Group
UK.

Law, SS & Zhu, XQ 2011, 'Moving loads- Dynamic analysis and and identification techniques', Taylor and Francis, London

Lee, JW, Kim, JD, Yun, CB, Yi, JH & Shim, JM 2002, 'Health-Monitoring Method For Bridges Under Ordinary Traffic Loadings ', *Journal of Sound and Vibration*, vol. 257, no. 2, pp. 247-64, viewed 01/03/2020, DOI 10.1006/jsvi.2002.5056.

Li, J & Hao, H 2014, 'Substructure damage identification based on wavelet-domain response reconstruction', *Structural Health Monitoring*, vol. 13, no. 4, pp. 389-405, viewed 01/03/2020, DOI 10.1177/1475921714532991.

Li, J, Hao, H & Lo, JV 2015, ' Structural damage identification with power spectral density transmissibility: Numerical and experimental studies. ', *Smart Structures and Systems*, vol. 15, no. 1, pp. 15-40, viewed 01/03/2020.

Li, J & Law, SS 2012a, 'Damage identification of a target substructure with moving load excitation', *Mechanical Systems and Signal Processing*, vol. 30, pp. 78-90, viewed 01/03/2020, DOI 10.1016/j.ymssp.2012.02.002.

Li, J & Law, SS 2012b, 'Substructural damage detection with incomplete information of the structure', *Journal of Applied Mechanics*, vol. 79, no. 4, p. 10 pages, viewed 01/03/2020.

Li, J, Law, SS & Ding, Y 2012, 'Substructure damage identification based on response reconstruction in frequency domain and model updating', *Engineering Structures*, vol. 41, pp. 270-84, viewed 01/03/2020, DOI 10.1016/j.engstruct.2012.03.035.

Li, J & Zhao, X 2006, 'A super-element approach for structural identification in time domain', *Frontiers of Mechanical Engineering in China*, vol. 1, no. 2, pp. 215-21, viewed 01/03/2020.

Li, ZH & Au, FTK 2014a, 'Damage detection of a continuous bridge from response of a moving vehicle', *Shock and Vibration*, vol. 2014, p. 7, viewed 01/03/2020.

Li, ZH & Au, FTK 2014b, 'Damage detection of bridges using response of vehice considering road surface roughness', *International Journal of Structural Stability and Dynamics*, vol. 2015, p. 7, viewed 01/03/2020.

Lim, TW 1991, 'Structural damage detection using modal test data', *AIAA Journal*, vol. 29, no. 12, pp. 2271-4, viewed 01/03/2020, DOI 10.2514/3.10873.

Lin, CW & Yang, YB 2005, 'Use of a passing vehicle to scan the fundamental bridge frequencies: An experimental verification', *Engineering Structures*, vol. 27, no. 13, viewed 01/03/2020.

Link, M & Weiland, M 2009, 'Damage identification by multi-model updating in the modal and in the time domain', *Mechanical Systems and Signal Processing*, vol. 23, no. 6, pp. 1734-46, viewed 01/03/2020, DOI 10.1016/j.ymssp.2008.11.009.

Liu, K, Law, SS, Zhu, XQ & Xia, Y 2014, 'Explicit form of an implicit method for inverse force identification', *Journal of Sound and Vibration*, vol. 333, no. 3, pp. 730-44, viewed 01/03/2020, DOI 10.1016/j.jsv.2013.09.040.

Lombaert, G & Conte Joel, P 2012, 'Random Vibration Analysis of Dynamic Vehicle-Bridge Interaction Due to Road Unevenness', *Journal of Engineering Mechanics*, vol. 138, no. 7, pp. 816-25, viewed 01/03/2020, DOI 10.1061/(ASCE)EM.1943-7889.0000386.

Lu, ZR & Law, SS 2007, 'Identification of system parameters and input force from output only', *Mechanical Systems and Signal Processing*, vol. 21, no. 5, pp. 2099-111, viewed 01/03/2020, DOI 10.1016/j.ymssp.2006.11.004.

Lu, ZR, Liu, JK, Huang, M & Xu, WH 2009, 'Identification of local damages in coupled beam systems from measured dynamic responses', *Journal of Sound and Vibration*, vol. 326, no. 1-2, viewed 01/03/2020.

Maia, NMM, Silva, JMM & Ribeiro, AMR 2001, 'THE TRANSMISSIBILITY CONCEPT IN MULTI-DEGREE-OF-FREEDOM SYSTEMS', *Mechanical Systems and Signal Processing*, vol. 15, no. 1, pp. 129-37, viewed 01/03/2020, DOI 10.1006/mssp.2000.1356.

Majumder, L & Manohar, C 2003, 'A time-domain approach for damage detection in beam structures using vibration data with a moving oscillator as an excitation source', *Journal of Sound and Vibration*, vol. 268, no. 4, pp. 699-716, viewed 01/03/2020.

Malekjafarian, A, McGetrick, PJ & OBrien, EJ 2015, 'A Review of Indirect Bridge Monitoring Using Passing Vehicles', *Shock and Vibration*, vol. 2015, p. 16, viewed 01/03/2020, DOI 10.1155/2015/286139.

Malekjafarian, A & Obrien, EJ 2014, 'Identification of bridge mode shapes using short time frequency domainn decomoposition of the responses measured in a passing vehicle', *Engineering Structures*, vol. 81, no. 386-397, viewed 01/03/2020.

Mazurek, DF & Dewolf, JT 1990, 'Experimental study of bridge monitoring techniques', *J. Struct. Eng.*, vol. 116, p. 2532, viewed 01/03/2020.

McGetrick, P, Kim, CW & Obrien, EJ 2010, 'Experimental investigation of the detection of bridge dynamic parameters using a moving vehicle', viewed 01/03/2020.

McGetrick, PJ & Kim, CW 2013, 'A parametric study of a drive by bridge inspection system based on the Morlet wavelet', *Key Engineering Materials*, vol. 569-570, pp. 262-9, viewed 01/03/2020.

McGetrick, PJ & Kim, CW 2014, 'An indirect bridge inspection method incorporating a wavelet-based damage indicator and pattern recognition', viewed 01/03/2020.

Miyamoto, A & Yabe, A 2011, 'Bridge Condition Assessment based on Vibration Responses of Passenger Vehicle', *Journal of Physics: Conference Series*, vol. 305, no. 1, p. 012103, viewed 01/03/2020.

Miyamoto, A & Yabe, A 2012, 'Development of practical health monitoring system for short and medium- span bridges based on vibration responses of city bus', *Journal of Civil Structural Health Monitoring*, vol. 2, no. 1, pp. 47-63, viewed 01/03/2020.

Modena, C, Sonda, D & Zonta, D 1999, 'damage localization in reinforced concrete structures by using damping measurements', *Key Engineering Materials*, vol. 167, no. 1, pp. 132-41, viewed 01/03/2020.

Múčka, P 2018, *Simulated Road Profiles According to ISO 8608 in Vibration Analysis*, vol. 46.

Mulcahy, NL 1983, 'Bridge response with tractor-trailer vehicle loading', vol. 11, no. 5, pp. 649-65, viewed 01/03/2020, DOI 10.1002/eqe.4290110505.

Narkis, Y 1994, 'Identification of Crack Location in Vibrating Simply Supported Beams', *Journal of Sound and Vibration*, vol. 172, no. 4, pp. 549-58, viewed 01/03/2020, DOI 10.1006/jsvi.1994.1195.

Nasrellah, HA & Manohar, CS 2010, 'A particle filtering approach for structural system identification in vehicle-structure interaction problems', *Journal of Sound and Vibration*, vol. 329, no. 9, pp. 1289-309, viewed 01/03/2020.

Nguyen, KV & Tran, HT 2010, 'Multi-cracks detectio of a beam-like structure based on the on-vehicle vibration signal and wavelet analysis', *Journal of Sound and Vibration*, vol. 329, no. 21, pp. 4455-65, viewed 01/03/2020.

Obrien, E, Carey, C & Keenahan, J 2015, 'Bridge damage detection using ambient traffic and moving force identification', *Structural Control and Health Monitoring*, vol. 22, no. 12, pp. 1396-407, viewed 01/03/2020, DOI 10.1002/stc.1749.

Ojio, T, Carey, C, Obrien, E, Doherty, C & Taylor, S 2015, 'Contactless Bridge Weigh-in-Motion', *Journal of Bridge Engineering*, vol. 21, viewed 01/03/2020, DOI 10.1061/(ASCE)BE.1943-5592.0000776.

Oliva, J, Goicolea, JM, Antolín, P & Astiz, MÁ 2013, 'Relevance of a complete road surface description in vehicle–bridge interaction dynamics', *Engineering Structures*, vol. 56, pp. 466-76, viewed 01/03/2020, DOI 10.1016/j.engstruct.2013.05.029.

Oshima, Y, Yamamoto, K & Sugiura, K 2014, 'Dammage assessment of a bridge based on mode shapes estimated by responses of passing vehicles', *Smart Structures and Systems*, vol. 13, no. 5, pp. 731-53, viewed 01/03/2020.

Ouyang, H 2011, 'Moving-load dynamic problems: A tutorial (with a brief overview)', *Mechanical Systems and Signal Processing*, vol. 25, no. 6, pp. 2039-60, viewed 01/03/2020, DOI 10.1016/j.ymssp.2010.12.010.

Pandey, AK & Biswas, M 1994, 'Damage detection in structures using changes in flexibility', *J. Sound Vib.*, vol. 169, p. 3, viewed 01/03/2020.

Pandey, AK, Biswas, M & Samman, MM 1991, 'Damage detection from changes in curvature mode shapes', *Journal of Sound and Vibration*, vol. 145, no. 2, pp. 321-32, viewed 01/03/2020, DOI 10.1016/0022-460X(91)90595-B.

Peeters, B, Maeck, J & De Roeck, G 2001, 'Vibration-based damage detection in civil engineering: excitation sources and temperature effects', *Smart Materials and Structures*, vol. 10, pp. 518-27, viewed 01/03/2020.

Peeters, B, Maeck, J & Roeck, GD 2001, 'Vibration-based damage detection in civil engineering: Excitation sources and temperature effects', *Smart Mater. Struct.*, vol. 10, p. 518, viewed 01/03/2020.

Piombo, BAD, Fasana, A, Marchesiello, S & Ruzzene, M 2000, 'Modelling and Identifiaction of the Dynamic Response of a Supported Bridge ', *Mechanical Systems and Signal Processing*, vol. 14, no. 1, pp. 75-89, viewed 01/03/2020, DOI 10.1006/mssp.1999.1266.

Ratcliffe, CP 1997, 'DAMAGE DETECTION USING A MODIFIED LAPLACIAN OPERATOR ON MODE SHAPE DATA', *Journal of Sound and Vibration*, vol. 204, no. 3, pp. 505-17, viewed 01/03/2020, DOI 10.1006/jsvi.1997.0961.

Rizos, PF, Aspragathos, N & Dimarogonas, AD 1990, 'Identification of crack location and magnitude in a cantilever beam from the vibration modes', *Journal of Sound and Vibration*, vol. 138, no. 3, pp. 381-8, viewed 01/03/2020, DOI 10.1016/0022-460X(90)90593-O.

Shimoi, N, Saijo, M, Cuadra, C & Madokoro, H 2015, 'Comparison of Natural Frequency Vibration Analysis for a Bridge Using Accelerometers and a Piezoelectric Cable Vibration Sensor', *International Journal of Instrumentation Science*, vol. 4, no. 1, pp. 1-9, viewed 01/03/2020, DOI 10.5923/j.instrument.20150401.01.

Siringoringo, DM & Fujino, Y 2012, 'Estimating bridge fundamental frequency from vibration response of instrumented passing vehicle: Analytical and experimental study', *Adv. Struct. Eng.*, vol. 15, p. 417, viewed 01/03/2020.

Sun, H & Betti, R 2014, 'Simultaneous identification of structural parameters and dynamic input with incomplete output-only measurements', *Structural Control and Health Monitoring*, vol. 21, no. 6, pp. 868-89, viewed 01/03/2020, DOI 10.1002/stc.1619.

Sun, Z, Zhang, Y & Tong, S 2013, *Review of bridge damage detection based on coupled vehicle-bridge vibration*, vol. 29.

Tee, KF, Koh, CG & Quek, ST 2009, 'Numerical and Experimental Studies of a Substructural Identification Strategy', *Structural Health Monitoring*, vol. 8, no. 5, pp. 397-410, viewed 01/03/2020, DOI 10.1177/1475921709102089.

Trinh, TN & Koh, CG 2012, 'An improved substructural identification strategy for large structural systems', *Structural Control and Health Monitoring*, vol. 19, no. 8, pp. 686-700, viewed 01/03/2020, DOI 10.1002/stc.463.

Wang, C, Du, C & Jiang, S 2018, 'Simultaneous identification of the load and unknown parameters of the structure based on the perturbation method', *Advances in Mechanical Engineering*, vol. 10, no. 10, p. 1687814018805664, viewed 01/03/2020, DOI 10.1177/1687814018805664.

Wang, H, Nagayama, T, Zhao, B & Su, D 2017, 'Identification of moving vehicle parameters using bridge responses and estimated bridge pavement roughness', *Engineering Structures*, vol. 153, pp. 57-70, viewed 01/03/2020, DOI 10.1016/j.engstruct.2017.10.006.

Wang, T, Wan, Z, Wang, X & Hu, Y 2015, 'A novel state space method for force identification based on the Galerkin weak formulation', *Computers & Structures*, vol. 157, pp. 132-41, viewed 01/03/2020, DOI 10.1016/j.compstruc.2015.05.015.

Womack, KC & Halling, MW 1999, *Forced vibration testing of the l-15 South Temple Bridge*, Federal Highway Administration, Utah Department of Transportation
Research and Development Division, viewed 01/03/2020.

Wu, D & Law, S 2004, 'Model error correction from truncated modal flexibility sensitivity and generic parameters: Part I - Simulation', *Mechanical Systems and Signal Processing - MECH SYST SIGNAL PROCESS*, vol. 18, pp. 1381-99, viewed 01/03/2020, DOI 10.1016/S0888-3270(03)00094-3.

Wu, SQ & Law, SS 2012, 'Statistical moving load identification including uncertainty', *Probabilistic Engineering Mechanics*, vol. 29, pp. 70-8, viewed 01/03/2020, DOI 10.1016/j.probengmech.2011.09.001.

Yabe, A, Miyamoto, A, Isoda, S & Tani, N 2013, 'Development of bridge monitoring system for short- and medium-span bridges based on bus vibration', *Journal of Japan Society of Civil Engineers, Series F4 (Construction and Management)*, vol. 69, no. 2, pp. 102-20, viewed 01/03/2020.

Yan, W-J & Ren, W-X 2012, 'Operational Modal Parameter Identification from Power Spectrum Density Transmissibility', *Computer-Aided Civil and Infrastructure Engineering*, vol. 27, no. 3, pp. 202-17, viewed 01/03/2020, DOI 10.1111/j.1467-8667.2011.00735.x.

Yang, YB, Chang, KC & Li, YC 2013, 'Filtering techniques for extracting bridge frequencies from a test vehicle moving over the bridge', *Engineering Structures*, vol. 48, pp. 353-62, viewed 01/03/2020.

Yang, YB & Chen, W-F 2016, 'Extraction of Bridge Frequencies from a Moving Test Vehicle by Stochastic Subspace Identification', *Journal of Bridge Engineering*, vol. 21, no. 3, viewed 01/03/2020, DOI 10.1061/(ASCE)BE.1943-5592.0000792.

Yang, YB, Li, YC & Chang, KC 2014, 'Constructing the mode shapes of a bridge from a passing vehicles: A theoretical study', *Int. J. Smart Struct. Syst.*, vol. 13, p. 797, viewed 01/03/2020.

Yang, YB, Lin, CW & Yau, JD 2004, 'Extracting bridge frequencies from the dynamic response of a passing vehicle', *J. Sound Vib.*, vol. 272, p. 471, viewed 01/03/2020.

Yu, L & Chan, THT 2003, 'Moving force identification based on the frequency–time domain method', *Journal of Sound and Vibration*, vol. 261, no. 2, pp. 329-49, viewed 01/03/2020, DOI 10.1016/S0022-460X(02)00991-4.

Yu, L & Chan, THT 2007, 'Recent research on identification of moving loads on bridges', *Journal of Sound and Vibration*, vol. 305, no. 1, pp. 3-21, viewed 01/03/2020, DOI 10.1016/j.jsv.2007.03.057.

Yun, C-B & Bahng, EY 2000, 'Substructural identification using neural networks', *Computers & Structures*, vol. 77, no. 1, pp. 41-52, viewed 01/03/2020, DOI 10.1016/S0045-7949(99)00199-6.

Yun, C-B & Lee, H-J 1997, 'Substructural identification for damage estimation of structures', *Structural Safety*, vol. 19, no. 1, pp. 121-40, viewed 01/03/2020, DOI 10.1016/S0167-4730(96)00040-9.

Zaurin, R & Catbas, FN 2011, 'Structural health monitoring using video stream, influence lines, and statistical analysis', *Structural Health Monitoring*, vol. 10, no. 3, pp. 309-32, viewed 01/03/2020, DOI 10.1177/1475921710373290.

Zhan, JW, Xia, H, Chen, SY & and De Roech, G 2011, 'Structural damage identification for railway bridges based on train-induced bridge responses and sensitivity analysis', *Journal of Sound and Vibration*, vol. 330, no. 4, pp. 757-70, viewed 01/03/2020.

Zhang, Q, Jankowski, #x141, ukasz & Duan, Z 2013, 'Simultaneous Identification of Moving Vehicles and Bridge Damages Considering Road Rough Surface', *Mathematical Problems in Engineering*, vol. 2013, p. 12, viewed 01/03/2020, DOI 10.1155/2013/963424.

Zhang, Q, Jankowski, Ł & Duan, Z 2010a, 'Identification of coexistent load and damage', *Structural and Multidisciplinary Optimization*, vol. 41, no. 2, pp. 243-53, viewed 01/03/2020, DOI 10.1007/s00158-009-0421-1.

Zhang, Q, Jankowski, Ł & Duan, Z 2010b, 'Simultaneous identification of moving masses and structural damage', *Structural and Multidisciplinary Optimization*, vol. 42, no. 6, pp. 907-22, viewed 01/03/2020, DOI 10.1007/s00158-010-0528-4.

Zhang, Q, Jankowski, Ł & Duan, Z 2012, 'Simultaneous identification of excitation time histories and parametrized structural damages', *Mechanical Systems and Signal Processing*, vol. 33, pp. 56-68, viewed 01/03/2020, DOI 10.1016/j.ymssp.2012.06.018.

Zhang, Y, Wang, LQ & Xiang, ZH 2012, 'Damage detection by mode shape squares extracted from a passing vehicle ', *Journal of Sound and Vibration*, vol. 331, no. 2, pp. 291-307, viewed 01/03/2020.

Zhu, H, Mao, L & Weng, S 2013, 'Calculation of Dynamic Response Sensitivity to Substructural Damage Identification under Moving Load', *Advances in Structural Engineering*, vol. 16, no. 9, pp. 1621-31, viewed 01/03/2020, DOI 10.1260/1369-4332.16.9.1621.

Zhu, X, Cao, M, Ostachowicz, W & Xu, W 2019, 'Damage Identification in Bridges by Processing Dynamic Responses to Moving Loads: Features and Evaluation', *Sensors*, vol. 19, p. 463, viewed 01/03/2020, DOI 10.3390/s19030463.

Zhu, X & Law, S 2007, *Damage Detection in Simply Supported Concrete Bridge Structure Under Moving Vehicular Loads*, vol. 129.

Zhu, XQ & Law, SS 2001a, 'Identification of moving loads on an orthotropic plate', *Journal of Vibration and Acoustics*, vol. 123, no. 2, pp. 238-44, viewed 01/03/2020.

Zhu, XQ & Law, SS 2001b, 'ORTHOGONAL FUNCTION IN MOVING LOADS IDENTIFICATION ON A MULTI-SPAN BRIDGE', *Journal of Sound and Vibration*, vol. 245, no. 2, pp. 329-45, viewed 01/03/2020, DOI 10.1006/jsvi.2001.3577.

Zhu, XQ & Law, SS 2002, 'Moving Loads Identification Through Regularization', *Journal of Engineering Mechanics*, vol. 128, no. 9, pp. 989-1000, viewed 01/03/2020, DOI 10.1061/(ASCE)0733-9399(2002)128:9(989).

Zhu, XQ & Law, SS 2006, 'Moving load identification on multi-span continuous bridges with elastic bearings', *Mechanical Systems and Signal Processing*, vol. 20, no. 7, pp. 1759-82, viewed 01/03/2020, DOI 10.1016/j.ymssp.2005.06.004.

Zhu, XQ & Law, SS 2015, 'Structural Health Monitoring Based on Vehicle-Bridge Interaction: Accomplishments and Challenges', *Advances in Structural Engineering*, vol. 18, no. 12, pp. 1999-2015, viewed 01/03/2020, DOI 10.1260/1369-4332.18.12.1999.

Zhu, XQ & Law, SS 2016, 'Recent developments in inverse problems of vehicle–bridge interaction dynamics', *Journal of Civil Structural Health Monitoring*, vol. 6, no. 1, pp. 107-28, viewed 01/03/2020, DOI 10.1007/s13349-016-0155-x.

Zhu, XQ, Law, SS & samali, B 2014, 'Indirect structural health monitoring of bridge structures using moving sensors', *23rd Australasian Conference on the Mechanics of Structures and Materials (ACMSM23)*, . viewed 01/03/2020.